Team S16

DSE - Lynx: Deployable UHF Transponder Payload

Technical Demonstration Mission of a Deployable Long Range UHF Transponder Payload to be Launched by the Lynx Spacecraft

L. De Backer	4233530	T. Celebi	4080270
I.A.M Bance	4271394	A. van den Hoed	4216954
P.J.C. Bentinck	4229827	I.A. Ruchser	4289609
M. Borst	4299159	J.S. Sonneveld	4303784
J.H. Bröcker	4079450	A. Van Eemeren	4302494

Final Report

Design Synthesis Excercise

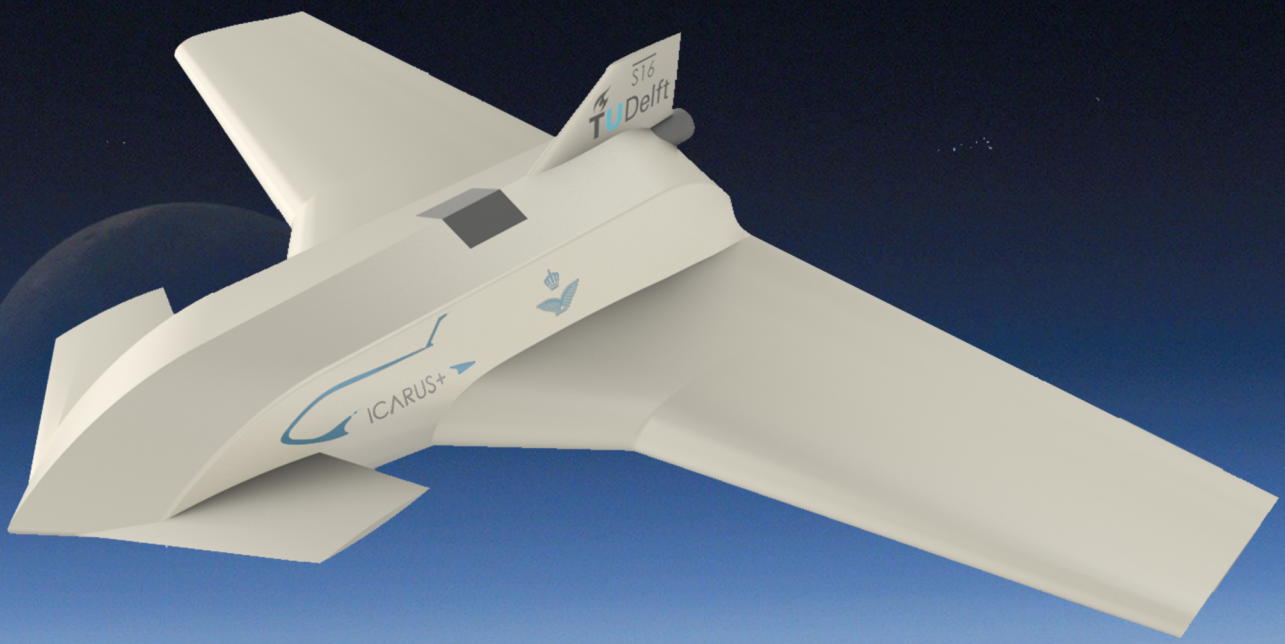

ICARUS+

TU Delft Delft University of Technology

Aerospace Engineering

June 20, 2016

Issues and Distribution Final Report

This is the first issue of the Final Report from DSE group S16, TU Delft.

Table 1: Update record.

Issue	Date	Pages Affected	Description of Update
Draft	20/06/16	all	New document

Table 2: Distribution list.

Distributed to	Company	Function
S16	TU Delft	designers
Trevor Watts	TU Delft	tutor
Ping Liu	TU Delft	coach
Gunther March	TU Delft	coach
Frank Matser	RNLAF	customer
Harry van Hulten	XCOR	customer

Image title page [1].

List of Symbols

C	Heat capacity	$J \cdot K^{-1}$
c	Specific heat	$J \cdot kg^{-1} \cdot K^{-1}$
N_0	White noise power	dB
Q	Thermal energy	J
d	Distance	m
$(\frac{V_c}{V})^2$	Velocity change of the canard surface	–
$\bar{c_e}$	Mean aerodynamic chord length of the part of the control surface behind the hinge line	m
$\ddot{x}_{GRMS}$	Overall response	g
$\delta_{e,max}$	Maximum deflection angle of the elevator	rad
$\frac{d\epsilon}{d\alpha}$	Down-wash gradient of the wing	–
γ	Ratio of specific heats	–
ϕ	Angle of displacement around the z-axis	rad
ψ	Angle of displacement around the x-axis	rad
ρ	Density	$kg \cdot m^{-3}$
σ_{bear}	Bearing stress	MPa
$\sigma_{ult,ten}$	Tensile ultimate stress	MPa
$\sigma_{yield,comp}$	Compressive yield stress	MPa
$\sigma_{yield,ten}$	Tensile yield stress	MPa
τ	Maximum shear stress	MPa
θ	Angle of displacement around the y-axis	rad
ξ	Damping factor	–
A	Aspect Ratio of the Wing	–
a	Lapse rate of an atmospheric layer	Km^{-1}
a_0	Lift curve slope of the airfoil	K
C_D	Total drag coefficient	–
C_f	Friction coefficient	–
C_L	Total lift coefficient	–
C_{D_i}	Lift induced drag coefficient	–
C_{D_p}	Parasitic drag coefficient	–
C_{D_w}	Wave drag coefficient	–
$C_{D_{trans}}$	Transonic drag coefficient component	–
$C_{D_{wl}}$	Wave drag coefficient due to lift	–
$C_{D_{wv}}$	Wave drag coefficient due to volume	–
C_{H_δ}	Hinge moment coefficient derivative of the elevator deflection angle	–
$C_{L_{\alpha_{A-c}}}$	Slope of the aircraft less canard lift-curve	–
$C_{L_{\alpha_c}}$	Slope of the canard lift-curve	–
$C_{L_{A-c}}$	Lift coefficient of the aircraft less canard	–
$C_{L_{c,max}}$	Maximum lift coefficient of the canard surface	–
C_{L_c}	Lift coefficient of the canard surface	–
$C_{L_{subsonic}}$	Lift coefficient for subsonic flight	–
$C_{L_{supersonic}}$	Lift coefficient for supersonic flight	–

C_{m_α}	Slope of the moment curve	–
C_m	Aerodynamic moment coefficient	–
e	Oswald factor	–
f_s	Structural safety factor	–
f_n	Natural frequency	Hz
h_0	Altitude at the boundary of an atmospheric layer	m
$H_{c,max}$	Hinge moment on the canard axis	Nm
$H_{e,max}$	Hinge moment on the elevon axis	Nm
k	Form factor	–
l	Total vehicle length	m
L_{A-c}	Lift of the aircraft less canard	N
L_C	Lift of the aircraft canard	N
l_c	Canard length (the distance between the aerodynamic centres of the wing and canard	m
M	Mach number	–
M_∞	Mach number for the free stream flow	–
M_{ac}	Moment around the aerodynamic centre of the wing	Nm
M_{crit}	Critical Mach number	–
M_{dd}	Drag divergence Mach number	–
n_{max}	Maximum load factor	–
p	Pressure of an ideal gas	Nm^2
p	Rotational velocity around the x-axis	rad/s
$P_{internal}$	Internal component heat generation	W
q	Rotational velocity around the y-axis	rad/s
Q_x	Statical moment of area of wing box cross section	m^4
r	Rotational velocity around the z-axis	rad/s
Re	Reynolds number	–
S	Wing surface of the aircraft	m^2
S_c	Canard surface of the aircraft	m^2
S_{cs}	surface area cross section	m^2
S_e	Elevon surface behind the hinge line	m^2
$S_{reference}$	Reference area	m^2
S_{wet}	Wetted area	m^2
T	Temperature of an ideal gas	K
T	Transmissibility	–
T_0	Temperature at the boundary of an atmospheric layer	K
T_h	Temperature at a certain altitude	K
$T_{initial}$	Initial internal temperature	K
$t_{insulation}$	Insulation thickness	mm
T_{melt}	Melting temperature	K
$T_{stagnation}$	Stagnation point temperature	K
W	Weight	kg
$z_{controllable}$	Longitudinal position of the centre of gravity limit due to controllability	m
$z_{controllable}$	Longitudinal position of the centre of gravity limit due to stability	m
$z_{hingeline}$	Longitudinal location of the hinge axis of the canard	m
$z_{n.p.}$	Longitudinal position of the neutral point	m
PSD	Power spectral density	$g^2 \cdot Hz^{-1}$
S.F.	Safety factor to go from neutral point to stable regime	–
λ	Wavelength	m
E_b	Energy per bit	dB
$\bar{z_{ac}}$	Dimensionless longitudinal position of the aerodynamic centre of the wing w.r.t. the M.A.C.	–
$\bar{z_c}$	Dimensionless longitudinal position of the aerodynamic centre of the canard w.r.t. the M.A.C.	–
$\bar{z_{np}}$	Dimensionless longitudinal position of the neutral point w.r.t. the M.A.C.	–
κ_a	Technological factor	–

List of Abbreviations

ADCS	Attitude Determination and Control System
ADS	Attitude Determination System
AWG	American Wire Gauge
CBS	Cost Breakdown Structure
CFD	Computational Fluid Dynamics
CLA	Coupled Loads Analysis
CPU	Central Processing Unit
CRM	Continuous Risk Management
COTS	Commercially-Off-The-Shelf
DMIPS	Dhrystone Million Instructions Per Second
DSE	Design Synthesis Exercise
EIRP	Effective Isotropic Radiating Power
FAA	Federal Aviation Authorities
FBS	Functional Breakdown Structure
FFBD	Functional Flow Block Diagram
FMEA	Failure Mode and Effect Analysis
FRAM	Ferroelectric Random Access Memory
GPIO	General Purpose Input/Output
GPS	Global Positioning System
IMU	Inertial Measurement Unit
ISA	International Standard Atmosphere
ICARUS+	Innovative Compact Autonomous long-Range UHF-transponder System
MAC	Mean Aerodynamic Chord
MDT	Mean Down Time
MOI	Moment of Inertia
MTBM	Mean Time Between Maintenance
MTR	Mid-term Report
MTTM	Mean Time To Maintain
NASA	National Aeronautics and Space Administration
PSD	Power Spectral Density
PWM	Pulse Width Modulation
RAM	Random Access Memory
RAMS	Reliability, Availability, Maintainability and Safety
RBD	Reliability Block Diagram
RF	Radio Frequency
RIDM	Risk-Informed Decision Making
RISC	Reduced Instruction Set Computing
RNLAF	Royal Netherlands Airforce
RTC	Real-Time Clock
Rx	Receiving
SDRAM	Synchronous Dynamic Random Access Memory
SPI	Serial Peripheral Interface
TPM	Technical Performance Measurement
TTCS	Telemetry, Tracking and Command System
Tx	Transmitting
UART	Universal Asynchronous Receiver/Transmitter
UHF	Ultra-High Frequency

List of Figures

3.1 Functional flow block diagram. . . . 4

4.1 Initial design drawing. . . . 5
4.2 Design iteration process. . . . 7

5.1 Layers of the atmosphere. . . . 11
5.2 Quasi-Biennial Oscillation in the stratosphere 12

6.1 Shape of the enclosure in Ansys Fluent®. . . . 14
6.2 Mesh of the design in Ansys Fluent®. . . . 14
6.3 NACA-43012A airfoil for the main wing. . . . 15
6.4 C_L - C_D and C_L - α curves for the NACA-43012A 16
6.5 Aerodynamic properties of NACA-43012A at high Reynolds numbers 16
6.6 Biconvex 8% t/c airfoil for the canard. . . . 17
6.7 Drag coefficient for the biconvex 8% airfoil 17
6.8 Normal coefficient for the biconvex 8% airfoil 17
6.9 Pressure drag coefficient of the biconvex airfoil 18
6.10 Lift coefficient of the biconvex airfoil 18
6.11 Drag coefficients for different geometries. . . . 19
6.12 Lift slope at different Mach numbers. . . . 19
6.13 Form factor against thickness ratio for the wing and canards. . . . 20
6.14 Form factor against thickness ratio for the wing and canards. . . . 20
6.15 Total drag versus Mach number for different C_L values at sea level. . . . 21
6.16 $C_L - \alpha$ and $C_M - \alpha$ graphs 22
6.17 $C_D - \alpha$ and $C_L - C_D$ graphs 22
6.18 Double- and single sweep on a wing planform. . . . 24
6.19 Schematic drawing of the canard and elevon actuating mechanism. . . . 25
6.20 Schematic drawing of the forces and moments acting on a canard aircraft 26
6.21 Spring damper system 29
6.22 Deployment mechanism for the UHF antenna. . . . 31
6.23 Wing box with double axes hinge. . . . 32
6.24 Wing unfolding stages. . . . 32
6.25 Clamping systems. . . . 33
6.26 The box cross section as airfoil replacement 34
6.27 Wing box cross section dimensions 34

6.28 The lower boundary of the stratosphere per latitude. . . . 41
6.29 The flight path of the ICARUS+. . . . 42
6.30 Mach number vs horizontal displacement of the ICARUS+ flight path. . . . 42
6.31 Mach number vs time of the ICARUS+ flight path. . . . 43
6.32 Dynamic pressure during flight of the ICARUS+. . . . 43
6.33 C_L and C_D plot during flight of the ICARUS+. . . . 44
6.34 C_{D_0} and C_{D_i} plot during flight of the ICARUS+. . . . 45
6.35 UHF antenna and tuning circuit specifications. . . . 48
6.36 Mirroring effects on the radiation pattern of the antenna 49
6.37 Radiation pattern reference UHF antenna. . . . 49
6.38 Data handling diagram 51
6.39 Electrical block diagram 54
6.40 Ambient air temperature and stagnation temperature versus flight time. . . . 55
6.41 Result comparison with mesh refinement. . . . 55
6.42 Computational time versus mesh refinement. . . . 55
6.43 Internal temperature versus flight time 56
6.44 Effect on internal temperature 57

7.1 Experimental C_L - α curve for the NACA-0012 airfoil 64
7.2 C_L - α curve comparison between (corrected) experimental simulated data 64
7.3 Experimental $C_L - C_D$ curve for the Cessna 177 65
7.4 Drag model prediction compared with experimental data for the Cessna 177 65
7.5 Experimental $C_D - C_L^2$ curve of the Concorde 66
7.6 Drag model compared to experimental data of the Concorde 66

8.1 $C_L - \alpha$ for different airfoils. . . . 72
8.2 UHF antenna power consumption and mass increase as a function of downlink data rate. . . . 78
8.3 UHF antenna power consumption and mass increase as a function of broadcasting distance. . . . 78
8.4 UHF antenna gain (i.e. directionality) as a function of downlink data rate 78
8.5 UHF antenna gain (i.e. directionality) as a function of broadcasting distance 78

9.1 Design of the first iteration. . . . 81
9.2 High pressure point on top of the nose. . . . 82
9.3 Design of the second iteration. . . . 82
9.4 Under-pressure behind the design. . . . 82
9.5 Design of the third iteration. . . . 82
9.6 Design of the final iteration. . . . 83

10.1 Render of the final design of the ICARUS+ in both folded and unfolded configuration. . . . 84
10.2 Hardware block diagram. . . . 87
10.3 Software block diagram. . . . 88
10.4 Communication diagram. . . . 89

12.1 Project design and development logic diagram. . . . 94
12.2 Logistics. . . . 97

13.1 Cost breakdown structure. 99

14.1 Government space budget growth, 2012-2014 105

16.1 Risk identification web. 110
16.2 Risk map. 112
16.3 Risk map after mitigation. 112

17.1 Relation between RAMS. 114
17.2 Reliability block diagrams. 116
17.3 Bathtub curve 116
17.4 Impacts in the scope of safety. 118

18.1 Mass contingency. 120
18.2 Cost contingency. 120

A.1 Functional breakdown structure. 126

B.1 Gantt chart of the entire ICARUS+ project. 127
B.2 DSE gantt chart part one. 128
B.3 DSE gantt chart part two. 129

C.1 Functional flow diagram stability and control. 130
C.2 Functional flow diagram flight mechanics. 131

D.1 Technical drawing of the external lay-out of the ICARUS+. 132
D.2 Technical drawing of the internal lay-out of the ICARUS+. 133

List of Tables

1 Update record. . . . I
2 Distribution list. . . . I

4.1 General parameters for the MTR design iteration. . . . 6
4.2 Performance results for the MTR design iteration. . . . 7
4.3 Requirement labels. . . . 8
4.4 Technical performance measurements for the Mid-Term review. . . . 10

6.1 Initial Parameters . . . 28
6.2 Characteristics of phosphor bronze. . . . 30
6.3 Spring properties. . . . 31
6.4 Stress values inside the ICARUS+ wing. . . . 36
6.5 Some characteristics of materials which are commonly used in aerospace. . . . 36
6.6 Flight trajectory results. . . . 45
6.7 Uplink budget. . . . 47
6.8 Downlink budget. . . . 47
6.9 Electrical subsystem components. . . . 53
6.10 Transient thermal analysis simulation settings. . . . 56
6.11 Temperatures for the insulation thicknesses and initial temperatures. . . . 57

7.1 ISA values . . . 59
7.2 Error of the simulation in Fluent® . . . 63
7.3 Parameter inputs for the Cessna 177. . . . 65
7.4 Parameter inputs for the Concorde. . . . 66
7.5 Variables for 1D thermal model verification. . . . 68
7.6 Comparison between Heisler and convection model. . . . 68
7.7 Temperature comparison between Heisler chart and convection model. . . . 68

8.1 Sensitivity parameters relating to aerodynamic performance. . . . 71
8.2 C_D values for different S_{wet}/S_{ref} and Mach numbers. . . . 71
8.3 C_D values for different sweep angles and Mach numbers. . . . 71
8.4 Sensitivity parameters relating to stability and control. . . . 74
8.5 Sensitivity analysis with respect to the stability height. . . . 74
8.6 Sensitivity parameters relating to the stresses induced by the flight loads. . . . 75
8.7 Sensitivity parameters relating to flight mechanics, effects on range. . . . 77
8.8 Sensitivity parameters relating to flight mechanics, regarding the attitude. . . . 77
8.9 Sensitivity parameters relating to thermal control. . . . 79

10.1 General parameters of the final design iteration. . . . 85
10.2 Performance results of the final design. . . . 86

12.1 Manufacturing data. . . . 95

13.1 Production costs. . . . 102
13.2 Total cost. . . . 102

14.1 Potential customers per segment. . . . 104
14.2 Overview of the government funding per segment. . . . 105

16.1 Relative rates for risk map. . . . 110

17.1 Criticality categories. . . . 115
17.2 Failure modes and probability of occurrence for the subsystems. . . . 115
17.3 Mean up time and mean down time ICARUS+. . . . 118

18.1 Contingency management. . . . 119
18.2 Contingency management results. . . . 119

19.1 Compliance matrix. . . . 122

E.1 Work distribution - Final Report. . . . 134

Summary

The Royal Netherlands Airforce (RNLAF), as a part of the Dutch Ministry of Defence, has a long term plan to build a satellite in their search for innovative ways to provide intelligence gathering. However, the development and building of a satellite requires large investments and thus results in high costs. For a first space asset of the RNLAF, a collaboration with XCOR was established. XCOR will provide commercial space travel with the Lynx Mark I, which will reach an altitude of 60 km. Two of the Lynx' outer payload bays can carry a deployable 2U-unit (22 x 10 x 10cm) and XCOR has offered the RNLAF the opportunity to use one of these payload bays during the first flights. Therefore, the RNLAF wants to build a deployable payload to perform a technical demonstration mission of a long range ultra high frequency transponder. The DSE team S16 from Delft University of Technology is tasked with the design of this system, named the ICARUS+. The goal of it is to reach a maximum range while being controlled autonomously.

In this report the design process that led to the final subsystem design of the ICARUS+ is given. In previous steps of this process a planning has been made, a baseline has been set up and based on this a concept selection has been performed. The selected concept was a deployable glider, in planform similar to the Lynx, that uses unfolding delta wings. This was the starting point for the process discussed in this report. The detailed design phase was done using an iterative process where six main engineering fields are combined to optimise the design. The fields are aerodynamics, stability and control, structures, flight mechanics, electronics and thermal control. During this process, important features were either changed, added or disregarded with respect to the initial concept. In order to design a controllable aircraft, a different airfoil was selected and a canard surface was added. The canard will contribute to the controllability in the supersonic flight regime, which occurs in the early stages of the mission. Other important aspects in the design process consist of the hinges in the wings and the UHF antenna, which deploys from the back of the spacecraft using a spring. Combining the results of all engineering fields finally resulted in a projected range of the payload, the estimated range of final design is 230 km. Besides the performance analysis, other parts of the design process were also investigated such as a the manufacturing and logistic processes, the costs that are to be expected, as well as a risk management strategy and a reliability, availability, maintainability and safety analysis. Furthermore, a look has been taken at other aspects namely a general market analysis and a sustainability analysis. Finally the previously established requirements were compared to the actual design in a compliance matrix, from which resulted that all but one requirements were met. It was found that in order for proper testing and certifying the allowed budget of €100,000 will not be sufficient.

Looking at the obtained results, it can be concluded that the design is not completely finished yet, and further details will have to be determined in the future. For example specific tests and analysis methods will have to be defined for the trans- and supersonic performance of the design. This is, among others, explained in an extensive recommendation chapter that has been included in this report.

Contents

List of Abbreviations **IV**

List of Figures **VII**

List of Tables **IX**

Summary **X**

1 Introduction **1**

2 Mission Overview **2**
2.1 Mission Purpose . . . 2
2.2 Possible Applications . . . 2
2.3 Current Design Stage . . . 2

3 Functional Breakdown **3**
3.1 Functional Breakdown Structure . . . 3
3.2 Functional Block Flow Diagram . . . 3

4 Design Process Overview **5**
4.1 Initial Design . . . 5
4.2 Design Process . . . 7
4.3 Requirements . . . 8
4.4 Budget Allowances . . . 10

5 Meteorological Analysis **11**
5.1 The Atmosphere . . . 11
5.2 Effects . . . 12

6 Performance Analysis **13**
6.1 Aerodynamics . . . 13
6.1.1 Software . . . 13
6.1.2 Airfoil selection . . . 14
6.1.3 Lift . . . 18
6.1.4 Drag . . . 19
6.1.5 Results . . . 21
6.1.6 Method changes . . . 22

6.2 Stability and Control . . . 23
6.2.1 Planform and Control Surfaces . . . 23
6.2.2 Flight Stability and Control . . . 25
6.2.3 Longitudinal Stability . . . 25
6.2.4 Free Fall Stability and Control . . . 27
6.3 Structures . . . 28
6.3.1 Launch Survivability . . . 28
6.3.2 Deployment . . . 30
6.3.3 Hinge Design . . . 31
6.3.4 Flight loads . . . 33
6.3.5 Material Selection . . . 36
6.4 Flight Mechanics . . . 37
6.4.1 Initial Conditions and Assumptions . . . 37
6.4.2 Flight Path Approach . . . 38
6.4.3 Elaboration on the Results . . . 41
6.5 Electronics . . . 46
6.5.1 Communication . . . 46
6.5.2 Actuation . . . 49
6.5.3 Navigation . . . 50
6.5.4 Command and Data Handling . . . 50
6.5.5 Power . . . 52
6.5.6 Electrical Subsystem . . . 52
6.6 Thermal Control . . . 53
6.6.1 Thermal Envelope . . . 53
6.6.2 Simulation Model . . . 54
6.6.3 Simulation Results . . . 55

7 Verification and Validation **58**
7.1 ISA Model . . . 58
7.2 Flight Mechanics Model . . . 59
7.3 Stability Height Model . . . 61
7.4 Ansys: Fluent® . . . 62
7.5 Drag Model . . . 64
7.6 Wing box model . . . 66
7.7 Thermal simulations, Ansys Mechanical® . . . 67

8 Sensitivity Analysis **70**
8.1 Aerodynamics . . . 70
8.2 Stability and Control . . . 72
8.3 Structures . . . 73
8.4 Flight Mechanics . . . 75
8.5 Electronics . . . 77
8.6 Thermal Control . . . 79

9 Design Iterations **80**
9.1 First Iteration . . . 80
9.2 Second Iteration . . . 81
9.3 Third Iteration . . . 81
9.4 Fourth Iteration . . . 83

10 Technical Design Overview **84**
10.1 Final Design and Performance Overview . . . 84
10.2 Hardware . . . 86
10.3 Software . . . 87
10.4 Communication . . . 89

11 Recommendations **90**
11.1 Aerodynamics . . . 90
11.2 Stability and Control . . . 90
11.3 Structural Analysis . . . 91
11.4 Flight Mechanics . . . 91
11.5 Electronics . . . 91
11.6 Thermal Control . . . 92
11.7 Recommendations Conclusion . . . 92

12 Project Design and Operations **93**
12.1 Project Design and Development Logic . . . 93
12.2 Manufacturing . . . 93
12.3 Operational Logistics . . . 96

13 Cost Breakdown **99**
13.1 Cost Breakdown Structure . . . 99
13.2 Total Costs . . . 101

14 Market Analysis **103**
14.1 Market Plan . . . 103
14.2 Detailed Market Analysis . . . 103
14.2.1 Demographics and Segmentation . . . 103
14.2.2 Target Market . . . 105
14.2.3 Market Need . . . 106
14.2.4 Competition . . . 106
14.2.5 Barriers and Opportunities to Entry the Market . . . 106

15 Sustainable Development **107**
15.1 Sustainable manufacturing approach . . . 107
15.2 Sustainable logistics and operations . . . 108

16 Risk Management **109**
16.1 Risk Management Approach . . . 109
16.2 Risk Assessment . . . 109

16.3 Risk Planning . . . 111
16.4 Track and Control . . . 113

17 Reliability, Availability, Maintainability and Safety (RAMS) 114
17.1 Necessity of RAMS . . . 114
17.2 Reliability . . . 114
17.2.1 Failure Mode and Effect Analysis . . . 115
17.2.2 Reliability Allocation . . . 115
17.2.3 Probability Distributions . . . 116
17.3 Maintainability . . . 116
17.4 Availability . . . 117
17.4.1 Definitions . . . 117
17.4.2 Analysis . . . 117
17.5 Safety . . . 118

18 Budget Allocation 119

19 Compliance Matrix 121

20 Conclusion 123

Bibliography 124

A Functional Breakdown Structure 126

B Gantt Chart 127

C Simulation Models Flow Diagrams 130

D ICARUS+ Technical Drawings 132

E Work Distribution 134

Chapter 1

Introduction

Until today, the Dutch Ministry of Defence has not owned space assets that are used for its military and civilian operations. However, it does have a space section at the Royal Netherlands Airforce (RNLAF), the space security centre, which investigates possible innovative solutions for intelligence gathering. Due to new technologies and cheaper possibilities, it will be possible for the RNLAF to develop their own satellite within a few years. XCOR Aerospace has offered the RNLAF to carry a payload on board of the Lynx Mark I spacecraft, which is expected to fly in 2017. During this mission, the RNLAF would like to investigate the possibilities of deploying a long range Ultra High Frequency (UHF) transponder payload from the Lynx at its apogee at an altitude of 60 km. This payload is designed in collaboration with Delft University of Technology.

So far a trade off between different concepts has been made with as a result the final concept, the ICARUS+. ICARUS+ stands for Innovative Compact Autonomous long-Range UHF-transponder System. The name is derived from the myth of Icarus, who flew to close to the sun and fell down from the sky. ICARUS+ will prove that with the current technology the limit for flying 'too high' does not exist anymore.

The aim of this report is to explain and guide the reader through the design process of the ICARUS+ down to subsystem level. Several iterations are made throughout the designing process to finally come to an optimum design. Six main engineering fields: aerodynamics, stability and control, structures, flight mechanics, electronics and thermal control are considered during these iterations. The main goal of the ICARUS+ is to fly as far as possible, however this will be limited by the possibilities of designing. Finally, an optimum design is given together with recommendations for future research.

This report is structured as follows. First of all a mission overview is given by including the mission purpose and possible future applications in Chapter 2. In Chapter 3 the functional breakdown of the mission is given. The design process overview so far can be seen in Chapter 4. Chapter 5 elaborates on the environmental conditions, since that will give the design some limitations and advantages. In the next chapter, Chapter 6, the performance analysis is given. This is divided in the six main categories: aerodynamics, stability and control, structures, flight mechanics, electronics and thermal control. In order to truly rely on the calculated results all the models need to be verified and validated, this is done in Chapter 7. Chapter 8 elaborates on sensitivity parameters, this is also done for each of the six categories. As follows the design iterations are explained in Chapter 9. The final design and performance overview is given in Chapter 10. Recommendations on the further design are given in Chapter 11. Chapter 12 and 13 elaborate on the project design and operations and the cost breakdown respectively. In order to be able to sell the product, a market analysis is done in Chapter 14. A sustainable development is given in Chapter 15. In order to know what the risks are and how they can be mitigated a risk analysis is given in Chapter 16. In Chapter 17 a RAMS analysis is done. A budget allocation of the product is given in Chapter 18. Finally, in Chapter 19 the compliance matrix of the design is given. Chapter 20 will terminate this report with a conclusion.

Chapter 2

Mission Overview

In this chapter a short explanation about the mission is given, which includes the mission purpose and possible applications of the final design. Furthermore, a brief recap about previous work is stated.

2.1 Mission Purpose

The purpose of this mission is to demonstrate the feasibility of sending a payload with the Lynx Mark I up to an altitude of 60 kilometres and deploy it in the surrounding environment. At 60 kilometres there is a very small density and almost vacuum conditions occur. However, still a gravitational acceleration of $9.8 m \cdot s^{-2}$ is present. This payload shall weigh no more than two kilogrammes and fit into the 2U external payload bay C of the Lynx Mark I. Furthermore, it shall be controllable and fly as far as possible. Thus, maximising its range by initiating its optimum gliding path at maximum altitude is an essential action in the design.

2.2 Possible Applications

The purpose of this specific mission is to demonstrate the general feasibility of the mission. This will be the foundation for different possible applications later on. Potential applications could be for example:

- Reconnaissance purposes above strange territories.
- Imaging of areas.
- Communication gateway where communication via other means (e.g. satellite connection) is hard or not possible at all.
- Radar jamming purposes.
- Delivery of packages.

Next to these potential applications, other applications are also possible. The applications are not limited by the ones mentioned in this list.

2.3 Current Design Stage

In this project of ten working weeks, design team S16 has been developing a design to fulfil the above mentioned mission. In previous reports the team organisation has been documented (Project Plan [2]) and the requirements and constraints have been derived from the needs of the involved parties which led to a broad design option tree (Baseline Report [3]). From this tree, five designs have been analysed in further detail in order to make an elaborated trade-off and choose a final design (Mid-term Report [4]). In this report, the Final Report, this design is elaborated on in detail and iterated in order to maximise its performance.

Chapter 3

Functional Breakdown

As the final design has been chosen, the Functional Breakdown Structure (FBS) will be updated in this chapter. In order to have a better visualisation of the functions of the payload, these will be presented in a Functional Flow Block Diagram (FFBD) as well.

3.1 Functional Breakdown Structure

Looking at the mission, different functions can be distinguished for the product to perform. To gain an overview, these functions have been organised in a pyramidal configuration with the top level functions on top, splitting up as the functions get smaller and more defined into sub levels. Essentially it is an AND tree, in which the main functions are split up into sub functions, as can be seen in Figure A.1 in Appendix A.

The main functions that have been identified are launching, activating the payload, deploying the payload and eventually operating the payload. The landing stage is not considered in this diagram, since at this point a smooth landing will not be designed for. This will be kept as a possible add-on for later design improvements.

3.2 Functional Block Flow Diagram

The functional breakdown from the previous section is useful to see everything the payload needs to be able to perform. However, for the designing process it is essential to order the functions chronologically as this facilitates a quick overview. Therefore the FFBD has been created (Figure 3.1). In the top row, again all main functions are stated. As follows they are chronologically further split up into sub functions.

The main functions are again launching, activating the payload, deploying the payload and eventually operating the payload. Conducting the launch simply includes the capability of the payload to survive the loads during launch. The second function is the activation of the payload. In order to save power, the payload will be in stand by mode until it is activated by the pilot of the Lynx, prior to deployment from the Lynx. Switching on includes turning on the active power supply to the payload in payload bay C, this will then initiate the system, including the board computer, the sensors and the UHF transponder. Finally, the system will check itself for proper functioning. The next main function shown in the diagram is the deployment of the payload. This includes opening the payload bay, releasing the box that contains the payload and finally checking for a proper deployment using the sensors. Once the box is falling, the payload has to be released from its adaptor, the box. This will be done again by a spring system separating both structures and a consequential deployment of the wings. Finally, proper deployment is checked again. At this stage the longest main function begins, the operating phase. This can be split into two main sub-functions, operating the UHF transponder and navigating. The first one consists of receiving, processing and sending signals. The second sub-function of the payload is to check its altitude and attitude, thus its overall position, but also to process and analyse the measured data and to give an according input to the control surfaces. These inputs will be most dominant in two parts of the flight path. The first one is the initiation of the pull out manoeuvre and the other one is the moment the pullout is completed and the gliding part is started. Apart from this, the function also checks and counteracts disturbances the payload encounters along its trajectory, such as winds or gusts. Finally, similar to the FBS, the landing is not taken into account as the payload is not designed to land at this point.

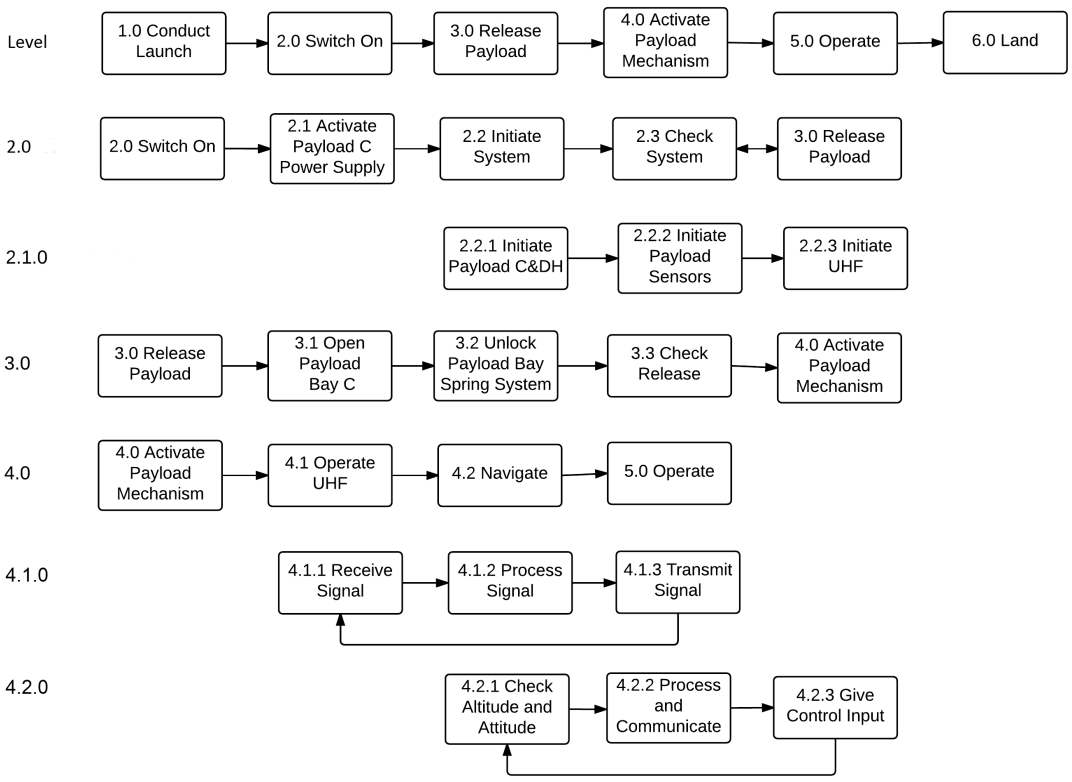

Figure 3.1: Functional flow block diagram.

Chapter 4

Design Process Overview

First of all, before beginning with an iterative subsystem level design process, the initial design has to be defined. This will be done in this chapter. Furthermore, the iterative approach is explained and the available budgets and technical performance measurements (TPMs) are given. Finally, this chapter is completed with the general requirements of the mission.

4.1 Initial Design

In the previous design steps, which are explained in the Mid-term Report (MTR) [4], a final conceptual design has been chosen. This is based on its superior characteristics and performance, compared to four other options. The resulting summarised data can be found in Table 4.1 and Table 4.2. This initial design will be used to start the final iteration process, which will be explained in the following section (Section 4.2). To visualise the chosen design, a drawing is shown in Figure 4.1.

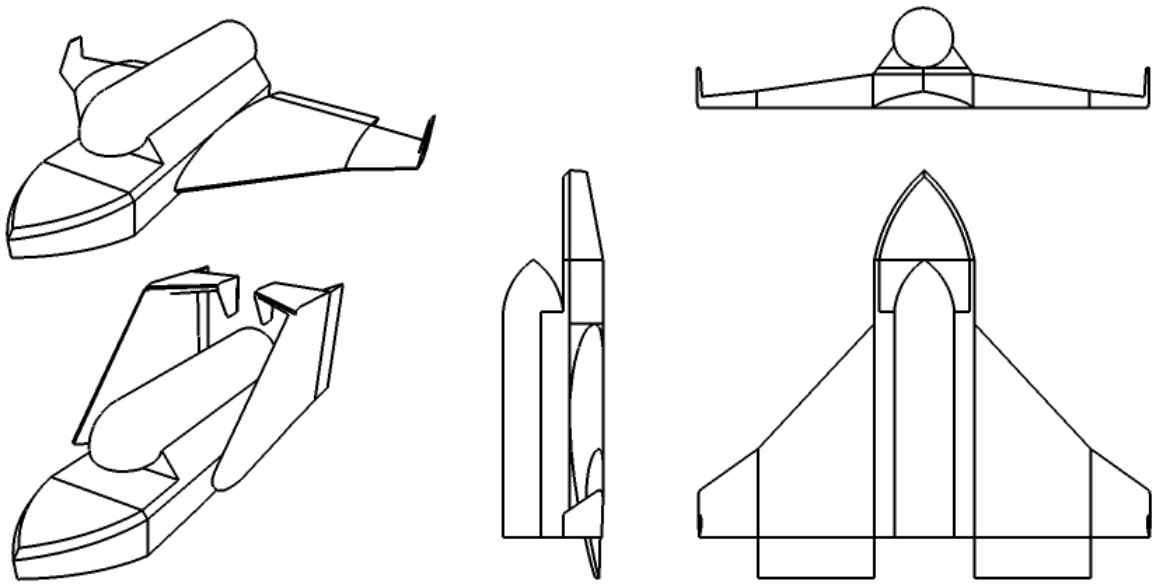

Figure 4.1: Initial design drawing.

As can be observed, the concept uses a delta wing configuration with deployable elevons and movable winglets. The elevons provide roll and pitch, whilst the winglets provide yaw control. Furthermore, the design offers

Dimensions		
Wing	Value	Unit
b	0.27	$[m]$
c_{root}	0.217	$[m]$
c_{tip}	0.03	$[m]$
$c_{M.A.C.}$	0.145	$[m]$
S	0.021	$[m^2]$
A	3.45	[-]
e	0.8	[-]
Γ	0	$[^\circ]$
Λ	0.138	$[^\circ]$
λ	47	[-]
$Airfoil$	NACA4412	[-]
Control surfaces	Value	Unit
$S_{elevons}$	0.002	$[m^2]$
$S_{winglet}$	0.0018	$[m^2]$
Fuselage	Value	Unit
$l_{fuselage}$	0.22	$[m]$
$w_{fuselage}$	0.06	$[m]$
$h_{fuselage}$	0.06	$[m]$
Payload	Value	Unit
$l_{payload}$	0.16	$[m]$
$w_{payload}$	0.04	$[m]$
$h_{payload}$	0.04	$[m]$

a)

Mass budget		
Parameter	Value	Unit
m_{system}	1.23	$[kg]$
$m_{payload}$	0.1	$[kg]$
m_{total}	1.24	$[kg]$

b)

Center of gravity and neutral point		
Parameter	Value	Unit
$\bar{x}_{c.o.g.}$	0	$[m]$
$\bar{y}_{c.o.g.}$	0	$[m]$
$\bar{z}_{c.o.g.}$	0.1216	$[m]$
$\bar{x}_{n.p.}$	0	$[m]$
$\bar{y}_{n.p.}$	0	$[m]$
$\bar{z}_{n.p.}$	0.166	$[m]$

c)

Moment of inertia		
Parameter	Value	Unit
I_{xx}	0.0085	$[kg{\cdot}m^2]$
I_{yy}	0.0105	$[kg{\cdot}m^2]$
I_{zz}	0.0075	$[kg{\cdot}m^2]$
I_{xy}	-	$[kg{\cdot}m^2]$
I_{xz}	0	$[kg{\cdot}m^2]$
I_{yz}	0	$[kg{\cdot}m^2]$

d)

Table 4.1: General parameters for the MTR design iteration with respect to a) dimensions, b) mass budget, c) centre of gravity and neutral point and d) Moment of Inertia (MOI).

a substantial amount of space for the payload with a total system weight of 1.24 kg.

The performance results of the MTR design are discussed below, within the different engineering fields.

- **Aerodynamics**: the aerodynamic performance is optimised for the subsonic flight regime. This is the determining factor for maximising range, which can be seen from the lift-to-drag ratio of 4.94 with a maximum lift coefficient of 1.36. At transonic and supersonic speeds the zero-lift drag coefficient approximations should be improved, as they are inaccurate.
- **Stability and control**: as can be seen, this design will be stable and able to start its flight at an altitude of 32 km. This is nearly half of the release altitude, thus further research should be done to investigate if this could be improved. Additionally, the aircraft is stable as can be seen from the negative pitching moment coefficient. However, the controllability of the concept should be investigated and quantified still at this stage of development. This is especially true for the controllability of the design during the supersonic flight phase.
- **Flight mechanics**: the range of this concept is 157 km with a flight time of 14 minutes. This performance is rather poor and other design solutions should be explored to increase it, even if this could reduce payload carrying capability.
- **Electronics**: the electrical subsystem requires 5.9 W of power over a 14 minute flight time. More

Aerodynamics		
Subsonic	Value	Unit
C_{D0}	0.062	[-]
C_{L_α}	0.0827	[-]
C_{Lmax}	1.36	[-]
$\frac{C_L}{C_D}_{max}$	4.949	[-]
C_M-α	-0.00156	[-]
Transonic	Value	Unit
C_{D0}	0.114	[-]
$T_{max,induced}$	252	$[K]$
Supersonic	Value	Unit
C_{D0}	0.0397	[-]
$T_{max,induced}$	755	$[K]$

a)

Flight mechanics		
Parameter	Value	Unit
Range	157	$[km]$
Endurance	13.7	$[min]$

b)

Electronics		
Parameter	Value	Unit
Power	5.865	$[W]$

c)

Stability and Control		
Parameter	Value	Unit
Stability height	32	$[km]$

d)

Table 4.2: Performance results for the MTR design iteration with respect to a) aerodynamics, b) flight mechanics, c) electronics and d) stability and control.

research has to be done in order to determine if this is feasible and accurate with the limited amount of space and mass.

4.2 Design Process

As the design becomes more complex, the different departments have to increase their communication and interaction. This is a relatively difficult task and in order to not lose the overview, the systems engineers have defined an iteration scheme which is shown in Figure 4.2.

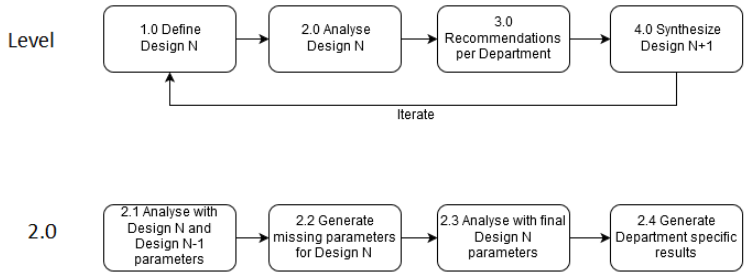

Figure 4.2: Design iteration process.

As can be seen, there are two flow diagrams to be distinguished. In the first flow diagram, the overall iteration process is shown. First, the entire team will start with one physical design configuration using the precise inputs previously defined. However, in order to generate certain values, such as C_{Lmax} or the neutral point, a sub iteration has to be done. For this, using the previously defined values (dimensions, airfoil etc) in a first round of computing, the missing parameters will be determined. Once these values are found, they can be used together with the already known dimensions of Design N to be analysed. Every department will now examine the values within a given range and see which changes will increase their specific performance. Once this is done, the recommendations will be collected by the systems engineers and synthesised into a new design iteration, Design N+1. Using these new values, the process will be repeated from the beginning. This iterative

process is being repeated several times within the time frame, as determined by the Gantt chart (see Appendix B). This will be done until an acceptable performance is obtained.

4.3 Requirements

In Table 4.3 the abbreviations used for the labelling of the requirements are stated. The requirements are structured as follows. First the type is given, that is whether it is a functional requirement or a constraint. The second part defines whether it is quantitative or qualitative requirement. After that the origin is stated and finally which part or subsystem it affects. In order to be able to distinguish between similar requirements, they are numbered. During the performance analysis, which is explained later on in this report (Chapter 6), several subsystem requirements arose limiting other departments. These requirements have been added to list below. Their explanation can be found in the respective section of Chapter 6.

Table 4.3: Explanation of the abbreviations used in labelling the requirements.

Abbreviation	Explanation
AER	Requirement derived from Aerodynamic engineering
ANT	Requirement specific to the UHF antenna
BAT	Requirement specific to the battery
COMP	Requirement specific to the board computer
CON	Requirement derived from a constraint
DAT	Requirement specific to data handling
ELEC	Requirement derived from Electrical engineering
ENV	Requirement categorised as being environmental
FLY	Requirement derived from Flight Mechanics engineering
FUNC	Requirement derived from a functional need
GS	Requirement specific to the ground station
LYNX	Requirement following from the Lynx interface document
PAY	Requirement derived from the payload
POW	Requirement following from the Lynx interface document specific to power
PROG	Requirement categorised as being programmatic
QUAL	Qualitative requirement
QUAN	Quantitative requirement
RAIL	Requirement following from the Lynx interface document specific to the rail system
REG	Requirement specific to the regulators
STAB	Requirement derived from Stability and Control engineering
STRUC	Requirement derived from Structural engineering

The battery should have a capacity of at least 10.11 Ah, which includes a 70% duty cycle. The voltage should be around 3-5 V with a maximum discharge current of at least 4 A. Finally, the temperature range should be at least from -40 to 60 $°C$.

CON-QUAN-ELEC-BAT-01 The battery shall have a capacity of 10.11 Ah, inlcuding a 70% duty cycle.

CON-QUAN-ELEC-BAT-02 The battery shall deliver a voltage between 3-5 V at a maximum discharge current of at least 4 A.

CON-QUAN-ELEC-BAT-03 The battery shall have a maximum discharge current of 4 A.

CON-QUAN-ELEC-BAT-04 The battery shall last at least 2 hours.

CON-QUAN-ELEC-BAT-05 The battery shall have a temperature range at least from -10 to 60 °C.

CON-QUAN-ELEC-COMP-01 The computer shall have at least 2 UART (Rx/Tx) ports.

CON-QUAN-ELEC-COMP-02 The computer shall have at least 4 PWM ports.

CON-QUAN-ELEC-COMP-03 The computer shall have 1 GPIO port.

CON-QUAN-ELEC-REG-01 The regulators shall be able to handle voltages between 0 and 28 V.

CON-QUAN-ELEC-STRUC-01 The temperature around the electronics shall be between -10 °C and 60 °C.

CON-QUAL-ENV-01	The payload shall be able to withstand thermal heating during its descent.
CON-QUAL-ENV-02	The payload shall avoid turbulent weather conditions at all times.
CON-QUAL-ENV-03	The design shall fly in the direction of the Quasi-Biennial winds when it is within the stratosphere.
CON-QUAN-ENV-01	The payload shall be able to operate in a -70 $^{\circ}C$ to +30 $^{\circ}C$ atmospheric temperature range.
CON-QUAN-ENV-02	The payload shall be able to operate in an absolute atmospheric pressure of 0.002196 Pa at 60 km [5].
CON-QUAL-LYNX-01	The payload shall be attachable to the Lynx Mark I.
CON-QUAL-LYNX-02	The payload shall be interfaceable with the payload bay power connector.
CON-QUAN-LYNX-01	The payload shall have a size of 10x10x22 cm.
CON-QUAN-LYNX-02	The payload shall have a total mass equal to or less than 2 kg.
CON-QUAN-LYNX-03	The payload shall survive the 6g launch loads with a safety factor to material yield of 1.5.
CON-QUAN-LYNX-RAIL-01	The rails shall have a minimum width of 8.5 mm.
CON-QUAN-LYNX-RAIL-02	The rails shall have a surface roughness less than 1.6 μm.
CON-QUAN-LYNX-RAIL-03	The edges of the rails shall be rounded to a radius of at least 1 mm.
CON-QUAN-LYNX-RAIL-04	At least 75% of the rail shall be in contact with the P-POD rails.
CON-QUAN-LYNX-RAIL-05	Aluminium 7075, 6061, 5005, and/or 5052 shall be used for the deployment rails of the payload.
CON-QUAL-PAY-ELEC-01	All subsystems shall fit within the allocated space.
CON-QUAL-PAY-ELEC-02	All subsystems shall stay within the defined mass budget.
CON-QUAL-PAY-ELEC-03	All subsystems shall stay within the defined power budget.
CON-QUAL-PROG-01	The payload shall be flying within the legal framework of every relevant country.
CON-QUAN-PROG-01	Each payload shall have a total cost lower than €100,000.
CON-QUAN-PROG-02	The preliminary design shall be made within 10 weeks, starting April 18th 2016.
CON-QUAN-PROG-03	The design and production of the system shall be ready to be launched by the first quarter of 2017.
CON-QUAL-STAB-COMP-01	The computer shall be able to compute the required control inputs.
CON-QUAN-STAB-ELEC-01	The elevator actuator shall be able to deliver a maximum torque of 0.049 Nm.
CON-QUAN-STAB-ELEC-02	The canard actuator shall be able to deliver a maximum torque of 0.0082 Nm.
CON-QUAN-STRUC-01	The hinge shall have a minimum turning angle of 100 degrees.
CON-QUAN-STRUC-02	The chord at the hinge shall be at least 52 mm.
CON-QUAN-STRUC-03	The structure shall be able to withstand any loads with a safety factor of 2.
CON-QUAN-UHF-ANT-01	The UHF antenna shall match the 395 MHz of the transponder.
CON-QUAN-UHF-ANT-02	The UHF antenna shall close uplink and downlink within a margin bigger than 7.8 dB.
FUNC-QUAL-01	The system shall be able to successfully detach the payload.
FUNC-QUAL 02	The system shall be able to communicate with the ground station.
FUNC-QUAL-03	The system shall provide power to the different subsystems.
FUNC-QUAL-04	The system shall be able to deploy a flying mechanism.
FUNC-QUAL-05	The system shall be able to control its attitude.

FUNC-QUAN-01	The system shall have the ability to communicate with a signal bandwidth of 225-400 MHz.
FUNC-QUAN-02	The system shall survive a maximum load factor ($n = \frac{L}{W}$) of 5 with a safety factor of 2.
FUNC-QUAN-03	The inside of the payload shall be within a -20 °C to +60 °C temperature range during the entire duration of the mission.
FUNC-QUAN-AER-01	The maximum lift coefficient shall be at least 1.0 at M = 0.6 at 25 km altitude.
FUNC-QUAN-AER-02	The lift over drag ratio shall be higher than 5.0 during the glide phase.
FUNC-QUAL-ANT-01	The UHF antenna shall be in sight of GPS satellites at all times.
FUNC-QUAL-ANT-GS-01	The ground station shall fulfil the requirements mentioned in the Link budget table.
FUNC-QUAL-FLY-STAB-01	The payload shall be able to stabilise itself at the latest at an altitude of 40 km.
FUNC-QUAL-GS-ANT-01	The payload shall have connection with the ground station at all times.
FUNC-QUAL-STAB-01	The design shall be stable for all flight conditions.
FUNC-QUAL-STRUC-ANT-01	The UHF antenna shall be strong enough to push the payload out.

4.4 Budget Allowances

Breaking down the budget first of all requires defining the different technical performance measurements (TPMs). These TPMs are derived from the mission requirements (see Section 4.3) and have been specified in Table 4.4, together with their maximum value as well as the current value if applicable. In previous design stages a higher contingency margin has been applied, that is up to 30%. However, considering that the design is approaching its final shape, the contingency margin varies between 5% and 15% for the Mid-Term review and will decrease down to 5% for the Final review. For the exact TPMs for all stages the reader is referred to the Mid-term Report [4].

Table 4.4: Technical performance measurements for the Mid-Term review.

TPM	MTR Contingency Margin	MTR Design Goal	MTR Design State
Mass [kg]	15%	1.91	1.24
Power [W]	10%	25.45	5.87
Cost [€]	15%	95,238	64,776
Schedule [days]	5%	40	40

As can be observed from Table 4.4, all the allowances are made at the Mid-Term design stage. The final and exact budget breakdown of the design, is presented in Chapter 18.

Chapter 5

Meteorological Analysis

When the extremely light-weight design is subjected to heavy weather conditions, it will lose most of its stability and controllability. However, some effects of the weather can also be used in the advantage of the flight path and increase the range. Therefore, the weather phenomena around the world should be analysed.

5.1 The Atmosphere

As can be seen in Figure 5.1, the design will fly in the troposphere, stratosphere and mesosphere. Since the ICARUS+ will be deployed at 60 km, only the phenomena up to 60 km will be briefly analysed. A more broad analysis of the weather is required in later design stages.

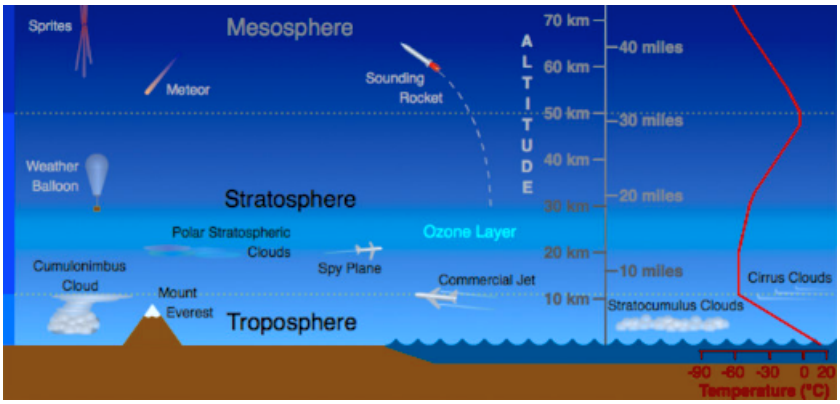

Figure 5.1: Layers of the atmosphere. [1]

The major part of the weather on Earth occurs in the troposphere. The movements of the air in the troposphere are caused by the pressure differences, which on their part are a result of the differences in the heating of the Earth. This movement also contributes to the different weather on earth. Which need to be taken into account when the final flight path of the design is being determined. In some situations, the effects of the wind are not only determined by the general circulation pattern as explained above. Due to topographical circumstances, specific regional wind patterns can arise. In those areas, wind speeds can reach up to 140 $km \cdot h^{-1}$. For the mission it is recommended to avoid those areas, since the high wind speeds will decrease the stability of the design significantly. [6] Once the design gets closer to the surface of the Earth, more small scale effects will occur, which have be taken into account.

The next layer is the stratosphere. This is the layer that also contains the ozone layer. Some of the weather conditions found in the section before also arise in this layer. However, this only appears in extreme conditions, like with cumulonimbus clouds, so called 'thunder clouds'. The air above those clouds might get very turbulent. Therefore, it is recommended to avoid those clouds. Another phenomena that occurs in the stratosphere is the Quasi-Biennial Oscillation. This is a constant wind going from West to East or from East to West, which

[1] URL `http://scied.ucar.edu/atmosphere-layers` [9 Jun 2016]

changes every 14 months. In Figure 5.2 the velocity and the pressure of the Quasi-Biennial Oscillation is shown with the altitude. Wind waves originating from the winds that started in the troposphere are enlarged in the stratosphere and mesosphere and will finally dissipate in the Mesosphere.

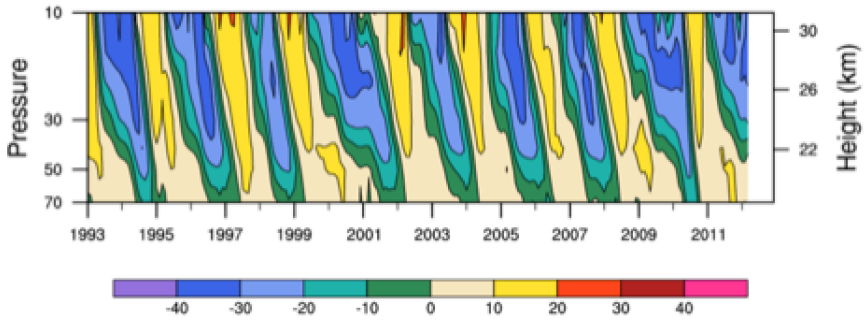

Figure 5.2: Quasi-Biennial Oscillation in the stratosphere, velocity expressed in $m \cdot s^{-1}$, pressure expressed in hPa. Positive velocities are westerly winds. [1]

Influenced by the Quasi-Biennial Oscillation, there are also jet streams. Jet streams are winds caused by particularly strong temperature gradients. They are usually found in the upper troposphere and lower stratosphere. The jet streams create a lot of turbulence caused by their strong wind shears. Taking the stability of the design into account, it is not recommended to stay in the streams for a long time.

As stated before, the mesosphere starts at 55 km and ends at 85 km. Normally, vehicles only pass through this layer, but will not stay in the layer long enough to make proper measurements. Therefore, not much is known about the mesosphere so far. However, in the mesosphere two main disturbances can be found. First of all nocticulent clouds and secondly 'sprites'. Nocticulent clouds, also named polar mesospheric clouds, are seasonal and will only form during summer, this is because the temperatures in the mesosphere will be lowest at that time of the year. Next, the sprites are large bursts of light that occur above a thunderstorm. Sprites only last for a small fraction of a second but nevertheless they can reach a diameter up to 50 km. Being in a Sprite should be avoided by the ICARUS+. Since thunderstorms should be avoided anyway, this is not going to be a problem.

5.2 Effects

Taking the phenomena mentioned in Section 5.1, an analysis can be performed to see what the consequences might be for the design. In the mesosphere, where the design will be deployed, it must avoid the nocticulent clouds and the sprites, since this might cause catastrophic failure of the design.

The Quasi-Biennial Oscillation is expected to be directed from West to East in 2017, the expected year of launch. The speeds of this wind, which are up to 35 $m \cdot s^{-1}$, can have a beneficial effect on the range. This is further explained in Section 6.4.

Finally, the design will enter the troposphere. Worldwide, the weather is very different and therefore hard to analyse when the exact place of deployment and the range are not yet known. However, it is highly recommended that the weather during the mission is taken into account. Meaning that the design will be launched in the right direction and that mountains and coast areas will be avoided. Even though the weather causes great risks for the mission, the mitigation is feasible. The weather is predicted precisely nowadays, resulting in the ability to allow for any unwanted circumstances.

[1] URL `https://climatedataguide.ucar.edu/climate-data/qbo-quasi-biennial-oscillation` [31 May 2016]

Chapter 6

Performance Analysis

This chapter contains the performance analysis of the design. The performance analysis is divided in six main sections: aerodynamics, stability and control, structures, flight mechanics, electronics and thermal control. Every section describes the approach taken for its analysis. The six engineering groups are all very dependent on each other, in one way they limit each other and in another way they allow each other for a better design. In the first section the aerodynamic approach is given, the second section elaborates on stability and control of the design. In the third section the structural analysis is explained with as follows the flight mechanics elaboration. Thereafter the electronics analysis is explained with in the last section an explanation of the thermal analysis.

6.1 Aerodynamics

In this section, the aerodynamic performance of the design will be analysed. Two methods are used for analysing the aerodynamic performance. The first method is for the subsonic performance and uses Computational Fluid Dynamics (CFD). The second method is used for transonic and supersonic analysis and contains information from literature.

6.1.1 Software

The program used for earlier aerodynamic analysis, SimFlow, proved to be adequate in earlier design stages. However, the program did not support a high number of mesh points and is as follows not sufficiently accurate. Therefore a different software is used for the aerodynamic analysis from now on. Fluent, a module of Ansys® allows for a more refined mesh and is capable of simulating accurate flows. The settings used for the analysis are presented below. First of all an explanation of the software used is given followed by the airfoil selection. In the next sections lift and drag are elaborated on. As follows the results of the aerodynamic analysis are given. This section ends with an elaboration on the different approach used.

Geometry and Meshing

The software allows for a .stp file (a 3D geometry file) to be imported. Since the simulation can be run with a symmetry plane, only half of the geometry is imported in order to increase the fineness of the mesh. First an enclosure is created around the model. Figure 6.1 shows the shape of the enclosure. The inlet is a sphere like shape, which is extended around the model. The program can easily change the direction of the flow in order to simulate different angles of attack, by changing the velocity components. This will not change the relative position of the model with respect to the enclosure, so it can be used for all simulations with a certain model.

The meshing is done automatically by the software. Sudden changes in geometry will make the mesh more refined. As can be seen in Figure 6.2, around the model the mesh is more refined compared to the rest of the enclosure. As stated before this mesh can be used for the analysis at different angles of attack, so no re-meshing is required. Only when starting with a new iteration, a new geometry and mesh has to be created.

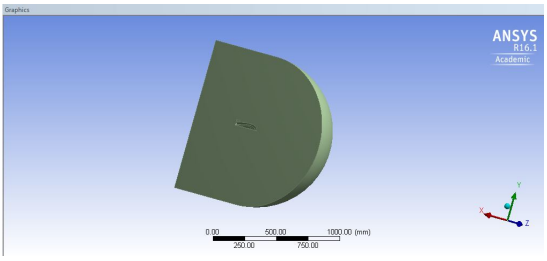

Figure 6.1: Shape of the enclosure in Ansys Fluent®.

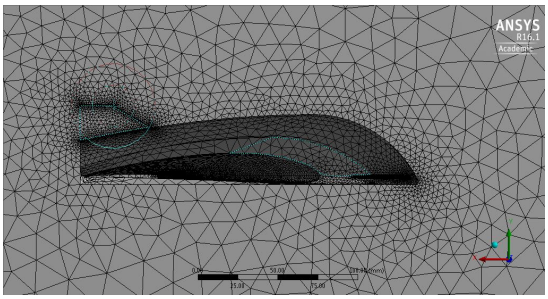

Figure 6.2: Mesh of the design in Ansys Fluent®.

Setup

After importing the geometry and creating the mesh, the setup for the simulation is chosen. The analysis is for compressible flow at subsonic flow conditions. The energy equation is enabled to account for compressibility. The k-omega-SST turbulence model is used. This model combines two models to be used for both low and high Reynolds numbers[7]. This model is capable of accurately simulating a turbulent flow that is close to the body of interest. The density is set to the one of a perfect gas, which means that the density is dependent on the pressure and temperature of the air. The flow conditions are given by Flight Mechanics engineering, that is the subsonic conditions as stated before. The flow conditions are defined using the boundary conditions, which will be elaborated on next.

Boundary Conditions

Boundary conditions are used to set the flow conditions. This means that all boundaries, except the symmetry plane and the model surface, are set to 'pressure far field'. Also, the Mach number and gauge pressure are set to the conditions that need to be analysed. The velocity components are set to the desired angle of attack. This use of boundary conditions makes sure that the Fluent® software simulates the model in a free stream compressible flow. Finally, the boundary condition for the model surface is set to 'wall', since it must be treated as a solid body. Also, the symmetry plane is set to symmetry.

Controls and Monitors

During the simulation, the lift and drag coefficients are monitored. In addition, the scaled residuals are monitored as well. Finally, the number of iterations are set to 150, to allow for the solution to converge. After the simulation, the lift-, drag- and moment coefficients are inspected and documented. Using the post-processing window, the solution can be visualised by means of gradients, streamlines and volume renderings of for example the pressure, velocity, Mach number, density and temperature. Inspecting these results can be used to visualise, for example, the stagnation points and the turbulent flow.

6.1.2 Airfoil selection

The aerodynamic performance is greatly influenced by the chosen airfoil. It is therefore of great importance to put effort into choosing the right airfoil. Airfoils have to be chosen for different parts of the design, which are the wings, the winglets and potential additional control surfaces.

Main Wing

The main function of the wings is to generate lift. However, since the vehicle has to operate in both supersonic and subsonic regimes, a selection for a single airfoil is not straightforward.

Looking at the flight path, which is elaborated on in Section 6.4, it can be concluded that during most of the mission the vehicle operates at subsonic speeds. Only during the pull-out a reasonable supersonic performance is desired. However, designing for both flight regimes will generate contradicting requirements for the shape

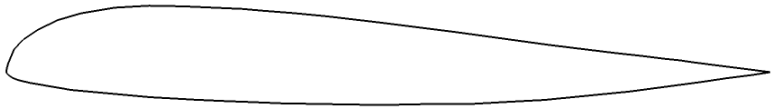

Figure 6.3: NACA-43012A airfoil for the main wing.

of the wings. For example, the airfoil will have to be thin to operate with low drag in supersonic speeds. On the other hand, for subsonic speeds, a thicker airfoil will generally have a better lift over drag ratio. According to Chapman[8], the shape of the airfoil in supersonic conditions mostly effects the drag force. However, this is not a major concern during the supersonic flight phase, since it is performing a pull-out. During this pull-out manoeuvre, slowing down is not a problem, as long as the lift is not influenced too much. Also, at higher C_L values, the volume component of the drag becomes less significant compared to the drag induced by the lift. During the pull-out, a relatively high C_L for supersonic speeds is desired. This means that a thin airfoil will lose on its performance, compared to a thick airfoil.

The lift over drag performance of supersonic airfoils is rather poor at subsonic speeds (≈ 7.5 at low α and ≈ 2 at high α) [9] and can only maintain a low drag coefficient at low angles of attack for supersonic speeds. Furthermore, a thin airfoil will stall at a lower angle of attack. Since the ICARUS+ will slow down during the gliding phase, the vehicle might not be able to generate the required lift anymore.

It can be reasoned that in order to find a compromise between sub- and supersonic performance, multiple airfoils can be incorporated in the wing. The effect of this is illustrated by comparing the lift performance of four wings. Two wings have complete subsonic airfoils, one wing has a subsonic airfoil up to halfway the half span where after the airfoil gradually changes to a supersonic airfoil at the tip. The last wing has a gradual change of airfoil from 1/3 to 2/3 of the half span. The subsonic airfoils that are used are the NACA-4412 and NACA-43012A, the supersonic airfoil that is used is the NACA-0006. The results of each wing are presented and discussed in section 8.1.

All considerations taken into account, it is decided to use a thick airfoil for the wing, designed to optimise the gliding part of the mission. For controllability considerations, a few additional requirements are set for the airfoil. C_{m_0} has to be larger than zero, where higher values are preferred. Also, the C_{L_α} value of the airfoil of the wing shall be higher than for the canard. The airfoil that is selected is shown in figure 6.3. The NACA-43012A airfoil has been designed for sailplanes and has an excellent gliding performance. In the figures below, the characteristics of this airfoil, as it has been taken from literature, is presented. In Figure 6.4, the lift and drag performance of the 2D airfoil is presented for low Reynolds numbers. In Figure 6.5, the characteristics at higher Reynolds numbers are shown. From the graphs it can be seen that the airfoil has a good performance at both high and low Reynolds numbers. Since the vehicle has to perform in a large range of velocities and thus Reynolds numbers, this performance is desirable. In addition it can be seen that the airfoil provides a high lift to drag ratio, which is desirable for an efficient gliding flight.

Control Surfaces

In order to provide stability during the pull-out and thus at supersonic speeds, a pair of canards is used. This surface has the main function to operate at these conditions and will therefore be optimised for supersonic flight. This can be done since elevons are used for subsonic control. The wing profile used has to provide enough lift to provide sufficient counter moment. Looking at fighter aircraft having canards as control surfaces, it can be seen that a biconvex airfoil is often used. Based on this observation, it has been decided to look at the performance of a biconvex airfoil with a maximum t/c of 8%, which can be seen in Figure 6.6. In Figure 6.7 and 6.8 the drag and normal force coefficients of the biconvex airfoil can be seen at subsonic conditions. It can be seen that the airfoil has a reasonable performance at subsonic speeds and can thus be used to control the vehicle during the gliding part of the mission. It can also be seen that the C_{l_α} is lower compared to the main wing airfoil, which is good for controllability.

In Figure 6.9 and 6.10 the pressure drag and lift coefficients of the biconvex airfoil at supersonic speeds are presented. This airfoil is capable of reaching sufficiently high lift coefficients at a low drag at supersonic speeds.

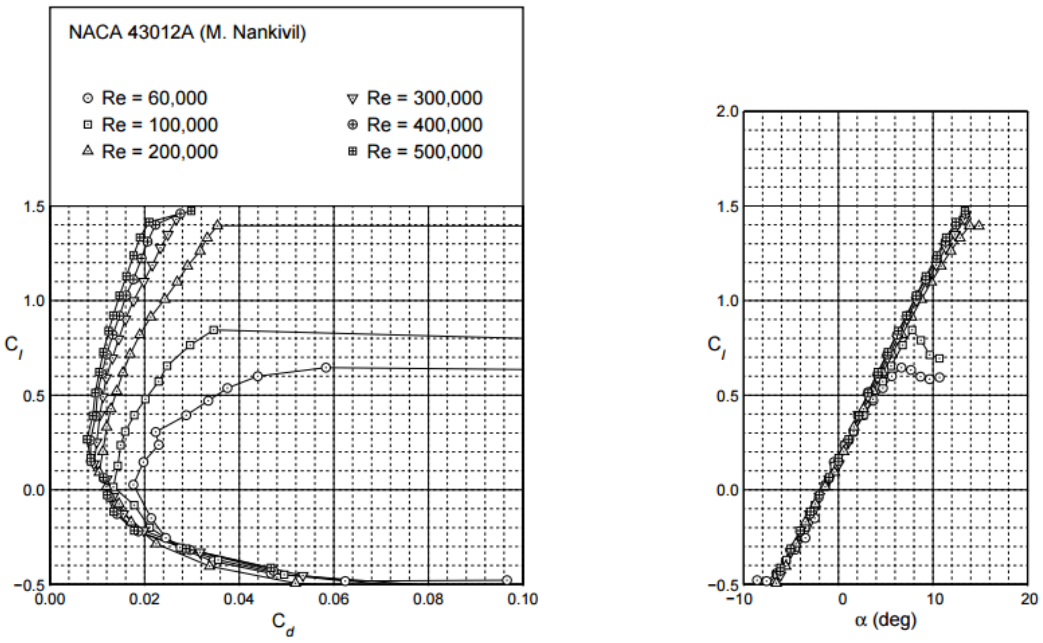

Figure 6.4: C_L - C_D and C_L - α curves for the NACA-43012A at low Reynolds numbers [10].

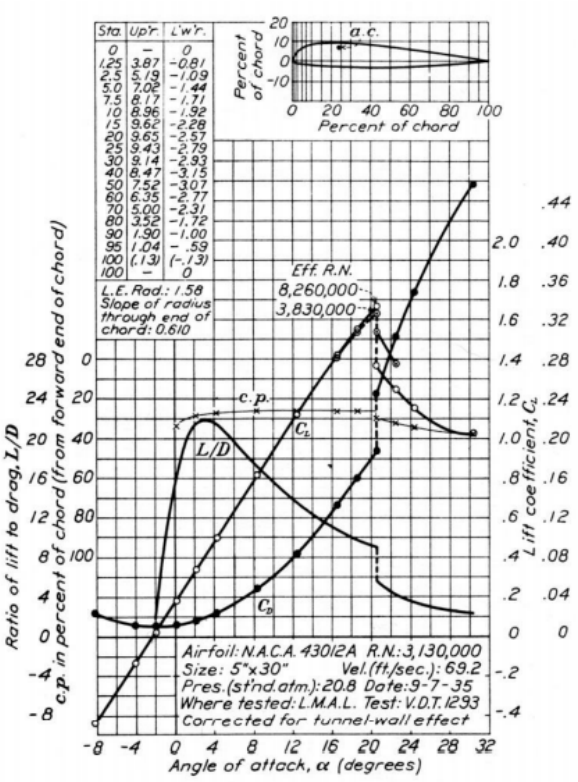

Figure 6.5: Various aerodynamic properties at different angles of attack for the NACA-43012A at high Reynolds numbers [11].

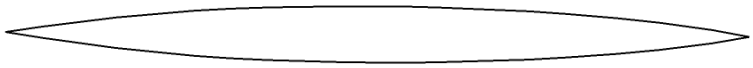

Figure 6.6: Biconvex 8% t/c airfoil for the canard.

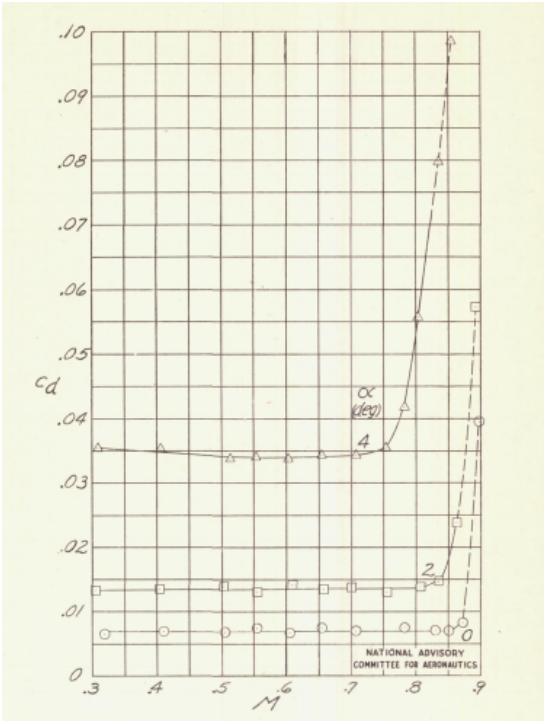

Figure 6.7: Drag coefficient for the biconvex 8% airfoil at subsonic speeds for a number of angles of attack [9].

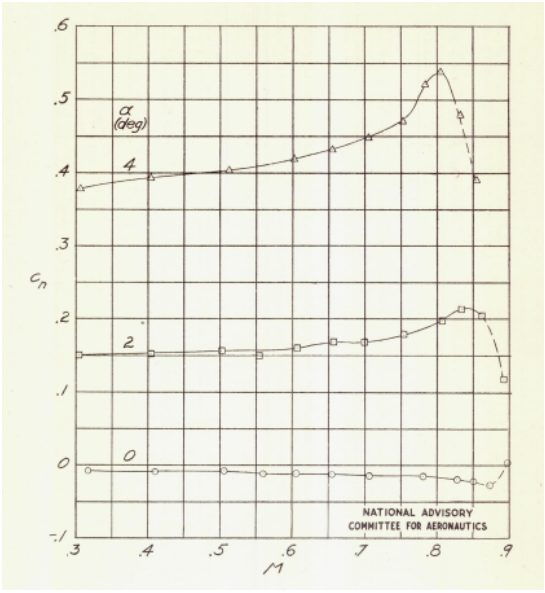

Figure 6.8: Normal coefficient for the biconvex 8% airfoil at subsonic speeds for a number of angles of attack [9].

Winglets

Winglets are widely used in commercial aircraft mainly to increase efficiency and thus range. Although, increasing the structural complexity, winglets reduce the induced drag and increase the effective aspect ratio. Winglets can also generate an additional thrust component. However, since commercial jets generally do not fly at supersonic speeds, it cannot easily be concluded that winglets are beneficial for the overall performance. According to Keenan [13], winglets on a low aspect ratio wing can be designed such that only a minor influence on the drag is present at supersonic speeds. These winglets have to be very small and will not have a large effect on subsonic performance. Based on the aforementioned and inspection of existing supersonic airplanes, it has been chosen to not implement winglets in the design.

Fuselage shape

Next to the wings, also the fuselage is important for the aerodynamic performance. The geometry of the fuselage is determined by combining engineering sense and literature. In Figure 6.11 the different drag coefficients found for different geometries are stated. When this is taken into account, it appears that a smooth shape is likely to perform better in sense of generating less drag than a rough shape.

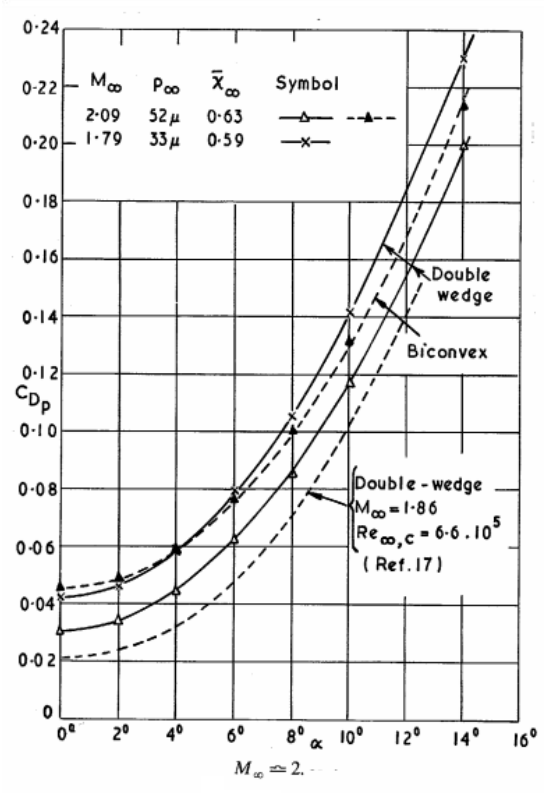

Figure 6.9: Pressure drag coefficient of the biconvex airfoil at number of Mach numbers at different angles of attack.[12]

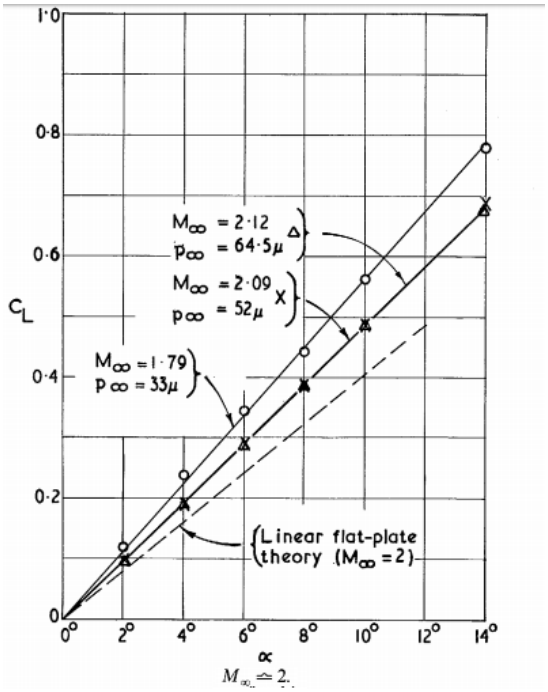

Figure 6.10: Lift coefficient of the biconvex airfoil at a number of Mach numbers at different angles of attack.[12]

6.1.3 Lift

For the determination of the performance, it is important to have a method that accurately estimates the lifting capabilities of the design. The software explained in Section 6.1.1 is used to determine the lifting characteristics of the design at subsonic speeds. An analysis at a number of angles of attack has been performed to create a $C_L - \alpha$ graph. The slope is corrected for subsonic compressible and supersonic conditions. For subsonic compressible conditions, the equation used is shown in Equation 6.1[1]. This is valid for Mach numbers between 0.3 and 0.8.

$$a = \frac{a_0 cos(\Lambda)}{\sqrt{1 - M^2 cos^2(\Lambda) + \left(\frac{a_0 cos(\Lambda)}{\pi A}\right)^2} + \frac{a_0 cos(\Lambda)}{\pi A}} \tag{6.1}$$

For supersonic conditions, the lift slope of an infinite swept back wing can be estimated using Equation 6.2. [14]

$$a_{\infty_c} = \frac{4 cos(\Lambda_{LE})}{\sqrt{M^2 cos^2(\Lambda_{LE}) - 1}} \tag{6.2}$$

This slope can be corrected for aspect ratio using Equation 6.3.

$$a_c = a_{\infty_c} \left(1 - \frac{1}{2A\sqrt{M^2 cos^2(\Lambda_{LE}) - 1}}\right) \tag{6.3}$$

[1]URL `http://www.srmuniv.ac.in/sites/default/files/downloads/class4-2012.pdf` [13 Jun 2016]
[1]URL `https://www.grc.nasa.gov/www/k-12/airplane/shaped.html` [13 Jun 2016]

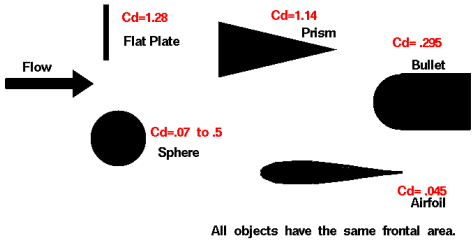

Figure 6.11: Drag coefficients for different geometries. [1]

These equations are valid for a Mach number above $sec(\Lambda_{LE})$ since the leading edge will still be within the Mach cone and therefore subsonic. Between Mach 0.8 and 1.15 (for $\Lambda_{LE} = 30°$), there is a transonic region where it is very hard to predict the lifting behaviour. Analytical models for analysing the lifting performance are not available at this time and is considered beyond the scope of this project. In Figure 6.12 the lift slope versus Mach number is presented for iteration four, and as can be seen, the transonic region is left out. The simulated lift slope is added as well. As can be seen, it is in accordance with the model. This model can be used to estimate the maximum lift coefficient, based on the angle of attack the vehicle can fly. An even better estimate can be made when the drag is known as well. A method for determining the drag is presented in the next section.

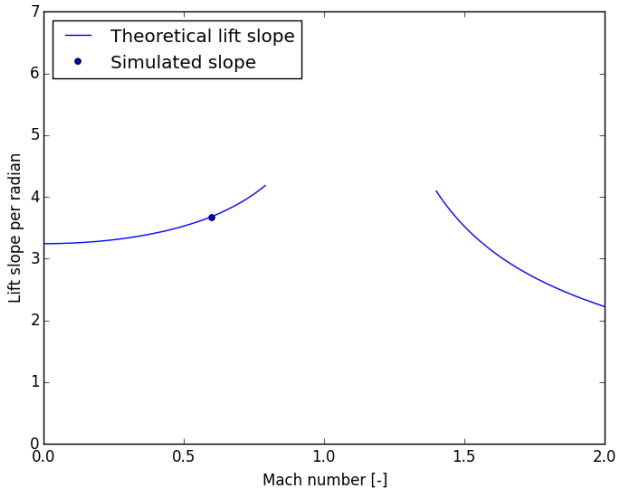

Figure 6.12: Lift slope at different Mach numbers.

6.1.4 Drag

Since the simulation method used is not accurate enough to define the drag coefficient in a reliable way, an estimation method has been used at different velocity regimes. This method gives an indication that is accurate enough for the applications that it is used for. The drag can be divided into a number of contributions. For subsonic conditions, the profile drag and induced drag can be identified. For trans- and supersonic conditions an additional wave drag component is added. This breakdown can be seen in Equation 6.4.

$$C_D = C_{D_p} + C_{D_i} + C_{D_w} \tag{6.4}$$

For calculating the profile drag, also known at parasitic drag, the following procedure can be used. [15] According to Equation 6.5, the parasitic drag can be calculated by summing the different drag components of the total vehicle. This has been split up into the wings, canards and the fuselage.

$$C_{D_p} = \sum k_i C_{f_i} \frac{S_{wet}}{S_{ref}} \tag{6.5}$$

Where k is the form factor, c_f is the friction coefficient and S_{wet} and S_{ref} are the wetted and reference surface respectively. The form factor can be estimated using reference data presented in Figures 6.13 and 6.14.

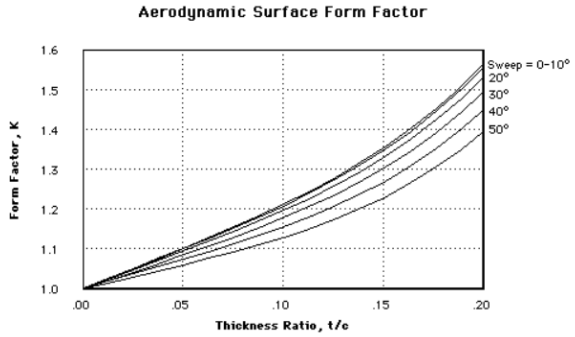

Figure 6.13: Form factor against thickness ratio for the wing and canards. [15].

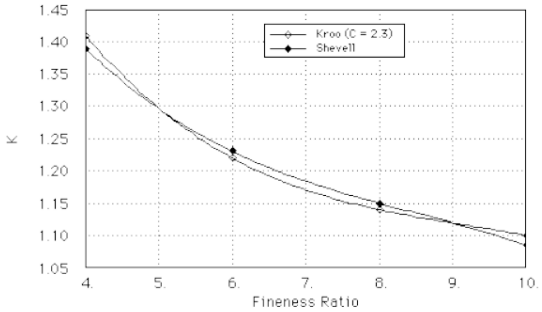

Figure 6.14: Form factor against fineness ratio for the fuselage. [15]

The friction coefficient can be calculated using Equation 6.6, according to the DATCOM [16] method that has been published in 1978. The friction coefficient depends on the Reynolds number and Mach number.

$$C_f = \frac{0.445}{\log(Re)^{2.58} \cdot (1+0.144M^2)^{0.65}} \tag{6.6}$$

Using the procedure explained above, Equation 6.5 can be used to determine the parasitic drag. The next step is to calculate the lift induced drag. This drag component can be calculated using the well known drag polar formula, as can be seen in Equation 6.7.

$$C_{D_i} = \frac{C_L^2}{\pi A e} \tag{6.7}$$

For the transonic regime, an additional wave drag component is added to the parasitic and lift induced drag. According to Vargas [17], the following method estimates accurate wave drag values for transonic speeds. First, the drag divergence Mach number, M_{dd}, is estimated for the wing.

$$M_{dd} = \frac{1}{\cos(\Lambda)} \left(\kappa_a - \frac{C_L}{10\cos^2(\Lambda)} - \frac{\left(\frac{\bar{t}}{c}\right)_w}{\cos(\Lambda)} \right) \tag{6.8}$$

Where M_{dd} is the drag divergence Mach number, κ_a is the technological factor (equal to 0.87 for conventional airfoils and 0.93 for supercritical airfoils [18]) and $\frac{\bar{t}}{c}_w$ is the average thickness over chord ratio of the wing. This has been converted to the critical mach number using Equation 6.9.

$$M_{crit} = M_{dd} - 0.108 \tag{6.9}$$

Finally, the drag coefficient can be calculated with Lock's fourth-power law [19], as stated in Equation 6.10. This component will be implemented up to a Mach number of 1.2, where after another model is used for the computation of wave drag.

$$C_{D_{trans}} = 20(M - M_{crit})^4 \tag{6.10}$$

The wave drag for speeds above Mach one can be split up into the wave drag due to volume and the wave drag due to lift. The latter can be calculated using Equation 6.11. This equation is valid for low aspect ratio wings and is in accordance with experimental data for a similar planform[1].

$$C_{D_{wl}} = \frac{\pi l^2}{16S} C_L^2 \left(\sqrt{1+(M^2-1)\left(\frac{4S}{\pi l^2}\right)^2} - 1 \right) \tag{6.11}$$

The volume wave drag can be estimated using Equations 6.12 to 6.14 [20]. These equations are based on the wave drag of ellipses with an equal area and length.

$$x = \frac{2}{\pi} \frac{\beta\left(\frac{b}{2}\right)}{l} \tag{6.12}$$

$$k_0 = \frac{2x^2+1}{(4x^2+1)^{3/2}} \tag{6.13}$$

$$C_{D_{wv}} = \frac{128}{\pi\left(\frac{b}{2}\right)} \frac{vol^2}{l^4} \cdot k_0 \tag{6.14}$$

Combining all drag components into one model results in a drag profile as shown in Figure 6.15. This is calculated at sea level at different C_L values, with a reference configuration of iteration three (Chapter 9). It must be noted that in order to smooth the curve, some corrections are applied to the transonic drag component, such that it reduces again after Mach 1. A drag rise can be observed at two places. First at very low Mach numbers. This is due to the parasitic drag dependence on Reynolds number, where a low velocity results in a low Reynolds number and thus a high parasitic drag (Equations 6.6 and 6.5). This behaviour is a well known and a studied phenomenon and mostly solved by just flying at higher Reynolds numbers. However, due to the small scale of the design and the high altitudes, and thus low densities, this cannot be achieved. The second drag rise is around Mach one and is a well known phenomena that is related to the sound barrier. As can be seen in Figure 6.15, this drag rise occurs earlier with a higher C_L. This could be expected from Equation 6.8. The maximum lift over drag ratio can be determined at different Mach numbers, using this model combined with the information from the lift model and simulated data.

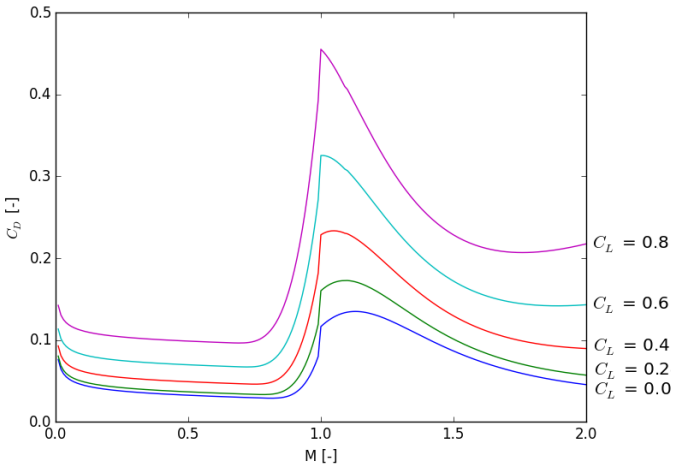

Figure 6.15: Total drag versus Mach number for different C_L values at sea level.

6.1.5 Results

In this section, the results of the Aerodynamic analysis are shown. A $C_L - \alpha$ graph and a $C_M - \alpha$ graph are presented in Figure 6.16. In the $C_L - \alpha$ graph, the four curves of the four iterations are presented. It can be seen that the lines of iteration one and iteration two produce more lift at low angles of attack, but due to the fact that the C_{L_α} of iteration three was bigger, this one would have the best C_{Lmax}. However, since the planform between iteration three and four has changed, the lifting performance of iteration four compared with three is slightly reduced. Nevertheless, the $C_M - \alpha$ graph shows also the curves for all four iterations. It can be seen, that the slope

[1] URL `http://mail.tku.edu.tw/095980/drag.pdf` [13 Jun 2016]

of iteration three is positive, while the slope of iteration four is negative. In order to be stable, the slope should be negative. Therefore, it is decided to keep the planform of iteration four, although the lifting performance is worse.

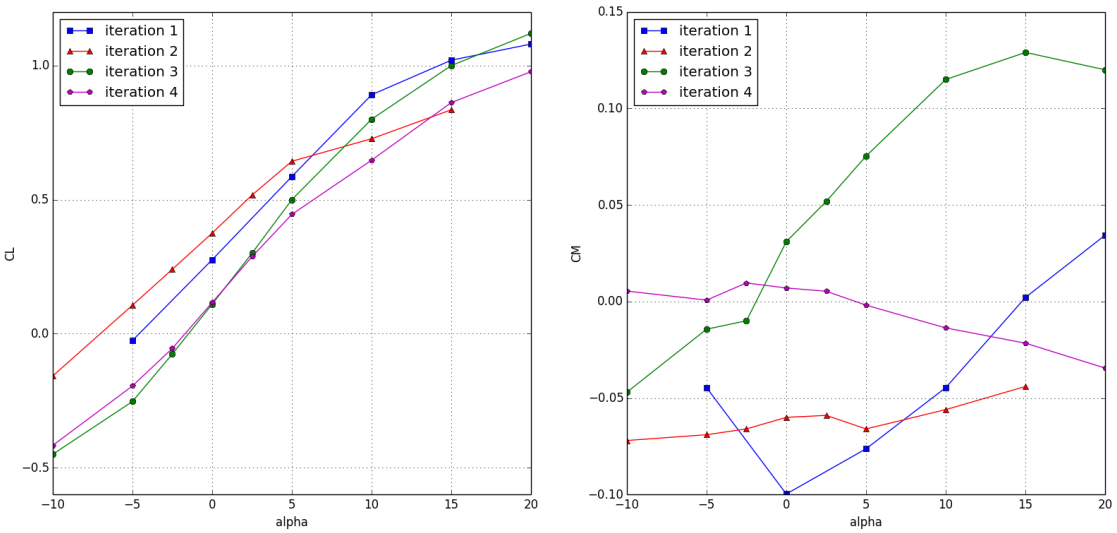

Figure 6.16: $C_L - \alpha$ and $C_M - \alpha$ graphs of the Aerodynamic performance(M = 0.6, Re = 52867).

In Figure 6.17 the $C_D - \alpha$ and the $C_L - C_D$ curves can be seen. While iteration four was not the best regarding lift, due to the choice of airfoil rather on the $C_{M_{ac}}$ than the C_L, the $C_D - \alpha$ performance of iteration four is the best compared with the other iterations. The $C_L - C_D$ curves are not very distinguishable from each other, but it seems that iteration four has also the best C_L over C_D ratio of the iterations.

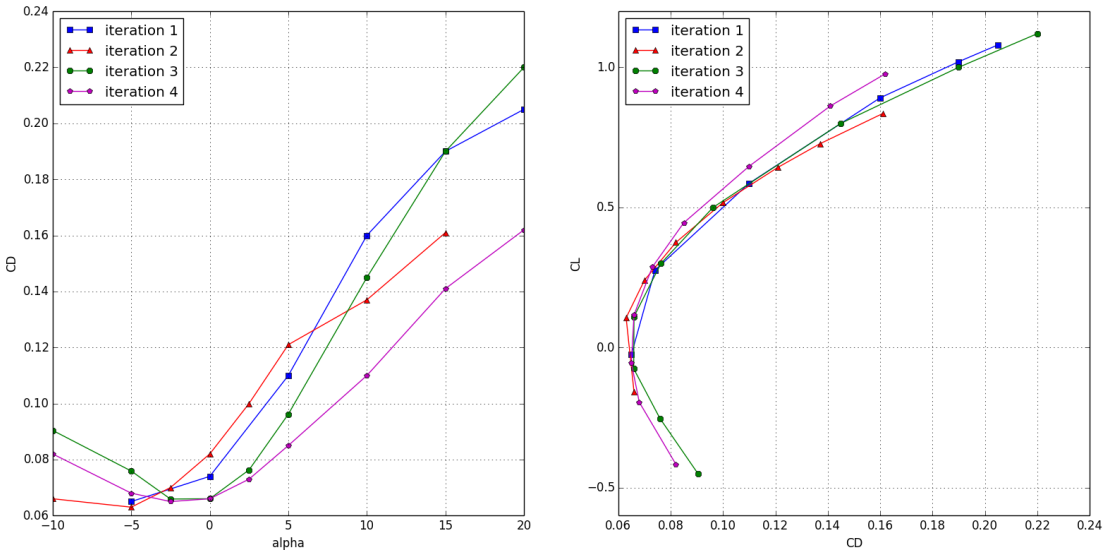

Figure 6.17: $C_D - \alpha$ and $C_L - C_D$ graphs of the Aerodynamic performance(M = 0.6, Re = 52867).

6.1.6 Method changes

In between iteration two and iteration three, the group discovered that CFD could not be used for transonic and supersonic flight regimes. This has as effect that the method to analyse the design in these regimes has changed from doing a CFD simulation, to a literature study. Futhermore it is chosen not to combine two

different airfoils anymore. Combining two airfoils would make the literature study too complex. Also, according to Chapman [8], a supersonic airfoil has only better drag performance in supersonic regime than a subsonic airfoil has in the supersonic regime. However, since the supersonic part of the trajectory is during the free fall phase of the ICARUS+, it does not matter how much drag is generated. Therefore it is recommended to use a subsonic airfoil for the next iteration.

6.2 Stability and Control

Since the goal of the design is to maximise range while having controlled flight, it is very important that the deployed aircraft is stable and controllable during flight. These two concepts can be defined as follows. First, stability is defined as the tendency of the aircraft to go back to its original position once a disturbance occurs. Controllability on the other hand, refers to how easy an aircraft is displaced after a control input from the pilot. In this section, the effect of control surfaces and the possible solutions, the stability and controllability during flight and the stability after deployment are explained.

6.2.1 Planform and Control Surfaces

According to the stability and control performance of the ICARUS+ a suitable planform is chosen for the wing. The decision for the planform is limited by the structural analysis of the model: for example, a control surface over the entire wing span is not possible, since there are already hinges needed to unfold the wings. The wing would then turn out to be too complicated. In this section, the planform of the ICARUS+ is discussed. First of all, the overall wing lay-out is elaborated. Secondly, the canard is discussed, followed by the elaboration on elevons.

Wing

A couple of parameters are important for the wing planform. These are first of all the surface area and the span, which lead to the aspect ratio. Other parameters are the tip- and root chord, the sweep angle and the taper ratio, which affect each other. As shown in Chapter 4, the initial planform is a delta wing planform with one sweep angle. Furthermore, wing tips are mounted on the wing tips to give an effective increase of the aspect ratio.

The selected delta wing planform has a couple of advantages. The first one is a larger stall angle due to to a phenomenon called vortex lift: a vortex is stuck on the upper part of the wing at high angles of attack and the airflow will as follows detach from the wing at even higher angles of attack. This is because the airflow is being sucked down by the vortex to the upper wing surface.[1]Secondly, the sweep of a delta wing delays the supersonic speed regime over the wing, that is the critical Mach number increases. As follows, drag is reduced for this Mach number [21]. Finally, a sweep angle improves the lateral stability by affecting stability derivatives, such as C_{l_β} and C_{n_β}. However, the main disadvantage is that delta wings only perform very good transonic and supersonic and lack good subsonic performance.

Some important considerations in the planform design come from the Structures and Flight Mechanics division. This is since it is beneficial for gliding performance to have a large aspect ratio. Thus a large span or a small surface area is desired. However, since the ICARUS+ must fit inside the box from which it is deployed, the span is limited. On the other hand, the surface area needs to be large enough to carry the aircraft with the selected airfoil. The aircraft cannot fly at a C_L value that is higher than $C_{L,max}$ and it is desired to glide at a maximum value of $\frac{C_L}{C_D}$.

Another configuration is evaluated as well: double sweep angles. Applying a second sweep angle can increase or decrease the wing surface, depending on whether the second sweep angle is smaller or larger than the first one. Applying this sweep angle has multiple effects. Assume for this explanation that the wing surface area is decreased due to a larger sweep on the inboard, $\Lambda_{new,1}$ and a smaller sweep on the outboard section, $\Lambda_{new,2}$, see Figure 6.18.

This change in the planform has the following consequences. First of all, the centre of gravity shifts backwards due to the removed area. This increases the tail arm, which is positive for trimming the aircraft. The negative consequence is that the aircraft will become less stable. This will be explained more thoroughly in Section 6.2.2. It is thus a trade off between a stable and a trimmable aircraft. A second consequence is that the surface area

[1]URL `http://adg.stanford.edu/aa241/highlift/sstclmax.html` [14 Jun 2016]

becomes smaller and thus the aspect ratio becomes larger. Finally, the vortex lift becomes more controlled with a double sweep, which also increases drag at low velocities. [1]

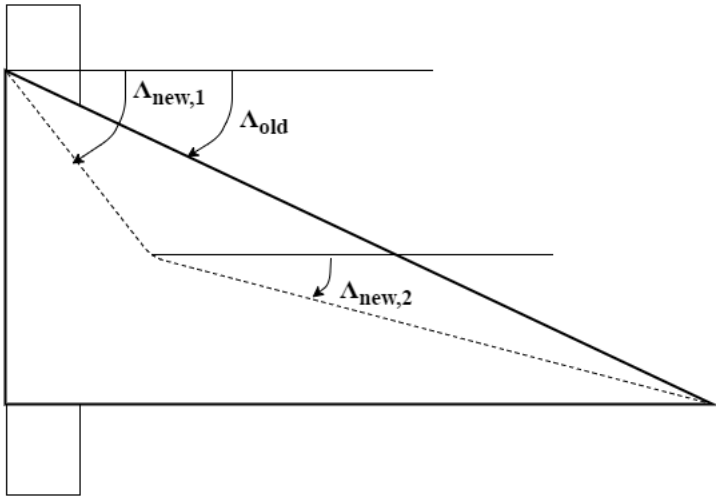

Figure 6.18: Double- and single sweep on a wing planform.

Canard

During the design process, the option of a canard surface is explored. Generally, a canard decreases the stability performance of an aircraft, since it has a positive C_{m_α}-curve. However, it does have a beneficial effect on the controllability of an aircraft, since the pitch-up moment generated by the canard can counter the pitch-down moment caused by the wing. In order to provide lateral control at supersonic velocities, the canards will be able to move independent from each other. This way they can introduce a rolling moment on the aircraft. In order to make this possible, two servos are needed to activate the canard. It is however important to check whether the selected servos can generate the torque needed for deflecting the panels.

The hinge moment on the canard surface is calculated using Equation 6.15. In this equation, $H_{c,max}$ is the maximum hinge moment on the canard, $C_{L_{c,max}}$ is the maximum lift coefficient of the canard and $z_{hingeline}$ and z_{ac_c} are the longitudinal positions of the hinge and the aerodynamic centre of the canard, respectively. This equation is used since the canard airfoil is symmetric and the moment in the hinge is assumed to be caused solely by the change in lift and the distance between the aerodynamic centre and the hinge line of the canard. This might be adapted if the arms of the servo and the axis are different, but for a start they are assumed to have the same size. Since this calculation is quite general, a relatively large safety factor of three is used to guarantee that the servo is suitable. Figure 6.19 provides an illustration of the actuation mechanism of the canard.

$$H_{c,max} = C_{L_{max,c}} \frac{1}{2} \rho V^2 S_c (z_{ac_c} - z_{hingeline}) \tag{6.15}$$

Elevons

The choice for elevons is based on the need for lateral and longitudinal control. By moving the elevons separately, yaw and roll motion can be obtained. By moving both of the elevons with the same angle at the same time, a pitch moment can be created. Sizing for these elevons is done with Equation 6.16 [21]. Constraints on the elevon sizing are given by the Structures department: due to the hinge lines in the wing, which are needed to fold and deploy the ICARUS+ into a 2U box, the size of the elevons is limited. The wing structure would be too complicated if the elevons have to pass such a hinge line. Furthermore, if the elevon wiring has to pass several hinge lines, the electrical structure would be too complicated. As follows the elevons are placed between the fuselage and the first hinge line over the full length in between. The maximum change in lift

[1] URL `http://www.456fis.org/THE_DELTA_WING.htm` [15 Jun 2016]

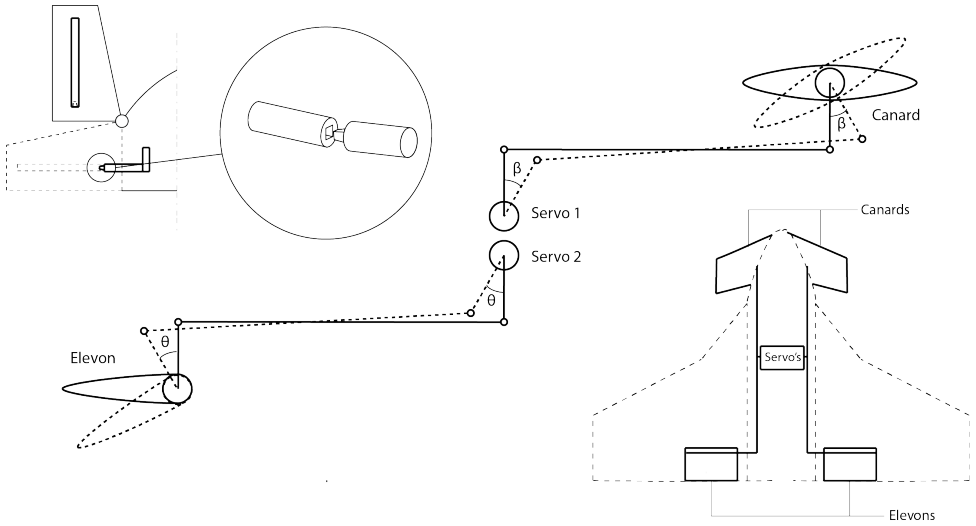

Figure 6.19: Schematic drawing of the canard and elevon actuating mechanism.

coefficient created by fully deploying the elevons can be calculated using Equation 6.16. In this equation, S_{wf} is the wing area over the span length where the control surfaces are located.

$$\Delta C_{L_{max}} = 0.9 \Delta C_{l_{max}} \frac{S_{wf}}{S} \cos\Lambda_{hinge-line} \tag{6.16}$$

Just as for the canard, it should be investigated whether the servos are suitable for carrying the hinge moment. The maximum hinge moment on the elevon is estimated with Equation 6.17[22]. In this equation C_{H_δ} is the hinge moment coefficient derivative of the elevator deflection and $\delta_{e,max}$ is the maximum elevon deflection. Furthermore, S_e and $\bar{c_e}$ are the surface area and the Mean Aerodynamic Chord of the part of the elevon behind the hinge axis. The hinge moment coefficient is estimated from literature [23], where it is checked for Mach- and Reynolds number [24]. Then, maximum elevator deflection angles of 20 ° and -20 ° are assumed and a safety margin of three is used again. In Figure 6.19 the actuation mechanism for the elevon is shown. The mechanism has to pass through the hinge, this introduces some complications. This is solved by separating the rod at the hinge, and letting it reconnect when unfolded.

$$H_{e,max} = C_{H_\delta} \delta_{e,max} \frac{1}{2} \rho V^2 S_e \cdot \bar{c_e} \tag{6.17}$$

6.2.2 Flight Stability and Control

During the mission the design will fly in various flight conditions and regimes. It is important that the aircraft, when deployed, is able to be controlled (trimmed) and that it is stable. Since stability and controllability limit each other - a very stable aircraft is not easily controlled - an optimum needs be found in order to produce a suitable design. The method to do so is explained in this section.

Figure 6.20 shows a representation of the forces and moments acting on a conventional aircraft. With this figure, both the criteria for stability as for controllability can be determined. It should however be noted that the design will be a canard aircraft, which is different from Figure 6.20. However, the only thing that will really change is the sign of the tail length l_c, which is the length between the two aerodynamic centres.

6.2.3 Longitudinal Stability

In order to guarantee static longitudinal stability the centre of gravity needs to lie in front of the neutral point. The neutral point is defined as the point where a change of the lift force acts. If the centre of gravity lies before the neutral point an increase in angle of attack would result in an increase of the pitch up moment, meaning

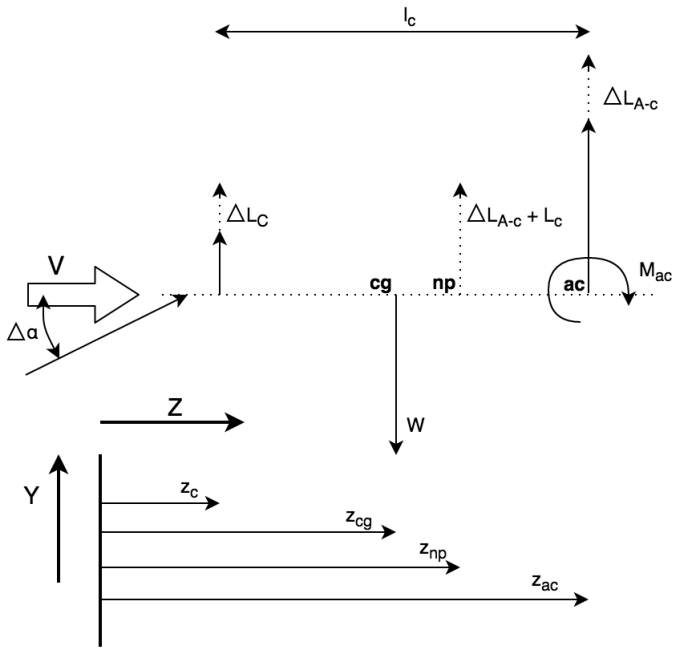

Figure 6.20: Schematic drawing of the forces and moments acting on a canard aircraft [25].

that the aircraft is statically unstable. The condition for longitudinal stability is represented by Equation 6.18. If the centre of gravity lies on the same location as the neutral point, the aircraft is neutrally stable and the inequality from Equation 6.18 becomes an equality.

$$\frac{dC_m}{d\alpha} = C_{m_\alpha} < 0 \tag{6.18}$$

The next step is substituting the forces and moments in this equation, which leads to Equation 6.19. When assuming that the canard length, l_c, can be approximated as done in Equation 6.20 and the equation is made dimensionless, it can be rewritten to Equation 6.21, which determines the location of the neutral point. In order to guarantee stability a safety margin of 5% [26] of the chord length is included, which is represented by Equation 6.22.

$$\Delta L_{A-c}(\bar{z_{np}} - \bar{z_{ac}}) - \Delta L_c(\bar{z_c} - \bar{z_{np}}) = 0 \tag{6.19}$$

$$z_h - z_{np} \cong l_c \tag{6.20}$$

$$\bar{z_{np}} = \bar{z_{ac}} + \frac{C_{L_{\alpha_c}}}{C_{L_{\alpha_{A-c}}}}(1 - \frac{d\epsilon}{d\alpha})\frac{S_c l_c}{S\bar{c}}(\frac{V_c}{V})^2 \tag{6.21}$$

$$x_{cg,\bar{stable}} = \bar{x_{ac}} + \frac{C_{L_{\alpha_c}}}{C_{L_{\alpha_{A-c}}}}(1 - \frac{d\epsilon}{d\alpha})\frac{S_c l_c}{S\bar{c}}(\frac{V_c}{V})^2 - S.M. \tag{6.22}$$

In these equations, the symbols mean the following. In Equation 6.19, L_{A-c} is the lift generated by the aircraft less canard and L_c is the lift generated by the canard; Δ indicates a change in lift. Furthermore, z_{np}, z_{ac}, z_c are the longitudinal locations of the neutral point, wing aerodynamic centre and tail aerodynamic centre, respectively. As was already the mentioned, l_c is the tail length. Then from Equation 6.21, $C_{L_{\alpha_c}}$ and $C_{L_{\alpha_{A-c}}}$ are the slopes of the lift curves of the canard and the wing. Values for these slopes can be estimated using

the DATCOM method [21] [27]. $\frac{d\epsilon}{d\alpha}$ is the downwash gradient for the wing and $(\frac{V_c}{V})^2$ is the canard velocity, which differs from the wing velocity due to perturbing effects of the fuselage [25]. Both these values are zero for a canard aircraft.

With these equations, a plot of $\frac{S_H}{S}$ versus the centre of gravity location can be made to find the stable centre of gravity location for a certain canard size. The line that is generated with this method indicates that a forward shifted centre of gravity leads to more stability. The other limit will be determined from the controllability analysis.

Controllability

In order to investigate the controllability, Figure 6.20 is used. The requirement for the controllability is that for every flight condition there should exist a combination of lift forces and moments that results in a total aerodynamic moment equal to zero. This is called trimming the aircraft. In order to check this, all moments will be evaluated. When looking at Figure 6.20, the big difference with the longitudinal stability is that the focus is now put on the actual moments instead of the changes in the moments. From Figure 6.20, Equation 6.23 can be set up. When these values are made dimensionless, an equation of the same form as Equation 6.22 is constructed, see Equation 6.24.

$$M_{ac}+L_{A-c}(x_{cg}-x_{ac})-L_c l_c=0 \tag{6.23}$$

$$\bar{x_{cg}}=\bar{x_{ac}}+\frac{C_{m_{ac}}}{C_{L_{A-c}}}+\frac{C_{L_c}}{C_{L_{A-c}}}\frac{S_c l_c}{S\bar{c}}(\frac{V_c}{V})^2 \tag{6.24}$$

In these equations, M_{ac} is the moment around the aerodynamic centre of the wing and $C_{m_{ac}}$ is the dimensionless coeficient for this moment.

This equation can be rewritten in the same way as was done for the stability equation, in order to generate a forward boundary for the centre of gravity location. This means that with these two curves, ideally, there is a range of the centre of gravity for which the system is both stable and controllable.

6.2.4 Free Fall Stability and Control

In this section, the self stabilising process will be elaborated. First of all, the model used for these calculations is explained. Afterwards, reaction wheels will be discussed, followed by the use of the control surfaces in the free fall phase.

It is necessary for the ICARUS+ that it can stabilise itself during the free fall phase, right after being released. The ICARUS+ will be released at a random orientation with a horizontal velocity and zero vertical velocity. First thoughts are that it will start tumbling and fall down in an arc. At a certain moment it needs to be orientated in such a way that it can start flying and it also needs to be stable at that moment. All possible orientations are taken into account and the most extreme is calculated with. Furthermore, also initial rotational velocities are taken into account to a certain extend. Afterwards, it is seen as a risk, as stated in Chapter 16. In agreement with the Flight Mechanics department, a stability height of 40 km is aimed for. Above that altitude flying will not add any range due to the low density. This decision was made by running the Flight Mechanics model several times at different starting altitudes with their velocities and location at that moment and comparing outputs.

Model

To get some insights of what would happen to the payload if it was simply dropped, a model has been made. This model assumes the initial conditions stated in Table 6.1. In Appendix C, the functional flow diagram of the stability and control model can be seen. In the model, the forces the payload is objected to are calculated and translated into three moments. One moment around each axis, located at the centre of gravity. These can as follows be translated into accelerations around each axis, which will result into a three dimensional

orientation. By plotting the results, it can be seen that the payload will oscillate as it falls down. The period and amplitude of the oscillation both get smaller with time, until at a certain moment the period is that small that for an actual object it would be impossible to move like that, but a computer is still able to calculate those values. At that time the payload is assumed to be stable. The flight path conditions at that moment are given to the Flight Mechanics group and as follows, the entire flight path can be given (Section 6.4).

Parameter	Value
h [m]	60000
V_{hor} [m/s]	94
V_{ver} [m/s]	0
ψ [rad]	$0-\pi$
θ [rad]	$0-\pi$
ϕ [rad]	$0-\pi$
p,q,r [rad/s]	<1

Table 6.1: Initial Parameters

Reaction Wheels

After previous calculations, it was recommended that reaction wheels have to be used to stabilise itself. By doing a literature study on reaction wheels, it was found that the smallest reaction wheels that would actually have a stabilising effect are too large to fit within the ICARUS+. However, they can be fitted into the box the payload is in, during its way up in the Lynx. The payload will then be released and stabilise itself in the box, and only when it is stable, the ICARUS+ would be released from the box. However this approach has two major disadvantages: the box needs a power supply and the payload would destabilise all over by deploying from the box. Therefore, reaction wheels are not a suitable option and they are not added to the design.

Control surfaces

Since reaction wheels cannot be used, the payload should be able to stabilise itself by using its elevons and canard. The change in lift coefficient, by fully deploying the control surfaces, is calculated in the previous section. This can be translated to moment coefficients. These moments will however be small at high altitudes due to the low density, but so are all the other forces acting on the ICARUS+ at those altitudes. By applying these moments in the model, it can be seen that they have a considerable influence on the stability. The maximum moment is able to create an angular acceleration in the opposite direction, so by applying optimised inputs from the control surfaces, in such a way that finally the resulting moment due to all forces is zero, the ICARUS+ can be stabilised. Up to a certain initial rotational velocity, the payload can be stabilised before it reaches a height of 40 km. The oscillation can be stopped by using the control surfaces before reaching 40 km. Therefore, the requirement of a 40 km stability height is met.

6.3 Structures

In order to perform the structural analysis of the design, different fields of interest have been identified. First, the loads during launch are examined. Next, a close look is taken into the folding mechanisms used for the design, which includes an analysis of the hinges. After this, the flight loads are examined. Finally, a material selection is made and elaborated on.

6.3.1 Launch Survivability

During launch, the payload will be subjected to different loads than during its flight after deployment. During launch, nearly constant acceleration is introduced, which is expressed in gravitational forces. The maximum acceleration that the design must be able to endure is a 9g force. Next to this load, random vibrations will occur. It is of great importance that the structure will be able to handle those loads.

In order to predict the influence of the loading during launch, Coupled Load Analyses (CLA) is performed. This approach uses the mathematical model of the spacecraft and launcher combined to calculate the internal forces, displacements and accelerations. The launch vehicle and the payload can be represented as a spring-damper system as shown in Figure 6.21. The method makes use of the Miles equation, shown in Equation 6.25, and is a simplified procedure to calculate the response of a single degree of freedom system to a random vibration base input. The input consists of the Power Spectral Density (PSD) from the launch vehicle, expressed in $g^2 \cdot Hz^{-1}$. As an output, the acceleration of the spacecraft is given expressed in terms of the gravitational constant g. f_n represents the natural frequency of the design and will be simulated using Ansys®. Finally, the damping factor is given by ξ. For now, it is assumed that the design is critically damped and therefore this value equals one.

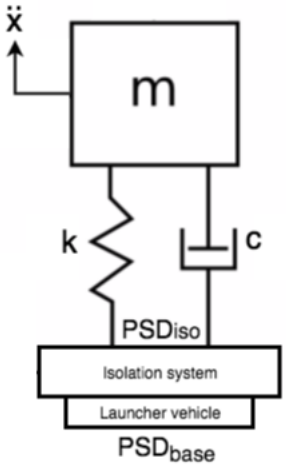

Figure 6.21: Spring damper system used for the prediction of launch loads.

$$\ddot{x}_{GRMS} = \sqrt{\frac{\pi}{2} \cdot PSD_{ISO} \cdot f_n \cdot \frac{1}{2\xi}} \tag{6.25}$$

$$PSD_{ISO} = T^2 \cdot PSD_{BASE} \tag{6.26}$$

The absence of the PSD values from the launch vehicle in early design stages can make it difficult to determine the launch loads. Since it is not desirable to over-design the spacecraft for this reason, another solution is found. By placing an isolation system in between the launch vehicle and spacecraft, the PSD value can be changed with the use of Equation 6.26. An example of such an isolation system is SoftRide®[1]. This method reduces the launch vehicle loading by decreasing the amplitude of the response of the payload. Different isolation systems can be chosen for the design with varying transmissibility factors (T). Since most of the isolation systems can be added to the design in later design phases, the design will be able to withstand different loads for different launch vehicles. In this way the flightpath loading can be the focus instead of the launch survivability. In the end, this will result in a fail safe design during launch, weight reduction and a design that can handle the deflections during launch without yielding. Next to this, the design has an increased operationally responsiveness, since other launch vehicles might be used as well. There will also be a slight risk reduction, because of the increased margins for the design. However, the isolation systems must probably be designed specifically for this design, since all the COTS products are meant for bigger spacecraft. This may result in increased costs for the development of this design and should be elaborated on when the total costs are analysed.

With the use of an isolation system, the value for $\ddot{x}_{GMRS}$ can be greatly reduced into a desirable value. Consequently, the vibrational loading during launch will not cause the design to fail. To perform the total analysis of the launch loads, the 9g force should be analysed too. This is done with the use of the simulation program Ansys®. The maximum stresses should not exceed the optimum loading values from the design. This mainly depends on the chosen material, which will be analysed later in this section.

[1]URL `http://digitalcommons.usu.edu/cgi/viewcontent.cgi?article=1316&context=smallsat` [31 May 2016]

6.3.2 Deployment

After launch the design will be deployed. As stated before, it is fitted within a 2U box. In the first stage of deployment, this box has to be ejected from the Lynx. A mechanism for this stage is built in the Lynx itself. When the 2U box left the Lynx, the design should be released. This is done by means of a special release mechanism, explained below. First, the general dimensions of the box are elaborated on.

2U Box

The box is initially the interface between the ICARUS+ and the launch vehicle. It can protect the design from yielding if needed. When the box is deployed, it should be able to release the design. The box is open at one side, which is the small side at the nose of the ICARUS+. From this side the design can leave the box.

The box has some special requirements which are set by XCOR and can be found in Chapter 4. Taking all the requirements into account, the following specifications regarding the 2U box can be stated. The dimensions are 10x10x22 cm and every corner contains a rail of 8x8 mm with 1 mm diameter rounded edges. The rails are made out of Aluminium 7075. The properties of this material can be found in Section 6.3.5. Additionally to those characteristics, the surface roughness of the material is less than 1.6 $\mu{\cdot}m$ when polishing is used during manufacturing. The rails are 100% in contact with the P-POD rails. The box itself is made out of 0.5 mm thick titanium sheets. The same titanium is used as for a big part of the design. This is further explained in Section 6.3.5.

Finally, the design must be connected with the Lynx. This connector is placed in the middle of the back of the box and is placed under an angle of 45°. The joining point of the ICARUS+ is place in the back of the design. However, this cannot be directly connected with the Lynx. Therefore, an extra connection bridge is place in between those two connection points.

Taking all the materials and dimensions into account, the total weight is calculated to be 0.375 kg. This also includes the weight of the rails. All restrictions caused by the carrying box are taking into account during all the design phases of the ICARUS+.

Release Mechanism

Since the design is too big to fit into the box in its final shape, a hinge system is used to fold the design. After the design is released from the box, it should unfold into its final shape. To make sure the design leaves the box out of the opening, a small initial force should be provided. Fortunately, this mechanism can be combined with another deployment mechanism. Namely, the deployment of the UHF antenna. This antenna needs to be outside the titanium shell of the fuselage and should therefore have a release mechanism too. This is done by means of a spring. The force created by this will also be used to push the design away from the box.

In Figure 6.22 a sketch of the mechanism is shown, in both before (1) and after (2) deployment configuration. It consists of a spring and the antenna, attached with a spring washer. Before deployment, the spring is loaded in compression and hold by a Dyneema® wire. A resistor, which is located in the washer, will cut this wire when a current is applied. Moreover this resistor can be found in Section 6.5.2. All the components of the mechanism are elaborated on in the following paragraphs.

The material chosen for the spring is Phosphor Bronze Grd A B159. A few characteristics of this material are shown in Table 6.2. This material is chosen for its non magnetic and relatively stiff behaviour. Another advantage is that it is very cheap. A proper custom made spring, with closed and squared ends, is found for this design. A few properties of the chosen spring can be found in Table 6.3

Table 6.2: Characteristics of phosphor bronze.

	E $[GPa]$	G $[GPa]$	ρ $[kg{\cdot}m^{-3}]$	T_{max} $[K]$
Phosphor Bronze Grd A B159	103	43.4	8860	225

Using those properties the force applied by the spring can be calculated with the use of Equation 6.27. [1]

[1] URL `http://www.acxesspring.com/spring-constant-calculator.html` [7 Jun 2016]

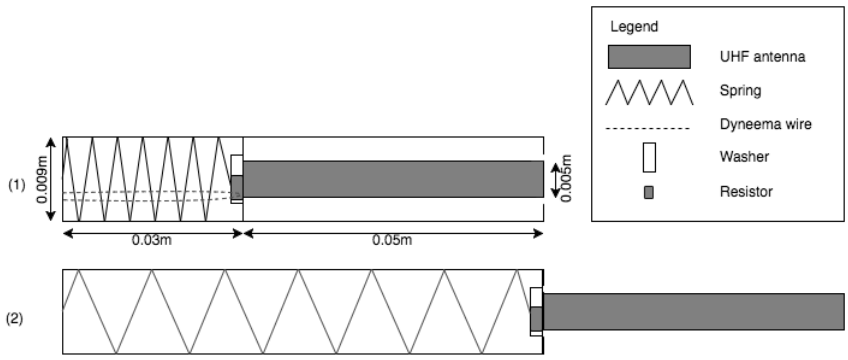

Figure 6.22: Deployment mechanism for the UHF antenna.

Table 6.3: Spring properties. [1]

	L_{free} $[mm]$	N_a [-]	D_{outer} $[mm]$	d_{wire} $[mm]$
Spring A C1500-9000-12.000-PB-80.000-C-N-MM	100	10	9	1.5

$$k = \frac{F}{x} = \frac{G d_{wire}^4}{8 D_{outer}^3 N_a} \tag{6.27}$$

The spring constant is represented by k and x represents the displacement of the spring relative to its free length. With a free length (L_{free}) of 100 mm, this displacement equals 0.07 m before deployment and 0.02 m after deployment. D_{outer} and d_{wire} are the outer diameter and the wire thickness of the spring respectively. G is the shear modulus of the material and finally N_a is the number of active coils. With the use of this equation, it is calculated that k equals 6512 $N \cdot m^{-1}$. Using this value it is found that the spring exerts a force on the antenna of 455.84 N before deployment and 130.24 N after deployment. This implies that the spring is slightly over designed. This is done for safety reasons.

The spring is hold by a wire made of Dyneema®. This material has its melting point at 424 K. The minimum available thickness is 6 mm and can hold forces up to 41.2 kN. The spring will never exert forces higher than this limit, which makes Dyneema® a proper material for the wire design.[2]

With this design, the only risk that may be present is that the spring can buckle during compression. To fix this problem the spring can be placed over a shaft, the wire diameter can be increased or the free length can be shortened. The decision to make one of those adjustments should be made after more test are done regarding this design.

6.3.3 Hinge Design

As is mentioned in the previous parts of this section, the design is deployed from a 2U box to guarantee structural stability and provide proper guidance during deployment from the Lynx spacecraft. To create a controllable and flying design undergoing these flight conditions, which fits in this small box, the design must be folded. In Figure 6.24a half of the the folded design can be seen as it would fit in the 2U box.

The design is placed in the box such that the fuselage is orientated straight with respect to the longest direction of the box. This is required to create enough space for all components which must be taken along. In order to obtain a surface area which generates enough lift and has an aspect ratio which is relatively high for good gliding performance, both wings are folded three times. For an effective use of space due to large folding angles, aerodynamic efficiency and optimal unfolding properties a double hinge as can be seen in Figure 6.23, was used at all folding lines.

[1] URL `https://www3.nd.edu/~manufact/FME_pdf_files/FME3_Ch17.pdf` [7 Jun 2016]

[2] URL `http://www.gvanderlee.com/_asset/_public/Hendrik-Veder-Group/Discover-the-power-of-Dyneema-based-ropes.pdf` [7 Jun 2016]

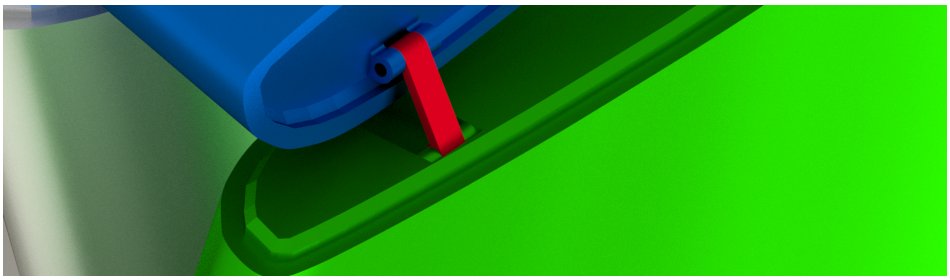

Figure 6.23: Wing box with double axes hinge.

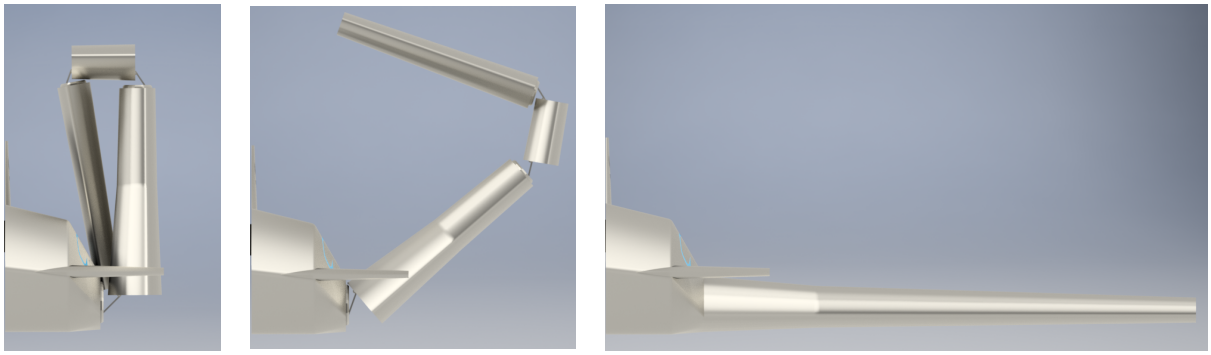

(a) Folded. (b) Unfolding. (c) Deployed.

Figure 6.24: Wing unfolding stages.

The double hinge consists of two rotation axes which both contain a spiral spring to initiate and guide the unfolding. Due to the distance between these two axes, the wing segments can make an angle of more than 90 degrees with respect to each other. This allows a broader range in angles and therefore gives more flexibility in folding options. This comes down to an increase in aspect ratio throughout the iterations in the design optimisation stage. The distance between these axes also comes along with a restriction. The minimum airfoil thickness is required to conserve a producible hinge design. This thickness at the folding line came along with a required chord of 52 mm.

The aerodynamic advantage of this hinge is obtained by the fact that the hinge is completely put away in the wing itself once the ICARUS+ is fully deployed as can be seen in the last stage of the hinge folding in Figure 6.24c. This reduces unnecessary drag by having the hinge axes outside the wing.

Another major advantage of this hinge are the unfolding properties. The progress of the unfolding hinge can be seen in Figure 6.24. As can be seen in the late stages of the unfolding the approach at the end is almost straight compared with a normal axis hinge. This allows the different segments to fold into each other with less required margin. The design its inner and outer parts will fit more tightly and therefore be able to carry the loads better.

Once the design is unfolded, rigidity must be guaranteed. The spiral springs are able to unfold the wings at high altitude where the air is very thin and the wings are not carrying any loads yet. However the springs do not create the required stiffness and strength to the wing at lower altitudes during flight. To carry the shear loads a mechanism of a smaller wing box folding in the bigger wing segment as shown in Figure 6.23 is used. But this does not deliver normal force carrying components. For that a clamping system is used. A pin at one of the wing segments will enter a slot at the other wing segment during the unfolding. A mechanism in the entered wing will clamp the pin to provide fixation. As for this clamping system two designs have been created focusing on the complexity in combination with the small size of the clamping systems. Both designs came out as feasible but require a more elaborate investigation to select the optimal clamping system. The clamping process of the two systems can be seen in Figure 6.25.

The design in combination with the clamping system seems fairly complex which is always bad regarding failure probability. However due to the double axis hinge for which the spiral springs initiate the unfolding motion, the hinge will endeavour towards its neutral position which is fully folded. Due to the two springs

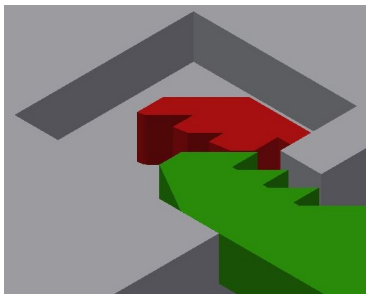

(a) Tie wrap system progress stage 1.

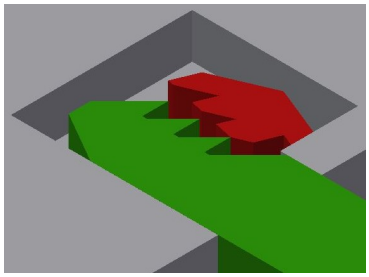

(b) Tie wrap system progress stage 2.

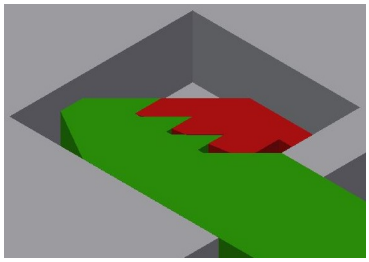

(c) Tie wrap system progress stage 3.

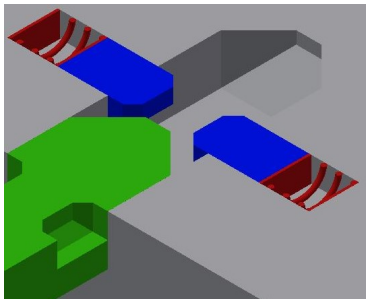

(d) Spring click system progress stage 1.

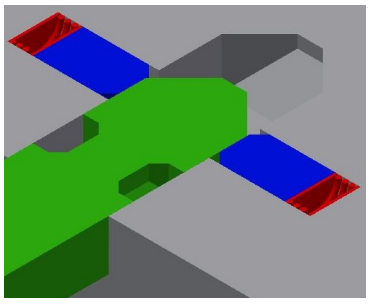

(e) Spring click system progress stage 2.

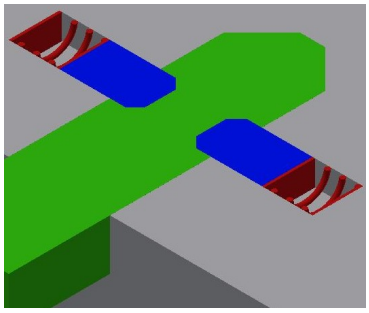

(f) Spring click system progress stage 3.

Figure 6.25: Clamping systems.

there is more mutual assessment and the mechanism can find its equilibrium more easily.

6.3.4 Flight loads

In this section of the report, the structural feasibility and optimisation of the wing is investigated considering the flown flight pattern. As design it was chosen to investigate a space shuttle and airplane like design. With rigid wings it is common to implement a wing box with potential reinforcement by eg. stringers. This approach was not applied in this design due to the small size of the ICARUS+ and the limited loadings it must be able to carry. Therefore the wing skin itself is calculated to be sufficient as structural element. In this section the approach of this calculation is explained.

First of all, structural properties are very difficult to calculate for complex shapes. Airfoils have been created by applying aerodynamics, however simplicity for structural calculations was discarded completely as can be understood very well. This resulted in complex shapes considering structures. Enough time and resources would allow a very detailed discretised solution for these calculations but this is not necessary for this design stage and not possible in the given time slot. Due to extensive experience of structural engineers in the aerospace world with airfoils, the estimation methods are very refined. For structural calculations the airfoil is approached as a rectangular box (wing box) for which the calculations are much more straight forward.

This estimation will be discussed later as first the lift force is calculated. The theoretical maximum is restricted to the maximum load factor n_{max} which will be flown during the flight. This would then be flown in the pull-up manoeuvre as explained in Section 6.4.2. The maximum load factor applied in these calculations is five. The load which is designed for is the theoretical maximum encountered load multiplied with the safety factor f_s. A factor of safety in aerospace engineering is generally around 1.5 but due to the limited comparable designs and the complexity of our flight this is taken to be two. This results in a design force calculated as shown in Equation 6.28. A point load though would not be a good estimate for the lift force. Lift is created over the whole wing due to the pressure difference above and below the wing. Therefore the lift is scaled with the surface area. This thus neglects the lower lift at the tip due to tip vortices and by that the loads are slightly overestimated. The scaled wing loading is performed as shown in Equation 6.29. The drag contribution is estimated by scaling the drag to the lift using the C_L/C_D factor for the main flight condition, which is optimum

glide. This is discretised over the wing by distributing the drag linearly with the frontal wing area. The calculations are identical to the lift distributed load calculation. This underestimates the drag at the wing tip slightly due to the drag induced by the tip vortices. The loads due to drag are much smaller compared to the lift [28] and lift is overestimated at the tip. Taking both into account this approximation may not be a problem.

$$L = n_{max} \cdot f_s \cdot W \tag{6.28}$$

$$q_L = \frac{L \cdot S_{cs}}{S} \tag{6.29}$$

From the distributed load in both x- and z-direction the moments at every cross section due to these loads can be calculated. The moments induced due to these loads can be calculated using the same approach. The moment in x-direction is shown in Equation 6.30 and the other moment must be calculated as is already stated beforein.

$$M_x(b/2-y) = \frac{(b/2-y)^2}{2} \cdot \sum_{i=0}^{(b/2-y)} q_i \tag{6.30}$$

Now that the loads have been discussed, the cross sectional approach can be explained more in depth. As explained, the airfoil is approached as a square box [28]. The wing box estimation is performed as can be seen in Figure 6.26. The overall cross sectional area is the same for both the airfoil and the box. From this point on structurally the airfoil will not be considered anymore and everything will be calculated using this box.

Figure 6.26: The box cross section as airfoil replacement.

The only contribution which remains from the airfoil is the attachment point of the loads which is at the aerodynamic centre of the airfoil. The wing is discretised along the span of the wing. This discretisation leads to a number of cross sections with very little depth. Considering the neutral point and the aerodynamic centre in every cross section, force and moment calculations can be performed. For this the neutral point, the section of both neutral lines, must be calculated for every cross section along the wing span. The neutral lines can be calculated as shown in Equation 6.31 applying the dimensions as they can be found in Figure 6.27. The equation for distance to the neutral line in z-direction can be found similar to the equation for the x-neutral axis.

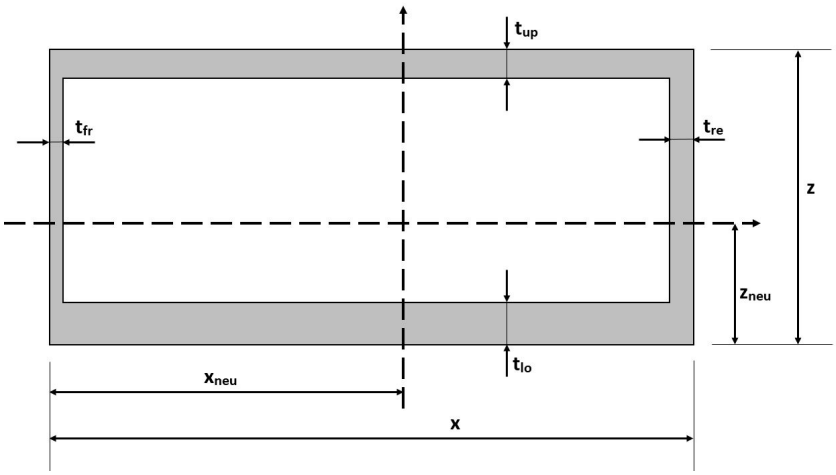

Figure 6.27: Wing box cross section dimensions.

$$(x-t_{fr}-t_{re})\cdot t_{up}+(z-z_{neu})\cdot(t_{fr}+t_{re})=(x-t_{fr}-t_{re})\cdot t_{lo}+z_{neu}\cdot(t_{fr}+t_{re}) \tag{6.31}$$

Once the neutral axes are known, the moments of inertia can be calculated around these axes. The moment of inertia around the z-axis, I_{zz}, can be solved as shown in Equation 6.32. For the moment of inertia around the x-axis the same method must be applied. For the second moment of inertia, I_{zz}, Equation 6.33 must be used.

$$I_{zz}=\frac{1}{12}\cdot z\cdot x^3-\frac{1}{12}\cdot(z-t_{up}-t_{lo})\cdot(x-t_{fr}-t_{re})^3 \tag{6.32}$$

$$I_{xz}=\sum \overline{x}_i\cdot\overline{y}_i\cdot A_i \tag{6.33}$$

The normal stress, σ_y, in the wing box was calculated in every discretised cross section over the wing span using Equation 6.34. The stress in the panels is not equal throughout the cross section and therefore all combinations of x and z encountered in the cross section must be calculated. The iteration over all x and z values for all cross sections is accompanied by computational limitations. The steps over which is iterated in x- and z-directions and the discretisation step cannot be taken small enough without consideration because of the maximum available computational power. The discretisation step must be chosen while taking into account the computational power limit and the minimum step required for an accurate calculation.

$$\sigma_y=\frac{M_z\cdot I_{xx}-M_x\cdot I_{xz}}{I_{xx}\cdot I_{zz}-I_{xz}^2}x+\frac{M_x\cdot I_{zz}-M_z\cdot I_{xz}}{I_{xx}\cdot I_{zz}-I_{xz}^2}z \tag{6.34}$$

The shear stresses, τ, in the wing box are induced by the shear forces (the lift and drag force) and by the torque, T, induced by lift and drag forces if these do not apply in the centre of gravity of the cross sections. For calculating the shear flow the first moment of area, Q, in both directions must be calculated. This can be done using Equation 6.35 for Q_x and the other way around in order to calculate Q_z. From these first moments of area in both directions, the shear stress at every point in a cross section can be calculated by applying Equation 6.36 in both the x- and z-direction.

$$Q_x(z)=\sum \overline{z}\cdot A \tag{6.35}$$

$$\tau_V=\frac{L\cdot Q}{I_{xx}\cdot t} \tag{6.36}$$

The shear stress induced by the torque, T, as explained above can be calculated by applying Equation 6.37. In this equation A_{enc} is the enclosed area of the cross section which is evaluated and t the skin thickness. The equation must be applied for all skins of the cross section. The torque is not only induced by the lift forces in the section but by summation of the distributed lift until the investigated section from the tip onwards. The equation gives an average over the cross section which is valid for a box shape since a box does not contain very high stress concentrations [28].

$$\tau_T=\frac{T}{2\cdot A_{enc}\cdot t} \tag{6.37}$$

A final stress analysis over the box requires Von Mises, however since the outcomes of the normal and shear stresses, shown in Table 6.4, are not even close to failing when the minimum manufacturable design is applied this analysis is not required. The minimum manufacturable design mainly implies a minimum thickness under which manageability and production induce problems.

As just explained the limits on the design are not imposed by the stress analysis but are dictated by the manufacturability. From this can be concluded that the stress analysis as is explained in this section is a required check which is performed throughout all iterations. In these iterations the feasibility of the design towards production is handled with great care.

Table 6.4: Stress values inside the ICARUS+ wing.

	$\sigma_{max,com}$ $[MPa]$	$\sigma_{max,ten}$ $[MPa]$	τ_{max} $[MPa]$
Max. Titanium	880	950	550
Wing	48.169	48.169	6.801

6.3.5 Material Selection

From the previous chapters it can be concluded that the design is exposed to fierce conditions. It should be able to handle all different kinds of loads, withstand the thermal conditions and stay within the weight limit of 2 kg. In order to withstand all these loads, proper material selection is crucial. Therefore, a few kinds of materials are examined on their performance in different areas. In the end, the most appropriate material is selected for the design, taking all the earlier mentioned fields of interest into account as well. Consequently, a good balance is established between meeting the technical requirements and staying within the constraints.

Commonly used materials in aerospace that will also be interesting for the design, are aluminium and titanium. Aluminium is mainly used for its high performance in strength in combination with a low density. Titanium, on the other hand, has a higher density, which may result in increased weights. However, titanium performs better under high loads and it also has better thermal propertie. For now, both materials are analysed, starting with titanium.

Titanium is produced in a high variety of applications. It can be selected for both resistance to corrosion and high strength. Clearly, for the ICARUS+, strength efficient materials should be examined, since corrosion is not one of the first concerns. For this practice, wrought titanium alloys are frequently used. Those have optimum tensile, compressive and creep strength at different temperatures. The combination of those attractive properties together with inherent workability makes titanium unique in use. The most promising types of titanium are Ti-6Al-4V (grade 5), Ti-6Al-2Sn-4Zr-2Mo+Si and Ti-10V-2Fe-3Al. [29] This is the selection of materials that are examined on their properties. The most important characteristics needed for this design can be found in Table 6.5.

Next, aluminium will be elaborated on. This material is widely used in the aerospace industry because of its relatively low density and high strength. The only downside of aluminium is the thermal resistance. The design will be subjected to high temperatures as stated in section 6.6. Consequently, aluminium might not be sufficient taking the thermal properties into account. Nevertheless some aluminium alloys have increased thermal resistance and are therefore also analysed in order to select a material for the design. The properties of three commonly used aluminium alloys in aerospace can also be found in Table 6.5.[1]

Table 6.5: Some characteristics of materials which are commonly used in aerospace.[2]

	ρ $[kg{\cdot}m^{-3}]$	$\sigma_{ult,ten}$ $[MPa]$	$\sigma_{yield,ten}$ $[MPa]$	$\sigma_{yield,comp}$ $[MPa]$	σ_{bear} $[MPa]$	τ_{max} $[MPa]$	T_{melt} $[K]$	E $[GPa]$
Ti-6Al-4V	**4430**	**950**	**880**	**970**	**1860**	**550**	**1877-1933**	**113.8**
Ti-6Al-2Sn-4Zr	4540	940	860	1070	1620	660	<1973	113.8
Ti-10V-2Fe-3Al	4650	1430	1240	1280	1690	760	588	110
Al-2024-T6	2780	440	345	-	855	283	775-911	73.1
Al-6061-T6	2700	310	276	-	386	207	582-651.7	68.9
Al-7075-T6	2810	572	503	-	-	331	750	71.7
Torlon®	1480	221	205	254	-	-	556	-

Finally, taking the calculated stresses and temperatures into account, a material can be selected. Looking at the stresses, only the hinges might cause a problem. However, still all the materials shown in the table might be sufficient in terms of internal stresses. More critical criteria are the thermal properties of the materials. As shown in section 6.6, the maximum temperature can reach a value of 420 K. All selected materials might be

[1] URL http://www.matweb.com/search/MaterialGroupSearch.aspx [27 May 2016]
[2] URL http://metalspecialist.continentalsteel.com/blog/aluminum-in-the-aerospace-industry [27 May 2016]

able to handle those temperatures. However, taking the early stage of design into account, the materials with temperature properties close to this limit will be eliminated. Two titanium alloys remain to be chosen for the design, Ti-6Al-4V and Ti-6Al-2Sn-4Zr. The weight of titanium with respect to aluminium is almost doubled. However, the weight limit of two kilogrammes is not likely to be exceeded and therefore this is not considered a problem. The titanium alloys have very similar properties, as can be seen in Table 6.5. For the final trade-off between the two materials, the availability in the market is taken into account. Ti-6Al-4V is more commonly used in the aerospace industry than Ti-6Al-2Sn-4Zr. Consequently, this alloy is widely available on the market in different forms, like sheets, bars, wires and more. Taking all the above mentioned factors into account, the material chosen for the design is the titanium alloy Ti-6Al-4V.

For aerodynamic reasons, the GPS antenna is placed within the fuselage. A new arising problem is that the antenna will not have any signal within a titanium shell. For this reason, another material is selected for the upper part of the fuselage. Since the fuselage is assembled in three parts, it is possible to replace one part with another material. The material chosen for this part is Torlon®. This is a unique high performance thermoplastic composite that will be able to passage the signal to the antenna. In Table 6.5 the properties of Torlon® can be found. It is clear that it will still be able to handle all the loads subjected to the design. In Chapter 12 the manufacturing techniques used for the three parts of the fuselage are stated. In this chapter the reason for choosing Torlon® is elaborated on more.

6.4 Flight Mechanics

This section gives an overview of all the important characteristics and approaches regarding the flight mechanics of the ICARUS+. Since the performance analysis is a large iteration process, the flight mechanics engineers will also refer to the other technical divisions.

During the mid-term process, five concepts were compared to each other with respect to their range, flight time and overall flight path. In this design phase, only the final design is discussed and iterated. First of all, the initial conditions and assumptions are described. The initial conditions are split up into environmental conditions and body conditions. In the second section, the flight path modelling approach is discussed. Regarding the approach, the flight path is split up into four stages. Also the effects of meteorology are discussed in this section, since those atmospheric conditions will have a significant effect on the flight path. Following to the flight path approach, the improvements with respect to the earlier design phase are discussed. The final section gives an overview of the results.

6.4.1 Initial Conditions and Assumptions

The initial conditions contain environmental conditions and body conditions. Both categories are elaborated on. Afterwards the assumptions are stated, these are divided into primary and secondary assumptions.

Environmental Conditions

The initial conditions result from several kinds of aspects. The overall start of the flight path is at an altitude of 60 km. At this point, the pressure and density are significant lower than the common values at commercial flight altitudes. The density is the most important environmental variable during the flight mechanics analysis, since the lift and drag force decrease with the density. Next to density, also the temperature changes with altitude. The temperature is important for calculating the Mach number, which is important for the drag computations.

Body Conditions

Furthermore there are body conditions that contribute to the initial conditions. First of all, the Lynx has a certain velocity at the moment of detachment. That velocity can be approximated by analysing the related flight path of the Lynx.[1] Another important condition is the altitude at which the payload will be stable and ready for flight. This is an input that results from the stability analysis, which is elaborated on in Section 6.2. At this altitude, the ICARUS+ starts flying by performing a pull-out manoeuvre. Other inputs for the flight mechanics model, regarding the altitude at which the ICARUS+ is stable, are the velocities and horizontal displacement at that stage.

[1] Harry van Hulten, personal communication, [8 Jun 2016]

Assumptions

In the model of the flight path some assumptions are made that will affect the computations. These assumptions are categorised by primary assumptions and secondary assumptions. The primary assumptions have a significant influence on the computed flight path. The secondary assumptions have negligible contribution.

Primary Assumptions

- At the instant the flight mechanics model initiates the computations, the payload is assumed to be perfectly stable. In reality it is possible that the payload is not completely stable. The effect of this assumption depends on the level of stability of the payload. An unstable payload decreases the total range, since in that case it is harder to maintain the C_L values for optimal flight.
- The decrement of the lower boundary of the stratospheric altitude from the equator to the poles is linearised. This could make a small difference on the overall flight characteristics, since the stratospheric range contains an assisting wind. This will affect the total flight time. This is because the lower boundary of the stratosphere is passed when the ICARUS+ is in its gliding phase, where the flight path angle is fixed for optimal glide. However, the velocity changes due to the assisting wind which falls away, which eventually changes the flight time.
- It is assumed that the ICARUS+ descends to sea level. However, if there are for example high mountains, the payload would stop flying or crash earlier during its flight. This makes a significant difference regarding the total range. If the payload would hit a high mountain, the total range would become much less.

Secondary Assumptions

- The Earth is assumed to have a constant mass distribution. This will not make a significant difference on the trajectory, since the fluctuation in gravitational acceleration is low (9.7639 $m{\cdot}s^{-2}$ - 9.8337 $m{\cdot}s^{-2}$).
- The Earth is assumed to be a perfect sphere. This does not have a significant effect on the total displacement of the payload, since the Earth is an almost perfect sphere and the scale on which the ICARUS+ is operating is relatively small compared to the scale of the Earth.
- The gravitational influences of the Moon and the Sun are neglected. This does not has a significant influence on the computations, since at an altitude of 60 km the Earth is far more dominant.
- The velocity changes due to the stratospheric winds are implemented immediately, instead of in an iteration over time. This would not make a significant change, since the time iteration would be short. Also the upper boundary of the stratosphere could fluctuate a little bit, so these effects would cancel each other out.
- Accelerations are assumed constant over a time step. However, since the period of time is very small ($< 0.001\ s$), this effect is negligible.
- For the flight path calculation a point mass is assumed, this will have a negligible effect since the ICARUS+ is so small.
- The latitude does not change during flight. It is only implemented as an initial condition. This will not make a significant change on the computations since the distance travelled by the ICARUS+ is relatively small compared to the size of the Earth.

6.4.2 Flight Path Approach

In this section the approach with respect to the flight path is discussed. The flight path is categorised in four stages. At first, the ICARUS+ starts with a free fall. During this free fall, the ICARUS+ will stabilise in order to be able to perform a controlled flight. After this, a constant pull-out will be performed. The stage that is initiated after the pull-out and holds until the final gliding stage is called the transition stage. The fourth stage is the final phase at which the optimal gliding flight will be performed. All stages will be elaborated on. After this, the effects due to meteorology will be discussed. The meteorology has already been discussed into depth in Chapter 5, but in this section the implementation in the flight mechanics model will be elaborated on. The final part of this section will contain an overview of the improvements of the present model, including an overview of the important parameters.

Free Fall Phase

The flight path starts when the ICARUS+ is being released from the Lynx Mark I. To know the velocities of the Lynx at that moment, the flight path of the Lynx has been analysed. A Mach number of 0.3 is found, which complies with a velocity of 94 $m \cdot s^{-1}$.[1]Since the ICARUS+ is released when the vertical velocity is zero, this is all horizontal velocity. In this phase of the flight path there is a very low density, which means that lift and drag have a minor effect on the payload. First of all, the payload has to stabilise itself with its nose pointing downwards, in order to have the ICARUS+ to be able to start its controlled flight. The stabilisation of the model is explained in Section 6.2.4.

Due to the horizontal velocity when the payload is released and the lack of density, the ICARUS+ will already gain some range during the free fall. The approach used for this part is an arc flight path until the payload is stable. Afterwards, the constant pull-out will start. By iterating the model several times, an altitude of 40 km is chosen as optimum altitude to start flying, and thus start the pull-out, in order to gain as much range as possible. This is a result of the trade-off between the ability to pull-out quickly due to density changing and the amount of vertical velocity that is present during each stage of the fall. It also has to gain enough velocity during the vertical fall, in order not to stall at the final approach of the flight path.

Constant Pull-out

The vertical velocity that is generated in the free fall stage, has to be transformed into a horizontal component in the most efficient way possible, in order to generate a flight path for maximum range.

After analysing different approaches to transform the velocity component, the outcome was convincing. The most efficient way to transform the velocity component would be to perform a constant pull-out. This manoeuvre causes an overall altitude decrement that is least compared to other manoeuvres. Furthermore a lot of velocity is maintained at the end of the pull-out. This is due to the fact that the velocity is transformed more efficiently when it pulls out as curvy as possible. The rougher the pull-out is, the more the total velocity decreases due to the almost-parallel working counter accelerations.

The limiting factor of the pull-out manoeuvre is the maximum load factor. The maximum load factor has been defined while performing the structural analysis, which is elaborated in Chapter 6.3. The maximum load factor determines the maximum value of C_L that can be used during the pull-out manoeuvre. The computation of C_L has been done by Equation 6.38.

$$C_L = \frac{n_{max} W}{\frac{1}{2}\rho V^2 S} \tag{6.38}$$

This is an important value for the computations, since the lift force is acting as the centrifugal force during this manoeuvre. The C_L value will have the maximum allowable value during the pull-out, in order to finish the manoeuvre at a high altitude. Since the velocity and density will increase during the pull-out, the C_L value has to decrease from a certain moment on, in order to not exceed the maximum load factor. At the end of the manoeuvre, the vertical velocity component is be zero. Therefore, the flight path angle is considered zero at the end of the manoeuvre, which is pure horizontal motion.

Transition stage

The transition stage is the flight path that starts directly after the pull-out and ends at the point where the gliding path will be initiated. The transition stage is split up intro three phases. During the first phase, the payload keeps on pulling out, until a certain flight path angle is reached. During the second phase, this particular angle will be maintained until the payload meets the optimal dynamic pressure criteria for optimal flight. The optimal dynamic pressure value can be computed by Equation 6.39, where C_{D_0} is the profile drag coefficient.

$$(\frac{1}{2}\rho V^2)_{opt} = \frac{W}{S\sqrt{C_{D_0}\pi A e}} \tag{6.39}$$

[1]Harry van Hulten, personal communication, [8 Jun 2016]

One of the characteristics of an optimal gliding path is the fact that this dynamic pressure value remains approximately constant during gliding flight.

After the second phase has been performed, the third phase will be initiated. Here, the C_L value will be set to zero, in order to pull-over towards horizontal flight and to start the optimal glide as soon as possible. Otherwise, the payload would lose too much energy during the climb and the dynamic pressure could get too low for the optimal glide.

When the dynamic pressure is too high, the payload will have to fly horizontally, in order to brake speed. This is the most optimal way of braking speed, considering the range. However, if the dynamic pressure after this third stage gets lower than the optimal dynamic pressure, there are two options that yield to a higher dynamic pressure.

- The first option is to let the payload oscillate. The oscillation causes the payload to gain and lose velocity during the oscillation, until it stabilises at the optimal dynamic pressure.
- The second option is maybe not the most apparent one. Here, the payload will fly at flight path angles between perfect horizontal flight and the optimal glide angle. This is an applicable approach for specific altitudes, where the velocity decrement is low compared to the increment of air density. Since the dynamic pressure is $0.5\rho V^2$, these values will factorise each other in order to let the dynamic pressure increase.

After these three phases are computed, a final iteration is done in order to achieve maximum range. The iteration has two variables. These are the specific flight path angle until the payload will pull-out and the factor for how long that condition will be maintained. The second variable, the mentioned factor, can cause some confusion, since it has been mentioned that the condition would be maintained until a certain dynamic pressure would be achieved. However, when the payload would initiate the final pull-over at the instant that the optimal dynamic pressure is reached, the payload will finish the pull-over at an altitude at which the dynamic pressure is definitely lower than the optimal dynamic pressure. The iteration leads to the optimal conditions for maximum range.

Final Gliding Stage

The final stage of the flight path is the optimal gliding path. At the start of this final stage, the payload orientates its angle of attack in order to generate the optimal C_L value for gliding flight. The value for optimal C_L can be computed by Equation 6.40.

$$C_L = \sqrt{C_{D_0} \pi A e} \tag{6.40}$$

This trajectory is characterised by the straight descending line in the graph of the flight path (see Figure 6.29). The C_{D_0} value is computed for every time step, since it depends on flight mechanical and aerodynamic parameters. The temperature, density, velocity and Mach number contribute to the C_{D_0} computations. As mentioned before, the dynamic pressure remains constant during the optimal gliding path: while the velocity decreases due to drag, the density increases. These two changes cancel each other out during an optimal glide, regarding the fluctuation of the dynamic pressure. Another characteristic of an optimal gliding path is that the profile drag and induced drag are perfectly equal to each other. [30]

Meteorology

The meteorology effects the flight path at stratospheric altitudes. The wind direction and velocity are elaborated on in Chapter 5. Having the wind coming from the back or from the front implies two different impacts for the flight characteristics. If for example, the wind is coming from the back, then the relative velocity to the ground increases. However, the relative air velocity decreases, due to which the C_L value increases. This approach is validated by airspeed models from NASA.[1]

For maximum range, it is optimal to have the wind coming from the back of the payload. This implies that a flight from west to east is most beneficial, since in Chapter 5 it is mentioned that the wind is heading from west to east.

[1] URL https://www.grc.nasa.gov/www/k-12/airplane/Animation/airrel/anrela.html [1 June 2016]

In the complete flight path, the wind assists the payload from the instant the payload drops below 50 km. The instant the payload passes the lower boundary of the stratosphere the wind stops assisting the payload. The lower boundary is determined by the latitude at which the payload is located above Earth. Around the equator, the lower boundary of the stratosphere is at about 16 km altitude. Around the North- and South Pole the lower boundary is at about 8 km altitude. An overview can be found in Figure 6.28. Because the stratospheric conditions hold longer above the poles, it can be concluded that flying near the poles is more efficient instead of flying near the equator.

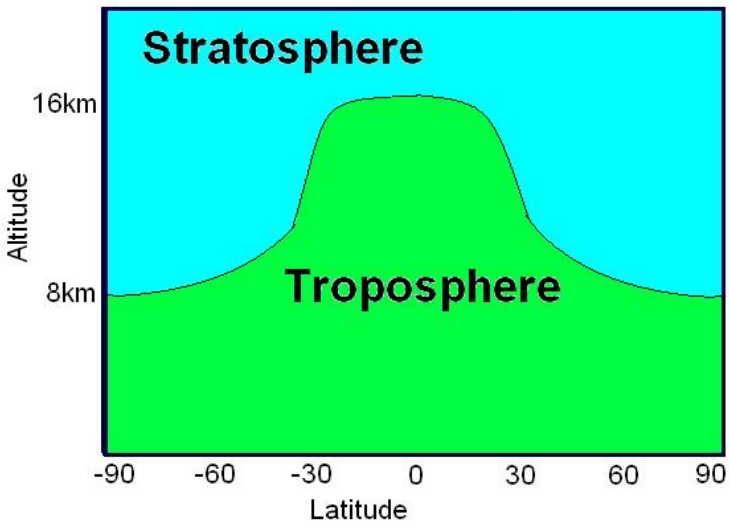

Figure 6.28: The lower boundary of the stratosphere per latitude.

Model Improvements and Main Parameters

Compared with earlier design phases there are some significant changes in the approach for the flight path calculations. The free fall, pull-up and constant glide stage are almost the same. The only difference at these stages is the fact that the computation of the gliding path in the current model is improved. The gliding path is now a linear descending path, as can be seen in Section 6.4.3.

The major difference is made in the transition flight stage. At earlier design phases it was considered more effective to have oscillations in the flight path for the following condition. At the lower maximums of the curved flight paths, the C_L values have been analysed regarding their value for the condition in which lift would equal weight. If this value is higher than the optimal C_L value for gliding flight, the ICARUS+ would start another oscillation. However, after more analyses have been performed, it could be concluded that having only one oscillation will result in higher ranges. This oscillation occurs after the pull-out has been performed. So, the transition flight stage can be considered as the only oscillation that occurs during the flight path. With more oscillations, the payload loses too much energy during the flight, due to the altitude and velocity changes.

Another major improvement is the implementation of the aerodynamic drag model. All drag components are now computed according to the steps that are elaborated on in Section 6.1. The aerodynamic coefficients are now computed very accurately for every time step. This makes the new model very reliable with respect to these coefficients.

During the iterations, there are a few inputs which are more important than other inputs regarding the range. In Chapter 8 these parameters are analysed regarding their sensitivity. The sensitivity is determined by examining the effect on the total range.

6.4.3 Elaboration on the Results

This section gives an overview of all the characteristics of the flight trajectory. The results are divided into five sections. The first section shows the resulting flight path, including the results of the total range and flight time.

The second part elaborates on the Mach number during flight. The third part elaborates on the dynamic pressure during flight. The fourth part contains the results of the lift- and drag coefficients during flight. Finally, the fifth part gives the results of the drag coefficient by plotting the values of C_{D_0} and C_{D_i} for the total flight path.

Flight Path Results

The flight path of the ICARUS+ is computed with the flight mechanics model. The approach of this model has been elaborated on in the previous sections of this chapter. All specifications of the ICARUS+ are implemented in the model in order to create a flight path that is customised for the ICARUS+. The environment, by means of the International Standard Atmosphere, implements the stratospheric wind effects and an accurate drag model in the model. The flight path can be seen in Figure 6.29.

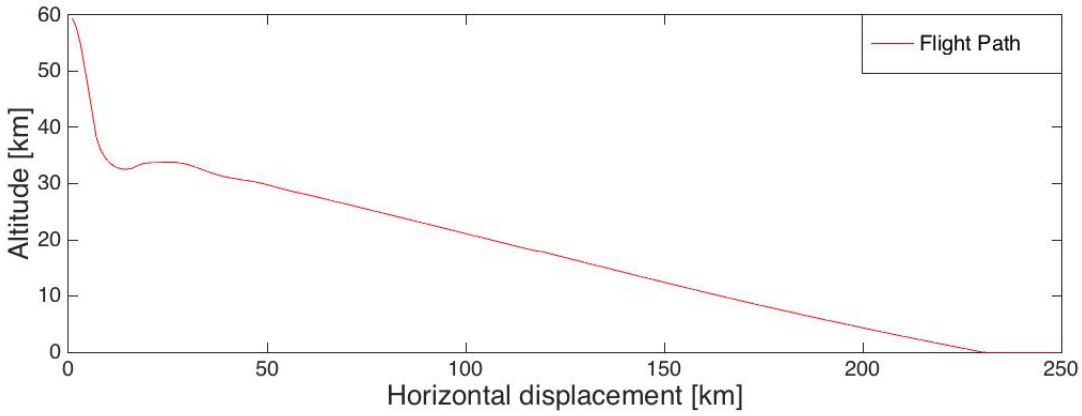

Figure 6.29: The flight path of the ICARUS+.

The maximum range the ICARUS+ can achieve is 230 km. The total flight time of this flight is 70 minutes. The pull-out is completed at an altitude of 32.5 km. After the ICARUS+ performed its ascending phase, it pulls over at an altitude of 33.7 km. From this altitude on, the optimal gliding flight is initiated.

Mach Number During Flight

The Mach number is an important parameter regarding the performance analysis. Different engineering divisions in this project need specific values regarding the Mach number analysis. Aerodynamics, for example, needs to know the maximum Mach number during flight. For thermal engineering the time span the ICARUS+ flies above a certain value is necessary. Control and stability engineering need to know what kind of velocities the ICARUS+ is flying in order to determine controllability and stability at each flight regime.

Figure 6.30 gives an overview of the Mach number during the horizontal displacement. Figure 6.31 gives an overview of the Mach number over time.

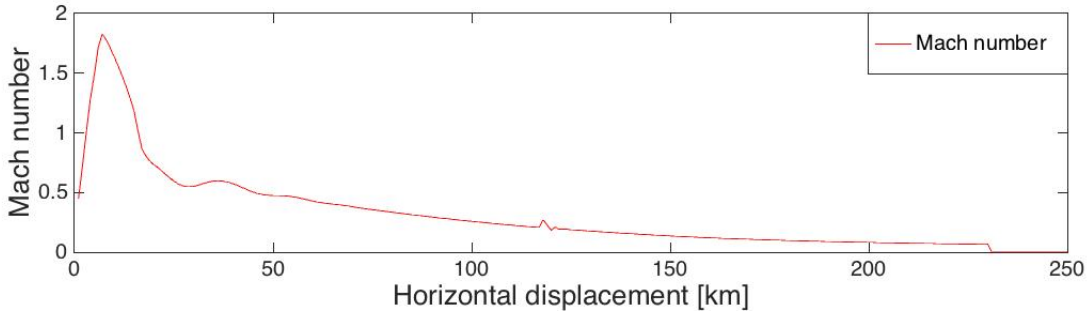

Figure 6.30: Mach number vs horizontal displacement of the ICARUS+ flight path.

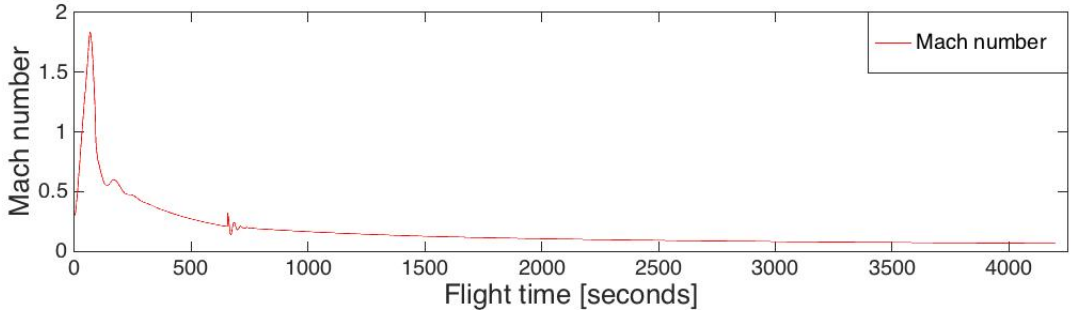

Figure 6.31: Mach number vs time of the ICARUS+ flight path.

As can be seen, the maximum Mach number during flight is 1.84, at an altitude of 39.5 km. The total flight time at which the ICARUS+ is flying faster than Mach 1 is 59 seconds, which is relatively small compared to the 70 minute flight time.

After a horizontal distance of 118 km and after a flight time of 710 seconds, an oscillation can be seen in Figure 6.30 and Figure 6.31. This is due to the lower boundary of the stratosphere. Below this boundary, the assisting wind of the stratospheric wind disappears. However, the velocity stabilises relatively quick, that is in 30 seconds. Also in the beginning of both figures, a high peak can be seen. The increasing Mach value is due to the free fall, after which it decreases during the pull-out. After the Mach number finishes decreasing, it suddenly starts to increase for a short while. This is due to the little oscillation after the pull-over. This oscillation is the result of the fact that the dynamic pressure is too low at the start of the optimal gliding flight. As follows, the ICARUS+ descends a little at the start of the oscillation, after which it quickly stabilises and continues with the gliding flight.

Dynamic Pressure Overview

The dynamic pressure is an important value during the computations of the flight path. As has been explained before in this chapter, it is very important regarding the final approach of the transition stage. Here, the dynamic pressure has to be optimal for gliding flight. The dynamic pressure is also important for the hinge moments of the control surfaces.

In Section 6.4.2 it is stated that the dynamic pressure should be approximately constant during the optimal gliding flight. This can be confirmed by taking a look at Figure 6.32. After the ICARUS+ passes the lower boundary of the stratosphere, the dynamics pressure tends to stabilise at some higher value. This is due to the fact that the velocity of the ICARUS+ relative to the surrounding air increases at that instant.

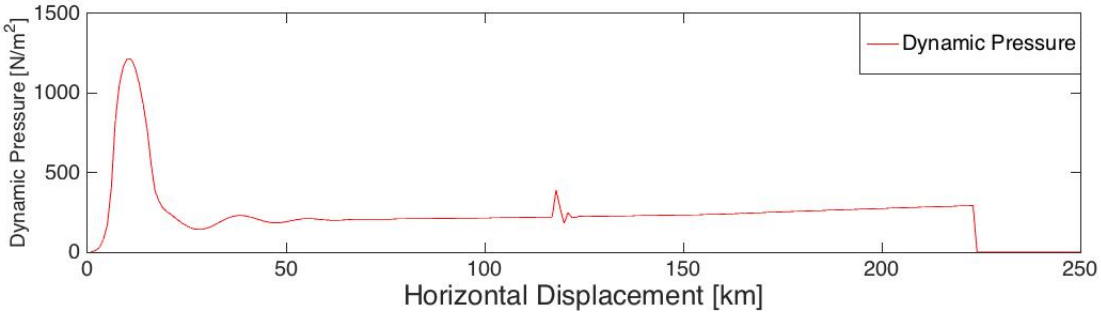

Figure 6.32: Dynamic pressure during flight of the ICARUS+.

The increment of the first peek is again due to the free fall. Here, the velocity and the density are both increasing. The decrement of that same peek is due to the pull-out manoeuvre, followed by the pull-over manoeuvre. Here, the velocity decreases rapidly. After the pull-out, also the density decreases during the ascending stage. The little oscillation after this peek is again due to the stabilisation of the optimal dynamic pressure.

At a maximum Mach velocity, the dynamic pressure is equal to 698.9 $N \cdot m^{-2}$. This is not the largest value for

dynamic pressure. The maximum value occurs after a horizontal displacement of 10.0 km, where the altitude is equal to 34.0 km. Here, the dynamic pressure is equal to 1217.1 $N \cdot m^{-2}$.

Lift- and Drag Coefficient Overview

This section will give an overview of the values of the lift- and drag coefficients. The lift values are determined according to the needs for an optimal flight. During the flight of the ICARUS+, the optimal values of C_L never exceed the value of the maximum C_L. The drag coefficient is computed by the drag model, which is elaborated on in Section 6.1.4. Figure 6.33 gives an overview of the C_L and C_D values during flight.

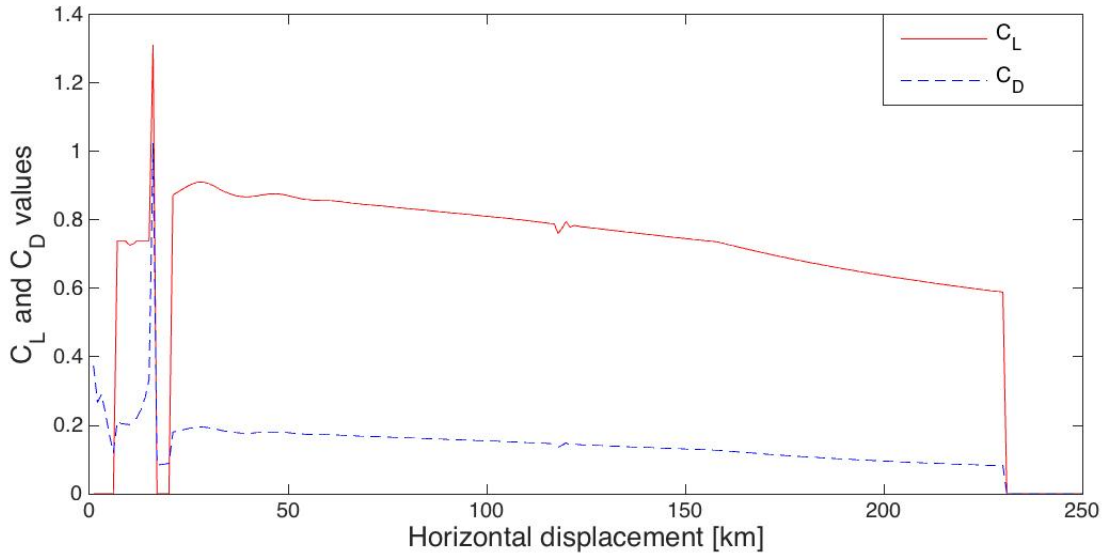

Figure 6.33: C_L and C_D plot during flight of the ICARUS+.

As can be seen, the C_L value at the beginning is almost zero. This occurs during the free fall trajectory, where the ICARUS+ is stabilising before controlled flight begins. After this, the C_L value is set to the maximum allowable value, with respect to the Mach number. There are three deviations for the $C_{L_{max}}$ value, divided over the subsonic, transonic and supersonic speeds. At the start of the pull-out, the C_L value is constant at $C_{L_{max}}$. There is a little curve in it, where the C_L value gets lower, in order to meet the maximum load criteria. At a certain point, the C_L value rises quickly. This is because of the rising Mach number, which allows a higher $C_{L_{max}}$. After this, the C_L value has been set to zero during the pull-over, which has been elaborated on in Section 6.4.2. When the pull-over is done, the C_L value increases again, this time for the gliding flight. It decreases during flight, since the value for C_{D_0} decreases.

The C_D value changes according the drag model that is elaborated on in Section 6.1.4. One can easily see the large peek during supersonic flight, relatively to the lower C_D values during the gliding flight.

Profile Drag and Induced Drag Overview

The drag coefficient is computed using five different sorts of drag. These are the profile drag, the induced drag, the transonic drag and two different supersonic drags. In Section 6.4.2 it has been mentioned that during an optimal gliding flight, the profile and induced drag should be equal to each other. This can be confirmed by taking a look at Figure 6.34.

The fluctuation of the C_{D_i} value looks similar to the fluctuation of the C_L value in Figure 6.33. This is due to the relation of the lift coefficient with respect to the induced drag, which has been stated in Equation 6.41.

$$C_{Di} = \frac{C_L^2}{\pi A e} \tag{6.41}$$

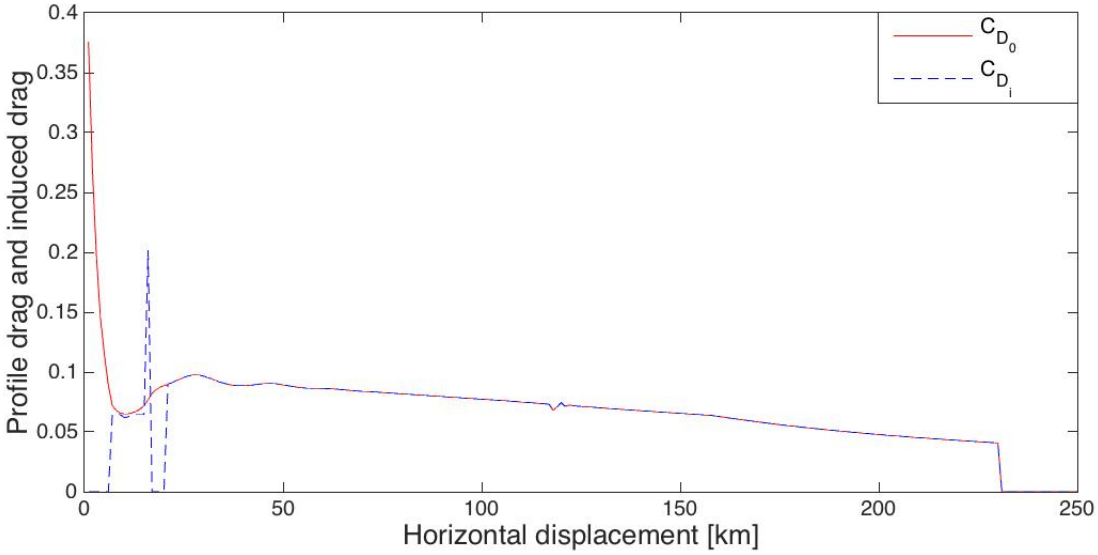

Figure 6.34: C_{D_0} and C_{D_i} plot during flight of the ICARUS+.

During the gliding path the profile and induced drag are exactly the same, so the theory about these values can be confirmed by considering these results. This can also be confirmed by substituting the C_L value for optimal glide from Equation 6.40 in Equation 6.41, which results in Equation 6.42.

$$C_{Di} = \frac{(\sqrt{C_{D_0}\pi Ae})^2}{\pi Ae} = C_{D_0} \tag{6.42}$$

The C_{D_0} changes according to the drag model from Section 6.1.4. At high altitudes, where the density is low, the Reynolds number becomes low. At low velocities, the Reynolds number gets even lower. A low Reynolds number results in a high C_{D_0} value, which can also be seen at the start of the C_{D_0}-plot in Figure 6.34. When the free fall is initiated, the density and velocity will both increase, due to which the Reynolds number increases. This is the reason why the value of C_{D_0} is decreasing relatively fast during the first flight stage. The formula for the Reynolds number can be found in Equation 6.43.

$$Re = \frac{V\rho\bar{c}}{\mu} \tag{6.43}$$

Table 6.6: Overview of the important flight trajectory results of the ICARUS+.

Parameter	Results
Total range	230 km
Endurance	70 min
Maximum Mach number	1.84
Pull-out altitude	32.5 km
Pull-over altitude	33.7 km
Maximum dynamic pressure	1217.1 $N{\cdot}m^{-2}$
C_L/C_D during glide	7.22
Glide angle in degrees	-7.886°
Flight time above Mach 1	59 s
End velocity at maximum range	22.1 $m{\cdot}s^{-1}$ (= 80.0 $km{\cdot}h^{-1}$)
Stall speed at sea level	16.2 $m{\cdot}s^{-1}$ (= 58.4 $km{\cdot}h^{-1}$)

Results Overview

The most important results from the final design are summarised in Table 6.6. Also some general results are added to this table, like for example the stall speed.

6.5 Electronics

The mission requirements imply that the design not only has to be autonomous, but also capable of communicating with a ground station in both uplink and downlink modes. This puts heavy requirements on the electrical subsystem of this mission, as many different capabilities have to be packed into a very small form factor.

In earlier stages of the design process different components have already been considered in order to obtain a rough estimate of costs, mass and volume. However, it is important to also take the electrical interface into account when designing and iterating this subsystem into further detail. Therefore a closer look is taken at the following capabilities: navigation, actuation, communication, command and data handling, interfacing and power.

This section first goes into detail of the components of the electrical subsystem. Afterwards, an overview and budget of this whole system is given. Finally, the data handling system is explained.

6.5.1 Communication

When designing the communication segment of a mission, a link budget first has to be made, as it defines the necessary antenna and power requirements. Afterwards, the selected antenna and UHF transponder is discussed.

Link Budget

The link budget is limited by the capabilities of the antenna, the ground station and the maximum distance between the ground station and the payload. Taking into account a horizontal displacement of the Lynx prior to deployment as well as an aspired range of about 1,000 km for now, a maximum distance of 1,000 km is used to compute the link budget. Computing the link budget requires several values, which are listed in Table 6.7 for the uplink and Table 6.8 for the downlink. Firstly, the ground station segment is discussed, followed by the path segment and lastly the spacecraft segment is evaluated.

For the ground station, a reference ground station is selected based on the AS100 antenna from GOMSpace. This antenna has a gain, pointing loss, power output, system temperature and transmission line loss as specified in the datasheet of the AX100 UHF Transponder. [1]

For the path segment, the atmospheric as well as the rain loss can be considered to be zero as they are reasonably small for this altitude range .[26] The ionosphere is just above the deployment height of 60 kilometres, and therefore this loss is zero as well. There is an additional 3 dB polarisation loss, due to the spacecraft antenna having linear polarisation and the ground station circular polarisation. Finally, the path loss that is based on transmission distance of 1,000 km is calculated using Equation 6.44.

$$path\ loss = 10 \cdot log\left\{\left(\frac{\lambda}{4\pi d}\right)^2\right\} = 10 \cdot log\left\{\left(\frac{0.75}{4\pi 1000000}\right)^2\right\} = -144.49dB \tag{6.44}$$

For the spacecraft segment, the linear polarisation antenna from Vishay^{TM} which has been selected as reference that has a power input close to 1 W, as this is what the power budget allows. The pointing loss, peak gain and system temperature for the antenna are defined in its datasheet [2]. Additionally, the required data rate of 9600 bps adds a loss of 39.8 dB. The signal to noise ratio threshold of 7.8 dB is based on the desired bit error rate of 10^{-5} and the selected Gaussian phase shift keying modulation technique .[26]

To come to the total signal-to-noise ratio, intermediate subtotals for a clearer overview of the spacecraft, ground station and transmission path budget contributions are determined. The margin is then obtained by looking at the threshold signal-to-noise ratio and comparing it to the actual one, mentioned previously. As can be seen,

[1] URL `http://gomspace.com/documents/ds/gs-ds-nanocom-ax100-3.2.pdf` [6 June 2016]
[2] URL `http://www.mouser.com/ds/2/427/VJ5301M400MXBSR_DS_Prelim-201076.pdf` [7 June 2016]

Table 6.7: Uplink budget.

Parameter	Value [dB]
Ground station transmitter power	14
Ground station total transmission line loss:	-1.6
Ground station antenna gain	17
Ground station EIRP (subtotal 1)	29.4
Ground station antenna pointing loss	-0.5
Ground-to-S/C antenna polarisation loss	-3
Path loss	-144.49
Atmospheric loss	0
Ionospheric loss	0
Rain loss	0
Isotropic signal level at ground station (subtotal 2)	-118.61
Spacecraft antenna pointing loss	-3
Spacecraft antenna gain	-8.7
Spacecraft total transmission line loss	-0.5
Spacecraft effective noise temperature loss	-23.69
Data rate loss	-39.82
Boltzmann constant	228.6
Eb/No (total)	34.58
Eb/No_{min} (thresh hold)	7.8
Margin	26.78

Table 6.8: Downlink budget.

Parameter	Value [dB]
Spacecraft transmitter power output	0
Spacecraft total transmission line losses	-0.5
Spacecraft antenna gain	-8.7
Spacecraft EIRP (subtotal 1)	-9.2
Spacecraft antenna pointing loss	-3
S/C-to-ground antenna polarisation loss	-3
Path loss	-144.49
Atmospheric loss	0
Ionospheric loss	0
Rain loss	0
Isotropic signal level at ground station (subtotal 2)	-159.69
Ground station antenna pointing loss	-0.5
Ground station antenna gain	17
Ground station total transmission line loss	-0.5
Ground station effective noise temperature loss	-30.01
Data rate loss	-39.82
Boltzmann constant	228.6
Eb/No (total)	15.07
Eb/No_{min} (threshold)	7.8
Margin	7.28

the margin for both uplink and downlink are positive, meaning that this antenna fulfils the communication requirements. Also noteworthy is that the uplink data rate can be increased to 115200 *bps* whilst still having

a positive link margin. For downlink however, the data rate can only be increased to 38400 *bps* due to the small antenna size of the payload.

UHF Antenna

With the required antenna power and gain known from the link budget, an antenna and a configuration can be designed for the mission. It is important to take into account the mirroring effects of the payload on the radiation pattern of the antenna, since the payload is made of titanium. Also important is the direction of the peak gain of the antenna with respect to the ground station throughout the flight.

With these considerations in mind, a monopole antenna with a capacitor-inductor circuit is selected and developed. A monopole antenna is chosen because of its simplicity and omnidirectional radiation pattern. For a monopole antenna, the length should be a quarter of the communication wavelength, which for a 395 MHz frequency would mean a 0.19 m long antenna. As this length is not achievable the capacitor-inductor circuit will have to be tuned to obtain the right frequency. The capacitance is a function of the percentage deviation from the quarter wavelength, and the inductance makes the antenna resonate at the desired frequency. The selected dimensions for the antenna, which fit in the available space, are 0.05 m in length and 0.005 m in diameter. The reduction in length means the gain is lower compared to the ideal 0.19 m length (quarter wavelength), but since the link budget allows for a very low antenna gain this is a viable solution. The dimensions of the antenna and values of the tuning circuit can be found in Figure .6.35

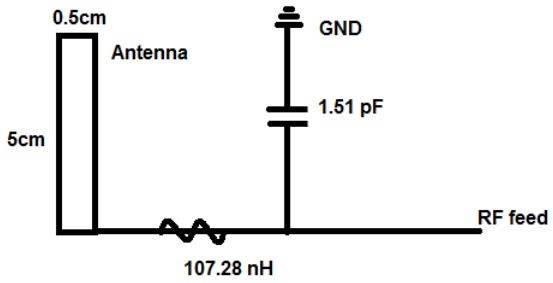

Figure 6.35: UHF antenna and tuning circuit specifications.

This antenna will extend from the rear of the fuselage just after deployment from the Lynx spacecraft. This configuration is chosen to keep the radiation pattern of the antenna within reach of the ground station. As it is mirrored slightly by the system made of titanium, the peak gains are moved slightly more aft as can be seen in Figure 6.36. Also, the expected non distorted radiation patten of the antenna is given in Figure 6.37 based on the reference antenna. [1] At this stage of development no RF simulation is made, although necessary for accurate analysis. This is because it is not a part of the aerospace Bsc. curriculum.

Finally, the antenna is made of titanium, as it will be subjected to temperatures close to those of the leading edge of the wing. Since there is only one antenna, half duplex communication has to be used. This means that half of the time the antenna is receiving and half of the time it is transmitting. This lowers the data volume by half, but the size constraints do not allow the addition of another antenna and as follows this is the only viable solution.

UHF Transponder

In the selection of a UHF transponder, the frequency range and power requirements are driving. It was decided to use the AX100 from GOMspace. It is space grade and has very low mass, power and volume specifications. Additionally, it falls within the required frequency range of 225-400 MHz with a data rate of 9600 *bps*. Noteworthy is that the data rate can be increased up to 115200 *bps* for uplink and 38400 *bps* for downlink due to the antenna size of the payload. The communication to the flight computer is also performed through Universal Asynchronous Receiver/Transmitter (UART) connection, which is compatible with most flight computer systems.

[1] URL `http://www.mouser.com/ds/2/427/VJ5301M400MXBSR_DS_Prelim-201076.pdf` [7 June 2016]

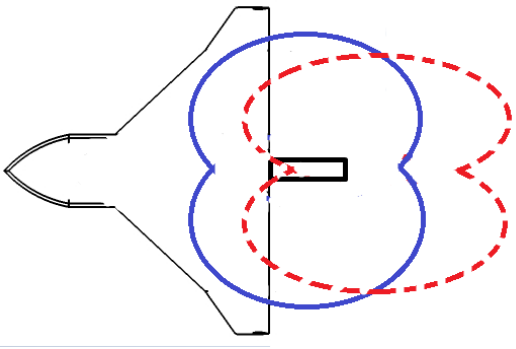

Figure 6.36: Mirroring effects (intermittent pattern) on the radiation pattern of the antenna compared to an undisturbed continuous pattern.

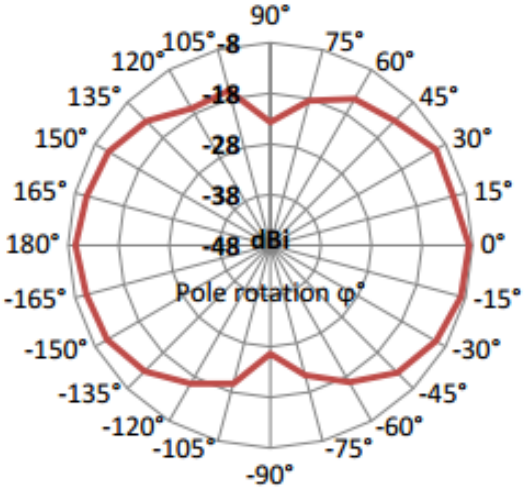

Figure 6.37: Radiation pattern reference UHF antenna.

6.5.2 Actuation

There are three components which require independent actuation in the system: elevons, canards and the deployment of the antenna. These are discussed separately below.

Control Surface Servo

For the actuation of the elevons and canards, four servos are used. The driving selection criteria here are the torque, operative temperature range and power consumption. Since the payload is quite small, very little torque is needed to move the control surfaces. From a controllability analysis it can be concluded that 0.084 $kg{\cdot}cm$ is necessary. Based on these criteria, high duty aluminium wing servos DS65-K from MKS were selected. These provide a torque of 2.2 $kg{\cdot}cm$ with a weight of 6.5 grams. To control these servos four PWM connections are used, which is also compatible with most flight computer systems. Since the operative temperature range of the electronics is desired to be $-40°$ to $60°$, insulation has to be applied around the servos, as they only have a minimum temperature of $-10°$. A possible solution for insulation is paraffin that is commonly used in aerospace systems .[31]

Release Activation Mechanism

The UHF antenna is spring loaded and will deploy after being released by the Lynx Mark I. The activation mechanism of this release should be lightweight, low cost and low power consuming. With these driving factors, a solution where a wire is cut through high applied heat has been selected. The wire made of Dyneema®, which is ultra high molecular weight polyethylene, holds the spring that extends the UHF antenna down during launch. When the Lynx deploys the payload, the connector (alternative power supply) will be detached. This will signal the payload that is has been deployed. This signals the flight computer to power one of the General Purpose Input/Ouput (GPIO) lines, which is connected to a redundant burn resistor that touches the Dyneema® wire. The applied heat will burn through the wire and unlock the spring to release the UHF antenna. This technique is commonly used on cubesats to deploy antennas.

The heating of the resistor (Joule heating) is described by Equation 6.45.

$$\Delta T = \frac{\Delta Q}{C} = \frac{P{\cdot}\Delta t}{m{\cdot}c} \tag{6.45}$$

Where T is temperature, Q thermal energy, C heat capacity, P power, t time, m mass and c specific heat. Since Dyneema® wire melts at $144°C$, the desired ΔT should result in the temperature being above this melting temperature. This can be achieved with an 0402 resistor that can reach temperatures up to $250°C$ and has

a specific heat of 1 $J \cdot g^{-1} \cdot K^{-1}$ whilst weighing only 1 mg. With a power applied of 0.1 W for 1.44 seconds, the temperature change of 144°C could be achieved.

6.5.3 Navigation

To have autonomous navigation capabilities, the payload has to know its position, velocity, attitude, angular acceleration and control derivatives. The first four variables can be found with a Global Positioning System (GPS) and an Inertial Measurement Unit (IMU). Important to note is that a GPS also needs an L-band antenna to function. These components are discussed in the sections below.

GPS and IMU

For the GPS and IMU function, weight, size, operating conditions and power consumption are driving parameters. Keeping this in mind, the VN-200 from VectorNav has been selected. It combines both in a very small size factor and is used in extreme environmental conditions for aerospace applications. Additionally, it uses Kalman filtering algorithms and also has a magnetometer and barometer included. The interface is performed through UART also at a bit rate of up to 921600 *bps*.

GPS Antenna

The antenna of the GPS has to be small in volume and low in power consumption. Important to note is that it cannot be hidden within the fuselage, as the radiation from the antenna will not go through the titanium skin. Thus the volume factor plays an even bigger role in the selection of the antenna. With this in mind the aerospace grade AM15-S from SANAV is selected. It is the smallest GPS patch antenna on the market today with a very low power consumption. This antenna will be placed below a patch of non conductive Torlon® in the top part of the fuselage to always be pointing towards the sky and allow the radiation waves to pass through. This is essential, since patch antennas are very directional in their radiation pattern.

6.5.4 Command and Data Handling

The command and data handling segment sends out commands and receives and redistributes data to the corresponding components through the flight computer. Next to that, additional memory might be necessary to store flight data and communication data. In this section, the above mentioned systems are discussed, and the data handling architecture is explained.

Flight Computer

With the actuation, sensing and communication components of the electrical subsystem being defined, an appropriate flight computer can be selected. The driving selection criteria here are the interface ports, computing power, size and power consumption. The computer should have 4 PWM lines, 2 UART lines (both Tx and Rx) and 1 analog GPIO line. Additionally, it is preferred that it also offers functions from a power supply by distributing appropriate voltages to the different components.

With the most important parameters defined the space grade NanoMind A3200 from GOMspace was selected. It offers all the necessary interface lines and has a very small size and power consumption. It uses an Atmel 32-bit Micro Controller Unit (MCU) which is performance efficient and provides a 32-bit architecture. It also provides 128MB of NOR flash, which does not require power to store data (ie. non volatile memory). With a flash capacity of 512 kB it offers sufficient computing power, as it is commonly used in cubesat missions which have similar mission objectives and requirements. Moreover, this computer also includes a gyroscope and magnetometer to determine attitude and magnetic field strength. This results in attitude determination being fail safe as it can be determined by the flight computer and the IMU.

Additional Memory

The flight computer has a flash memory of 128 MB, which for the given maximum data rates of the UHF antenna, GPS and IMU would be insufficient as they could generate up to 841 MB with a two hour flight time.

Thus a micro sd card could be connected through a Serial Peripheral Interface (SPI) to the flight computer to extend the storage capabilities by several gigabytes at very little extra cost, mass and power consumption. This would only be necessary if all the flight data has to be recorded. As follows it is left as a design option for the user and its intended purpose.

Data Handling

The data handling system distributes data and commands from and to specific system components as can be seen in Figure 6.38.

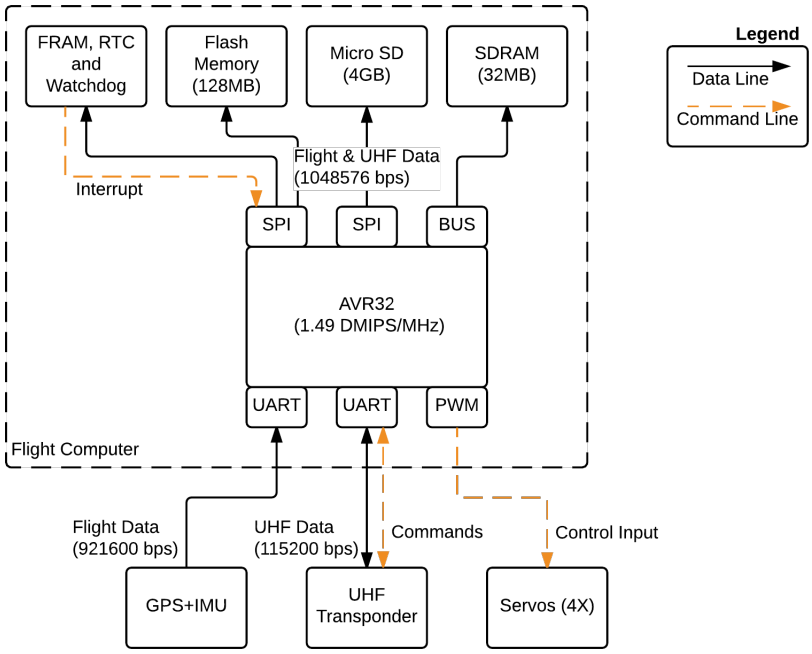

Figure 6.38: Data handling diagram with continuous data lines and intermittent command lines.

It can be observed that at the core of the system, the high performance and low power AVR32® microprocessor can be found. It interfaces all components with a 32-bit Reduced Instruction Set Computing (RISC) architecture. This architecture reduces the necessary amount of computing cycles per CPU instruction. Also, the 32 bit data buses and registers offer IEEE 754 floating point support, which is important for computational accuracy. Moreover, the computational power of this processor is 1.49 Dhrystone Million Instructions per Second (DMIPS) per microsecond. This enables the data handling system of storing data at rates of 1 Mbit/s to the four memory locations (i.e. SDRAM, micro SD, flash and FRAM).

The flash memory of 128 MB provides easy access storage of data and the micro SD card extends this memory capacity by four gigabytes. Both are connected through SPI and provide more storage than can be generated and received during the entire mission. The RAM can also be extended with 32 MB of Synchronous Dynamic Random Access Memory (SDRAM) and 256 Kb of Ferroelectric Random Access Memory (FRAM). For the former this means that the RAM is optimised for the processor clock speed and thus more instructions can be performed. For the latter this means that the non-volatile memory can undergo much more write-erase cycles. The FRAM is part of the FM33256B processor, which also includes a watchdog and Real-Time Clock (RTC). The watchdog will reboot the system when the AVR processor does not send out signals anymore, to prevent the system from crashing.

Interfacing with the GPS/IMU and UHF transponder is done through UART at data rates of 921600 and 115200 bps respectively. The flight data comes from the GPS/IMU module and the UHF data and commands are to and from the UHF transponder. Finally, PWM command signals are sent to the four servos controlling the canards and elevons.

6.5.5 Power

To power all the components a source of energy (battery and Lynx power supply), a connection (wiring) and a distribution system (power regulator) have to be selected. These are discussed individually in the sections below.

Battery

The driving requirements for the battery are the temperature range, power density and power volume. Furthermore, the battery should have a capacity of at least 10.11 Ah, which includes a 70% duty cycle. The voltage should be around 3-5 V with a maximum discharge current of at least 4 A. Finally, the temperature range should be at least from -40 to 60 °C. These values come from the total power budget, which is given and discussed in Section 6.5.6. With the total power of all the components and the voltage of the battery, the required discharge current can be found. It is also important to take the required capacity into account based on a two hour flight time estimate.

With this in mind, the aerospace grade M20HR battery from Saft was selected. It is a lithium manganese dioxide battery with a capacity of 11.5 Ah at 3 V with a maximum discharge current of 4 A. Moreover, it has an operative temperature range of -40 to 70°C.

Power Regulator

The function of the power regulator is to adjust the voltage and current of the battery to that of the components. This is necessary for the link between the battery and the flight computer, but also for the link between the battery and the servos. A voltage regulator is a very cost effective solution with low volume, mass and power requirements. Thus, two types of step-up voltage regulators have been selected. The first one converts 3 V to 3.6 V and the second one 3 V to 4.8 V. Two more step down voltage regulators are required to convert the Lynx supplied voltage of 28 V to 3.6 V for the flight computer and 3 V for recharging the battery. Since these conversions do not have a 100% efficiency, there is a power loss estimated at 0.015 W for 95% assumed efficiency.

Wiring

For the wiring initial sizing, two circuit segments are considered. Firstly, the wiring between the battery and the voltage regulators at 3 V and 4 A is analysed. This requires 15 American Wire Gauge (AWG) copper wire which has a maximum rating of 4.7 A and a diameter of 1.45 mm. With an estimated length of 20 cm at 3 V and 4 A, the total power loss of the wire can be computed to be 0.017 W. Secondly, the wiring between all other components is considered and simplified to be at 3.6 V and 0.8 A. This requires 29AWG copper wire which has a maximum rating of 1.2 A and a thickness of 0.29 mm. With an estimated length of 1 m at 3.6 V and 0.8 A, the total power loss of the wire can be computed to be 0.43 W.

Lynx Connector

The payload will be linked to the power supply to the Lynx with a connection running through the back of the fuselage and the box into the payload bay. There are two reasons for this design option. Firstly, the payload might be put inside the Lynx for an extended period of time before launch. This means that the battery would discharge a little and not be able to be deployed at full capacity. Secondly, this offers an easy way for the payload to know that it has been deployed, as it will be able to deduce that from the external power supply being cut off when deploying. Thus no other communication link will have to be implemented, reducing cost and complexity. The power supplied by the Lynx is 28 V at maximum 1 A, implying that two voltage regulators are required to convert the 28 V to 3.6 V for the flight computer and 3 V for recharging the battery.

6.5.6 Electrical Subsystem

As can be observed, most of the components are COTS components, except for the UHF antenna. This has the benefit of being cheaper and more reliable, as most components originate from aerospace industries. A total overview of the electrical subsystems can be found in Table 6.9.

Table 6.9: Electrical subsystem components.

Component	Voltage $[V]$	Current $[mA]$	Power$[W]$	Temperature range $[°C]$	Mass $[kg]$
GPS sensor	3.6	139	0.5	-40 to 85	0.016
GPS antenna	3.6	10	0.04	-40 to 85	0.004
Servos (4X)	4.8	380	7.3	-40 to 60	0.026
Burn resistor	3.6	28		-55 to 250	0.000001
UHF transponder	3.3	800	2.64	-40 to 60	0.0245
UHF antenna	3.6	278	1	1604 (max)	0.0043
Flight computer	3.3	40	0.13	-40 to 60	0.014
Power regulator	3 (in)	4000 (in)	0.015	-40 to 85	0.04
Wiring	3, 3.6, 4.8	4000, 800, 380	0.41	-40 to 75	0.0035
Battery	3	4000	12	-40 to 72	0.117
Total	-	-	12.13	-40 to 60	0.23

It can be observed that the total electrical system mass is only 230 gr, which is relatively little compared to the total payload mass. Important to note is that the total wattage of 12.13 W seems to not fit the 12 W battery. This is, however, not true as all the components will not be turned on at the same time. Additionally, the UHF transponder only uses 55 mA when receiving, which is half of the time with the communication link being half duplex. Also, the servos will not be working at max power most of the time. Taking this into account a power of 7.16 W is estimated as average power consumption throughout the mission lifetime.

As can be seen the electrical power subsystem has to be kept in a temperature range of -40 to 60 $°C$. This is mainly done by heat shielding the underside of the fuselage with heat resistant material. If this would prove to be insufficient in further analyses, paraffin wax can be applied around this subsystem. This would take up excess heat by being a phase changing material that turns into liquid when heat is added.

To get an oversight of all the different interactions between the components, the data and power lines are given in an electrical block diagram found in Figure 6.39.

As can be observed from this diagram, there are two power sources for the system. The first one is the Lynx power supply, which powers the flight computer and recharges the battery when the ICARUS+ is still inside the Lynx. For this, two voltage regulators are used to convert the 28 V to the appropriate voltages. After release, the connection with the Lynx is ruptured and the whole system is powered by the 3 V onboard battery going through two voltage regulators. When the GPS and IMU detect that the payload can be released from its containment box, the burn resistor is turned on for a few seconds. This burns the Dyneema® wire holding back the spring release mechanism, which is responsible for release from the containment box and deployment of the UHF antenna. Finally, the flight computer distributes and receives data and commands from the UHF transponder, receives flight data from the IMU/GPS and sends commands to the servos to control the canards and elevons.

6.6 Thermal Control

The ICARUS+ is subject to a wide range of temperatures. The payload bay is exposed to the outside atmosphere during the launch, but the rocket engine of the Lynx is also located right next to this payload bay and further tests by XCOR should be done to identify this temperature envelope. After deployment the ICARUS+ is only inb contact with the outside air. This temperature envelope depends on two factors, the altitude and the heating due to friction and compression of the surrounding air. The first one is determined by the flight path and the second one is difficult to determine without the use of complex CFD models and is therefore estimated with the flight speed.

6.6.1 Thermal Envelope

The altitude and velocity versus the flight time are determined in section 6.4. This is converted to temperature versus time using the International Standard Atmosphere (ISA) model which can be found in Section 7.1. Without experimental data it is difficult to predict the exact temperature range of the design during its flight.

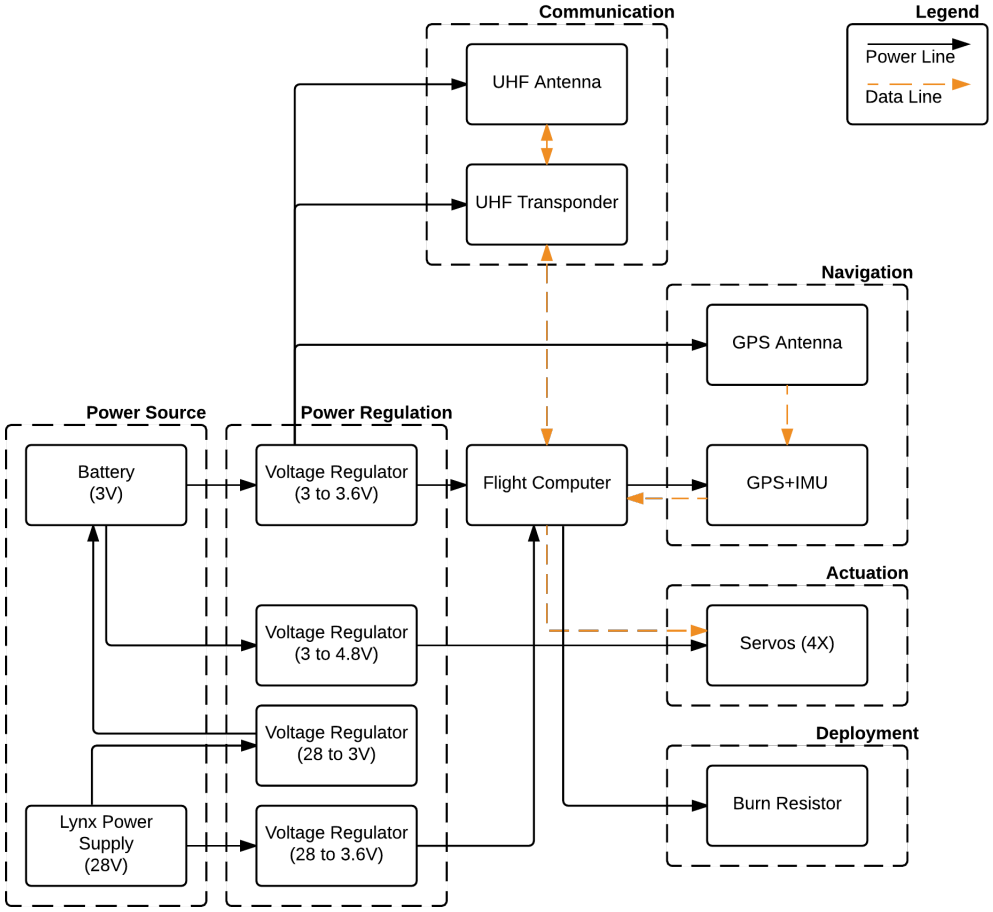

Figure 6.39: Electrical block diagram with intermittent data and command lines and continuous power lines.

However, the stagnation temperature can be estimated based on the the outside air temperature and the true airspeed at each point of the trajectory. Due to the small size and lack of reference data or actual test data it is assumed that the stagnation temperature will propagate throughout the entire fuselage. The stagnation temperature is computed using Equation 6.46.

$$T_{stagnation} = (1 + \frac{\gamma - 1}{2} M^2) T_h \tag{6.46}$$

Where $T_{stagnation}$ is the temperature in the stagnation point, γ the specific heat ratio of air, M the mach number and T_h the temperature at a certain altitude. The expected thermal envelope can be seen in Figure 6.40. The temperature spike in the first part of the graph is induced by the high velocity of the first part of the trajectory. After 500 seconds the difference between the stagnation temperature and the ambient temperature becomes negligible.

6.6.2 Simulation Model

The next step is setting up a model that is representable, whilst keeping limited computing resources- and time in mind. For these reasons a 1D plate model was chosen to compute the transient response of varying insulation thicknesses. 1D models assume that the width and height of the plate are much larger than the thickness and therefore can be seen as perfectly insulated. This is a very rough estimation as our entire design is small, but given the two major constraints it is the best option to get a sense of the necessary insulation thickness. The model consists of two layers, the first resembles the titanium outer skin and the second resembles the insulation layer, which

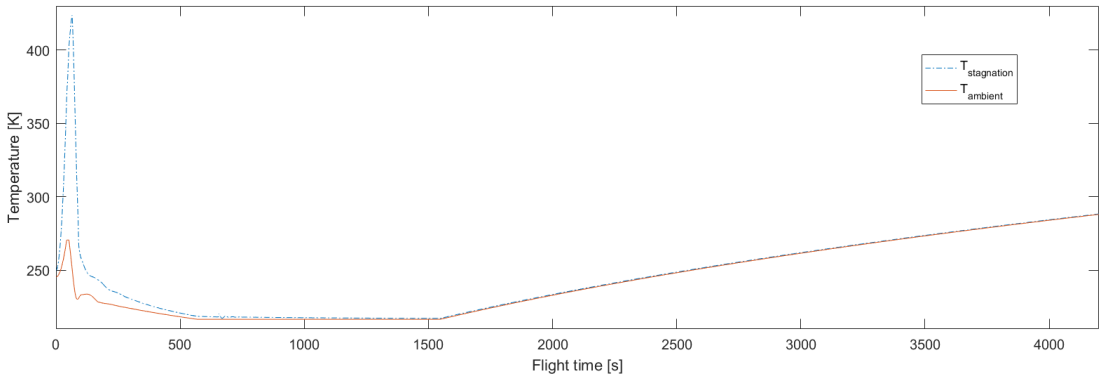

Figure 6.40: Ambient air temperature and stagnation temperature versus flight time.

is made from Silica Aerogel, because it has both a very low density and a very coefficient of thermal conductivity [1].

This model is then made in ANSYS® Mechanical for the transient thermal analysis. A 2D plate can be modelled as a 1D problem by putting perfectly insulated boundaries on the 4 sides of the plate. The plate is also meshed in this program. The effect of refining the mesh on the results and computation time can be seen in Figure 6.42 and Figure 6.41. Refining the mesh along the thickness has a negligible effect on the results. However, the required computational time increases linearly with increasing mesh refinement. The face mesh does not affect the results, because of the 1D discretisation. To minimise the simulation time, a mesh of 10 divisions along the thickness is applied to all future simulations.

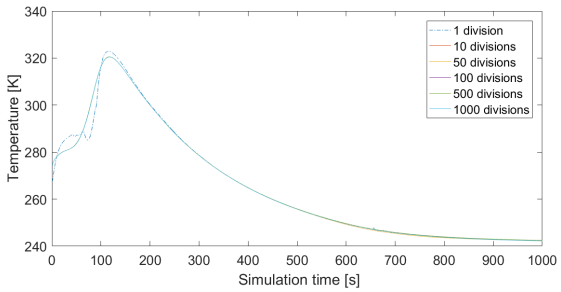

Figure 6.41: Result comparison with mesh refinement (3 mm insulation thickness, 7.16 W internal power generation).

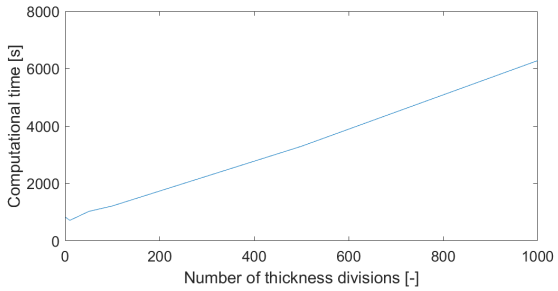

Figure 6.42: Computational time versus mesh refinement (3 mm insulation thickness, 7.16 W internal power generation).

Next, the temperature envelope is loaded as a time dependent table and is applied to the outside of the titanium skin. Finally the components on the inside of the fuselage also produce heat, this is modelled by scaling the average power consumption to the surface area of the inside of the fuselage compared to the surface area of the plate. There are three variables that can be changed to ensure the operating temperature of the internal components namely, the insulation thickness, the initial temperature and to some extend the power consumption of the internal components. The operating limits of the internal components are 233.15 K and 333.15 K and the average power consumption is 7.16 W which is seen as a fixed variable for now, these parameters can be found in Section 6.5.

6.6.3 Simulation Results

In total nine simulations were performed with varying insulation thicknesses and initial temperatures, the internal heat generation is kept the same for each simulation at the average 7.16 W. An overview of the simulation boundary variables can be found in Table 6.10.

[1] URL `http://www.matweb.com/search/datasheet.aspx?MatGUID=c864d25c235648d6b11711fd324b64d4&ckck=1` [cited 13 Jun 2016]

Table 6.10: Transient thermal analysis simulation settings.

Simulation	$t_{insulation}$ $[mm]$	$T_{initial}$ $[K]$	$P_{internal}$ $[W]$
1	4	268.15	7.16
2	4	273.15	7.16
3	4	278.15	7.16
4	3	268.15	7.16
5	3	273.15	7.16
6	3	278.15	7.16
7	2.5	268.15	7.16
8	2.5	273.15	7.16
9	2.5	278.15	7.16

The results of the simulations with an initial temperature of 273 K are displayed in Figure 6.43. The two horizontal lines represent the operational limits of the internal components. A safety margin of 5 K on both limits has been taken, so the lower limit is 238.15 K and the upper limit is 328.15 K. From these results it can be concluded that, with the same internal power generation, an increase in insulation will result in a lower heat spike in the supersonic part of the trajectory. Furthermore, the lower temperature bound shifts up and the end temperature increases.

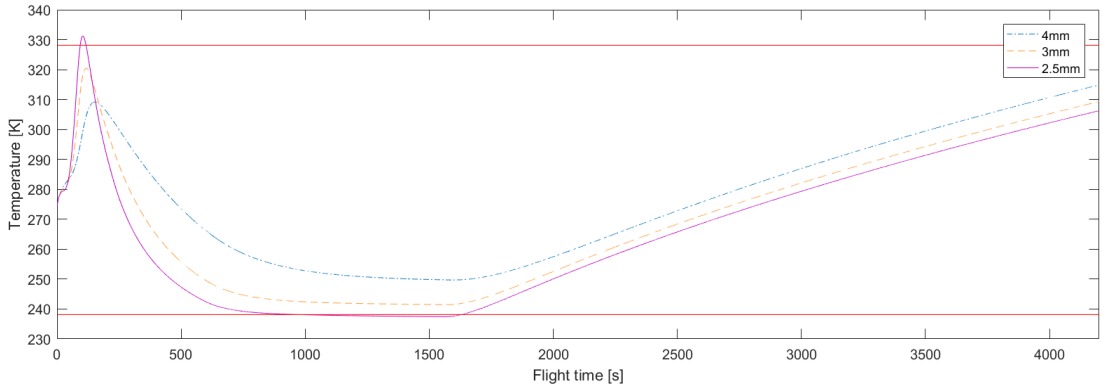

Figure 6.43: Internal temperature versus flight time with varying insulation thickness for an initial temperature of 273 K.

The effect of changing the initial temperature has less impact on the differences between the insulation thicknesses, as can be seen in Figure 6.44. It changes the starting temperature and it changes the temperature spike. A 5K increase in initial temperature results in roughly a 2.5K increase of the spike. After 500 seconds the difference becomes negligible.

The minimum and maximum temperatures of all the simulations can be found in Table 6.11. From these results it can be concluded that the minimum temperature only depends on the insulation thickness and not on the initial temperature. Furthermore the maximum temperature of the 4 mm insulation does not depend on the initial temperature, because the end temperature is actually higher than the spike temperature. Also, the lower bound of the internal temperature scales linearly with the insulation thickness. Taking the limited internal space into account, going for the smallest insulation thickness is desirable. 2.5 mm was not enough, but with the linearity and the 5K safety factor in mind, 2.6 mm of insulation should be sufficient. However, it should be stressed that further research and testing is necessary to minimise the risk of thermal failure.

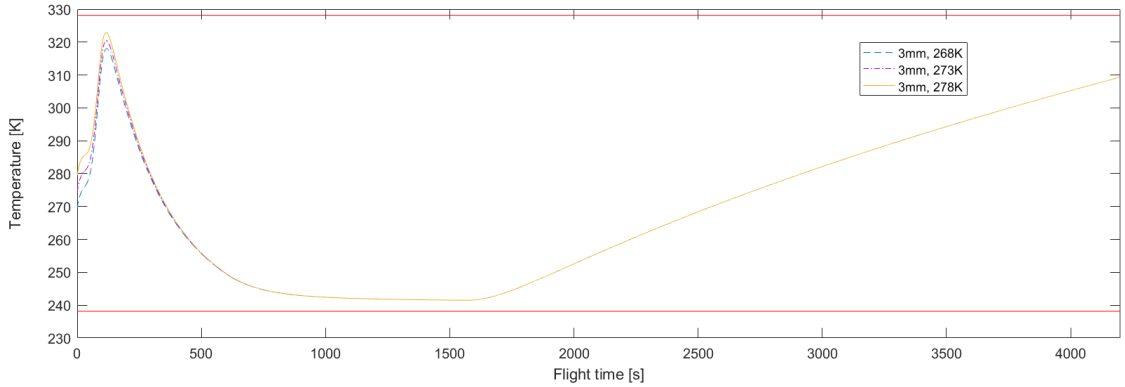

Figure 6.44: Effect on internal temperature with different initial temperatures with an insulation thickness of 3 mm.

Table 6.11: Minimum and maximum temperatures for the different insulation thicknesses and initial temperatures.

Simulation	$t_{insulation}$ $[mm]$	$T_{initial}$ $[K]$	$P_{internal}$ $[W]$	T_{min} $[K]$	T_{max} $[K]$
1	4	268.15	7.16	249.7	314.9
2	4	273.15	7.16	249.7	314.9
3	4	278.15	7.16	249.7	314.9
4	3	268.15	7.16	241.5	318
5	3	273.15	7.16	241.5	320.5
6	3	278.15	7.16	241.5	323
7	2.5	268.15	7.16	237.4	329.4
8	2.5	273.15	7.16	237.4	331.2
9	2.5	278.15	7.16	237.4	333.1

Chapter 7

Verification and Validation

During the performance analysis multiple models were used to analyse the design. All these models need proper verification and validation, which is discussed in this chapter. First of all the ISA model is verified and validated. This model is used in several other models. Secondly the flight mechanics model is discussed followed by the stability height model. Afterwards the aerodynamics analysis is verified and validated and the structural analysis is discussed. Finally the Thermal analysis is discussed For each model the assumptions are stated followed by the verification and validation method.

7.1 ISA Model

This model has been developed in order to provide the atmospheric values at a given altitude to both, the Stability & Control- and the Flight Mechanics group.

Assumptions

The assumptions made for this model are listed below:

- Geopotential altitude is used.
- Humidity of the air is neglected.
- Air is considered to be a perfect gas. (R and γ are considered for air)
- Air is assumed to have the same composition everywhere and always. For example the Ozone layer is neglected.

As these assumptions have not been explained in the text yet, their effects are stated in this section. Using geopotential altitude assumes a changing gravitational acceleration. This results in ta more realistic pressure, density and temperature at higher altitudes. Humidity is neglected because the exact weather conditions are unpredictable. These differences can be quite big, however they are largest at very low altitudes, which only represent a really small percentage of the entire flightpath. Here the density of the air and also the pressure might change (and thus the temperature will change as well, especially in tropic areas). Furthermore the humidity also affects the values of R and γ. These values might also be subject to change at certain altitudes such as the Ozone layer. The reason this is neglected is its small size of a few millimetres, which the ICARUS+ will pass in a fraction of a second.

Verification

Verification of this model is relatively straight forward as the model is simply using the gas law (Equation 7.1) and the relations between temperature, pressure and density (Equations 7.2 and 7.3).

$$p = \rho R T \tag{7.1}$$

$$dp = -\rho g dh \tag{7.2}$$

$$T = T_0 + a(h - h_0) \tag{7.3}$$

Syntax errors have been indicated by the compiler. Randomly setting values to zero will result in an error in the compiler and thus give the expected result. There are no differences between the values obtained from the computer model and the analytical calculations, as in this case the program has more the function of an extensive calculator rather than using complex numerical methods to obtain results. Thus it is of no use to further explain the values obtained in the verification process.

Validation

In order to validate the functions used for the ISA model, data-check points at different altitudes have been compared to the obtained values. As the standard atmospheric values are by definition commonly used in aerospace, the values of the program are exactly as the ones that can be found in literature .[32] The checked points are summarised in the Table 7.1.

Table 7.1: ISA values from the course Introduction to Aerospace Engineering .[32]

Geopotential Altitude $[m]$	ISA Pressure $[Pa]$	ISA Temperature $[K]$	ISA Density $[kg \cdot m^{-3}]$
0	101,325	15.0	1.225
11,000	22,632	-56.5	0.3639
20,000	5,474.9	-56.5	0.0881
32,000	868.02	-44.5	0.0132
47,000	110.91	-2.5	0.0014
51,000	3.564	-2.5	0.000845

7.2 Flight Mechanics Model

The flight mechanics model has been developed during this project using Matlab®. It is customised according to the needs of the mission of this project. In this section, the assumptions will be listed first. After this, the verification and validation of this program will be explained. A functional flow block diagram can be found in Appendix C.

Assumptions

During the computation of the flight path, there are some assumptions (also mentioned in Section 6.4.1) that will effect the computed flight path. These assumptions are categorised by primary assumptions and secondary assumptions. The primary assumptions will have a significant influence on the computed flight path. The secondary assumptions will have no significant contribution. The assumptions are listed below. The specific effects will also be elaborated on.

Primary Assumptions

- At the instant that the flight mechanics model initiates the computations, the payload is assumed to be perfectly stable. In reality, it is possible that the payload is not perfectly stable at the initiated altitude. The effect of this assumptions depends on the level of stability of the payload. An unstable payload would decrease the total range, because it would get harder to maintain the C_L values that are computed for optimal flight.
- The decrement of the lower boundary of the stratospheric altitude from the equator to the poles has been linearised. This could make a little difference on the overall flight characteristics, since the stratospheric range contains an assisting wind. This will effect the total flight time. This is due to the face that the the altitude of the lower boundary occurs during the gliding phase, at which the angle is already fixed for optimal glide. However, the velocity would change due to the assisting wind.
- The model assumes that it has to descent to sea level. However, if there are for example high mountains, than the payload would stop flying or crash earlier during its flight. This makes a significant difference regarding the total range. If the payload would hit a high mountain, the total range would become much less, because it could not fly any longer.

Secondary Assumptions

- The Earth is assumed to have a constant mass distribution. This will not have a significant impact on the trajectory, since the fluctuation in gravitational acceleration is low (9.7639 $m \cdot s^{-2}$ - 9.8337 $m \cdot s^{-2}$).
- The Earth is assumed to be a perfect sphere. This does not have a significant effect on the total displacement of the payload, since the Earth is an almost perfect sphere and the scale on which the ICARUS+ is operating is relatively small compared to the scale of the Earth.
- The gravitational influences of the Moon and the Sun are neglected. This does not has a significant influence on the computations, since at an altitude of 60 km the Earth is far more dominant.
- The velocity changes due to the stratospheric winds are implemented immediately, instead of using an iteration over time. This would not make a significant change, since the time iteration would be short. Also the upper boundary of the stratosphere could fluctuate a bit, so these effects would cancel each other out.
- Accelerations are assumed constant over a time step. However, since the period of time is very small (< 0.001 s), this effect is negligible.
- For the flight path a point mass is assumed, this will have a negligible effect since the ICARUS+ is so small.
- The latitude does not change during flight. It is only implemented as an initial condition. This will not make a significant change on the computations.

Verification

There are different kinds of tests with which we can verify the model. For example, when the C_L and C_D would be zero, the flight path would be a simple free fall. The verification tests are listed below:

- Setting C_L and C_{D_0} to zero and gravitational acceleration constant should lead to a simple free fall. The velocity after a free fall from 60 km altitude can be computed as follows:

$$a \cdot ds = v \cdot dv \tag{7.4}$$

$$9.81 \cdot 60000 = 0.5 \cdot V^2 \tag{7.5}$$

$$V = 1085 \ [m \cdot s^{-1}] \tag{7.6}$$

  Performing this in the model leads to a velocity of V = 1085 $m \cdot s^{-1}$. This corresponds to the value from the analytical solution, provided above.
- Setting all surface areas to zero should give the same result as above. Implementing the value zero for the surface areas in the model leads to a velocity of V = 1085 $m \cdot s^{-1}$, which is the same result as the analytical solution.
- If the ICARUS+ has a larger initial horizontal velocity, then the range should become higher. This can be tested by implementing such a value in one of the models. If for example the first model would have a inertial horizontal velocity of 10 $m \cdot s^{-1}$, then the range goes for example from 157 km to 161 km. This is indeed higher, so this verification test is correct.
- If the lifting surface areas would slightly decrease, the gliding path should be less steep. This is due to the fact that the lifting surface areas is a part of the aspect ratio. When the area of the lifting surfaces decreases and the span stays constant, the aspect ration increases. The aspect ratio contributes to the computations of the optimal C_L value for gliding flight (see Equation 7.7) and the C_D (see Equation 7.8) values.

$$C_L = \sqrt{C_{D_0} \pi A e} \tag{7.7}$$

$$C_D = C_{D_0} + \frac{C_L^2}{\pi A e} \tag{7.8}$$

  For an increasing aspect ratio, the value for C_L should increase and the value for C_D should decrease. This would increase the C_L over C_D ratio during glide, due to which the gliding path should be less steep. This has been tested and confirmed.
- A lower stability height should decrease the overall range, since less altitude is left to glide from. This has been tested and confirmed.
- During optimal glide, the induced drag and the profile drag should be perfectly equal to each other. The flight mechanics model approves this, so the implemented drag model can be verified.

Validation

The validation for this model is relatively hard to set up. The specific approach is not a commonly used approach, due to which their are no reference materials to compare with. There would be several tests possible to validate the model.

It is possible to drop a small scale aircraft nose down from a certain altitude, while the attached wings have an initial angle. This will result in a certain C_L, after which the flight path could be analysed. This should have the characteristics of the pullout manoeuvre.

Another approach could be to centrifuge a rock, after which it is analysed at which detaching angle it would have the longest range. This could validate the approach that an angle of 45 degrees is the optimal angle to stop lifting the payload after the pullout.

7.3 Stability Height Model

The program used for the stability height is a comprehensive version of the program used for the mid-term analysis.[4] The biggest difference is that it is now a three dimensional model instead of a two dimensional model. In this section the assumptions of this model are stated with their effect and afterwards the model is verified and validated. The ISA model, vfrom Section 7.1, is used in this model. In Appendix C the functional flow diagram of the model is shown. The model is written in Matlab.

Assumptions

In this program there are some assumptions made that will affect the final results to a certain amount. These assumptions are divided into primary assumptions and secondary assumptions, where the primary assumptions will have the largest impact. Apart from the following list all the assumptions stated in the flight mechanics verification and validation section are also used. These assumptions can be seen in Section 7.2.

Primary Assumptions

- Lift is assumed to be zero at transonic and supersonic speeds. At these speeds very small angles of attack are flown with, which gives a very small lift coefficient. At transonic and supersonic speeds this lift coefficient will be even smaller, therefore for now it is assumed to be zero. This will have an minor acceptable effect since the lift coefficients are really small compared to drag coefficients at these speeds.

Secondary Assumptions

- Accelerations are assumed constant over a small period of time. However since the period of time is very small (< 0.0001 s) this effect is negligible.

Verification

In this section the verification of the stability and control model is given. Each block of the functional flow diagram (Appendix C) is verified followed by the verification of the entire program.

Lift and Drag Calculation

First of all the lift and drag are calculated at every time step. The formula used for the lift and drag calculation can be seen in Equation 7.9 and 7.10. The same values are found if this calculation is done manually. The values for the drag coefficient differ per Mach number, angle of attack and Reynolds number, these values are received from the Aerodynamics group and are verified and validated in that section (Section 7.4).

$$D = C_D 0.5 \rho V^2 S \tag{7.9}$$

$$L = C_L 0.5 \rho V^2 S \tag{7.10}$$

Flight Path

In order to verify the second block of the program, which is the velocity and altitude simulation, the velocity is set negative, which states that the payload is going up. At a certain moment the velocity should go down due to gravity forces, in the simulation this happens. These values can be checked by using the equations of motion for a projectile stated in Dynamics from Hibbeler .[33] In the model the drag is set to zero, since that is also a contribution to the acceleration next to gravity. Furthermore the gravitational acceleration is set to a constant value. When calculating, the same numbers are found for chosen moments in time for velocity and altitude. The governing equations are shown in Equations 7.11 and 7.12. Concluding, the falling simulation is verified.

$$V = V_0 + at \tag{7.11}$$

$$h = h_0 + V_0 t + \frac{1}{2} a t^2 \tag{7.12}$$

Moment Calculation

The moment calculation can also be seen as one big calculator, once a force is given a moment will be calculated. When calculating these moments by hand at several orientations of the ICARUS+ exactly the same values are found as the ones found by the program. Furthermore when the neutral point and the centre of gravity have exactly the same location all the moments will be zero, this is also verified in the program.

Angular Acceleration - Velocity - Displacement

If the moment is zero the angular acceleration is also zero, and this can be seen in the results. This principle is based on the second law of Newton. Furthermore if the moment is huge and lasts for a long time it can be seen that the rotating motion of the product is also huge and infinite.

Change in control surfaces

If the acceleration is set to zero the angular velocity will also be zero and the angles of orientation around the three axis will all be constant. An input of a control surface is a moment which will be added for a small period of time, this will result in an angular acceleration. This is tested and verified when a change in orientation can be seen with the same magnitude as expected by using the moment-acceleration equations based on Newton's second law.

Entire program

If the velocity is going upwards the payload should stabilise with its nose directed upwards, that is its centre of gravity pointing up. This can be checked by running the entire program simultaneously. While the payload has a velocity going upwards it can be seen that it stabilises the other way around compared to when it is falling down. After a certain time the payload will start falling downwards and stabilise around the opposite angle. Concluding the entire program is verified.

Validation

So far no validation has been done yet for this program since there is no real reference data for it. However, in a later stage sections of the program could be quality checked.

To validate the velocity profile values of a re-entry vehicle can be used. The initial velocity and altitude of the simulation program can be changed so that the re-entry vehicle will be simulated. The outcomes of the program and the re-entry can be compared. The rotation of the payload also has to be validated in a later design stage, however for now no appropriate reference data is found.

7.4 Ansys: Fluent®

In this section, the verification and validation of the software used for the aerodynamic analysis is discussed. This program, Fluent®, is discussed in Section 6.1.1.

Assumptions

- The flow is steady, the inlet flow shows no accelerations, in reality the flow will show small perturbations but this can be assumed to be negligible.
- Turbulence is assumed to be correctly modelled by the K-omega SST turbulence model. This model is can accurately model turbulence close to the body and is widely used for similar simulations.
- Flow is uniform and thus equal in magnitude and direction at the boundaries.

Verification

In order to make sure the settings used when running the simulations are resembling reality, a verification procedure is established. The program is run using the same settings as used for the analysis, for a number of geometries at Reynolds numbers for which experimental data is available.

First, a NACA 0012 airfoil incorporated in a rectangular wing with span of 2m and a chord of 1m is placed in the same enclosure as used for the performance analysis. Experimental data is available for the lift and drag of the NACA-0012 airfoil. This data is for the 2D airfoil and has to be corrected before it can be used as a comparison. The correction is done using equation 7.13 as obtained by H. B. Helmbold, valid for low aspect ratio wings. This equation is based on a standard slope of 2π per radian for 2D airfoils. Which can also be observed in Figure 7.1, which shows experimental data of the NACA-0012 airfoil at a Reynolds number of $6{\cdot}10^6$.

$$C_{L_\alpha} = \frac{a_0}{\sqrt{1+\left(\frac{a_0}{\pi A}\right)^2}+\frac{a_0}{\pi A}} \tag{7.13}$$

Filling in this equation for an aspect ratio of 2 produces a slope of 2. per radian. In Figure 7.2 the experimental curve together with the corrected version and the results of the simulation are presented. The simulation is performed using the wing described above at a Reynolds number of $6{\cdot}10^6$. The Reynolds number is calculated using Equation 7.14, using sea level conditions and a chord of 1 meter. This means that the simulation will be performed at a Mach number of 0.26 or V = 88.4 m/s. Looking at the corrected curve and the results of the simulation it can be seen that only a small difference can be observed. The exact errors at the measurement location are shown in Table 7.2. The aforementioned results prove that the software accurately simulates the 3D effects of a finite wing on the lifting performance of a wing.

$$Re = \frac{\rho \cdot V \cdot \bar{c}}{\mu} \tag{7.14}$$

Table 7.2: Error of the simulation compared to the corrected verification data at a number of angles of attack.

	0°	5°	10°	15°
simulated C_L	0.0005	0.27	0.56	0.835
corrected experimental C_L	0	0.28	0.572	0.859
error	<1%	3%	2.2%	4.3%

Validation approach

Validation of the aerodynamic model can be done by comparing test data or data of comparable missions with the outcome of the model. However, since there are no comparable missions at this moment and the model is not tested yet, an approach on how to validate the model will be described here more than an actual validation.

When a model of the design is available, the size of the design allows it to be tested in a wind tunnel. Since the aerodynamic model is only capable at this moment to do a subsonic analysis, it is most important to test the model in a subsonic wind tunnel. Such a wind tunnel is present at the faculty of Aerospace Engineering.

[1] URL `http://turbmodels.larc.nasa.gov/naca0012_val.html`.

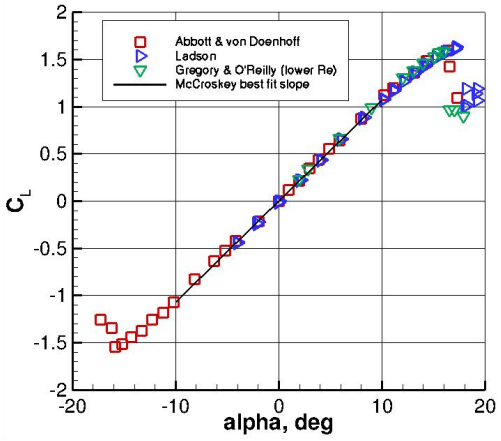

Figure 7.1: Experimental C_L - α curve for the NACA-0012 airfoil at a Reynolds number of $6 \cdot 10^6$. [1]

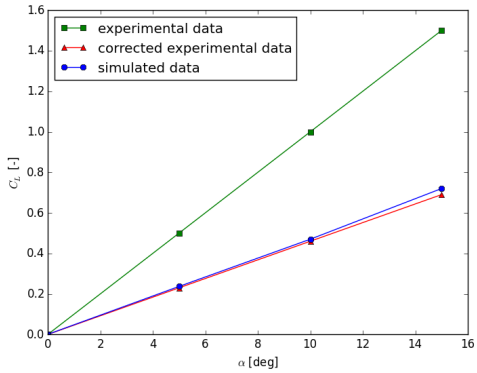

Figure 7.2: C_L - α curve comparison between (corrected) experimental simulated data, Re = $6 \cdot 10^6$.

After the test, the lift coefficient from the test can be compared with the lift coefficient from Fluent®. If these have a difference of not more than 10 %, the model can be considered validated.

7.5 Drag Model

In this section, the drag model used for aerodynamics is verified and validated. This model was explained in Section 6.1.4. First the assumptions made in the model are presented.

Assumptions

- The flow is assumed to be fully turbulent over the skin of the vehicle. This will underestimate the skin friction at very low Reynold numbers but will be more accurate at higher numbers, and thus be more useful over the entire flight path.
- The lift induced drag is assumed to vary with C_L^2, this is a widely used and accurate assumption and can be considered correct.
- The wave drag can be modelled by taking an equivalent ellipse with an equal span, area and volume. According to Kuchemann this gives accurate results.[34]

Verification

For the verification of the program a number of small tests are performed to make sure the program solved the equations correctly.

- The Parasitic drag is calculated by hand using the equations presented in section 6.1.4 and compared to the model output with the same inputs, and turned out to be correct.
- The lift induced drag calculation is verified with an analytical calculation of the drag for different lift coefficients. These results are compared to the model output.
- The transonic drag calculation is verified by comparing the results with analytical calculations. These turn out to be the same. The formula only simulates the drag rise and does not include the decline that can be seen on Figure 6.15. Since no analytical expressions are available, a comparison to real life data is used to verify the shape of the drag decline, and is considered verified.
- The wave drag components due to lift and volume, as represented by Equations 6.11 until 6.14, are verified by comparing the results to analytical calculations.

- The complete model is verified by adding the components of the drag relevant for a number of Mach numbers and comparing to the model output and turned out to be correct.

Validation

Validation of the program is done using drag data from a reference aircraft and comparing it with the model's output. The reference plane used is the Cessna 177. In Table 7.3 the parameters used as input for the drag model are presented. In Figure 7.3 the reference data is presented and Figure 7.4 shows the results of the drag model and the experimental data in one plot. As can be seen the data fits well with the estimation the model provides. This simulation is done at subsonic speeds, for the validation at supersonic speeds another experimental case is used.

The drag model is also used for the Concorde at supersonic speeds. In Table 7.4 the input parameters used for the Concorde are shown.[1] As can be seen the parameters for the tail are set to zero since the Concorde has no tail. In Figure 7.5 the reference data is presented and in Figure 7.5 the drag model results combined with the experimental data are shown. The data follows the same trend but has a slight offset as compared to the model outputs. The error reduces with increasing C_L and is therefore not considered a problem. This since the drag values are estimated to be slightly higher than reality, and thus on the safe side.

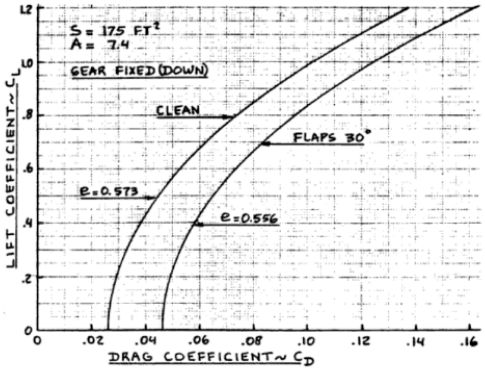

Figure 7.3: Experimental $C_L - C_D$ curve for the Cessna 177 at subsonic speed.[35]

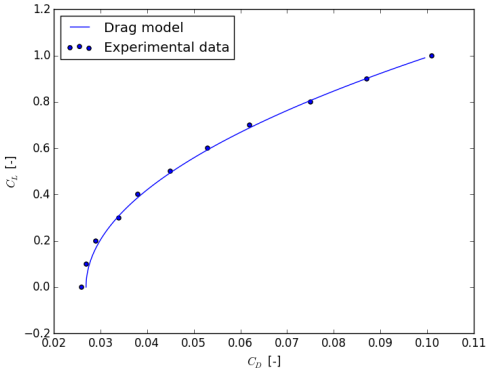

Figure 7.4: Drag model prediction compared with experimental data for the Cessna 177 at $Re = 14 \cdot 10^6$.

Table 7.3: Parameter inputs for the Cessna 177.

Parameter	Value	Unit	Parameter	Value	Unit
b	10.7	$[m]$	c_{wing}	1.52	$[m]$
A	7.5	[-]	c_{tail}	0.82	$[m]$
S_{wing}	15.2	$[m^2]$	$c_{fuselage}$	7.0	$[m]$
$S_{wet,wing}$	30.4	$[m^2]$	k_{wing}	1.2	[-]
S_{tail}	3.2	$[m^2]$	k_{tail}	1.1	[-]
$S_{wet,tail}$	6.4	$[m^2]$	$k_{fuselage}$	1.3	[-]
$S_{fuselage}$	4.7	$[m^2]$			
$S_{wet,fuselage}$	23.3	$[m^2]$			

[1] URL`http://www.concordesst.com/dimentions.html`[16 June 2016]

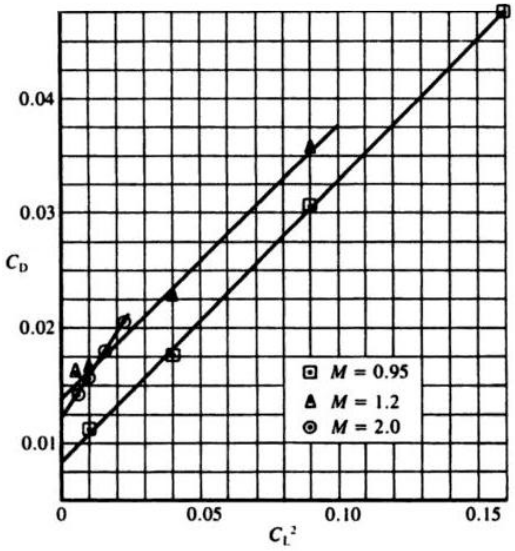

Figure 7.5: Experimental $C_D - C_L^2$ curve at different Mach numbers for the Concorde.[1]

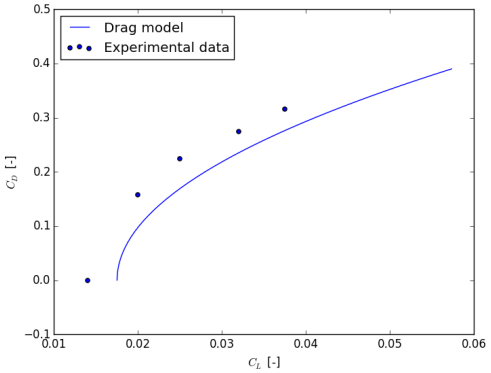

Figure 7.6: Drag model prediction compared with experimental data for the Concorde at M = 1.2.

Table 7.4: Parameter inputs for the Concorde.

Parameter	Value	Unit	Parameter	Value	Unit
b	25	$[m]$	c_{wing}	17	$[m]$
A	1.55	[-]	c_{tail}	0.0	$[m]$
S_{wing}	314.3	$[m^2]$	$c_{fuselage}$	70	$[m]$
$S_{wet,wing}$	629	$[m^2]$	k_{wing}	1.05	[-]
S_{tail}	0.0	$[m^2]$	k_{tail}	0.0	[-]
$S_{wet,tail}$	0.0	$[m^2]$	$k_{fuselage}$	1.1	[-]
$S_{fuselage}$	227	$[m^2]$			
$S_{wet,fuselage}$	579.5	$[m^2]$			

7.6 Wing box model

The wing box program is created in Matlab® and calculates the stresses in the wing box, which is the structural element in the wings. Because of the size the wing and the wing box are the same. To allow feasible calculations the wing box cross section was assumed to be rectangular. In this section the verification and validation of the wing box program are explained. For this the assumptions have been summed which are explained more extensive in section 6.3.4.

Assumptions

In this section the used assumptions will be stated.

- Maximum load factor: $n_{max} = 5$
- Factor of safety: $n_f = 2$
- Weight at moment of pull-up is two kilograms.
- Drag is scaled to lift by the glide ratio C_L/C_D.
- Wing box geometry is a rectangular box with width and height equal to the outer values of the airfoil size.
- Lift and drag are distributed considering a linear relationship with the cross section surface area and the frontal cross section area respectively.

[1] `http://gtae6343.wikia.com/wiki/File:Concorde_CD_CL2_drag_polar.jpg` [14 Jun 2016]

- Analytical methods are applied to calculate the stresses.
- Shear stress throughout the thickness of the skin is constant.

Verification

The program calculates the shear and normal stresses throughout the whole wing box. For the verification a simple straight wing box is given as an input. This means no taper, no dihedral and no sweep are implemented. Also the thickness throughout the wing box is constant. This allows verification by hand made calculations. Next to that the variation in thickness and the taper, dihedral and sweep are checked separately. One variation each time can be reasoned, something which becomes more difficult when more things are changed at the same time.

Validation

Validation of this model is difficult. No comparable planes which must perform a similar flight pattern exist and therefore validation by comparable concepts was not possible. Validation by different methods is difficult due to the required computational power and knowledge exceeds our resources. The most accurate validation it might be considerate to make a model of the structural part only and submit this to a bending test.

7.7 Thermal simulations, Ansys Mechanical®

In this section the verification and validation for the thermal simulations is discussed. The simulation were all performed with the software package, Ansys Mechanical®. First the assumptions are elaborated on, followed by the verification and validation.

Assumptions

To minimise the computational load a 1D or infinite plate model was chosen, to assess the thermal effect on the inside temperature. The following assumptions were used for this analysis.

- 1D transient problem, infinite plate.
- Sides of panel are perfectly insulated, this is done to make the actual 2D model represent a 1D scenario.
- Convective cooling/heating by the surrounding air is simplified by applying a temperature to the exposed surface, effectively replacing the convection by conduction.
- The temperature rise due to the airspeed is modelled by using the stagnation temperature.
- The heat transfer due to radiation is neglected to minimise computational effort and this transfer mechanism could be used to increase the temperature or decrease the temperature depending on the paint used on the final product.

Verification

The first two assumptions together form the basis of the simulation by converting the 2D model to a 1D problem, the settings in Ansys Mechanical® can be verified by applying the necessary boundary conditions to a single material plate and comparing the results with the expected values obtained using the Heisler chart. [36] The necessary conditions are, uniform initial temperature, constant surrounding temperature, constant convective heat coefficient and the body does not generate heat itself.

The panel has an initial temperature of 273.15 K and the front and the back of the panel are subjected to a constant 373.15 K air flow with a constant convective heat coefficient of 100 $W \cdot m^{-2} \cdot K^{-1}$.[1]The four sides have a perfectly insulated constraint on them, to ensure that the heat flow direction is from the panels to the middle only. Finally the panel itself does not generate any heat.

The next step is determining the Biot number and Fourier number for this specific plate, which are given by Equation 7.15 and 7.16. Where h is the convective heat coefficient, L_c is the effective length (halve the

[1]URL `http://www.engineersedge.com/heat_transfer/convective_heat_transfer_coefficients__13378.htm` [13 Jun 2016]

thickness for the symmetric plate), k is the thermal conductivity of the plate, α is the thermal diffusivity (Equation 7.17) and t is time.

$$Bi = \frac{hL_c}{k} \quad (7.15) \qquad \tau = \frac{\alpha t}{L_c^2} \quad (7.16) \qquad \alpha = \frac{k}{\rho c_p} \quad (7.17)$$

The plate is made from Silica Aerogel and as mentioned before the convection is done by dry air, all relevant values are summarised in Table 7.5. Using these values yields a Biot number of 16.67 and a Fourier number of $0.0143 \cdot t$. The Biot number is used to choose the corresponding line on the Heisler chart and the Fourier number translates the x value into the corresponding time.

Table 7.5: Variables for 1D thermal model verification.

Variable	Value	Unit
h_{air}	100	$W \cdot m^{-2} \cdot K^{-1}$
L_c	5	mm
$k_{aerogel}$	0.03	$W \cdot m^{-1} \cdot K^{-1}$
$\rho_{aerogel}$	100	$k \cdot m^{-3}$
$c_{p,aerogel}$	840	$J \cdot kg^{-1} \cdot K^{-1}$

The Heisler chart is used to find the time it takes for the midplane to get to 323.15 K and to 353.15 K. These temperatures are then compared to the temperatures of the simulation at the same time. The results are displayed in Table 7.6. The difference is sub 1%, which is negligible, so the simulation can accurately model the 1D transient thermal problem.

Table 7.6: Temperature comparison between Heisler chart and convection model.

Time $[s]$	Reference $[K]$	Convection model $[K]$	Difference [%]
28	323.15	320.4	-0.9
56	353.15	351.2	-0.5

Validation

The validation of the 1D representation of the fuselage consists of two parts, the first is validating the third assumption and the second part is a method which could be used to validate the accuracy of the 1D representation.

The assumption that the convection of the air can be modelled as a constant temperature on the contact surface can be validated by comparing the results of the convection simulation with the results of a simulation, which sets the temperature of the contact surfaces to a constant 373.15 K. The same model as before is loaded in Ansys®, with the same boundary conditions and the convection is changed to a constant 373.15 K. The results of this simulation can be found in Table 7.7 together with the reference values from the verification section.

Table 7.7: Temperature comparison between Heisler chart and convection model.

Time $[s]$	Reference $[K]$	Constant temperature $[K]$	difference [%]
28	323.15	325.6	0.8
56	353.15	355.4	0.6

The difference between the reference values and the constant temperature simulation are also in the sub 1% range, therefore this assumption is assumed to provide a reliable transient thermal response.

Unfortunately there are no comparable missions or research papers. Therefore the transient thermal response curves of the insulation models cannot be properly validated. Future research should focus on making an accurate convective heat coefficient model for the atmosphere to replace the constant temperature assumptions. Furthermore, including the effect of radiation heat transfer to fine tune the heat transfer should be included.

Lastly the most important improvement would be to make an accurate fuselage model, complete with insulation and possible internal structures and the heat generation of each component.

Chapter 8

Sensitivity Analysis

In this chapter the sensitivity analysis will be performed for each division. To do the sensitivity analysis, the main influencing parameters have to be identified first. Afterwards, the sensitivities are computed for -10% and $+10\%$ changes of those driving parameters. Finally, the results are presented and discussed in a comprehensive overview. First of all the aerodynamics analysis is given followed by the stability and control sensitivity analysis. After this the structural parameters are analysed on their sensitivity. As follows both flight mechanics and electronics are examined on sensitivity. In the end the thermal analysis is given.

8.1 Aerodynamics

The important parameters for the aerodynamic analysis are the fuselage shape, the airfoil chosen and the sweep angle. These parameters are of major influence on the aerodynamic performance and therefore determine the shape of the design. During the aerodynamic analysis, the influence of these parameters has been discovered and used to optimise the design.

Sensitivity Parameters

In this section, the method on how to research the influence of the parameters is given. At first for the fuselage shape, secondly for the airfoil type and at last for the sweep angle. These can be divided in parameters which can be quantified and parameters which cannot. The airfoil type cannot be quantified, as this is a combination of different values. Therefore the effect of changing the airfoil will be discussed in a high level. The sweep angle is a quantifiable parameter and will therefore be discussed more accurate. The fuselage shape is quantified by using the S_{wet} over S_{ref} value.

Fuselage shape The influence of the fuselage shape on the drag is researched by doing a literature study to different geometries and their drag. In the Section 6.1.2 there is already stated that a smooth shape will generate less drag and is therefore better than a blunt shape. The fuselage shape has a major contribution to the zero lift drag generated by the design. However, to quantify this, it is chosen to change the S_{wet}/S_{ref} ratio. Changing this by 10 % will effect the drag, thus the effect on the drag coefficient is quantified.

Airfoil type The influence of the airfoil is determined by implementing the wing geometry in the CFD program used, Ansys Fluent®. The NACA 4412, and the NACA 43012 are compared, just as two different combinations of the NACA 4412 and the NACA 0006. This is done to see what the influence is of combining separate airfoils on the $C_L - \alpha$ curve.

Sweep angle The influence of the sweep angle is tested by changing the sweep angle by 10% up and down in the program used to estimate the drag. By seeing how the drag is influenced, the effect of sweep on the drag is determined. The start value of the sweep is 30 degrees.

In the next section the results of the mentioned analysis methods are given.

Aerodynamics Sensitivity Results

In this section, the results of the sensitivity analysis regarding aerodynamics are given. In Table 8.1 the results of all quantifiable parameters are presented.

Table 8.1: Sensitivity parameters relating to aerodynamic performance.

Parameters	- 10 %	+ 10 %
Effect on	Drag coefficient (C_D)	
Fuselage shape, subsonic	-3.1 %	+3.2 %
Fuselage shape, transonic	-0.8 %	+0.5 %
Fuselage shape, supersonic	-1.1 %	+0.5 %
Sweep angle, subsonic	0 %	0 %
Sweep angle, transonic	+10.4%	-10.2%
Sweep angle, supersonic	0 %	0 %
Airfoil type	-	-

In Table 8.1 the effect of changing the fuselage and thereby the ratio of S_{wet} over S_{ref} can be seen. When the ratio is lower, the drag coefficient will decrease and when the ratio is higher, the drag coefficient will increase. In Table 8.2 it is seen that the effect of changing the ratio is higher for subsonic velocities than for transonic and supersonic velocities.

Table 8.2: C_D values for different S_{wet}/S_{ref} and Mach numbers.

Parameters	C_D@$M=0.6$	C_D@$M=1.0$	C_D@$M=2.2$
$S_{wet}/S_{ref} = 2.286$	0.0966	0.392	0.187
$S_{wet}/S_{ref} = 2.063$	0.0936	0.389	0.185
$S_{wet}/S_{ref} = 2.509$	0.0997	0.394	0.189

Also in Table 8.1 the relative change when changing the sweep angle with 10 % for sub-, trans- and supersonic flow can be found. The results of the tests for the sweep angle can be found in Table 8.3. It can be seen that a higher sweep angle is beneficial for transonic velocities, but has no effect for subsonic and supersonic performance. From literature it is known that increasing the sweep angle will influence the lift generation negatively near the root and increase lift near the tip[1].

Table 8.3: C_D values for different sweep angles and Mach numbers.

Parameters	C_D@$M=0.6$	C_D@$M=1.0$	C_D@$M=2.2$
Sweep = 30°	0.0966	0.392	0.187
Sweep = 33°	0.0966	0.352	0.187
Sweep = 27°	0.0966	0.433	0.187

The influence of the airfoil on the lift coefficient can be seen in Figure 8.1. The four airfoils in this figure have about the same slope, but their C_L at $\alpha=0°$ is different and so is their behaviour at higher angles of attack. The NACA4412/NACA0006 and the NACA4412/NACA0006/NACA0006 airfoils are combinations of the airfoils mentioned in the name. The first has a smooth gradient from the one to the other, the latter has 2/3 of this transition and the last 1/3 till the tip has the NACA0006 airfoil.

It can be seen in the Figure 8.1 that the influence of the airfoil is mainly on the C_L values. Also it can be seen that combining airfoils is particulary bad for higher angles of attack, due to the worse slope for higher angles of attack. It must be noted that although the NACA43012A airfoil has lower C_L values, it is still preferred over the NACA4412 because of the positive $C_{M_{AC}}$, which is better for stability.

[1] URL `http://adg.stanford.edu/aa241/wingdesign/geomnldistn.html` [15 Jun 2016]

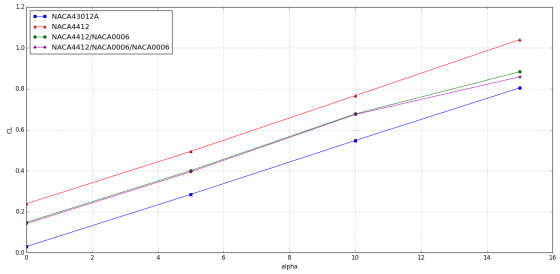

Figure 8.1: $C_L - \alpha$ for different airfoils at $Re = 500{,}000$.

8.2 Stability and Control

For the sensitivity analysis of stability and control, two models are analysed. These are the longitudinal flight- and the free fall stability model, discussed in Sections 6.2.2 and 6.2.4, respectively. For both models, the important parameters will be identified and the impact of changes to these parameters is evaluated.

Sensitivity Parameters

Both models have different outputs that determine the performance or restrictions of the design. Furthermore, both models have different parameters that affect these outputs and therefore they are discussed separately. This section will describe the outputs and the evaluated inputs per model.

Longitudinal Stability

As explained in Section 6.2.2 the longitudinal stability is evaluated with a spreadsheet model that estimates the centre of gravity range for which the aircraft is both trimmable and stable. If the centre of gravity is shifted more forward, the aircraft cannot be trimmed anymore and if it shifts backward, it will become unstable. For the design it is however decided that the lower centre of gravity limit from controllability is a harder requirement than the upper limit of stability. This is due to two reasons. First of all, the stability limit has a safety margin included which means that the aircraft is not unstable as soon as it exceeds the limit. Secondly, if the centre of gravity actually lies behind the neutral point, the actual stability limit, a flight control computer can counter these effects.

For this analysis, there are multiple important parameters that will be evaluated. These are the following:

S	The surface area of the wing affects the centre of gravity range in many ways, directly or indirectly. First of all, the wing surface, or more specifically the surface ratio between the wing and the canard, directly influences the centre of gravity range as was explained in the equations in Section 6.2.2. Furthermore, the surface area affects numerous other parameters such as the aerodynamic centre of the wing or the aspect ratio. These influence the calculations indirectly as well and thus the consequences due to a change in surface area are difficult to estimate.
$\bar{c}$	The mean aerodynamic chord affects the centre of gravity location directly since it used to make the equations dimensionless.
Λ_1	The first sweep is the sweep closest to the symmetry axis of the aircraft. Besides the fact that it affects the surface area it also affects the estimated quarter- and half chord sweep, which are used in the calculation of C_{L_α} of the DATCOM[16] method.
Λ_2	The second sweep effects the design in the same way as the first.
b_w	The wing span affects the aspect ratio and the surface area and does thus influence the performance in quite some ways.
S_c	The canard surface affects the results through the surface ratio of the wing and the canard. Furthermore, it affects the canard lift curve slope through the aspect ratio.
C_{m_0}	The zero-lift moment coefficient of the wing airfoil has a large influence on the moment coefficient around the aerodynamic centre, which is important for the controllability calculations. For stability, this has no effect.

$C_{L_{c,max}}$	The maximum lift coefficient of the canard is important for controllability since it determines whether the aircraft can be trimmed. Just as C_{m_0} does it not affect the stability location.
z_{ac_c}	The location of the canard aerodynamic centre affects the tail length which influences both the stability and controllability limit.
l_c	The tail length is an important parameter since it affects both the stability and the controllability limit directly.
$C_{L_{\alpha_c}}$	Lift curve slope of the canard less aircraft is important for the stability limit but does not affect the controllability.
$C_{L_{\alpha_{A-c}}}$	The lift curve slope of the canard affects the results in the same way as the slope of the tail less aircraft.

Free Fall Stability

I_{xx},I_{yy},I_{zz}	The moment of inertia's around the different axis systems determine how a moment affects the angular acceleration. The larger the moment of inertia, the larger the moment needed to initiate a rotation.
θ	θ is the pitch angle, this angle will change according to the location of centre of gravity, even without an initial rotation. By changing θ a different stability height will be found, this depends on how close θ is to its desired value.
S	The higher the surface the higher drag will be, and as follows the higher the stability height.
$\Delta C_{M_{max}}$	The maximum change in moment by moving the control surfaces also has an influence on the stability height. The higher the moment can be the better, but however at a certain moment a limit is reached and higher changes in moment are seen as an overdesign.

Stability and Control Sensitivity Results

Table 8.4 shows the results of the sensitivity analysis for the flight stability and control calculations. To get to these results, the parameters discussed in the previous section were increased adjusted to evaluate the effect on the results. The results in these calculations are the locations of the centre of gravity limits and the range of the centre of gravity. It can be seen that the length of the mean aerodynamic chord and the wing span have the largest influence on the limiting centre of gravity locations. Furthermore it can be seen that the centre of gravity range varies a lot more with respect to the original situation. The important reason for this is the small size of the original value of the centre of gravity range. Finally it can be seen that some parameters, such as $C_{L_{c,max}}$ and $C_{L_{\alpha_{A-c}}}$, only affect one of the limits of the centre of gravity. This is easily explained when looking at the equations used to calculate the results, as provided in Section 6.2.3.

In Table 8.5 the sensitivity results with respect to the stability height can be seen. The values shown are all calculated for the same control input of control surfaces in order to be able to compare data. The parameter which has the most influence is the initial pitch angle, which makes sense since that angle defines the necessary change in pitch angle needed until the ideal angle is reached.

8.3 Structures

The structural parameters subjective to changes are mainly focused in the stress calculation of the wing. For the vibrational loads an approach to perform the sensitivity analysis is given rather than an analysis of the values due to the limited knowledge as will be explained later in this section. Therefore, the stress calculations section is the part where the values are elaborated on.

Sensitivity Parameters

The parameters influencing the stress calculation outputs can be devided in three major sections. First the wing loading depending parameters are discussed. After that the parameters depending on the planform are

Table 8.4: Sensitivity parameters relating to controllability, stability, location of the neutral point and the centre of gravity range.

Current distance	[m]	$z_{controllable}$ 0.126	$z_{stability}$ 0.128	$z_{n.p.}$ 0.133	Centre of Gravity Range 0.0022
Parameters	Input Change	Change [%]	Change [%]	Change [%]	Change [%]
S	+10 %	1.58	0.83	0.80	-42.7
	-10 %	-1.83	-0.94	-0.91	50.6
$\bar{c}$	+10 %	-5.93	-6.12	-5.48	-16.9
	-10 %	6.02	6.20	5.56	16.9
Λ_1	+10 %	1.46	0.80	0.76	-38.1
	-10 %	-1.30	-0.66	-0.64	36.1
Λ_2	+10 %	0.49	0.26	0.25	-13.4
	-10 %	-0.50	-0.26	-0.25	13.8
b_w	+10 %	1.89	1.89	1.82	1.7
	-10 %	-2.29	-2.39	-2.29	-8.3
S_c	+10 %	-1.07	-0.16	-0.15	52.5
	-10 %	1.07	0.20	0.19	-50.2
C_{m_0}	+10 %	-0.32	0	0	18.9
	-10 %	0.32	0	0	-18.9
$C_{L_{c,max}}$	+10 %	-1.07	0	0	62.0
	-10 %	0.53	0	0	-31.0
z_{ac_c}	+10 %	0.35	0.26	0.25	-5.1
	-10 %	-0.35	-0.26	-0.25	5.1
l_c	+10 %	-1.07	-0.79	-0.76	15.4
	-10 %	1.07	0.79	0.76	-15.4
$C_{L_{\alpha_{A-c}}}$	+10 %	0	-0.79	-0.76	-46.6
	-10 %	0	0.79	0.76	46.6
$C_{L_{\alpha_c}}$	+10 %	0.49	0.26	0.25	-13.4
	-10 %	-0.30	-1.17	-1.13	-51.8

Table 8.5: Sensitivity analysis with respect to the stability height.

Parameters Effect on	- 10% Stability height	+ 10%
I_{yy}	0.31	0.04
S	1.42	0.04
θ_0 (change in ° not %)	-9.71	8.34
ΔC_m	-1.43	0.26

considered towards sensitivity, this is in order to finalise the stress part with the cross sectional parameters of the wing. As for the Launch loads no values will be analysed separately. For this subject an approach is given since the analysis must still be improved from mathematical point of view.

Launch Loads

The PSD values of the launch vehicles may only be known in the later stages of the design. The same counts for the loads acting on the ICARUS+ in launch by the Lynx spacecraft. Since most of the values are not known

at this time in the design, a proper sensitivity analysis can not be performed yet. However, as stated in Section 6.3.1, a mitigation solution is found. Using an isolation system between the payload and the launch vehicle will extend the limit in which the payload will be able to work. Choosing a sufficient isolation system will reduce the risks that might occur during a sensitivity analysis. Therefore, this part can be stated as examined for now.

Stresses

The stress analysis for the flight loads have been explained in Section 6.3.4. As is explained in this section the stresses in the structure do not impose a limit on the design. For the performed flight the design could not be fully optimised structurally due to manufacturability. If manufacturability improves, the design may be more optimised and also the design can be scaled later on. Therefore a sensitivity analysis of the structural stresses is still important, this is since some sensitivity analysis outputs are that insignificantly small these have been compounded.

L	An increase in the design lift would induce a higher loading on the wing. Since this is the main loading the contribution of this change is significant. The design lift can be changed by a change in the encountered weight, the load factor or the safety factor. These parameters are not discussed separately since the consequence will be the same.
D	The drag force will change along with the lift force since drag is scaled from lift using the C_L/C_D ratio as was explained in Section 6.3.4. If this ratio would change, the drag would change separately from the lift wherefore this is discussed.
S	If the same loads are applied on a different different surface area the stresses will increase and decrease with a decrease and increase of surface area respectively. Changing the surface area compounds a change in span and root cord because these changes are comparable.
Λ	The sweep in both the first and the second part will influence the stresses since a change sweep will induce a positively correlated change in torque. Since the torque does not contribute to the final stress in large proportions the change will not induce a big problem.
$I_{xx,cs}$,$I_{zz,cs}$,$I_{xz,cs}$	The cross sectional moments of inertia at every discretised cross section is a compound of the small changes which would occur when all the thicknesses, the width and the height are changed of the cross section.

Structures Sensitivity Results

Table 8.6: Sensitivity parameters relating to the stresses induced by the flight loads.

Parameters Effect on	- 10% $\sigma_{max,com}$ $[MPa]$	+ 10% $[MPa]$	- 10% $\sigma_{max,ten}$ $[MPa]$	+ 10% $[MPa]$	- 10% τ_{max}	+ 10% $[MPa]$
L	-10	10	-10	10	-10	10
D	-1.39	1.39	-1.39	1.39	-1.38	1.38
S	2.68	-2.68	2.68	-2.68	-4.71	4.71
Λ	-0.02	0.02	-0.02	0.02	-0.43	0.43
$I_{xx,cs}$,$I_{zz,cs}$,$I_{xz,cs}$	5.76	-5.76	5.76	-5.76	3.81	-3.81

8.4 Flight Mechanics

In this section, the parameters of the flight mechanics model will be tested in the form of a sensitivity analysis. First of all, the sensitivity parameters will be be listed, including the approach for testing those parameters. After this section, an overview of the results will be given.

Sensitivity Parameters

The characteristics of the payload that effect the range most are listed below. It is important to take into account that the importance of these characteristics are only based on the flight mechanics model for range. The other

effects as stability, controllability and structural visibility are not taken into account. The parameters below have been examined by changing their values in the flight mechanics model. The effects of changing these parameters are listed in Section 8.4. The sensitivity is based on the effects on the total range. The tests have been done for the final design values. For these conditions, the sensitivity analysis is specific for the current design.

Aspect ratio This influences almost all of the aerodynamic coefficients during the flight. During glide for example, the optimal value for C_L depends on the value of the aspect ratio, as has already been stated in Equation 6.40. The C_D value also depends on the aspect ratio, since the induced drag component is included in these computations. The equation for the induced drag, C_{Di}, computation can be found in Equation 8.1. The aspect ratio is an output of the span and the surface area of the wing. Since the span is a maximised value for this payload, the surface area is the parameter which could be changed. At a certain point, the wing surface will be too low to be able to perform the optimal flight.

$$C_{Di} = \frac{C_L^2}{\pi A e} \tag{8.1}$$

C_{D_0} These values affect the C_D equation, as stated in Equation 8.2.

$$C_D = C_{D_0} + \frac{C_L^2}{\pi A e} \tag{8.2}$$

All values for C_{D_0} have been in- and decreased during the computations in order to perform the analysis.

$C_{L_{max}}$ $C_{L_{max}}$ will be distinguished for subsonic, transonic and supersonic flight. These values are important during the pull-out manoeuvre. When the maximum load factor at a specific point of flight allows to increase the value of C_L to its maximum value, this maximum value determines how fast the pull-out can be performed. This sensitivity analysis has been performed by combining the three parameters to one parameter, by changing all three values of $C_{L_{max}}$ at once.

$V_{initial}$ This velocity determines what the initial values for the horizontal and vertical velocities are be for flight. This value can increase of decrease the final range.

Direction This is important for how the wind is contributing to the overall velocity at stratospheric altitudes. The initial direction is from west to east. In order to perform the sensitivity analyses, the direction has been changed to a direction from east to west.

Latitude The latitude determines the range of the stratospheric altitudes, where the wind contributes to the velocities during the computations. The initial latitude is around the equator. Changing the location to the poles will give the sensitivity of this parameter.

Total mass This is important with respect to the maximum load factor during the pull-out manoeuvres. In order to perform the sensitivity analysis, the mass has been modified.

Stability height From this altitude on, the payload will be able to perform the optimal flight, according to the flight mechanics model. If the payload will become stable at a low altitude, there is less altitude left to perform the flight. Different altitudes are tested in order to perform the sensitivity analysis. These altitudes have been centred around the stability altitude of the current design. This gives a different view on the sensitivity, compared to an altitude that is not optimised. At an altitude of 30 km for example, it would be both sensitive to increase and decrease the altitude. However, at the current altitude of 40 km, the parameter is only sensitive for decreasing the altitude. The elaboration on the optimisation of the stability height has been done in Section 6.4.2.

Flight Mechanics Sensitivity Results

In this section, the results of the sensitivity analysis for the flight mechanics division are summarised in Table 8.7 and Table 8.8.

The results imply that the most sensitive parameters regarding the total range are the aspect ratio, the values for C_{D_0} and the altitude at which the payload is stable. This can be explained by considering the flight trajectory.

Table 8.7: Sensitivity parameters relating to flight mechanics, effects on range.

Change in parameters	-10%	+ 10%
Effect on	Range	
S ($A = \frac{b^2}{S}$)	+4.42%	-4.29%
C_{D_0}	+5.63%	-4.83%
$C_{L_{max}}$	-0.54%	+0.68%
V_{Lynx}	-0.53%	+1.02%
mass	+0.34%	-0.27%
h_{stable}	-6.61%	+2.17%

Table 8.8: Sensitivity parameters relating to flight mechanics, regarding the attitude.

Parameters	Direction	Latitude
Parameter variation	π rad	$\pi/2$ rad
Range variation	-1.36%	+0.34%

The three most sensitive parameters have an active effect on the trajectory for the total flight path. The five other parameters only effect the first part of the flight trajectory. The direction, latitude and the velocity of the Lynx will mainly cause the payload to finish the trajectory quicker and decreasing the possibility of reaching stall speed. This is due the fact that the angles of the flight path are mostly determined by other parameters, instead of the velocity. The mass and $C_{L_{max}}$ values will only effect the pull-out manoeuvre, regarding the total range.

8.5 Electronics

The electronics subsystem significantly changes with the communication requirements set for the UHF link with the ground stations. This sensitivity analysis looks into what these effects are and how much impact they have on the whole design.

Sensitivity Parameters

The two parameters that can be set as main requirements for the UHF link are the data rate and the broadcasting distance. These are driving as they determine how far and how fast data can be sent through the UHF transponder. However, they have a significant effect on the performance of the whole system. Therefore, the effect of changing these requirements on the antenna power, antenna gain and battery size is quantified as explained below.

To be able to quantify the impact, the link budget is utilised and tested for different configurations of data rate, broadcasting distance, antenna power and antenna gain. The increase in power can be linked to an increase in battery mass by using the the power mass density of custom made Saft $Li-MnO_2$ batteries. It is important to note that the uplink data rate of 115200 *bps* is already maximised with the current configuration, since the transponder can not handle higher data rates. Thus it is not effective to increase the antenna capabilities for the uplink connection. The downlink connection, however, can still be increased from 38400 *bps* to 115200 *bps* by increasing the antenna capabilities.

Data rate Two things can be done to accommodate an increase in data rate. The first solution is to increase the antenna power, which will increase the battery size as more power is consumed. The second solution is to increase the antenna gain, by changing the antenna type to one that is more directional. This will make it more challenging to have a connection at all times and pointing the antenna in the right direction more important.

Distance The above mentioned considerations are valid here too.

Electronics Sensitivity Results

The effect of changing the downlink data rate on the required UHF antenna power is computed. Increasing the antenna power also implies an increase in battery mass, which is also given as a function of data rate in Figure 8.2. Furthermore, the effect of changing the broadcasting distance on the required UHF antenna power and the increase in battery mass are given in Figure 8.3.

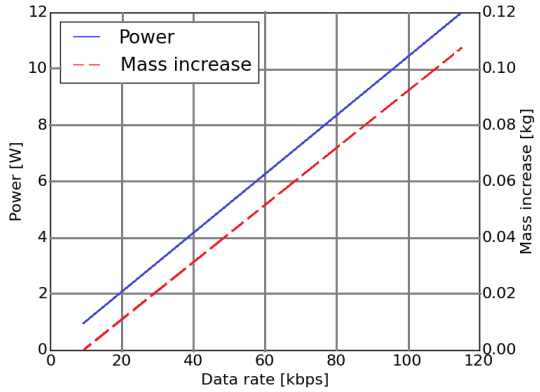

Figure 8.2: UHF antenna power consumption and mass increase as a function of downlink data rate with a broadcasting distance of 1000 km.

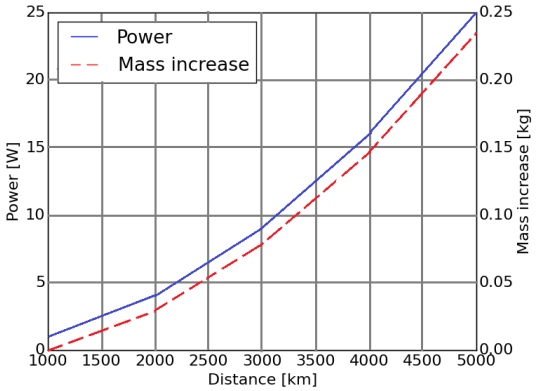

Figure 8.3: UHF antenna power consumption and mass increase as a function of broadcasting distance with a data rate of 9600 bps.

As can be seen in Figure 8.2, the mass increase of the battery for a downlink data rate of 115200 *bps* is a bit more than 100 grams and thus implementable, if the size of the fuselage would be increased to house the additional battery size. This would, however, mean a drag increase and therefore a range decrease. It is up to the customer to decide where the priority lies (i.e. the data rate or the range). Additionally, it can be observed in Figure 8.3 that the broadcasting distance could be extended to 5000 *km* with an increased battery mass increase of 250 grams. Once again, this means a performance decrease in range due to the drag increase coming from the enlarged fuselage.

The effect of changing the downlink data rate on the required UHF antenna gain is given in Figure 8.4. Also, the effect of changing the broadcasting distance on the required UHF antenna gain is given in Figure 8.5.

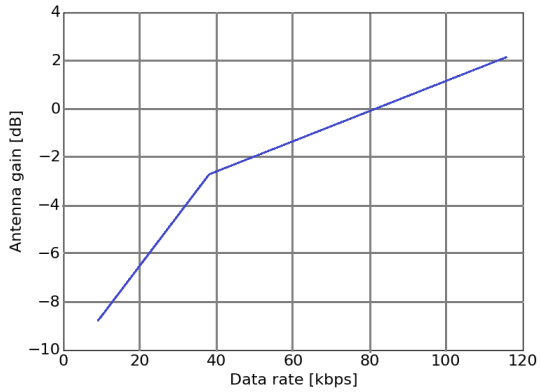

Figure 8.4: UHF antenna gain (i.e. directionality) as a function of downlink data rate with a broadcasting distance of 1000 km.

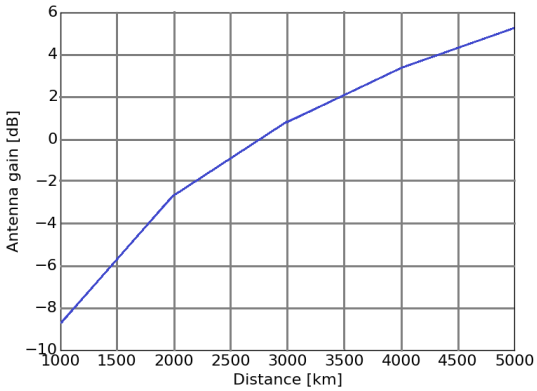

Figure 8.5: UHF antenna gain (i.e. directionality) as a function of broadcasting distance with a data rate of 9600 bps.

To achieve a downlink data rate of 115200 *bps*, a UHF antenna gain above 2 *dB* would be necessary as can be seen from Figure 8.4. This is possible with a different antenna type that is much more directional, but this would make it very hard to keep the connection with the ground station throughout the mission. The reason being that high gain antennas have a very directional radiation pattern. The same is true for the required antenna gain for

a broadcasting distance of 5000 km. A gain of more than 5 dB would be required, as can be seen from Figure 8.5. This is practically not feasible and thus a much better solution is to increase the antenna power and battery size.

8.6 Thermal Control

In this section the effects of changing the thermal control parameters on the minimum and maximum temperature of the inside of the fuselage are examined.

Sensitivity Parameters

There are three variables which are easily quantifiable and can be adjusted to fine-tune the minimum and maximum internal temperature. The temperature envelope is determined by the flight trajectory and therefore assumed to be an input and not a variable.

Insulation thickness This parameter determines the effective available volume in the fuselage.
Internal power generation This parameter is determined by the power consumption of the internal components.
Initial temperature This parameter is unknown because the payload bay temperature at the moment of deployment by the Lynx is still an unknown, so this is varied to find the effect on the result.

Not all of these parameters are tested with a 10% in- and decrease, due to the computationally intensive simulations. Only the internal power generation is changed in this manner. The other parameters have been changed to find the necessary insulation thickness, but in different increments. The results are gathered in the next section.

Thermal Control Sensitivity Results

The effects of the changing the three variables on the internal temperatures have been tested and the results are gathered in Table 8.9.

Table 8.9: Sensitivity parameters relating to thermal control.

Current temperature	$[K]$	T_{min} 241.5	T_{max} 320.5
Parameters	Input Change	Change $[K]$	Change $[K]$
$t_{insulator}$	+33.3 %	8.5	-5.6
	-16.7 %	-4.1	10.7
$T_{initial}$	+5 K	0	-2.5
	-5 K	0	1.5
$P_{internal}$	+10 %	2.2	2.6
	-10 %	-2.6	-0.7

From these results it can be concluded that the insulation thickness has the largest impact on the internal temperature ranges. Increasing the insulation increases the lowest temperature, which is expected. The maximum temperature at the end of the flight is higher, however the thermal spike in the first part of the trajectory causes higher temperature for a short period of time. Decreasing the insulation has the opposite effect as expected. Changing the initial temperature has no effect on the minimum temperature and only slightly affects the maximum. Finally the internal power generation can shift the whole curve up or down, but the effect is small compared to the insulation thickness.

Chapter 9

Design Iterations

The design process implemented in this project uses iterative cycles to improve and fine tune the design performance systematically and continuously. In this chapter the four design iterations that have been done during this design phase are elaborated on and the results are presented. This includes specific design changes and the reasoning behind it. The manner through which the designs are evaluated can be found in Section 4.2. It is noteworthy that these iterations illustrate the major design changes and that the optimal solution for each configuration (i.e. iteration) is also found through another iteration cycle that is not elaborated on in this report for conciseness.

9.1 First Iteration

To come to the first design iteration, recommendations were made based on the results of the Mid-Term Review design. The following design changes were recommended to be implemented to come to the first design iteration.

- **Dual airfoil wing**: in order to have a reasonable performance in both sub- and supersonic flight regimes a dual airfoil wing is used instead of using a single airfoil. A relatively thick subsonic airfoil is combined with a thin supersonic airfoil where the thick part is located at the root of the wing due to structural considerations. It is chosen to have a gradual transition between the airfoils to prevent abrupt thickness changes in the wing.
- **Fuselage streamlined**: the fuselage of the initial design showed a largely inefficient fuselage shape. In order to improve this, the fuselage is made more streamlined by incorporating the payload within the fuselage shape and thus reducing air resistance.
- **Canards**: the canard is recommended for multiple reasons. First of all, since the elevator effectiveness (and thus also the elevon effectiveness) decreases at supersonic speeds [37] a canard can be used to improve the controlling performance of the aircraft. Especially since it is suggested to give this canard surface a supersonic airfoil and make the two sides (independently) completely moveable, this canard can ideally control the aircraft without help of the elevons. A second reason for the canard is that it is beneficial for trimming the aircraft. The pitch-up moment generated by the canard counters the pitch-down moment of the wing due to its longer arm.
- **Increased span**: a 3D visualisation of the folded Mid-Term Review design showed the possibility to increase the span by adding another hinge to each wing.
- **Wing built-in elevons**: at first the idea of the elevons was to have the elevons as extended flaps on the wing as was presented in Figure 4.1 in Chapter 4. However, after the first iteration it was decided that it would be a better option to incorporate the elevons in the wings as is done in general for elevons. This way, the elevons are part of the wing profile and can deflect upwards and downwards to control the aircraft. The main function of the elevons is to control the aircraft in the subsonic flight regime, since their effectiveness is decreased at high Mach numbers, as was discussed before [37].
- **Remove winglets**: due to supersonic performance and structural considerations it is decided to remove the winglets. Winglets can be designed to have minimal effect on the supersonic performance but will be very small and have little effect in subsonic flight [13]. In addition structurally it will be very challenging to fit the winglets inside the 2U unit when fully folded. It is therefore decided not to include them in the design.

The resulting design of this iteration can be seen illustrated in Figure 9.1.

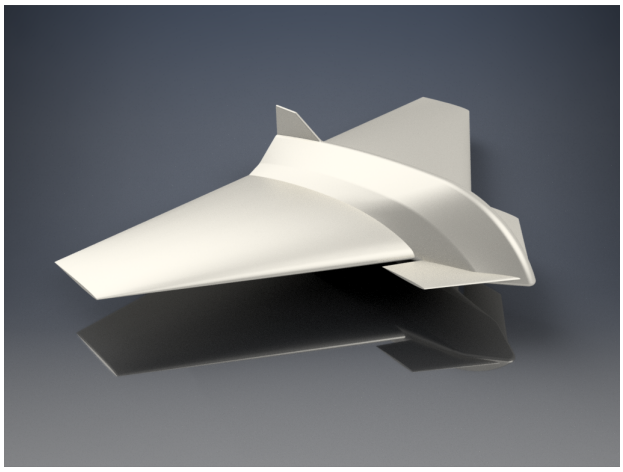

Figure 9.1: Design of the first iteration.

9.2 Second Iteration

To come to the second design iteration, recommendations were made based on the results of the first design iteration. The following design changes were recommended to be implemented to come to the second design iteration.

- **Wing incidence angle**: the performance of the design is very poor at low angles of attack. Therefore, it is suggested to let the wings have an initial angle of attack with respect to the body. This way the body still can be straight, while the wings will generate more lift due to a higher angle of attack they experience.
- **Increased supersonic wing section**: there is a major difference in the subsonic and transonic/supersonic performance. The subsonic performance is sufficient, while in transonic/supersonic flow the design does not generate enough lift, while generating a lot of drag. As is already mentioned in Section 6.1.2, the wing exists of a combination of two airfoils. One of these airfoils is designed for subsonic flow, while the other is designed for supersonic flow. By enlarging the part of the wing which consists of the latter airfoil, at cost of reducing the part of the wing which consists of the first, the subsonic performance will be worse than before, while the transonic/supersonic performance will be better.
- **Increased axial symmetry of fuselage nose**: after the first aerodynamic analysis it appeared that the pressure on top of the nose is much higher than underneath it, as can be seen in Figure 9.2. Because of this, the body will have a negative contribution to the lift. To prevent this to happen, it is chosen to implement a symmetric nose.
- **Rod on fuselage nose**: Aircraft designed for supersonic velocities often have a sharp rod at their nose [1]. This rod is to initiate the shock wave earlier. In this way the shock wave does not hit the wings and therefore creates less drag than when it would hit the wings. For the next iteration, a sharp rod is added to the nose.
- **Reduced wingspan**: the span was increased too much in this iteration to be able to unfold properly, so it has to be reduced to ensure proper deployment.

The resulting design of this iteration can be found in Figure 9.3.

9.3 Third Iteration

To come to the third design iteration, recommendations were made based on the results of the second design iteration. Next the recommended design changes for the third iteration are stated.

- **Smoothen aft part of fuselage**: right now the back is quite abrupt and goes straight down. Because of this, a large under pressure exists behind the design, as can be seen in Figure 9.4. This under-pressure creates an additional drag, thus in order to decrease the drag, a smoother transition is required.

[1] URL `https://www.nasa.gov/centers/dryden/multimedia/imagegallery/X-1A/E-2889.html` [14 Jun 2016]

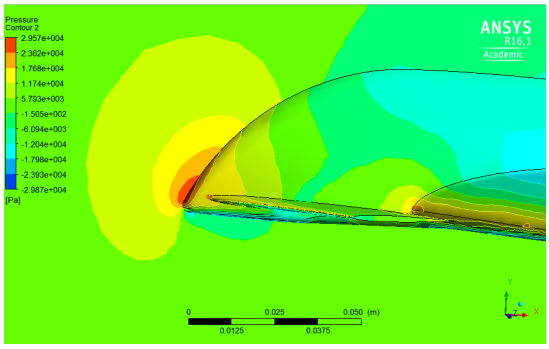

Figure 9.2: High pressure point on top of the nose.

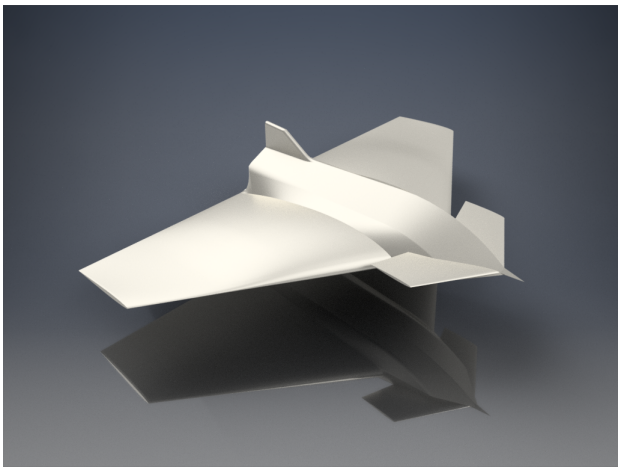

Figure 9.3: Design of the second iteration.

- **Remove rod on fuselage nose**: although the sharp tip after iteration one already makes a difference in initiating the shock-wave, it proved impossible to get the centre of gravity at the desired location. Furthermore, removing the spike will allow for an increase in overall length of the fuselage, and thus fully utilise the space available. It is therefore recommended to remove the spike altogether.
- **Increased span**: the new hinge concept created the possibility to increase the span, by reducing the wasted volume created by the regular hinges.
- **External UHF antenna**: an internal UHF antenna is not a viable solution, since the radiation signal can not pass through the titanium fuselage and wings. Thus, the only solution is to have an external antenna, which means it has to be made from titanium to be able to resist the external heating. Moreover, the mechanism used for deployment of this antenna has the dual functionality of pushing the ICARUS+ out the containment box. More specifications of this mechanism can be found in Section 6.3.2.
- **Double-swept wings**: the choice for double swept wings was made by considering several advantages. First of all the aspect ratio could be increased by decreasing the surface. The centre of gravity would locate itself more afterwards which makes the ICARUS+ more controllable. Furthermore by using a double sweep the vortex lift is more controllable.

The resulting design of this iteration is illustrated in Figure 9.5.

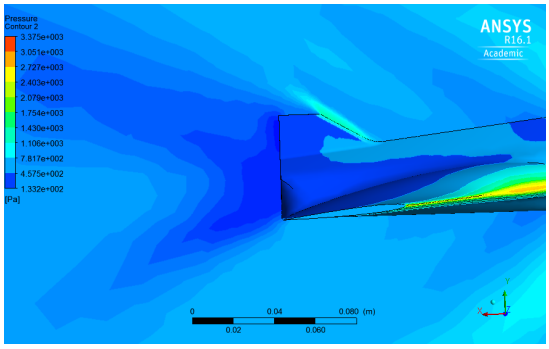

Figure 9.4: Under-pressure behind the design.

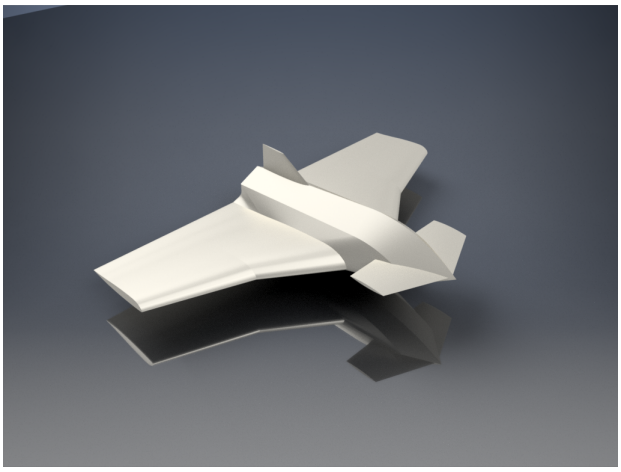

Figure 9.5: Design of the third iteration.

9.4 Fourth Iteration

The fourth and final design is made after iteration four. Next, the recommendations for this iteration can be found below. Those recommendations are made based on the results of the third design iteration.

- **Smoothen aft part of fuselage**: the design still offers room for a smoother aft section of the fuselage, which would reduce the zero-lift drag coefficient of the design even more so.
- **Increased span**: in the previous iteration the span was increased conservatively to avoid overshooting, therefore the span could be increased further once more.
- **Increased fuselage width**: due to the reduced root chord and corresponding root thickness, the fuselage could be made wider, however this was never an issue, so it is kept as a margin for future research.
- **Increased aspect ratio**: increasing the aspect ratio would increase the $(\frac{C_L}{C_D})_{max}$. This will increase the total range, due to the extension of the gliding path.
- **Fuselage top section made of Torlon® composite**: the same problem is raised for the GPS antenna as for the UHF antenna: radiation signals can not pass through the titanium fuselage and wings. Therefore, a patch of Torlon® composite, which is non conductive, thermally resistant, lightweight and strong has been selected as optimal solution. This patch is placed on top of the fuselage, where a cutout will be made in the titanium. This makes it possible to place the GPS antenna within the fuselage and still get a fix with the GPS satellites above. More explanation about this feature can be found in Section 6.3.5.

The final design can be seen illustrated in Figure 9.6.

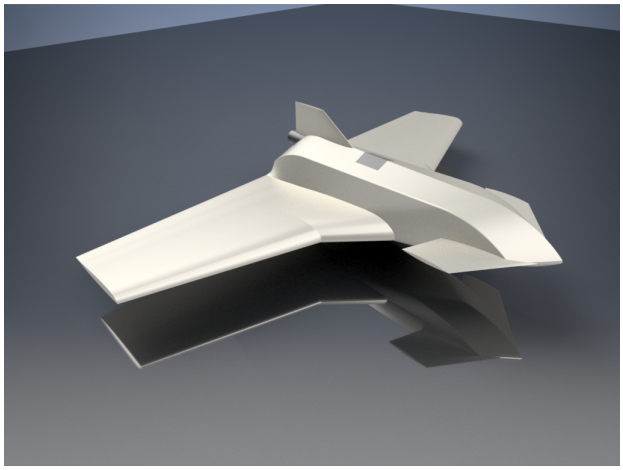

Figure 9.6: Design of the final iteration.

Chapter 10

Technical Design Overview

In this chapter a general overview of the final design and its performance is given. Afterwards, the hardware and the corresponding software diagram is discussed. Finally, the communication flow block diagram of the ICARUS+ is given.

10.1 Final Design and Performance Overview

The final design of the ICARUS+ can be seen depicted in Figure 10.1 with the specifications given in Table 10.1. Detailed drawings of the external and internal layout can be found in Appendix D.

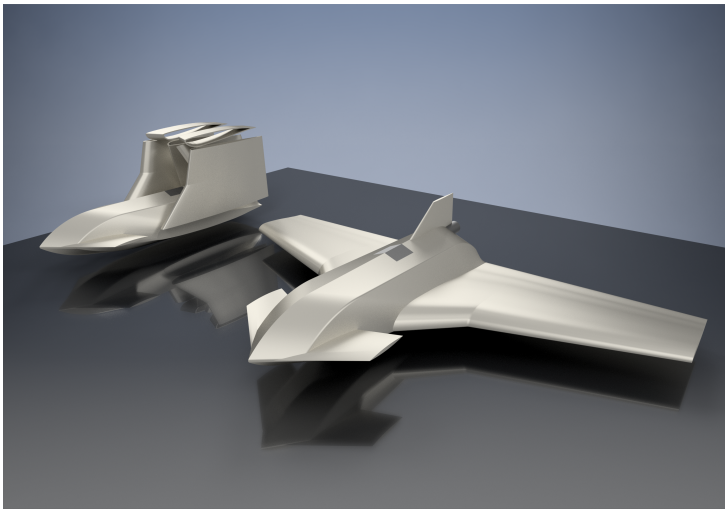

Figure 10.1: Render of the final design of the ICARUS+ in both folded and unfolded configuration.

As can be observed, a compound delta-canard wing configuration is used with a fixed vertical stabiliser, fully movable canards and wing built-in elevons. The canards offer control at transonic and supersonic speeds with their supersonic airfoil, whilst the elevons provide control at subsonic speeds. Furthermore, the vertical tail improves the lateral stability of the ICARUS+. Also, the aircraft has double-swept wings to postpone stall and decrease surface area. Noteworthy is that the total mass of the flying system is slightly over 0.600 kg and the supporting box structure adds only 0.375 kg which is significantly lower than the 2 kg allowable maximum mass. As can be noted the box will not be further mentioned in this chapter, as it does not add anything to the performance of the payload itself. Furthermore it was not part of the iteration process and its specifications have been constant throughout the design process which is stated in Section 6.3.

The performance of this design in all the different engineering fields is summarised in Table 10.2. Furthermore the performance results of the final design are discussed below within the different engineering fields.

- **Aerodynamics**: the aerodynamic performance is optimised for the subsonic flight regime, as this is

Dimensions		
Wing	Value	Unit
b	0.36	$[m]$
c_{root}	0.155	$[m]$
c_{tip}	0.057	$[m]$
$\bar{c}$	0.105	$[m]$
S	0.0337	$[m^2]$
A	3.85	[-]
e	0.88	[-]
Γ	0	$[^\circ]$
Λ_{inner}	43	$[^\circ]$
Λ_{inner}	18	$[^\circ]$
λ	0.368	[-]
$Airfoil_{inner}$	NACA43012	[-]
Control surfaces	Value	Unit
$S_{canards}$	0.0045	$[m^2]$
$S_{elevons}$	0.0015	$[m^2]$
S_{rudder}	0.00057	$[m^2]$
$Airfoil_{canard}$	NACA0006	[-]
Fuselage	Value	Unit
$l_{fuselage}$	0.06	$[m]$
$w_{fuselage}$	0.22	$[m]$
$h_{fuselage}$	0.045	$[m]$
Payload (UHF)	Value	Unit
$l_{payload}$	0.065	$[m]$
$w_{payload}$	0.04	$[m]$
$h_{payload}$	0.0065	$[m]$

a)

Mass budget		
Parameter	Value	Unit
m_{system}	0.581	$[kg]$
$m_{payload}$	0.0245	$[kg]$
m_{box}	0.375	$[kg]$
m_{total}	0.98	$[kg]$

b)

Center of gravity and neutral point		
Parameter	Value	Unit
$\bar{x}_{c.o.g.}$	0	$[m]$
$\bar{y}_{c.o.g.}$	0.02	$[m]$
$\bar{z}_{c.o.g.}$	0.128	$[m]$
$\bar{x}_{n.p.}$	0	$[m]$
$\bar{y}_{n.p.}$	-	$[m]$
$\bar{z}_{n.p.}$	0.126	$[m]$

c)

Moment of inertia		
Parameter	Value	Unit
I_{xx}	0.00186	$[kg{\cdot}m^2]$
I_{yy}	0.004481	$[kg{\cdot}m^2]$
I_{zz}	0.002751	$[kg{\cdot}m^2]$
I_{xy}	0.000127	$[kg{\cdot}m^2]$
I_{xz}	0	$[kg{\cdot}m^2]$
I_{yz}	0	$[kg{\cdot}m^2]$

d)

Table 10.1: General parameters of the final design iteration with respect to a) dimensions, b) mass budget, c) c.o.g and n.p. and d) MOI.

the determining factor for maximising range. This can be seen by the lift-to-drag ratio of 6.11 with a maximum lift coefficient of 1.1. At transonic and supersonic speeds the range performance significantly lowers, due to the heavily increased zero-lift drag coefficient.

- **Structures**: the structure is designed to take a maximum load factor of five with the maximum encountered stresses of 18.17 MPa, which is acceptable. Moreover, a thermal insulation layer of 0.26 cm is necessary to shield the internal components from the re-entry heating.
- **Flight mechanics**: The final range of the ICARUS+ is 230 km with a flight time of 70 minutes. This is achieved with a pull-out at 32.5 km height and a pull-over at 33.7 km.
- **Electronics**: the electrical subsystem requires 12 W of power at 3 V and 4 A with a total capacity of 4500 mAh for a two hour flight. Using state of the art $Li-MnO_2$, this can easily be accommodated by the battery.
- **Stability and control**: as can be seen, the ICARUS+ will be stable enough at an altitude of 40 km to start its flight. Additionally, the design requires a maximum hinging moment for the elevons of 0.0491 $N{\cdot}m$, which is within the 0.216 $N{\cdot}m$ range of the servos. Moreover, the design is stable and controllable as can be deduced from the negative $C_M-\alpha$ curve and the centre of gravity position of 0.128 m that lies within the controllabilty and stability limits.

Aerodynamics		
Subsonic	Value	Unit
C_{D0}	0.031	[-]
C_L-α	0.064	[-]
C_{Lmax}	1.1	[-]
$\frac{C_L}{C_D}_{max}$	6.11	[-]
Transonic	Value	Unit
C_{D0}	0.12	[-]
C_L-α	2.23	[-]
C_{Lmax}	-	[-]
$\frac{C_L}{C_D}_{max}$	1.7	[-]
Supersonic	Value	Unit
C_{D0}	0.045	[-]
C_L-α	0.025	[-]
C_{Lmax}	0.7	[-]
$\frac{C_L}{C_D}_{max}$	3.2	[-]

a)

Structures		
Parameter	Value	Unit
n_{max}	5	[-]
$t_{insulation}$	0.0026	$[m]$
t_{skin}	0.001	$[m]$
$\sigma_{tens.,max}$	48.17	$[MPa]$
$\sigma_{comp.,max}$	48.17	$[MPa]$
τ_{max}	6.8	$[MPa]$

b)

Flight mechanics		
Parameter	Value	Unit
Range	230	$[km]$
Glide ratio	-7.89	[°]
Pull-out height	32.5	$[km]$
Pull-over height	33.7	$[km]$
Endurance	70	$[min]$

c)

Electronics		
Parameter	Value	Unit
Power	12	$[W]$
Circuit current	3	$[A]$
Circuit voltage	4	$[V]$
Capacity	4500	$[mAh]$

d)

Stability and Control		
Parameter	Value	Unit
Stability height	40	$[km]$
C_M-α	-0.254	[-]
$C_{M,ac}$	0.0388	[°]
$H_{e,max}$	0.0491	$[Nm]$
$H_{c,max}$	0.0027	$[Nm]$
$c.g._{min}(Control)$	0.128	$[m]$
$c.g._{max}(Stability)$	0.133	$[m]$

e)

Table 10.2: Performance results of the final design with respect to a) aerodynamics, b) structures, c) flight mechanics, d) electronics and e) stability and control.

10.2 Hardware

The interaction and are linkage between system components can be summarised in a hardware block diagram, which can be found in Figure 10.2. This diagram illustrates all the mechanical links and data and power lines running throughout the system.

The Lynx payload bay C provides power to the ICARUS+ while inside the spacecraft, which is the configuration shown in Figure 10.2. The power connection is achieved through a DB9 connector that goes through the containment box and into the back of the fuselage of the payload. This power supply charges the battery, which in turn powers all the components passing through specific voltage regulators. The components that are powered by the battery include: antennas, sensors, servos, flight computer and transponder.

When the ICARUS+ and the containment box are deployed from the Lynx, the external power supply is cut off. This functions as the signal for the flight computer that the deployment has taken place. Once sufficient separation between the Lynx has been created, the burn resistor is turned on, thereby deploying the UHF antenna and pushing the design out of the containment box. At this point, the nominal mission operation mode can start.

It can be seen that flight data flows from the GPS/IMU to the flight computer. Afterwards, signals are sent to the servos to actuate the canards and elevons independently. Moreover, there is a data link between the

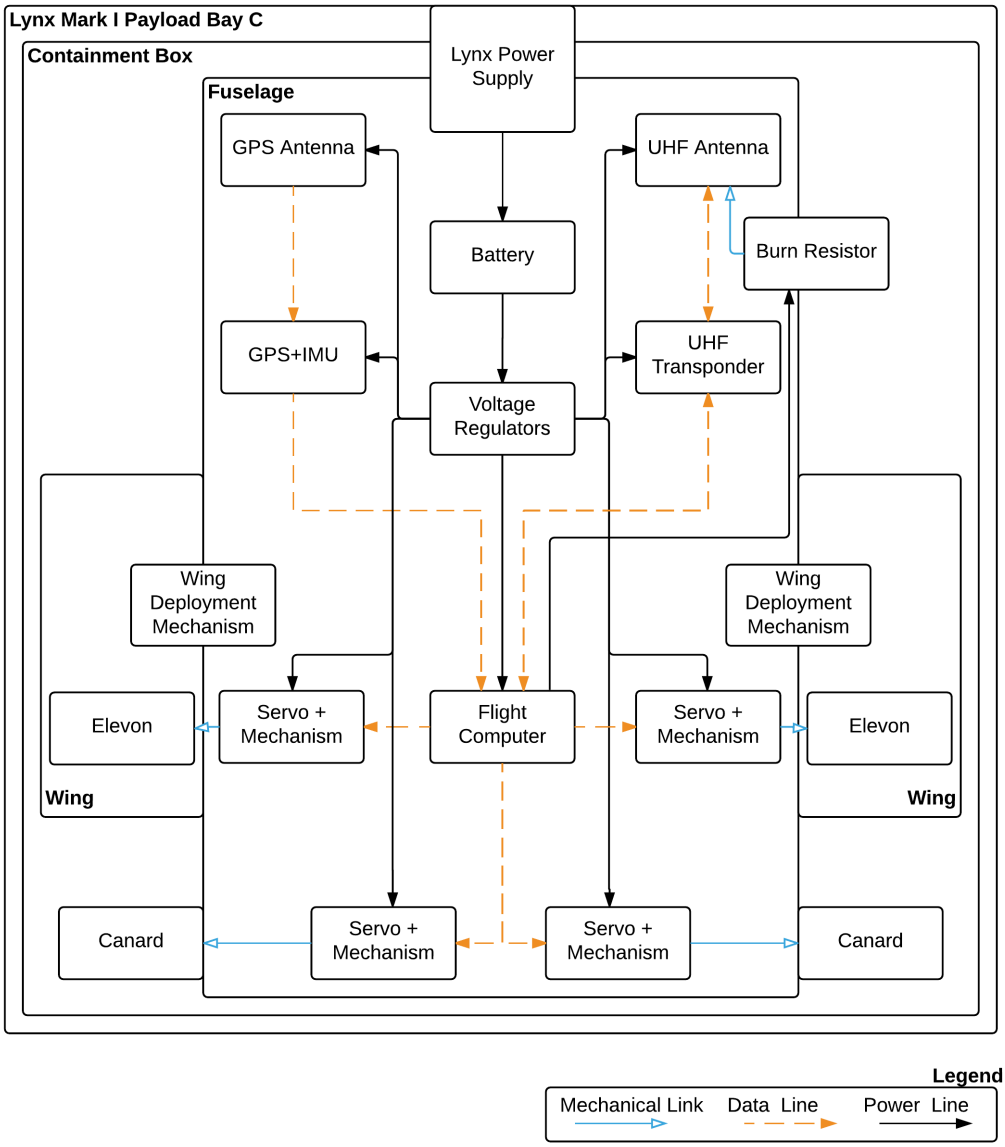

Figure 10.2: Hardware block diagram.

UHF transponder and the flight computer to send flight data and encrypted messages to a ground station. This data link is also used in opposite direction, where commands and encrypted data can be sent to the flight computer for trajectory changes or storage.

10.3 Software

The software flow block diagram of the ICARUS+ is given in Figure 10.3. As can be observed from this block diagram, multithreading (concurrent running of processes) is used as multiple tasks have to be performed at the same time. Such capabilities have already been implemented in AVR microcontrollers in the past [38], which are present in the flight computer of the ICARUS+. The three threads running simultaneously are the sense, UHF and main thread.

The main thread is in charge of processing and storing UHF data and signalling the watchdog. If the watchdog, located on the side processor of the flight computer, does not receive this signal for a certain amount of time,

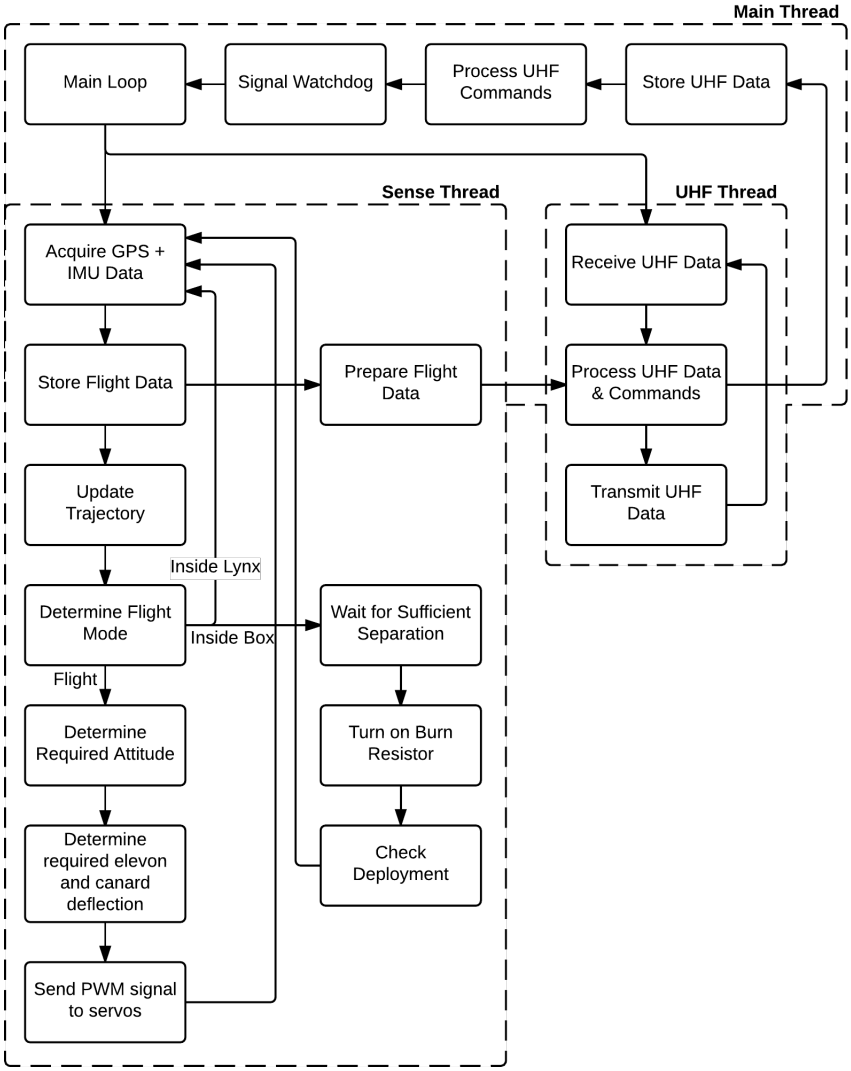

Figure 10.3: Software block diagram.

it reboots the system. This is to prevent the system from crashing or getting stuck on a singularity. The main thread is also in charge of initiating and coordinating the two other threads.

The sense thread processes the flight data and controls the payload. This is done by first acquiring the GPS and IMU data from the sensors. This data is then stored in case it is needed to analyse the flight after mission completion. Afterwards, the flight trajectory is updated based on the current conditions. Then the flight mode (inside Lynx, inside box, falling, pull-out, pull-over, glide or land) is determined based on the position within the flight path at the moment. If the ICARUS+ is still within the Lynx, only the trajectory gets updated. If the ICARUS+ is released by the Lynx, but still within the containment box, another mode is entered. For this, separation of the Lynx is awaited and then the burn resistor is turned on to release from the containment box and deploy the UHF antenna. Finally, if the ICARUS+ has its wings deployed, the required attitude and the according elevon and canard deflections for the current flight trajectory are determined. This is then translated into a PWM signal and sent to all the servos. This process repeats throughout the mission.

The UHF thread is in charge of the communication segment of the mission. It first receives the UHF data and commands from the transponder. Afterwards, the data is processed and sent to the onboard storage (this might be essential as the uplink data rate is more than double the downlink data rate). Next to that, the

commands from the ground station are processed and the according settings are changed. The flight data can also be sent to the ground station to continuously know the status of the ICARUS+. Finally, the UHF and flight data are sent to the transponder for transmission.

10.4 Communication

The communication flow diagram provides an insight into how the data flows through the system hardware components and to the outside environment as can be seen in Figure 10.4.

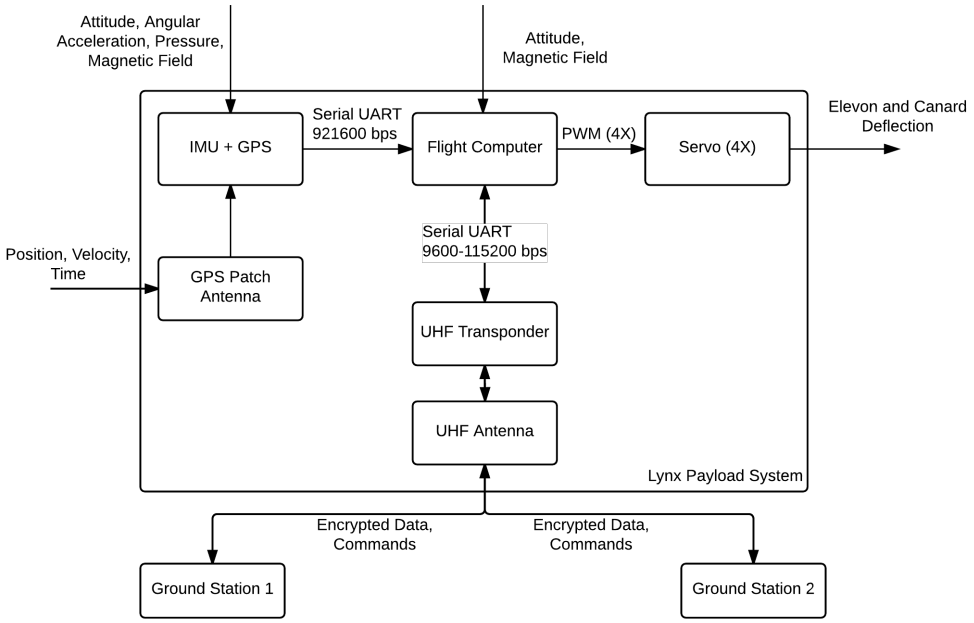

Figure 10.4: Communication diagram.

It can be observed that the outside environment for this mission are the ground stations communicating through UHF with the payload at a data rate between 9600 to 115200 *bps*. This is true for uplink. However, downlink has a maximum data rate of 38400 *bps* due to small payload antenna size. Through this communication link encrypted data and commands can be sent and received within a radius of 1000 km. This data is received and retransmitted by the UHF transponder and can be sent to the flight computer through UART if processing is necessary. Thus an abort mission command or change target command can be given to the payload. Additionally, the payload can update the ground stations of its status. However the communication link is half duplex, meaning that for a two hour mission 50 MB can be received and 16.5 MB can be transmitted. These data volumes can be tuned by changing the transmitting to receiving time ratio according to mission needs.

The outside environment also provides the position, time and velocity through the GPS receiver by passing through the L-band patch antenna located on the top of the fuselage. Furthermore, the IMU measures the attitude and angular acceleration. The barometer measures the pressure and the magnetometer the magnetic field strength. All this data is sent to the flight computer through UART at a baud rate of 921600 *bps*, which adds up to 791 MB over a two hour flight time.

All this flight data is then processed in the flight computer to determine the required elevator and canard deflection using control derivatives and a Proportional Integral Derivative (PID) controller. These are as follows converted to PWM signals for the four servo inputs, which results in deflection and a flight path change.

Chapter 11

Recommendations

Design group S16 is assigned with the task to design the payload for the Lynx Mark I. However, the group had only nine weeks to come up with a design and to simulate, verify and if possible validate everything. It is therefore not expected that the project is completely finished after these first design phases. Therefore, recommendations are given, to stimulate further research and make sure future work is done effectively.

This chapter elaborates on recommendations for further development of the final design. These recommendations for the post-DSE design and development phase have been categorised according to the different engineering fields.

11.1 Aerodynamics

From the aerodynamics point of view, a number of recommendations can be made on possible future research. The recommendations are mainly focused on the models used and how to improve and validate these.

- A more extensive optimisation should be performed for the selection of an airfoil. Due to the ever changing flight conditions during the iteration process many more iterations will have to be performed to arrive at the most efficient airfoil.
- In order to have a better understanding of the aerodynamic performance of the entire configuration in different flow conditions and at different angles of attack, a professional licence for Fluent should be acquired. This will allow for a finer mesh and thus more reliable results for the drag at higher speeds.
- A more reliable way to determine the maximum lift coefficient should be investigated, since the CFD software cannot accurately simulate stall.
- The drag model can be made more precise using more accurate estimates that have not yet been implemented due to time constraints. This includes estimation methods using more detailed dimension parameters describing the design.
- Wind tunnel tests should be performed to have a more accurate validation of the models used.
- More investigation into the effect of changing some design parameters like sweep angle, aspect ratio and taper ratio has to be performed.

11.2 Stability and Control

The recommendations regarding stability and control are given in this section. The stability and control department has done a lot of modelling. Therefore, their recommendations are focused on the models made. Next to this, the physical components of control and stability are taken into account.

- The free fall stability program should be combined with the flight mechanics model to make both more accurate.
- The free fall stability model should be made by using the stability derivatives for lateral and longitudinal stability and control .[22] Within the time constraint it was too difficult to make estimates on all the stability derivatives. However in a more detailed stage these values could all be calculated precisely.

- A computer controlled tool with feedback loops should be added to the model to optimise the control surfaces performance. This system should act as an automatic pilot.
- Supersonic control should be analysed in greater detail.
- The servos needed to bring motion to the control surfaces should be designed to a more detailed extent. This also implies that the hinge moments on the canard and the elevons need to be evaluated more thoroughly.

11.3 Structural Analysis

The most important aspects that should be investigated regarding the structural analysis are the expected loads during the launch and the feasibility and reliability of the hinge mechanism. The recommendations are focused on these aspects.

- Future tests performed by XCOR should identify the vibrational, acoustic and shock loads during the launch phase inside payload bay C. These loads are necessary to ensure launch survivability.
- The feasibility, reliability and manufacturability of the hinge should be explored. Due to the limited chord thickness these parts have to be very small, which might cause unforeseen problems.
- The structural feasibility for the clamping system requires a more detailed investigation. A proper trade-off must be made between the two possible clamping designs. The hinge unfolding in combination with the clamping system must then be optimised depending on the traded clamping design.

11.4 Flight Mechanics

The current flight mechanics model has a few aspects that can be improved, these aspects are listed below. Most improvements have to deal with making assumptions more accurate and implementing parts of code which are not included yet because of the assumptions.

- The effects of the winds in the atmosphere should be computed more accurately. The stratospheric winds are now assumed to be constant, but these will fluctuate for a certain range in reality. Also the winds below the stratospheric lower boundary can be implemented. These can be implemented close to the launch date, since the winds could be predicted more accurately at that time.
- The maximum lift coefficient should be implemented more accurately. The current model contains three values regarding the maximum lift coefficient. One is for subsonic flight, another for transonic flight and the third value is for supersonic flight.
- The mass distribution of the Earth should be implemented. Since the fluctuation of the gravitational acceleration is very small (9.7639 $m \cdot s^2$ - 9.8337 $m \cdot s^2$), it would not make a significant change on the total range, but it will make the model more accurate.
- For accuracy, the Earth has to be modelled as a non-perfect sphere.
- The exact attitude of the ICARUS+ also has to be implemented in the model. It is already in the initial conditions, but for example the latitude does not change during flight. This would make the model more accurate. However, it would not make a significant change.
- The lower boundary of the stratosphere should be computed more accurately. In the current model, this boundary is linearised.
- The obstacles that the ICARUS+ may hit on higher altitudes should be implemented. For example, mountains that can be implemented in the model. Due to the implemented attitude computations, the model can check if it would hit anything during flight.

11.5 Electronics

The recommendations with respect to the electronics are given for the fields that have been left out of research due to time constraints. Also aspects which could not be included yet are given below.

- If a higher downlink data rate is required, the power going to the UHF antenna has to be increased at the cost of an increased battery size. Since the fuselage can still be expanded, enough room for this increased battery can be created with decreased range performance. This is caused by the increased drag of the larger fuselage, which reduces the lift-to-drag ratio. In this manner the downlink data rate can be increased to 115200 bps, coming from 38400 bps.
- The containment box as it is now falls without slowing its descent and landing. This is an unsustainable solution, that can be improved upon. Possible solutions could be a built in parachute or airbag that deploy when landing. This requires an additional small electrical subsystem for the containment box alone. A small processor and battery with a simple parachute activation system can offer a viable solution. The parachute could deploy when a certain time has elapsed after deployment, which could be identified for example by a gyroscope that is able to measure the tumbling that occurs due to the separation between the ICARUS+ and the box itself. Moreover, if the box has to be recovered, it can also include a GPS module and radio transmitter to track its location.
- To make the ICARUS+ land successfully, the location data has to be more accurate. This can be achieved by using the VN-300 module from VectorNav that features two GPS receivers for increased accuracy. A second GPS antenna is then required, but that should not pose a problem, since it is small, low power and can be placed under another Torlon® composite section on the top part of the fuselage.
- Another alternative to landing the ICARUS+ like an aircraft is to use a parachute or airbag to break its fall. For this a larger fuselage is necessary, the parachute system will have to be custom designed to make use of the limited space that could be made available inside the fuselage.
- Finally, an external payload can be taken along, since the mass and size budget still offer significant mass and space increase possibilities. However, this would come at the cost of range and glide performance.

11.6 Thermal Control

The recommendations from the thermal engineering field are based on the lack of current knowledge of the thermal envelope, making the used simulation model more accurate and realistic and on a material study that could solve more then one problem in one go.

- The expected temperature envelope should be examined more in depth, preferably together with the aerodynamics department to develop a reliable CFD model, which models the skin heating due to friction and compression of the air.
- Complete fuselage temperature tests should be performed to ensure that the inner components do not exceed the allowed temperature range. The current approach gives a very rough estimation of the performance of the insulation and the large thermal envelope and tight allowable range should not be underestimated.
- If the temperature envelope allows the use of composites instead of titanium, that would be beneficial with respect to the thermal control. As many composites have a lower coefficient of thermal conductance compared to metals.

11.7 Recommendations Conclusion

Most recommendations in this chapter are focused on improving the models made, but also on implementing things which are left out due to the time and computational constraints. It is clear that there are currently too much uncertainties about the performance of this design, so further research should be performed to successfully perform the technical demonstration.

Chapter 12

Project Design and Operations

Actually finalising and producing the ICARUS+ needs quite some logistic planning and organisation. Therefore, the first section of this chapter elaborates on the project design and development logic and the testing. The second section focuses on the manufacturing process and the third section gives an overlook over the entire logistic process.

12.1 Project Design and Development Logic

In the post-DSE phases of the project, the ICARUS+ will be designed into further detail and qualified for flight. The logical sequence of activities of the detailed design and qualification can be found in the project design and development logic diagram, given in Figure 12.1.

As can be observed from the diagram, the three month detailed design phase followed by the one month qualification phase are planned in order to come to the final design. The overall planning of the ICARUS+ project can be found in Appendix B. These phases combine activities in parallel including design, testing, production, tooling, verification and qualification.

The detailed design and development phase has two branches running in parallel. The first one is made up of two segments: detailed design and development testing. For the detailed design segment, further research will be done in all the fields where more depth is needed. The specific areas of research can be found in the diagram. Afterwards, the development testing segment can start with the use of prototypes to test out and validate specific design solutions. The specific tests to be performed can be found in the same diagram. Noteworthy is that most of these tests only concern parts of the design and will thus not test the full model. The second branch of this phase concerns the production and qualification of the ICARUS+. Firstly, the production and product verification methods will be set up. This will be followed by the set-up of qualification methods. These will then be confirmed and a qualification model will be produced. This is to be used in the qualification phase of the development process.

The qualification phase also has two branches running in parallel. The first one is the qualification testing performed on the qualification model. This will include various tests on the full model. This is done to validate the design solutions from all the different design fields. These are all specified in the development diagram. For detailed information on what some of these tests include, the systems engineering slides of the TU Delft [39] can be used. The second branch will start off with the confirmation of the production and product verification techniques. Finally, it will be possible to produce the necessary tooling with the manufacturing process known. This sets the stage for the production process to start off with the finalised design of the ICARUS+.

12.2 Manufacturing

Once the development and the testing of the prototype has been completed, a look at the production is taken. In Table 12.1 all the sub parts of the ICARUS+ are presented. It can be noted from this table that the wing has to be split up. This is because of the hinges for the folding mechanism required to fit into the 2U box. Furthermore, also the fuselage is split up into three parts. One upper and one lower part, which is required by the manufacturing process, but also the nose will be separately. The reason for this is the fact that the best

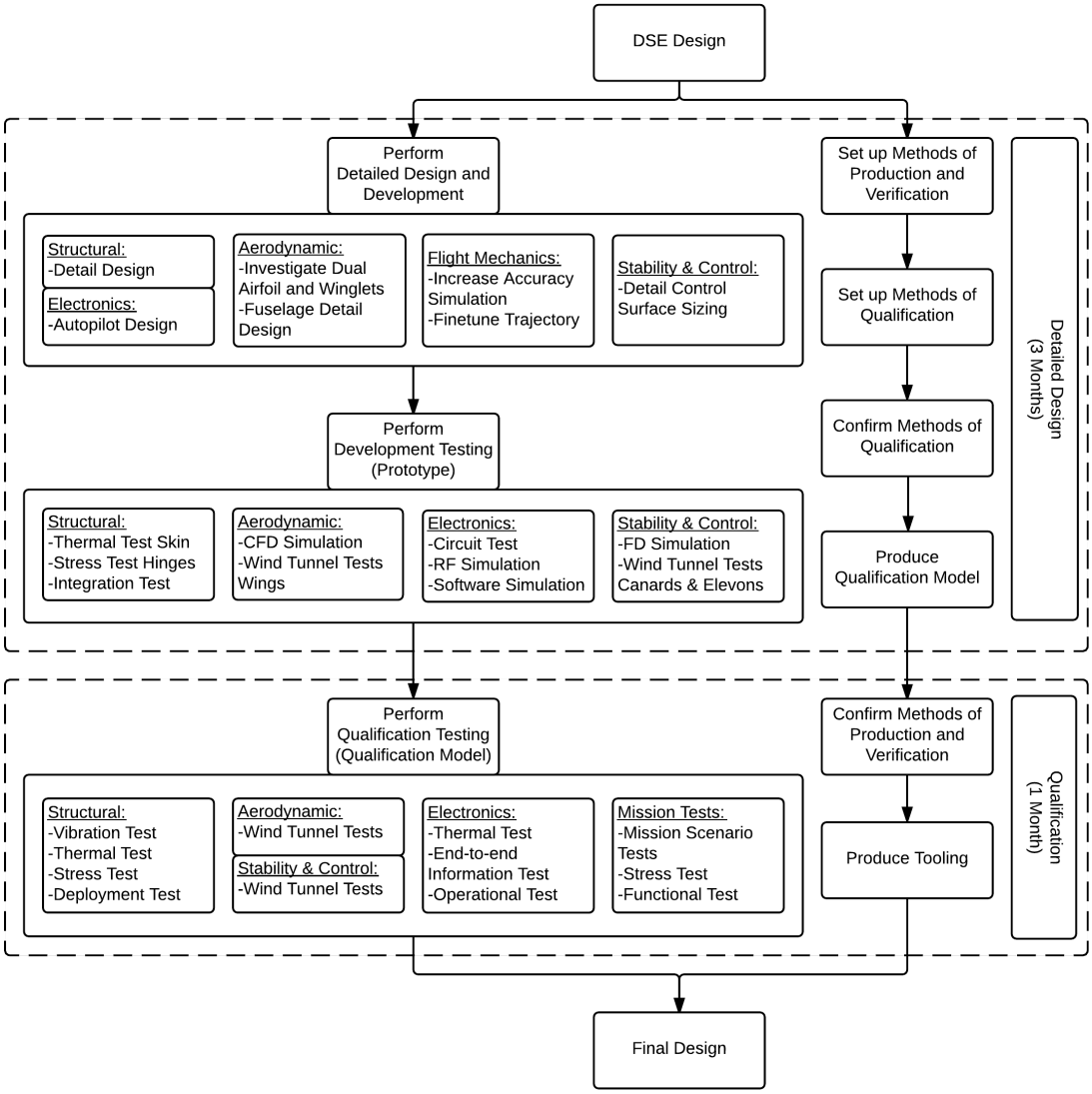

Figure 12.1: Project design and development logic diagram.

way of joining two titanium components is welding. However the heat generated during this process is too high for the electrical components inside. Therefore the upper and lower part will be welded together first together with the hinges and the wings. Then the electronics will be installed and finally the nose will be joined onto the structure with the help of adhesive bonding. The structure is cut in such a way that the pressure of the incoming air on the nose will strengthen this connection, which will increase the reliability of this design solution.

Most parts are COTS (Commercially Off The Shelf) components, as these have already undergone several verification and validation processes and have themselves proven to be reliably functioning. However, some parts cannot be bought and thus have to be produced or custom made. For example, the outer structure and the UHF antenna. Eventually everything has to be integrated and assembled into one structure. All this is part of the process. In order to gain a first overview, the lead time of the parts to be ordered, as well as the estimated manufacturing time and the additionally required tools and materials to manufacture the remaining parts are included in Table 12.1. Some values in the table are indicated only with a slash as they are too complex to be quantified in a simple table. These values can be found in the respective data sheets of the components. Furthermore, the lead time of several components is hard to determine as the respective companies require a quote to provide this kind of information and therefore these fields have been left with a question mark.

Table 12.1: Manufacturing data.

Component	Material	Method (Company)	Equipment	Lead Time
Servo	Titanium	Buy (MKS)	/	2 weeks
Computer	/	Buy (Gomspace)	/	?
GPS antenna	/	Buy (San Jose Technology, Inc.)	/	?
UHF	/	Buy (GomSpace)	/	?
UHF antenna	Ti-6Al-4V	Buy, Cut (Ti-Shop)	Cutting tool	2 weeks
GPS	/	Buy (VectorNav)	/	2 days
Power regulator	/	Buy (Mouser Electronic)	/	3 weeks
Battery	Li-Mn-O2	Buy (Saft)	/	3 weeks
Resistor	/	Buy (Mouser Electronic)	/	2 weeks
Wiring 15AWG	Copper	Buy (Mouser Electronic)	Cutting tool, Bending tool, Adhesive	3 weeks
Wiring 29AWG	Copper	Buy (Mouser Electronic)	Cutting tool, Bending tool, Adhesive	3 weeks
Patch	Torlon®	Machine	Milling tool	?
Fuselage Parts	Ti-6Al-4V	3D Print (GPI Prototype)	Welding tool/ Adhesive	7 Days
Wing Parts	Ti-6Al-4V	3D Print (GPI Prototype)	Welding tool/ Adhesive	7 Days
Control Surfaces	Ti-6Al-4V	3D Print (GPI Prototype)	Welding tool/ Adhesive	7 Days
Box	Ti-6Al-4V	3D Print (GPI Prototype)	Welding tool	7 Days
Hinges and Mechanisms	Ti-6Al-4V	CNC Mill	Milling tool, Welding tool/ Adhesive	2 Weeks
UHF Antenna Spring	Phosphor Bronze	Buy (Acxess Springs)	/	2 Weeks
UHF Antenna Housing	Torlon®	Buy (Drake Plastics)	Cutting tool	?
Power Connector	/	Buy (Mouser Electronics)	/	3 Weeks
Dyneema® Wire	/	Buy (Touwenwinkel)	Scissors	2 Days
Adhesive	Amide-Imide	Buy (Expoxy International)	Impregnation Treatment	2 Weeks

From analysing Table 12.1 it can be seen that three major steps have to be taking in the production process, which are ordering parts, manufacturing parts and assembling them. It can be noted that the maximum lead time is three weeks. However, in order to mitigate the risk of parts being delivered wrongly or broken, these components should be ordered six weeks in advance, forestalling a production delay.

The to be 3D printed components of the structure as well as the hinges will be produced by an external company specialised in 3D printing, for example GPI Prototype and Manufacturing Services[1]. However the UHF antenna will be manufactured at the TU Delft itself, using a simple cutting tool to shorten the ordered rod to the required length.

The casing of the GPS antenna, as well as the patch inserted in the upper half of the fuselage will be made of Torlon®. Torlon® is a composite material containing short glass-fibres which contribute to its outstandingly high performance, which is the reason why it is commonly used in aerospace applications. Looking at its mechanical properties it can be seen that they are quite satisfying concerning the tasks and restrictions this design has to meet. This might cause one to wonder now, why not produce the entire fuselage out of Torlon® as this would imply a much simpler structure and more reliability in terms of less joined parts. The reason for this is the fact that right now the product to be designed is a single product only, which does not involve a cost intensive process such as compression or injection moulding, which require a strong and very detailed mould. If this design was to be pro-

duced in higher quantities it would definitively be advantageous to use Torlon®, as 3D printing is very time intensive. Another possibility would be to machine the composite. However the accuracy that can be reached at this point is not sufficient to take into account the small details such as the airfoil shape. This is thus something that could possibly be considered in a few years from now, once technology has further evolved. For these reasons, only the parts around the antennae will be made out of composite in order to enable proper functioning. The casing for the UHF antenna will be ordered as a seamless rod. The patch however will be ordered as a plate and its exact shape will be obtained by machining. This is a process that can be done in the lab of the TU Delft by a structural specialist. The time estimated for this will be about half a day (five hours) including pretreatment and final polish.

Further parts to be manufactured by an external company are the hinges and actuating mechanisms. An example manufacturer specialised in this is GKN Aerospace[2], but there are many other companies on the market that are certified to do this.

The last step that remains is the assembly itself. This again consists of two sub parts, the electrical circuit assembly and the assembly of the entire structure. For the first, an electrical specialist will be hired for two consecutive working days. He will not only be responsible for the integration of all the electrical sub components, but also run the system a few times to ensure a proper connection. The second step will again be done by a structural specialist, as this requires welding (for the upper and lower part of the fuselage and possibly the hinges) and adhesive bonding for the remaining hinges, the composite patch and finally the closing of the fuselage. The time planned for this is two days as well, and will involve collaboration of the two hired specialists. Once the fuselage is closed, the manufacturing part of ICARUS+ is completed and it can be either stored or shipped to the desired location, as explained in the following section.

12.3 Operational Logistics

Next to defining the exact production plan as well as the testing methods, the logistics of the entire project have to be planned as well. The overall planning of the ICARUS+ project can be found in Appendix B. The logistics plan, depicted in Figure 12.2, illustrates six different phases of the entire logistics process. These will be explained below.

Production

The input into the logistics flow diagram is the tested and certified design made by the DSE group S16, playing the role of the vendor. The RNLAF is the customer on the other side of the operational logistics with the final aim to conduct the mission. The manufacturing (production) process is the first and probably most time consuming step. The single steps are explained more detailed in the previous section.

Shipping

Once the ICARUS+ has been produced, it has to be shipped to the launch location. Since at the launch site several tests have to be conducted as well, additional support material, such as measurement equipment, battery chargers or spare parts (wires etc.) have to be transported along with the payload or arranged at the location itself. Another action point to be taken is proper packing of the payload, to prevent any damages and of course to avoid any stresses in the structure or in the electronics caused by rough handling or high temperature differences. The shipping itself is advised to happen by air, train or truck, as shipping is very time consuming. Once the shipment has arrived at the location of the launch it should be received and stored until the acceptance test and the operations readiness test. The shipping is expected to take between three days if the launch site is nearby and twenty days for longer intercontinental shipments. Should there be no budget for air shipping, the product could be shipped by ship as well, however that could increase the the shipping time up to several months.

[1]URL `http://gpiprototype.com/` [10 Jun 2016]
[2]URL `http://www.monroeengineering.com/custom-manufacturing.php` [10 Jun 2016]

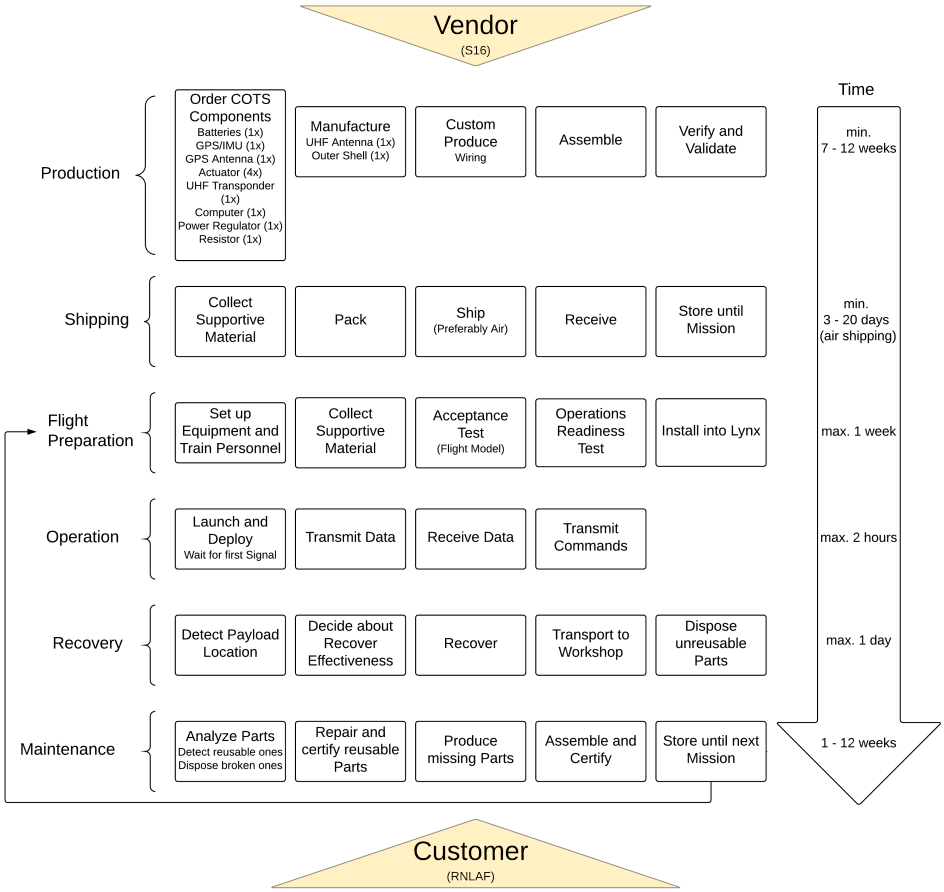

Figure 12.2: Logistics.

Flight Preparation

Before launching a few tests have to be conducted. Namely the acceptance test as well as the operations readiness test. For this, as well as for the proper installation in the Lynx and the data handling at the ground station, the available staff will need a short training and briefing. This should take about two to three days for the first launch and can be reduced to half a day after several launches. The acceptance test only has to be conducted once and will take up an entire day as well. The operations readiness test will take up about one day as well for the first launch. The time for this can possibly be reduced for future launches as well. The last step that has to be taken is the installation into the Lynx. Once this has been done several times this can be a routine exercise and should not take up more than half an hour. However, as this is the logistics plan for the first launch, and entire day will be scheduled for this activity as well. As can be seen from this, the time frame of one week can be significantly reduced after several successful launches.

Operation

This step is a relatively short one, however it is a crucial step as it is the goal of the entire project. The launch will take about five minutes until the payload can be deployed from the Lynx at 60 kilometres altitude. As soon as the payload is deployed it will detach from the box, as has been explained in Chapter 3, and start sending its position, speed and status. From this moment onward it is possible for the entire flight time of about 40 minutes to send or receive data to or from another ground station and to generate flight data. Furthermore, the option of sending commands to change the gliding trajectory is included in the software, giving the ground station partial control over the flightpath. The ground station can be chosen freely, as long as it will close the link budget presented in Section 6.5.

Recovery

Even though it is quite likely that the payload will end up in the Caribbean Sea if launched from Curacao, its exact position can be determined using the GPS sensor implemented in the design. After determining its location a decision can be made regarding the landing. If the area is considered to be accessible an attempt to recover the payload should be made, as this limits the contamination of the environment, as well as it provides possible reuse of some parts or materials. Once the payload has been found, it has to be transported back to the workshop either on site or back in the Netherlands where it can be repaired. The latter option is not included in the time-line as sending back will only be recommended if the payload needs complete rebuilding, which is quite similar to a new production process.

Maintenance

If only minor scratches are present, the payload can be inspected at the location and the damaged parts repaired or replaced. After assembling and verification, the payload can be stored until the next mission is planned. For this, one has to start at the third phase, the Flight Preparation phase again. In the worst case scenario, the device will have to be produced again and one has to go back to the Production phase.

Chapter 13

Cost Breakdown

When developing a new product or design, many different factors have to be taken into account when estimating the total cost. Therefore, it is very important to properly manage all parts of the process, including the production costs. This prevents an excess of the allowed budget of €100,000. In this chapter, the origin of all costs will be presented by means of a Cost Breakdown Structure (CBS) as well as the overall costs of this project.

13.1 Cost Breakdown Structure

First of all, a look at all the occurring costs has to be taken. In Figure 13.1 all the costs arising during a project, work breakdown, system breakdown and life cycle breakdown, are summarised in a CBS.

As can be seen from the structure, the costs can be divided into three main groups; development costs, production costs and operations and maintenance costs. As this project is still at a very early development stage, most of these costs can only be estimated very roughly, if at all. As this project differs from general

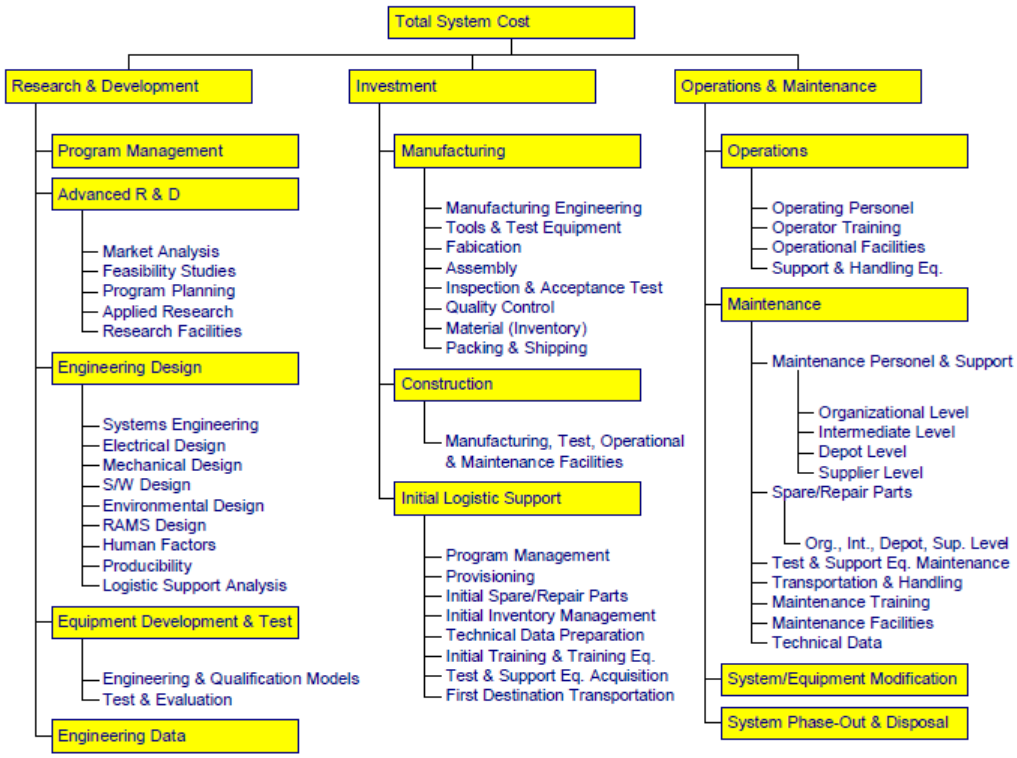

Figure 13.1: Cost breakdown structure. [40]

products, since only one device will be produced for now and it will only be used once, the development costs will form the biggest part. The production costs are as well quite high compared to the remaining costs. However, the maintenance and operations costs are relatively low. Apart from the intensive testing, all of the occurring costs will be recurring as the payload at this point is rather unlikely to survive the landing. Generally the costs for a product consist of product development costs, production costs which include recurring and non-recurring costs, operations and maintenance costs and finally disposal costs. However this project differs from general products, as only one device will be produced for now and it will only be used once. Therefore Their components and distributions are further explained in the following.

Research and Development

- **Program management costs**: these costs are the costs arising from the organisational part of the entire project. In a conventional design process every team has a manager. However in this case the DSE group S16 manages themselves and thus do not produce any costs for the customer. For more detailed information the interested reader is referred to the Project Plan .[2] However, the design will be handed over by the design team and needs managing from the first of July onwards until the end of March, after its mission. It is estimated that this task requires one person working about one day per week for the entire time span of 34 weeks until recovery of the launched payload.
- **Advanced Research and Development**: these planning and organising tasks are as well initially done by the design team S16 and will thus not result in any costs for the customer. However later on this will be one of the tasks of the project manager to further look into these areas.
- **Engineering design costs**: in theory, the work done by the engineering team has a market value of about €300,000 .[41] However, similarly to the management costs this part of the cost structure will remain cost free for the customer as it will be done by the design team S16. This includes all the work that has been done up to this point and is represented in this report. Possibly further design development will be necessary, as the students working on this project might not yet have the required background and experience, which for now is assumed will be done by the hired engineers.
- **Equipment and development costs**: these costs include the required verification and validation process for the design, as well as producing a prototype and conducting all the different tests mentioned in Section 12.1. These tests then will have to be evaluated and the design will have to be certified. The testing itself is difficult to price, however it can be assumed that for proper certification and quality control, a quality engineer plus three other experts will be hired full time for the period of four months.
- **Engineering data costs**: these costs arise when collecting data and producing graphs. Again this is partially already done by design team S16 within the design process. However more data will be generated during the qualification tests which is not part of this teams work and will have to be accounted for by the customer. This data collection will be done mainly by the responsible engineer, as well as the other hired staff.

Investment

- **Manufacturing costs**: the manufacturing costs, as can be seen in Figure 13.1 consists mainly of the material costs and the fabrication of the product. Another important, often forgotten, part of the costs is the tooling. In this design most of the production, except for the assembly itself, will be done by external companies. Therefore tooling costs will play a rather small role. However, if the product will be produced in larger quantities in the future, a switch of material will be beneficial in terms of costs and then the mould for the composite will form a large part of the production costs. This material choice is also another nice example where one can see the influence of the cost budget on the design.
- **Construction costs**: the construction costs are closely related to the manufacturing and the testing costs. However they focus more on the required facilities as well as the facilities needed for operations, for example the ground station. These costs have not been evaluated at this stage of the design and only partially fall into the provided budget for the development of the product.
- **Initial logistic support costs**: these costs in this project are mainly the costs involved with order costs for the COTS components and the management of the entire logistics process. The first one will be analysed in the next section, while the latter will be left to the customer, as this is not part of the design process anymore.

Operations and Maintenance

- **Operations costs**: these costs include all costs during the operations itself, including the training for the operating personnel. One part of these costs are the launching costs of €20,000, which are however not within the budget of the design team. Furthermore, the project manager along with the two engineers that assembled the design will be present for one week fulltime.
- **Maintenance costs**: the maintenance costs of this project will be rather small compared to other projects. This is because maintenance will, most likely only include the recovery of the design. At this point it is very likely that the product will not survive and has to be replaced entirely. Possibly some parts can be reused, but at this point that is not very likely. Especially as the planned launch location is an island, which increases the chances of the product landing and sinking in the Caribbean Sea.
- **System/Equipment modification costs**: these costs are very likely to occur, as the final altitude of the Lynx Mark II is aimed to be much higher than the Lynx Mark I. Furthermore the design might be used for different applications. This will involve quite some design modifications, if not a redesign. Additionally, this has never been done before, therefore a lot can be learned and probably improved and implemented in the future to render the mission more effective and efficient. At this point it is however impossible to estimate the costs of this.
- **Disposal costs**: it is very likely that it will not be possible to recover the design. Unless some fines for environmental pollution might have to be paid. Dependent on the country, this will not cause any costs. If the product can be recovered it will have to be disposed at a local scrap metal merchant. The costs involved will, based on the size of the design, be so small that they can be neglected compared to the other cost factors involved in this project.

13.2 Total Costs

Looking at each of the main cost sections, the design process, the manufacturing and the operation costs can be distinguished. However, the research and development costs have not yet been analysed in detail, as too little factors are known at this stage.

- **Staff**: as has been mentioned in the previous section a project manager will be required throughout the entire remaining time of the project. This will be 34 weeks, one day per week. A project manager on average earns €70 an hour, which amounts to €19,040. Furthermore, for the testing a quality engineer and three other different experts will be hired fulltime for a total of four months. With an estimated hourly salary of €30 this will amount to €76,800. Next to this, an electrical engineer, a software engineer and a structural engineer will be hired to further develop the design and assemble it. This is assumed to take a total time of about two months total. With an estimated hourly salary of €50 this will amount to another €24,000. Furthermore they will be travelling together with the project manager to conduct the mission and evaluate the collected data. Another two weeks will be planned for this, including preparations, which adds an additional €8,000. A more detailed planning can be found in Chapter 12. The mentioned average wages have been derived from a international website specialised in salaries.[1]
- **Facilities and equipment**: it is known that the launch itself will cost €20,000. The testing facilities and equipment will not be included in this cost estimate, since at this point of the design stage, it has not yet been defined how and where tests will be conducted exactly. This decision will be left to the customer, in consultancy with the engineers. The same applies to storing and assembling facilities and equipment.
- **Logistics**: the order costs are already included in the manufacturing part. For the transport part from the Netherlands to Curacao it can be estimated that shipping a package will not be more expensive than €3,000 as this will be a normal price for an actual person, including a safety margin. The reason for this rather high estimate is the fact that this also includes the shipment of possible spare parts or equipment that needs to be taken. This does not include the transport of the staff or any other logistic act, such as transport from storage to launch site or the storage itself for example.
- **Manufacturing**: the manufacturing costs are however at this point quite known already and therefore more extensively summarised in Table 13.1. Some values are estimates based on similar reference components, when the actual component price was not available. Not all categories are applicable to

[1] URL `http://www.payscale.com/` [16 Jun 2016]

all components and are therefore marked with a dash. Furthermore, several shipping costs are set into brackets as they are delivered together with other components by the same supplier (see Section 12.2). Some price have been converted from USD to €, as they are from American companies.

Finally there are the operation costs, which for example include the support of the ground station and the recovery and disposal, which are included in maintenance. However these costs are at this point very hard to estimate as they are absolutely unknown. After assessing all the different factors that play a role in the total costs, they can be rounded and summarised as follows in Table 13.2. Some of the actions are marked with an asterisk, for further information about what is included in the budget the reader is referred to the specifications in the text.

Table 13.1: Production costs.

Component	**Amount**	**Material Cost [€]**	**Manufacturing Costs [€]**	**Delivery Cost [€]**
Servo	4	240.00	-	5
Computer	1	ca. 4,500.00	-	ca. 15.00
GPS antenna	1	15.00	-	0
UHF	1	ca. 8,500.00	-	ca. (15.00)
UHF antenna	1	53.72	-	10.00
GPS	1	2292.47	-	48.49
Power regulator	4	5.16	-	20
Battery	1	50	-	35.00
Resistor	1	0.20	-	15.00
Wiring 15AWG	1	3.50	-	20.00
Wiring 29AWG	1	2.07	-	(20.00)
Patch	1	383.00	-	15.00
Fuselage Parts	3	0	1,500.00	20.00
Wing Parts	6	0	1,100.00	(20.00)
Control Surfaces	4	0	1,000.00	(20.00)
Box	1	0	1,000.00	(20.00)
Hinges and Mechanisms	10	ca. 1000	ca. 1000	ca. 10
UHF Antenna Spring	1	3.74	-	101.96
UHF Antenna Housing	1	140.00	-	(15.00)
Power Connector	1	28.55	-	(20.00)
Dyneema® Wire	1	0.50	-	4.5
Adhesive	1	7.99	-	34.34
Total	-	€17,961.38	€17,100.00	€349.29

Table 13.2: Total cost.

Action	**Cost Estimate**	**Accounting for budget**
Design Development	300,000.00	0.00
Project Management	19,040.00	19,040.00
Engineering Assembly	24,000.00	24,000.00
Testing & Certification*	76,800.00	76,800.0
Manufacturing	35,410.00	35,410.00
Logistics*	3,000.00	3,000.00
Launch	20,000.00	0.00
Operations*	8,000	0.00
Maintenance*	tbd.	tbd.
Total	**€486,250.00**	**€158,250.00**

Chapter 14

Market Analysis

A market analysis is a quantitative and qualitative assessment of a market. It looks into the size of the market, both in volume and value. Furthermore, a market analysis looks into the various customer segments and buying patterns, the competition and the economic environment in terms of barriers to entry and regulation. A market analysis is the foundation of the marketing plan. In this chapter, the first section will shortly describe the set up of a market plan and in the second section the market analysis will be elaborated on.

14.1 Market Plan

A market plan is structured by four main parts, which have their own subdivisions. These four main parts will be discussed below.

- **Part 1 - Conducting a situation analysis**: first, the goals of the company are considered. After this, the current marketing advantages and challenges of the company are examined. The target market has to be researched and the company has to examine on external opportunities or threats.
- **Part 2 - Researching the strengths and weaknesses**: the strengths and weaknesses of a company have to be examined in order to set up the optimal approach regarding the marketing strategy. This can be done by performing different kind of surveys, which are directed to current customers or external parties. This can be done by for example mail, by phone or by personal interviews.
- **Part 3 - Brainstorming on the marketing plan**: the surveys can be reviewed in order to determine the strategy of the company. After this, everyone that is responsible for the marketing of the company is been assigned a specific role. The marketing goals are declared and the marketing strategy has to be determined in order to meet those goals. After these steps, the budget for this strategy has to be set up.
- **Part 4 - Writing the marketing plan**: this is the part where everything comes together. Writing the marketing plan has to start with an executive summary. After this, the target market has to be described and goals have to be listed. The marketing strategy has to be identified and the budget will be written out into detail. At least, also an annual plan will be maintained.

14.2 Detailed Market Analysis

The objectives of the market analysis are to show investors that the company knows its market and that the market is large enough to build a sustainable business. In this section, the market analyses will be discussed in detail. This will be done in five steps. The first step of the market analysis consists of assessing the size of the market. Secondly, there will be elaborated on the target market. Than the market needs are examined. During the fourth step the competition in the target market will be elaborated on. At last, the barriers and opportunities to entry the market will be discussed.

14.2.1 Demographics and Segmentation

When assessing the size of the market, the approach for the assessment will depend on the type of the business. For example, if someone wants to open a new pizzeria, the size of the market can be limited to the local city.

The RNLAF is interested in a small UHF payload that will be detached at 60 km altitude from the Lynx, in cooperation with XCOR. Making this payload fly for a long range is even more progressive regarding technical developments. Because of the relative low costs predicted for this project and the opportunities towards technical development, a lot of worldwide technical divisions could be interested in this project. Space agencies, large space companies and national defence divisions, as the RNLAF itself, could be interested. Depended on the market, it could also be preferable to separate it into different segments, in order to have a clear overview and have the possibility for quick comparisons. Regarding the space industry, the market can be split up into six major segments. These are the United States of America, Europe, Russia, Brazil, China and India.

There are two factors that need to be investigated before assessing the size of the market. These factors are the number of potential customers and the value of the market. First, these two factors will be elaborated on. After that, an overview will be given of the demographics and segmentation.

Potential Customers

The potential customers for the type of payload that is going to be produced would be the kind of parties that are described in Section 14.2.2. Potential customers that will be discussed during this section, will be the space companies that have the ability or the co operations to launch a small payload for relatively low costs. Also the companies that are interested in the technical investigations at this scale will be potential customers. The potential customers per segment are summarised in Table 14.1.

Table 14.1: Potential customers per segment.

Segment	Europe (26)	USA (9)	Russia (10)	Brazil (5)	China (7)	India (4)
Potential Customers	ESA RNLAF Others DLR NLR SRON TNO Thales Alenia Airbus Defence RUAG Space Kongsberg Def. CNES INTA ALR BIRA UKSA SRI-BAS CSA DNSC-DSRI DTU Space ISARS ASI NRS ASR SNSB SSO	NASA Boeing Defence Andrews Space Lockheed Martin Orbital ATK SSL General Dyn. Dynetics SpaceDev	Roskosmos JSC-ISS Polyot ISC JSC Khartron MKB Raduga NPO Molniya Khrunichev NPO Lavochkin RSC Energia	AEB Star One Embraer Avibras XMobots	CNSA 602nd ADI AVIC CASIC CASC CCF CATIC	ISRO HAL NAL TASL

As can be seen, there are a lot of potential customers. Europe contains a lot of national space research centres, while the five other segments are concentrating on one single country.

Market Value

The market value is often more difficult to asses than the number of potential customers. In order to give the market value per segment, there is searched for reference material. The values that have been found are based on the market value at the start of 2015. For example, the global space industry grew by 9% in 2014, reaching a total of $330 billion worldwide.[1]The market value per segment is hard to determine, since the values that are available are mostly the values of the government funding. However, this will still give a good indication about how the markets activity is structured. The countries with a lot of government space fundings are often active on the space market. The 'government' funding value of Europe will be determined by summing the government funding values of the countries with the strongest economy. The government funding values of the USA, Europe, Russia, Brazil and India can be determined from Figure 14.1. The government funding value for China is found to be around $6.1 billion.[2]

Country/Agency	Currency	2012 Funding	2013 Funding	2014 Funding	2013-2014 Change
United States	U.S. Dollar	$47.041 B	$41.749 B	$42.956 B	2.9%
Brazil	Real	R$0.369 B	R$0.350 B	R$0.336 B	-3.8%
Canada*	Canadian Dollar	C$0.320 B	C$0.414 B	C$0.462 B	11.8%
European Space Agency (ESA)	Euro	€4.020 B	€4.282 B	€4.102 B	-4.2%
France*	Euro	€1.141 B	€1.122 B	€1.289 B	5.5%
Germany*	Euro	€0.586 B	€0.439 B	€0.451 B	2.7%
India	Rupee	₹48.947 B	₹67.920 B	₹72.380 B	6.6%
Israel	Shekel	₪0.050 B	₪0.180 B	₪0.090 B	-50.0%
Italy*	Euro	€0.251 B	€0.236 B	€0.161 B	-31.8%
Japan	Yen	¥298.000 B	¥322.100 B	¥382.700 B	18.8%
Russia	Ruble	₽140.000 B	₽165.223 B	₽165.814 B	0.4%
South Korea	Won	₩295.708 B	₩392.356 B	₩509.500 B	29.9%
Spain*	Euro	€0.032 B	€0.021 B	€0.023 B	6.5%
United Kingdom*	Pound	£0.029 B	£0.057 B	£0.075 B	31.4%

*National budget only (Excluding ESA contributions)

Figure 14.1: Government space budget growth, 2012-2014. [42]

Overview

The results of the analysis regarding the potential customers and market values have been summarised in Table 14.2.

Table 14.2: Overview of the government funding per segment.

Segment	USA	Europe	Russia	Brazil	China	India
Potential Customers	9	26	10	5	7	4
Government Fundings [· Billion US Dollars]	42.96	6.85	2.53	0.096	6.10	1.08

14.2.2 Target Market

The target market is the type of customers that the company targets on within the market. The type of customer that could be interested in this product are in general the kind of companies that produce or use flying payloads, aircraft or spacecraft. This product will have relatively low costs, regarding relatively small range missions.

[1]URLhttps://www.spacefoundation.org/sites/default/files/downloads/The_Space_Report_2015_Overview_TOC_Exhibits.pdf [7 June 2016]

[2]URLhttp://edition.cnn.com/interactive/2015/05/world/china-space/ [7 June 2016]

Companies that are interested in technical researches, regarding very small payloads which are able to fly, will be interested in this product. Also from a military point of view it would be an interesting product, regarding the different applications. The product could be used for communicative purposes or for carrying a very small payload with different purposes.

Until now, a project like this has never been performed before at such a small scale. Therefore, there are a lot of opportunities for further research, in order to improve the performance of a mission on this scale. Cost-wise this could be beneficial in the future for certain missions, so there will be a lot of interest in this product.

14.2.3 Market Need

The market need gets into detail regarding the need for this product. In this case there is no product like it at the current market on this scale. From a military point of view it will be a very demanded product. The product travels at high speed, which makes it hard to detect. Due to this, it is able to cover a certain area that would be dangerous to cross at ground level. Also, its small size reduces detectability.

The technical field of interest is a relatively new field regarding the overall technical developments. Due to the interest in and opportunities of this design, research towards these concepts will flourish, which will create more work for engineers.

14.2.4 Competition

While entering the market, the product will be in demand. It will be something new, in which other companies will be interested. However, after a while a lot of companies will try to do the same with their own resources. In other words, while entering the market, all potential customers will at the same time also actually be potential competitors.

14.2.5 Barriers and Opportunities to Entry the Market

This section is all about answering two main questions from the investor, in this case the RNLAF:

1. What prevents someone from producing the same product and taking over the market?
2. What will make this product so successful in trying to enter the market?

Some of these questions are already a bit elaborated on in the previous sections. The probability that the other technical companies will try to produce a product like this is significant. The probability that it will take over the market will be low, since this project group already has a leading start regarding the technical investigations. Because of the fact that this technical field is relatively new, there will be a lot of opportunities for improvements after a first design. It will take some time for other companies to get on the same performance level.

At the instant that this product enters the market, it will be successful due to the diversity of the possibilities that come with this product. From a military and technical exploration point of view, this product will be very demanded. Due to the relatively low costs of this product, this product could enter all markets from the investigated segments.

Chapter 15

Sustainable Development

In this chapter the sustainable development strategy of the ICARUS+ is given and elaborated on. This chapter is meant as a guideline. Functionality is more important than sustainability, especially since this is a demonstration mission. When a sustainable approach is not possible without decreasing the functionality in such a way that the aims of the mission will not be met, a less sustainable approach is preferred. A sustainable approach is however used up to the possible limits of implementing these.

15.1 Sustainable manufacturing approach

A sustainable development strategy starts from the manufacturing on. Up to manufacturing, sustainability is only taken in mind for designing the payload. For a sustainable manufacturing approach several things have to be taken into account. These things are: manufacturing methods, materials, waste and labour conditions.

Manufacturing methods

The ICARUS+ fuselage and wings are completely 3D printed. The material used is titanium, which has a melting temperature of 1877 K. [1] Due to the high melting temperature and high enthalpy of fusion, 1,158.4 Joule per gram is required to melt titanium and print something with it. However, the total energy required is still lower than the energy required to make a reusable mould and cast the design. This makes manufacturing with the use of 3D printing more sustainable for low numbers of products than traditional manufacturing methods. However, for high numbers of products a traditional manufacturing method is more sustainable than 3D printing due to the higher energy cost and manufacturing time for 3D printing separate designs.

Materials

The materials used are: titanium Ti-6Al-4V for the fuselage and wings and Torlon® for the the antenna patch. The titanium Ti-6Al-4V alloy can be recycled and is tried and tested, without decreasing the performance of the material, according to McDonald. [43] Therefore, waste chips of other manufacturers can be recycled to be used for the ICARUS+. Torlon® is however not recyclable.[2] When the Torlon® patch fails, the whole part should be replaced. Torlon® can therefore not be considered sustainable.

Waste

Waste is defined as "unwanted matter or material of any type, especially what is left after useful substances or parts have been removed".[3] When products are manufactured, waste material is the material left, which is not used for the design. With conventional manufacturing methods, waste is always present. Over time, the waste during manufacturing has already been limited by so called Lean Manufacturing methods. These

[1] URL `http://www.livescience.com/29103-titanium.html` [14 Jun 2016]
[2] URL `http://drakeplastics.com/wp-content/uploads/2016/01/Frequently-Asked-Questions.pdf` [14 Jun 2016]
[3] URL `http://dictionary.cambridge.org/dictionary/english/waste` [14 Jun 2016]

methods optimised the use of raw materials in such a way, that the most of useful parts are made from the least material required.

Nowadays a new manufacturing method exists. In Section 15.1 it is mentioned that 3D printing of titanium is used to make the fuselage and wings of the ICARUS+. An advantage of 3D printing is that there is no waste material.

Labour conditions

In a sustainable development process, also the labour conditions are considered. The labour conditions should be safe for the employees, without decreasing the efficiency of the process. Because of the manufacturing method used, which is 3D printing, the labour conditions are very well for the employees. There are no hazards as cutting and milling machines. An employee just has to run the program from a distance of the machine, and the machine does all the work.

COTS

Next to the shell of the ICARUS+, also the internal subsystems have to be made. All internal systems are commercially off the shelf components and are therefore likely to be sustainable.

15.2 Sustainable logistics and operations

This section elaborates on how the sustainable approach fits in the operations and logistics of the ICARUS+.

Logistics

When the design is manufactured, it must be transported to the launch location. Although the launch location is determined by XCOR Aerospace, it is recommended to pick a launch location close to the factory, or a factory close to the launch location. When the location is close to the factory, shipping costs and emissions can be saved. Also the time between production and launch can be reduced by limiting the distance the design has to travel.

Keeping sustainability in mind, it is important that there is no stock. A stock of ICARUS+ will cost space and will also produce emissions by the extra transport and facilities required.

Operations

The design is designed to perform its tasks autonomously, so little ground operations during the mission are required. Although it is not possible to limit this to zero activities, the aim is to limit the activities during the mission as much as possible.

After the performed mission, thus deployment out of the Lynx Mark I and flight to the Earth, the payload comes down on the Earth. When the payload lands, it should be retrieved in order to minimise the effect on the environment. In Section 12.3 it is already told that a trade-off has to be made between retrieving the object and disposing it because the costs and/or effort is too high. This is also seen from an environmental perspective. If the emissions and waste produced by retrieving the product are more harmful than the environmental impact of leaving the payload where it landed, the payload should be abandoned.

In the case the payload is retrieved, it should be checked on damage. The outer shell has to be replaced entirely in case of damage. The titanium can be recycled and be used in production again. The Torlon® is not recyclable and therefore should be stored until other applications are found. The internal components can be repaired in case of damage and can later be used again.

Chapter 16

Risk Management

It is very important to have a clear view on the risks of the mission. In this chapter the approach for this project's risk management is explained first. Next, the risks are assessed. This includes identification as well as analyses for their likelihood to occur. Later, a plan for reducing the risk of these scenarios is made. Finally, an approach for tracking and controlling the plans is given.

16.1 Risk Management Approach

Risk is always present in projects. According the NASA risk management handbook, risk is defined as "the potential for performance shortfalls, which may be realised in the future, with respect to achieving explicitly established and stated performance requirements" [44]. Those shortfalls can occur in different fields, such as safety, technical considerations, cost and schedule. They can occur separately from each other, but experience shows that most of them have some interdependency. To sufficiently analyse the total risk of the project, all the risks should be taken into account. Therefore, next to planning risk management at the start of the design, it is also important to take risk management into account during the whole design process. This is done by integrating two processes: Risk-Informed Decision Making (RIDM) and Continuous Risk Management (CRM). [44] Where RIDM mainly addresses the selection of alternative solutions to accomplish the set targets for the design, CRM focuses on meeting the requirements while implementing these alternative solutions. Using RIDM and CRM simultaneously will result in good risk management. To manage these processes in every subsystem in the final design the responsibilities for the subsystems are divided among the team members. To ensure that the risk for the total design is also small enough to be negligible, two members of the team are responsible for the integration of all subsystems.

In order to perform the RIDM and CRM sufficiently, a few steps need to be taken, which will also cover the content of the next sections. The first step is the risk assessment, which includes identifying the risks and analysing them. The initial risk identification is divided into two main categories, namely technical and programmatic risks. Technical risks take the shortfalls that might occur in the designing, engineering and test procedure phases into account. On the other hand, programmatic risks point up the uncertainties in the operating, financial and social sections. The identification is done by means of a risk web. Next, for analysis, those risks should be analysed to find the likelihood and magnitude of the consequence. The planning will be taken as third step and includes actions that need to be taken in upcoming design stages in order to reduce the risks. The fourth and final step is the the track and control of actions.

16.2 Risk Assessment

The first step that has to be taken in the risk management approach is to identify all involved risks. This is done by means of a risk web. As explained before, the risks are divided into technical and programmatic risks. For both categories a risk web is made. It can be found in Figure 16.1. In these webs the most important risks are identified.

Those risks should be analysed in order to estimate their likelihood and severity. In general the most severe and negative outcome is taken into account in order to guarantee a safer design. All the risks can be found in the risk map in Figure 16.2. Programmatic risks are indicated by a "P". The "T" stands for technical

[1] URL `http://www.hq.nasa.gov/office/codeq/doctree/NHBK_2011_3422.pdf` [cited 18 May 2016]

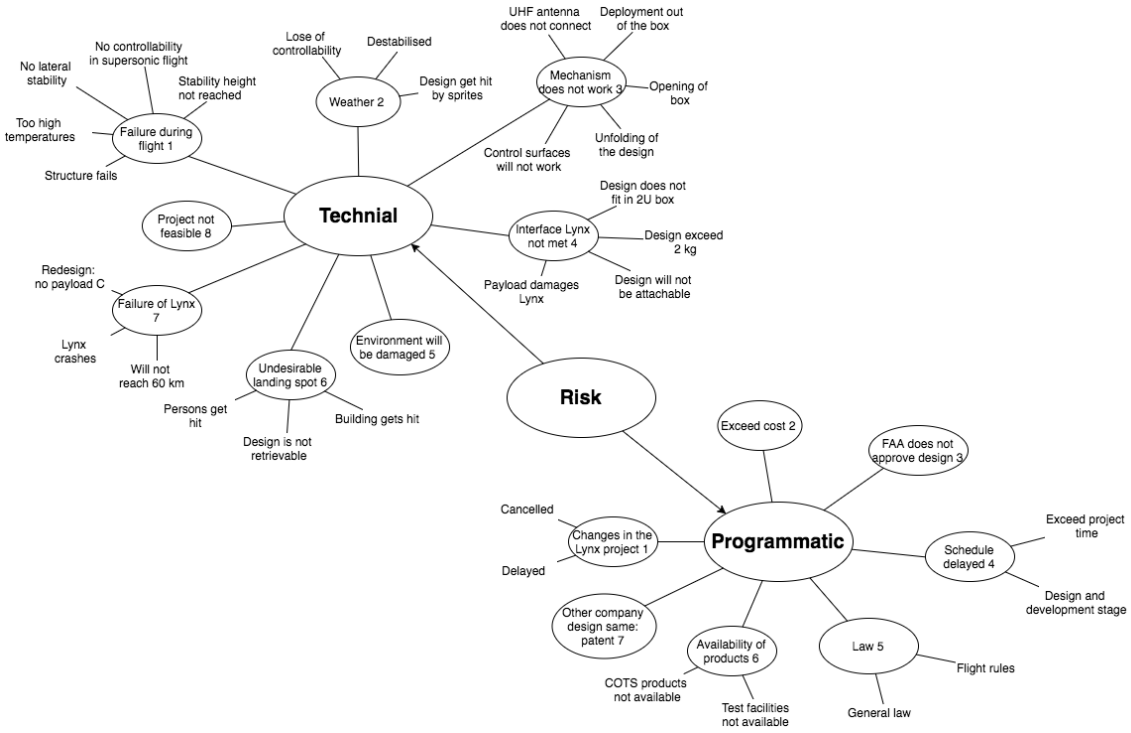

Figure 16.1: Risk identification web.

risks. The numbering used is the same as shown in the risk webs. Table 16.1 shows the relative rates for the indicated letters and numbers.

Table 16.1: Relative rates for risk map.

Level	Likelihood	Probability
5	Almost certain	100%
4	High Likelihood	80%
3	Likely	60%
2	Low Likelihood	40%
1	Not likely	20%

Level	Consequence
E	Risk will endanger project
D	Significant consequence
C	Moderate consequences
B	Minor consequences
A	Minimum consequences

As can be seen in the risk map, three divisions are distinguished, which are low, medium and high risk. The risks that are categorised in the low risk section are assumed to be negligible. They either are not very likely to happen ($<15\%$) or the consequence will be minimum. However, some risks do have a severe consequence and should be analysed further in order to mitigate the consequences. Those risks can be found in the medium and high risk zone and are briefly explained next.

- **Risk T1**: naturally there will be a risk that the design fails during its flight. For this risk, a positive outcome of the first part of the mission is assumed, which includes proper deployment. The risk can be found in the high risk zone. The reason being that the design can fail in a lot of different fields. The mitigation of this risk will be explained later on.
- **Risk T2**: depending on the launch time, the weather has a stronger or smaller effect on the mission. In all cases the weather is, even with modern technology, not absolutely predictable, which might cause surprises during operation. However, this is to be anticipated and some weather tolerance is therefore be taken into account during the design process. The probability that influential weather will arise during the mission is around 60%. However, the consequence is significant, since the weather might cause the design to be uncontrollable, destabilised or even badly damaged.

- **Risk T3**: one of the technical risks states the probability that deployment mechanisms do not work. As can be seen in the map, the probability for this event to occur is around 40%. However, the consequences might be harsh when a part of the deployment does not work. Therefore, it is graded high on impact. However, both values are the worst case taken. Naturally, the deployment mechanism consists of multiple parts, as stated in Figure 16.1. All those parts are carefully designed which already reduces the likelihood for this risk to occur.
- **Risk T5**: it is most likely that the payload will end up somewhere in the nature. Depending on the materials used, as well as the ground material on the actual final impact location, this can have very bad consequences on the environment. Especially if the mission is done repeatedly. This causes this risk to have a moderate consequence and to be something that has to be taken into account during the design process and during the risk mitigation procedures.
- **Risk T6**: the payload will come down with a high velocity. Therefore, the risk of hitting a person, an animal or the risk of the ICARUS+ doing any other damage has to be considered. This risk however is a product of two risks, the risk that the ICARUS+ will become uncontrollable together with the risk that the flying mechanism does not work well enough to slow the payload down. Since two events need to occur in order for it to be an actual risk, the event is less likely to happen. However, the consequences would be severe as it could hit inhabited areas on Earth. Therefore the impact is rated with an E.
- **Risk T8**: the feasibility of the ICARUS+ is an important section of the mission, since most of the requirements will not be met when the design will not be finished within the project. Therefore, this risk will have moderate consequences. The chance that the design will not be feasible is stated to be around 30% in this design stage.
- **Risk P1**: one of the programmatic risks states the risk that some changes might occur in the Lynx project. It can both be cancelled or delayed. The probability that it gets delayed is higher than that it will get cancelled. However, it is hard to state, since XCOR is responsible for this risk.
- **Risk P2**: the risk that the costs of the project will be exceeded is dependent on a lot of factors. Multiple mitigation techniques needed for other risks might result in increased costs. For this risk, proper trade-offs should be made in order for it to be mitigated. This is further explained in the next section.
- **Risk P3**: before the final design will perform its mission, it needs to be approved by the Federal Aviation Authorities (FAA). When the design is not allowed into space, it will have a significant consequence on the project. Probably it needs adjustments to fit the requirements given by the FAA. This will probably result in exceeded time and costs. For now, this risk is assumed to be very likely, since the FAA did not completely specify those requirement yet. So taking the worst case into account, it is quite likely that these requirements will not be met. The biggest concern are the high velocities during the free fall, since this increases the possible impact it would have on Earth.
- **Risk P4**: just as for the risk that the cost will be exceeded, the risk for schedule delay is dependent on multiple factors too. There can either be delay in the project stages of group S16 as well as in the design and development stage after the project. During the project, recommendations and expectations regarding the stages after the project are made. Those indicated that the risk for delay in schedule might be high, caused by further designing and research that might need to be done.

16.3 Risk Planning

The risks that fall within medium and high risk should be handled carefully, since they can compromise the mission. In the following paragraph the third step in risk management will be performed. Meaning that those risks will be evaluated to find proper solutions for the consequences they might bring. First, there must be decided what action should be taken. Possibilities are acceptance, mitigation, wait and watch the development, do more research or elevate that risk. All risks will be categorised within those actions and are analysed for the new impacts and probabilities they might cause. The low risks will for now be accepted, since their effect will not be severe or they are not likely to happen, as stated before.

Mitigation can be used for the risk that the design will land in an undesired spot. Looking at the risk map, this has a medium risk. Even though the chance that the device will land in a cultivated area is very small, it is still not small enough to neglect the risk. Naturally, there are multiple ways to control the path of the payload to a certain extent. Firstly, the location where it will be deployed can be chosen in such a way that the chances to land in an undesired location are reduced. During the mission, the weather and other meteorological

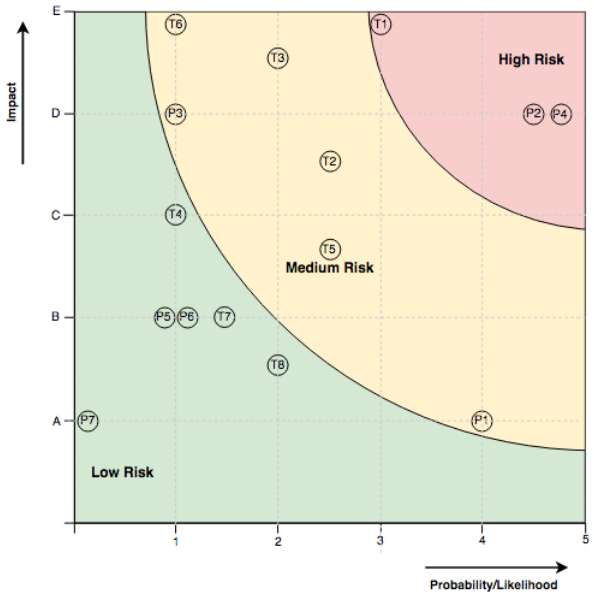

Figure 16.2: Risk map.

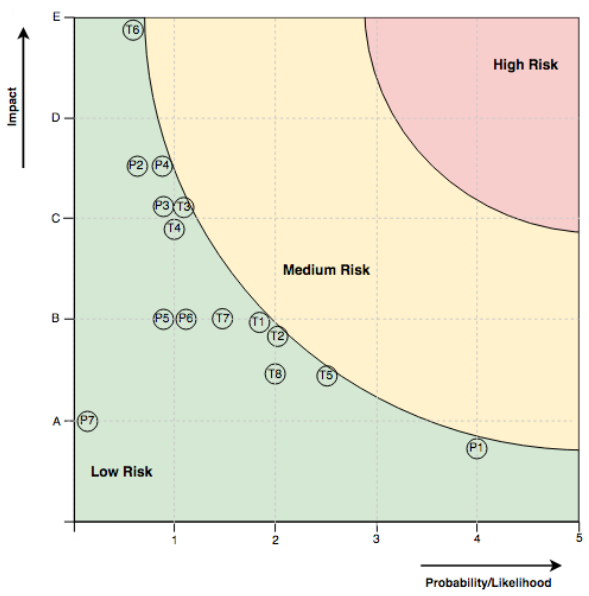

Figure 16.3: Risk map after mitigation.

phenomena can alter the path of the payload slightly. Some of those perturbations can be counteracted by implementing path and attitude control. However, this will result in more weight and thus it might not be feasible. Next to this, the weather phenomena can also be used to the benefit of the mission. For this reason, those phenomena should be investigated before the start of the mission. Doing this will cause the likelihood for this risk to decrease. Clearly, these methods are strongly interrelated with the risk stating the occurrence of unexpected weather. This risk can also be mitigated. The ICARUS+ should be designed in such a way that it is able to withstand various unexpected weather conditions, causing the impact of the phenomena to be reduced. Given that the Lynx will be flying several times a day, the launching time is also rather flexible and the design will not have to withstand a 100-year storm as that is an event that can be foreseen even a week in advance. This will reduce the likelihood for this risk too. The same counts for risk T5, that is concerned with the environment. Given that one of the aims of the project is that sustainability shall be taken into account, this is an aspect the team will definitely work on. Furthermore, during the design process a strong effort will be made to use environmentally friendly materials. Since the product should not only be launched once, it would be beneficial if the design could be reused. This would include a steering mechanism making the payload retrievable, which then again would reduce this risk to almost zero. However, the payload could be retrieved if the impact on the environment would be too harsh. Moreover this subject can be found in Chapter 15.

For the risk regarding the FAA, it is necessary to wait for their restrictions. Once known, they will be taken into account immediately. The impact will probably be lower than expected before. Therefore, the risk can be categorised in the low risk zone. The same counts for the risks regarding the Lynx project. The project group does have a low influence on this project and should therefore wait and watch the developments of XCOR. However, this risk can be slightly mitigated when the ICARUS+ is designed in a way that it might be implemented in other space vehicles too. This results in a lower impact for the project when the Lynx will not be developed any further.

In the next design stages, more research will be done regarding possible solutions to meet the requirements, which will reduce a few risks. For example, the flight path and mechanism will be further developed. This makes the possibility for failure much lower. On the other hand, the project feasibility might increase, when new found solutions fit the requirements. Naturally, the risk that a design fails can never be reduced to absolute zero. However, that risk can be significantly lowered by proper verification and validation processes that should be part of any design. This should not only be done at the end but throughout the entire process. If the mechanism fails, there is probably not enough time to analyse its predicted landing location. It could still be shot out of the air, or a small explosive devise could be used to destroy it before impact with the ground.

For both the risk of exceeding the cost and delaying the schedule a proper balance should be made. Spending more time or money on the project should only be done when it will reduce other risks that endanger the

project. For example, more research should be done when the design is very likely to fail during flight. However, when all the risk are mitigated in a proper way and fall within the low risk zone it can be chosen to leave the design as it is and start the mission. The interdependency with all the other risks makes predicting the schedule time and costs tough. However, it is very flexible and at this point in the design not very likely to be exceeded. Therefore, the risk can be categorised in the low risk zone.

After the mitigation is performed correctly, no more risk occurs in the medium and high risk zone anymore, as can be seen in Figure 16.3. Consequently, the risks can be accepted after the mitigation techniques are preformed.

16.4 Track and Control

The fourth and final step in risk management is to track and control all the analysed risks. As mentioned in the beginning of this chapter, CRM is used in combination with RIDM. This continuous management implies that the effects of the plans made should be evaluated. Obviously, new risks might come up during the detailed designing phase. Those should be documented and analysed continuously, so that their possible consequences can be taken into account within the design. Likewise, severe changes in the design might cause existing risks to change. This might in the end lead to a different planning.

If a risk does not behave as expected, actions should be taken to control it again. In order to do this proper feedback must be given. Therefore, the third step, planning, will be revised.

Chapter 17

Reliability, Availability, Maintainability and Safety (RAMS)

RAMS stands for Reliability, Availability, Maintainability and Safety and has become an essential part of aerospace design. This chapter first explains the general necessity of the analysis in Section 17.1. Using this information the four pillars of the analysis are examined in the remaining four sections.

17.1 Necessity of RAMS

RAMS is a recognised management and engineering discipline and can give recommendations to draw attention to the specifications of the design. Due to previous failures in spaceflight and therewith an increasing loss of operation, the safety impact is growing. Together with both the growing complexity and cost of aerospace systems, this causes RAMS analysis to be essential in the design stages of spacecraft. The analysis covers the complete life cycle of the mission and keeps operation, maintenance and disposal cost at an accepted level[1].

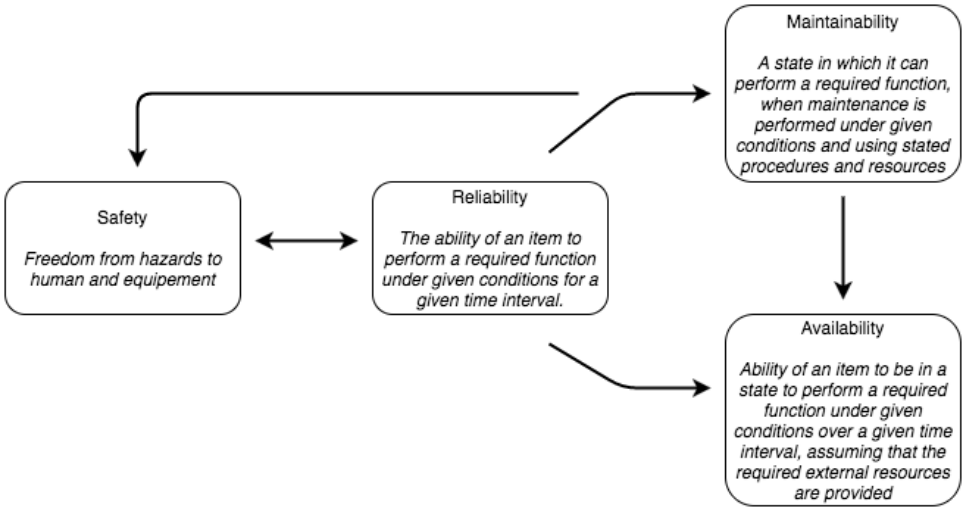

Figure 17.1: Relation between RAMS [45] [2].

17.2 Reliability

First, the reliability is going to be analysed. This is done with the use of failure rates. Therefore, the accuracy of the calculations depends on the knowledge about the failure modes of the different subsystems of the design. In

[1] URL http://www.dimat.unina2.it/marrone/dwnld/Proceedings/ESREL/2006/Pdf/S-247.pdf [13 Jun 2016]
[2] URL http://ntrs.nasa.gov/archive/nasa/casi.ntrs.nasa.gov/20120007117.pdf [10 Jun 2016]

order to calculate the total reliability, first a Failure Mode and Effect Analysis (FMEA) should be performed. After the failure modes are defined, a Reliability Block Diagram (RBD) is constructed. Using this information, the probability distributions for the reliability can be defined and final actions that must be taken can be identified.

17.2.1 Failure Mode and Effect Analysis

The objective of FMEA is to identify the severity of the failure modes that occur in the subsystems of the design. This information is used to determine the reliability of the design. Table 17.2 shows a list of systems with their failure modes, severity class and probability of occurrence. The criticality categories used in this table can be found in Table 17.1. For clarity reasons, only the worst failure mode is taken into account. The quantity of the subsystems used for the design is stated by n.

Table 17.1: Criticality categories.

Category	Severity	Impact
1	Catastrophic	Causes permanent injury
2	Critical	Causes severe injury or major property damage
3	Major	The system cannot operate
4	Significant	The system is partially operable

Table 17.2: Failure modes and probability of occurrence for the subsystems.

Type	n	Failure mode	Effect	Severity class	% of event
GPS sensor	1	Wrong calibration	Wrong data is passed on	3	30
GPS antenna	1	No fix with satellite	No actuation possible	1	10
Servos	4	Lose or open connection	No rotation	2	30
Burn resistor	1	Open circuit	No deployment	3	5
UHF transponder	1	Total loss of connection	No data available	2	20
UHF antenna	1	No fix with ground station	No communication possible	2	20
Flight computer	1	Common mode errors	Communication failure	2	20
Power regulator	4	Short circuit	No regulation	1	20
Wiring	$\sim$	Fried wiring	No connection	1	40
Battery	1	Overheated or exploded	No power available	1	10
Lynx power	1	No connection	Limited power available	2	5

17.2.2 Reliability Allocation

Now that the failure modes are identified a RBD is made. The purpose of the Reliability Block Diagram is to show the relationship of essential elements to system operational success[1]. For this design stage the diagrams are rather simplified. Consequently, a good reliability analysis can be performed. The two relationships that are distinguished are parallel and in series. For a parallel relation, all the components must fail in order to make the whole system fail. When the components are related in series, only one part has to fail in order to make the entire system work improper. The reliability of the two relations can be calculated using Equations 17.1 and 17.2, respectively.

$$R_{parallel} = 1-(1-R)^n \qquad (17.1) \qquad\qquad R_{series} = R_a + R_b + R_c \qquad (17.2)$$

Figure 17.2 shows the reliability diagrams for four different fields. Those fields cover the communication, navigation, actuation and deployment as also stated in 6.5.

[1] `http://ntrs.nasa.gov/archive/nasa/casi.ntrs.nasa.gov/19720006837.pdf` [13 Jun 2016]

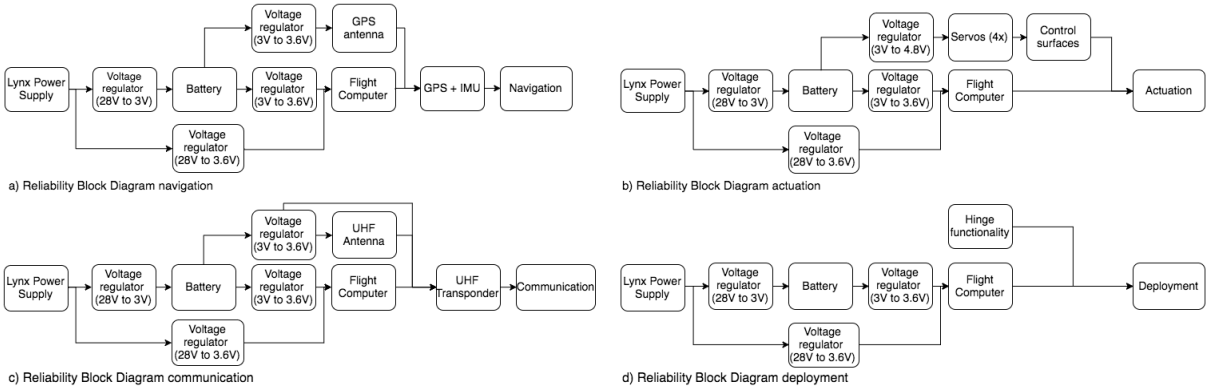

Figure 17.2: Reliability block diagrams.

17.2.3 Probability Distributions

Now that the relations between all the reliabilities are defined, an approach for the probability distributions can be found. Figure 17.3 shows the failure rate in time, where the failure rate is defined as in Equation 17.3. As can be seen, three different phases in the life time of the design can be defined. They all have their own probability function.

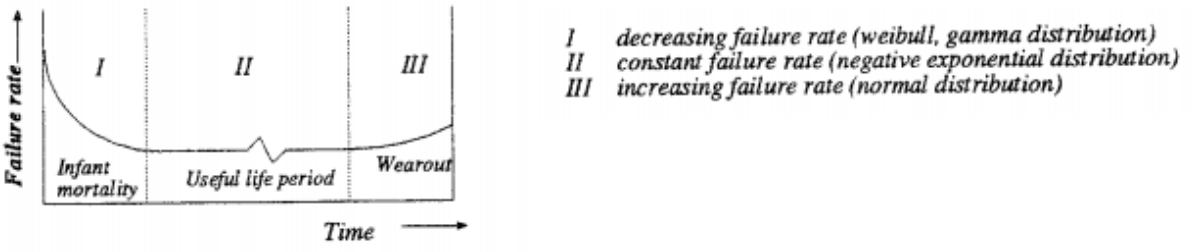

Figure 17.3: Bathtub curve. [45]

$$Failure\ rate = \frac{number\ of\ failures}{total\ operating\ time} \tag{17.3}$$

For this design phase, only phase II shown in the bathtub curve is analysed, since it will cover the main part of the life time of the design. The reliability can be calculated with the use of a negative exponential probability distribution. The corresponding equations for both parallel as series relations are given in Equations 17.4 and 17.5, respectively. Those are derived from Equations 17.1 and 17.2.

$$R_{parallel} = 1-(1-e^{-(\lambda \cdot t)})^n \tag{17.4}$$

$$R_{series} = e^{-(\sum_{i=1}^{n}\lambda_i)\cdot t} \tag{17.5}$$

In this equation λ represents the instantaneous failure rate and t is the time. In order to calculate the reliability of the design, the failure rates for the different subsystems must be found. This can be done by either testing or looking for internal databases of failure information on the devices or systems needed.

17.3 Maintainability

Maintainability is defined as the ability of an item to be maintained. It is essential for long term mission success. However, taking into account that the ICARUS+ carries a risk that it may not be retrieved after entering the Earth surface, it can be seen as a single use spacecraft. Consequently, it might need little or no maintenance requirements. Nevertheless, further investigation in landing possibilities will be performed in the

next phases of the design. Taking into account that the likelihood for the design to land safely increases, a proper maintainability approach should be examined.

The Mean Time To Maintain (MTTM) refers to the time required to perform both preventive and corrective maintenance action. [45] The time needed for maintainability can be reduced by increasing the labor-hours. However, this might result in additional cost. The frequency of maintenance is determined by the Mean Time Between Maintenance (MTBM) and is calculated using Equation 17.6. In the equation the subscript represent unscheduled (u) and scheduled (s) maintenance. Mostly, the reliability affects this design characteristic.

$$MTBM = \frac{1}{\frac{1}{MTBM_u} + \frac{1}{MTBM_s}} \tag{17.6}$$

Before the MTBM can be determined, the maintainability of the subsystems should be examined. All the electronic parts shown in Table 17.2 are COTS products and are therefore relatively easy to replace. However, a proper balance between cost and time should be found in this case.

The structure is mainly made out of titanium, as stated in Chapter 12. The initial higher cost for production will be counteracted by the reduction of maintainability costs for titanium as a result of the long life of titanium. Since the ICARUS+ is over-designed for stress forces, wear or failure is not expected. However, the fuselage is welded and glued during manufacturing. Consequently, when one of the electronic parts fail the fuselage should be taken apart too. This may result in unrepairable damage to the fuselage. Consequently, this part of the fuselage should be replaced as well and therefore also higher maintainability costs will arise.

Next, condition monitoring should be performed. Inspection requirements should be implemented when looking at reusable vehicles. All the parts should be inspected in order to check their operation. The failure of the electronics parts can be examined easily by looking at their reliability as stated in Section 17.2. For the titanium structure and the hinges, other inspection techniques must be used. Preferably, non-destructive test methods are performed, like visual inspection, X-ray inspection or ultrasonic inspection. Using those techniques, cracks in the material can be found that might lead to wear or even failure of the structure. In order to maintain the materials, coatings might be a good mitigation solution. They serve as additional stress, thermal and erosion protection.

Mean Down Time (MDT) is defined as the time spend on logistical delay next to the time used for active maintenance under current market conditions. Consequently, it considers the time that the design is unavailable to use. This is strongly interrelated with the availability of certain components and will therefore be further explained in the next section.

17.4 Availability

As is shown in Figure 17.1, availability is a product of both reliability and maintainability. The availability can be divided into three parts. These are the inherent availability (A_i), the achieved availability (A_a) and the operational availability (A_o). Those three types will be explained first. After this the analysis regarding the availability is performed, using two factors, the Mean Up Time and Mean Down Time. Up time is defined as the time that the design is in a state to perform its required function under given conditions.

17.4.1 Definitions

The inherent availability is defined as the probability that the design is available taking ideal conditions into account. Among other things, this includes readily available tools and personnel. The achieved availability also includes scheduled maintenance actions. However, logistic and administrative delays are still excluded. Finally, the operations availability states the probability that the design will operate as it should when it is needed.[45]

17.4.2 Analysis

Next, a rough estimation of the availability of the ICARUS+ will be made. The availability can be calculated using equation 17.7. For this calculation, A_i is taken into account, since the time span that should be taken for maintenance is hard to predict. Mean Up Time and Mean Down Time are stated in Table 17.3. The MDT

consist of preventive maintenance, like calibration, and repair time. This includes production and lead times. Most of those times are already stated in Chapter 12.

$$A_i = \frac{Up\ Time}{Total\ Time} = \frac{Mean\ Up\ Time}{Mean\ Up\ Time + Mean\ Down\ Time} \tag{17.7}$$

Table 17.3: Mean up time and mean down time ICARUS+.

Mean Up Time		Mean Down Time		
Time before deployment [hours]	Flight Time [hours]	Lead Time [days]	Manufacturing Time [days]	Assembling Time [days]
8.3	1.16	7-21	2	4

Using those values, the A_i is calculated to be 1.44 %, taking the worst MDT into accounts. This is the probability that the ICARUS+ is in an operational state when it is needed at a random point in time. However, for this calculation it is assumed that the design will not be reusable. This results in a total new full manufacturing process for each mission, which takes a lot of time. When reusability and line production is taken into account this value will increase significantly.

17.5 Safety

Finally, the safety of the mission is elaborated on. The safety is inherent with the risks of the mission, stated in Chapter 16. In that chapter effective mitigation techniques for most of the found risks are already stated making all the risks being categorised in the low risk zone. For that reason, this will not be examined in this section anymore. However, the impact those risk still might cause must be analysed in order to deliver a safe system. Figure 17.4 states all the impacts that safety might have. At a high level, the safety is divided into human safety, environmental safety and safety of equipment and property. More information on the environmental part can be found in Chapter 15. The other risks are elaborated in the risk management in Chapter 16.

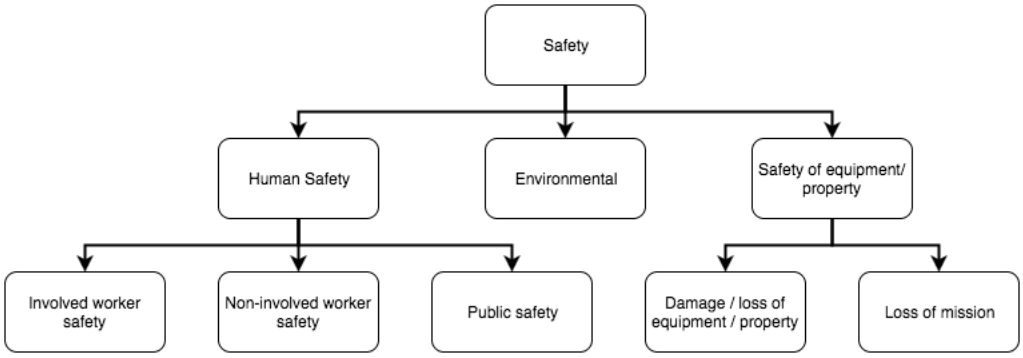

Figure 17.4: Impacts in the scope of safety. [1]

[1] URL `http://www.hq.nasa.gov/office/codeq/doctree/NASASP2010580.pdf` [14 Jun 2016]

Chapter 18

Budget Allocation

In order to keep track of the required budgets, it is very important to monitor the defined different technical performance measurements (TPMs). In this chapter the contingency margins of the entire project have been summarised and compared to the actual value.

Contingency management is used to ensure compliance with the requirements during the whole design process. This is done by identifying the important resources and assigning safety margins to each resource. At each milestone the margins can be lowered, because the design is more definitive. This project only has two mandatory milestones after the Baseline Review (BLR), namely the Mid-term Review (MTR) and the Final Review (FR). Most projects have more milestones, thus two additional independent design reviews have been introduced, namely the pre-MTR and pre-FR, so that the systems engineer has more control points. The contingency management for this project can be found in Table 18.1 and is based on spacecraft systems engineering examples [46]. Usually in projects like this one, the contingency margin of the schedule is decreasing with progress of the project. However, in this project, several deadlines have been set along the way, which reinforced being on schedule. Therefore, only a margin of 5% was used.

Table 18.1: Contingency management: the percentages indicate the contingency margin at each design step.

TPM	BLR	pre-MTR	MTR	pre-FR	FR
Mass	30%	20%	15%	10%	5%
Power	20%	15%	10%	5%	5%
Cost	25%	20%	15%	10%	5%
Schedule	5%	5%	5%	5%	5%

The compliance of the TPMs with the set contingency values has to be checked at every milestone. To visualise this, the TPMs of mass as well as power have been plotted in Figures 18.1 and 18.2. Only during the later design power was evaluated. Therefore a plot of the power budget has not been made. Also a plot of the schedule was considered redundant, as all the deadlines have been met. The achieved contingency values have been summarised in Table 18.2. Behind the achieved values, the actual contingency margin is mentioned in brackets. A negative contingency margin indicates that the TPM goes beyond the set requirement. It can be seen that the final costs are exceeded by 36.8%.

Table 18.2: Contingency management results with the actual values of the design and the corresponding actual contingencies between brackets.

TPM	BLR	pre-MTR	MTR	pre-FR	FR
Mass $[kg]$	1.54 (30%)	1.53 (30.7%)	1.24 (61.3%)	0.81 (146%)	0.98 (104.1%)
Power $[W]$	-	-	5.9 (374.6%)	8 (250%)	12 (133.3%))
Cost [€]	80000 (25%)	83300 (20%)	64776 (54.4%)	64776 (54.4%)	158,250 (-36.8%)
Schedule [days]	40 (5%)	40 (5%)	40 (5%)	40 (5%)	40 (5%)

For the actual detailed breakdowns of the respective TPMs the reader is referred to Chapter 10 for the mass,

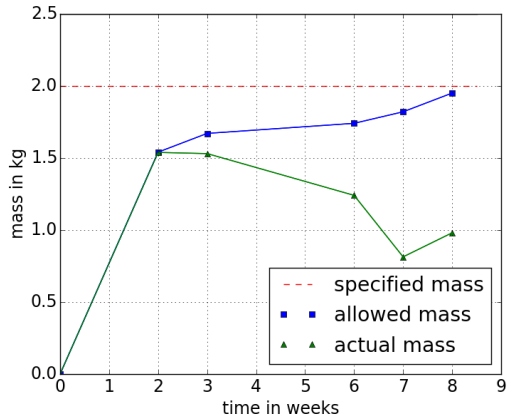

Figure 18.1: Mass contingency performance throughout the design phases.

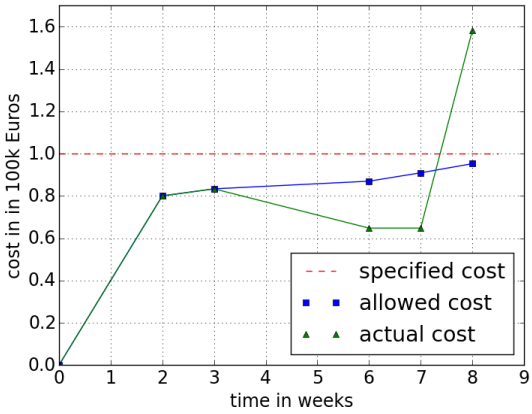

Figure 18.2: Cost contingency performance throughout the design phases.

to Section 6.5 for the power, to Chapter 13 for the cost and to Appendix B for the schedule. In those sections the reasons for not meeting the cost requirement are explained in further detail.

Chapter 19

Compliance Matrix

At the end of the conceptual design, it is important to take a look back at all the requirements that have been established earlier on and ensure that all of them have been met. Therefore, a requirements compliance matrix is given in this chapter.

In the beginning of this report (Section 4.3) an overview of the requirements has been given. Now that the design process has been completed, it is important to ensure that not only the subsystem requirements are met and that everything interfaces well, but also that the needs of the customer has been fulfilled. Therefore a compliance matrix has been establish in Table 19.1. In the left most column, the identifier of the requirement is stated. After that, for simplicity, only a short indication of the value or function of this requirement is mentioned. For a more detailed explanation about the requirement the reader is referred to Section 4.3. In the next column the actual value of the design is given. This is followed by the percentage of deviation from minimum or maximum value. These two columns have not been filled in for all requirements, as qualitative requirements do not have any values. Furthermore, some requirements give, for example, a temperature range, which cannot be expressed in percentages and therefore this is expressed in degrees of the smaller margin. Finally, the last column indicates whether or not the requirement has been met. The used indicators are explained below.

- **tbd**: only two requirements are indicated with tbd (to be determined). Both of them are requirements on the mission itself, and are not yet known whether they will be met or not as this will be purely dependent on the launch itself. This is also something that cannot be tested beforehand and should therefore be seen as a restriction to the launch window, rather than a requirement on the actual design.
- *: requirements marked with one star are requirements that have been designed for, but they cannot be approved as fulfilled and they will have to be verified with further tests other than pure inspection. This especially concerns qualitative requirements.
- **: there are only three requirements marked with two stars. The first requirement defines the resistance of the design towards the outside environment. As this is a function of time (the design will only experience the cold temperatures for a few minutes) this requirement is fulfilled for this mission. However, if the design was to stay at -70°C for a longer period of time, the battery might not survive. The other one defines the minimum pressure the design can survive. The structures department has determined that it can easily survive the minimum pressures occurring. However, a lower limit for this requirement is not determined yet. The third requirement is the requirement concerning the load factor. Due to the very strong material chosen, this requirement is being easily met. However, it was not possible yet to find the actual maximum load factor this structure can withstand.
- ***: two requirements are marked with three stars. These are the requirements defining the required actuator force. As can be seen they have been heavily overdesigned, which might look surprising. However, the reason for this is that the actuator chosen is already one of the smallest commercially available. There are smaller and lighter and thus weaker and maybe more suited actuators available, but due to the more detailed technology this will increase the cost. Therefore, as the chosen ones fit into the structure, the cheaper option has been selected.
- **No**: there is only one requirement that has not been met. This is the cost budget, which is exceeded by about 58%. The reasoning for this can be found in Chapter 13.

Table 19.1: Compliance matrix.

Requirement Identifier	Requirement	Value	Margin	Compliant
CON-QUAN-ELEC-BAT-01	Battery, 10.11Ah, (70% duty cycle)	10.11	0%	Yes
CON-QUAN-ELEC-BAT-02	Battery, 3-5V	3V	0%	Yes
CON-QUAN-ELEC-BAT-03	Battery, $\geq$ 4A	4A	0%	Yes
CON-QUAN-ELEC-BAT-04	Battery, $\geq$ 2 hours	2 hours	0%	Yes
CON-QUAN-ELEC-BAT-05	Battery, $\geq$ -40 to 60°C	-35.75 to 59.95°C	-	Yes
CON-QUAN-ELEC-COMP-01	Computer, $\geq$ 2 UART ports	2	0%	Yes
CON-QUAN-ELEC-COMP-02	Computer, $\geq$ 4 PWM ports	4	0%	Yes
CON-QUAN-ELEC-COMP-03	Computer, $\geq$ 1 GPIO port	1	0%	Yes
CON-QUAN-ELEC-REG-01	Regulator, 0 - 28V	0-28V	0%	Yes
CON-QUAN-ELEC-STRUC-01	Electronics, $\leq$-40 - 60°C	-40 - 72°C	12°C	Yes
CON-QUAL-ENV-01	Environment, thermal heating	-	-	Yes*
CON-QUAL-ENV-02	Environment, winds	-	-	tbd
CON-QUAL-ENV-03	Environment, winds	-	-	tbd
CON-QUAN-ENV-01	Environment, $\geq$ -70 - 30°C	-	-	Yes**
CON-QUAN-ENV-02	Environment, $\geq$ 0.002196Pa	-	-	Yes**
CON-QUAL-LYNX-01	Attachable to Lynx	-	-	Yes
CON-QUAL-LYNX-02	Power interface Lynx	-	-	Yes
CON-QUAN-LYNX-01	Size, 10x10x22 cm	10x10x22 cm	0%	Yes
CON-QUAN-LYNX-02	Mass, $\leq$ 2kg	0.905kg	54.75%	Yes
CON-QUAN-LYNX-03	Loads, $\geq$ 6g	9g	450%	Yes*
CON-QUAL-LYNX-RAIL-01	Aluminium 7075,6061,5005,5052	A 7075	-	Yes
CON-QUAN-LYNX-RAIL-01	Rails, $\geq$ width 8.5mm	8.5mm	0%	Yes
CON-QUAN-LYNX-RAIL-02	Rails, $\leq$ 1.6μm	1.6μm	0%	Yes
CON-QUAN-LYNX-RAIL-03	Rails, edge radius $\geq$ 1mm	1mm	0%	Yes
CON-QUAN-LYNX-RAIL-04	Rails, contact $\geq$ 75%	100%	25%	Yes
CON-QUAL-PAY-ELEC-01	Subsystems, fit into space budget	-	-	Yes
CON-QUAL-PAY-ELEC-02	Subsystems, fit into mass budget	-	-	Yes
CON-QUAL-PAY-ELEC-03	Subsystems, fit to battery	-	-	Yes
CON-QUAL-PROG-01	Legal framework	-	-	tbd
CON-QUAN-PROG-01	Cost, $\leq$ €100,000	158,250	-58.25%	No
CON-QUAN-PROG-02	Time, $\leq$ 10 weeks	10 weeks	0%	Yes*
CON-QUAN-PROG-03	Launch time, 1st quarter 2017	March 2017	0%	Yes*
CON-QUAL-STAB-COMP-01	Computer, control input	-	-	Yes*
CON-QUAN-STAB-SUB-01	Actuator elevator, $\geq$0.049Nm	0.216Nm	340.8%	Yes***
CON-QUAN-STAB-SUB-02	Actuator canard, $\geq$0.0082Nm	0.216Nm	2534%	Yes***
CON-QUAN-STRUC-01	Hinge, turning angle $\geq$ 100 degree	104	3.85%	Yes
CON-QUAN-STRUC-02	Chord at hinge, $\geq$ 52mm	79mm	51.9%	Yes
CON-QUAN-STRUC-03	Load safety factor $\geq$ 2	2	0%	Yes*
CON-QUAN-UHF-ANT-01	UHF antenna, 395 MHz	395 MHz	N/A	Yes*
CON-QUAN-UHF-ANT-02	UHF antenna, margin $\geq$ 7.8dB	15.07	248%	Yes*
FUNC-QUAL-01	System, detach	-	-	Yes*
FUNC-QUAL 02	System, communicate	-	-	Yes*
FUNC-QUAL-03	System, power supply	-	-	Yes*
FUNC-QUAL-04	System, flying mechanism	-	-	Yes*
FUNC-QUAL-05	System, attitude control	-	-	Yes*
FUNC-QUAN-01	Communication, 225-400 MHz	395 MHz	-	Yes
FUNC-QUAN-02	Load factor, $\geq$ 5(L/W)	-	-	Yes**
FUNC-QUAN-03	Temperature $\geq$ -20 to 60°C	-35.75 to 59.95°C	0%	Yes*
FUNC-QUAN-AER-01	at M=0.6 $C_{L_{max}} \geq 1$	1.1	10%	Yes*
FUNC-QUAN-AER-02	Gliding, L/D $\geq$ 5	7.22	44.4%	Yes*
FUNC-QUAL-ANT-01	Antenna, in GPS sight	-	-	Yes*
FUNC-QUAL-ANT-GS-01	Grounstation, compatible with antenna	-	-	Yes*
FUNC-QUAL-FLY-STAB-01	Stability height, $\geq$ 40km	40km	0%	Yes*
FUNC-QUAL-GS-ANT-01	Antenna, in ground station sight	-	-	Yes*
FUNC-QUAL-STAB-01	Stability	-	-	Yes
FUNC-QUAL-STRUC-ANT-01	Antenna, push payload out	-	-	Yes*

Chapter 20

Conclusion

In collaboration with RNLAF and XCOR the ICARUS+ was designed by DSE project group S16 from Delft University of Technology. The ICARUS+ is a deployable long range UHF-transponder which will be dropped by the Lynx Mark I from XCOR at an altitude of 60 km. In this report the design process that led to the final design of the ICARUS+ down to subsystem level is presented. This design is established through an iterative process performed by the collaboration of six main engineering fields: aerodynamics, stability and control, structures, flight mechanics, electrical engineering and thermal control. These fields each limit and support each other during the design phases. The final lay-out of the ICARUS+ is a compound delta wing-canard configuration.

The main limiting requirements of the ICARUS+ is the size limit of 2U. The ICARUS+ is designed in such a way that a maximum wing span can be reached by using special designed hinges in optimum locations. As follows, when the payload is fully folded, it fits into a 2U box. When deployed, a wing span of 360 mm is reached. The total system mass of the ICARUS+ including its box resulted to be 0.980 kg.

In order to obtain optimum performance, a NACA 43012A airfoil was chosen. This airfoil has a good gliding performance at low Reynolds numbers and a positive moment around the aerodynamic centre. This airfoil is used on a compound delta wing, also known as a double swept wing, which is preferable at high speeds and delays stall due to a phenomenon called vortex lift. Furthermore, a canard is added to the configuration to increase the controllability of the ICARUS+. in order to obtain lateral stability a vertical tail surface is added. The canards are made movable and additional elevons are added to the wings to increase controllability. The material chosen for the design is titanium as it is very strong and has a good resistance against high temperatures. In the ICARUS+ a UHF-transponder with antenna is integrated. Finally, it has been found that the customer will need to make a trade-off between quality and testing and the budget as the estimated cost of €158,250 is exceeding the set budget of €100,000.

With a long range as main goal of the design, the flightpath pattern is mayor importance and thus has been examined into further depth. Initially, when the payload is released, it will immediately deploy from the box and start a free fall. However, the initial horizontal velocity from the Lynx will make it fall in an arc. When the density is high enough the ICARUS+ will perform a pull-up followed by a pull-out. Afterwards it will start its optimum glide flight path. All these design specifications together accumulate to a final range of 230 km with an airborne time of 70 minutes.

Recommendations for future research are establishing a more detailed design of the ICARUS+ and performing a more into depth quality control throughout the entire design process. This should be done by qualified engineers. Overall more testing should be done to the design whilst staying within the €100,000 budget. Considering this final budget, it is advised to think about different applications the ICARUS+ could be used for in the future.

Bibliography

[1] Valare S. Lynx spacecraft to give big boost to space tourism. *RocketSTEM*, Jan. 2014.

[2] DSE Group S16. Dse - lynx: Deployable uhf transponder payload - project plan. Technical report, Delft University of Technology, 2016.

[3] DSE Group S16. Dse - lynx: Deployable uhf transponder payload - baseline report. Technical report, Delft University of Technology, 2016.

[4] DSE Group S16. Dse - lynx: Deployable uhf transponder payload - mid-term report. Technical report, Delft University of Technology, 2016.

[5] Anderson J.D. *Introduction to Flight.* Mc Graw Hill Higher Education, fifth edition, 2005.

[6] Vrijhof B. *Meteorologie en navigatie.* QDM Luchtvaart, fifth edition, 2014.

[7] Menter F.R. Improved Two-Equation $k-\omega$ Turbulence Models for Aerodynamic Flows. Technical report, NASA Ames Research Center, 1992.

[8] Chapman D.R. Airfoil profiles for minimum pressure drag at supersonic velocities- general analysis with application to linearized supersonic flow. Technical report, Ames Aeronautical Laboratory, 1951.

[9] Hall C.F. Lift, drag, and pitching moment of low-aspect-ratio wings at subsonic and supersonic speeds. Technical report, National Aeronautics and Space Administration, 1953.

[10] Williamson W.A. Summary of low-speed airfoil data. Technical report, Department of Aerospace Engineering University of Illinois at Urbana-Champaign, 2012.

[11] Corby J. Starlet wing rib section. online, Jul. 2005.

[12] Berry J.C. Rogers E.W.E. Experiments with biconvex and double-wedge aerofoils in low-density, supersonic flow. Technical report, Aerodynamics Division N.P.L., 1970.

[13] Kuhl J.M. Keenan J.A. The effects of winglets on low aspect ratio wings at supersonic mach numbers. Technical report, National Aeronautics and Space Administration, 1991.

[14] Cook M.V. *Flight Dynamics Principles: A Linear Systems Approach to Aircraft Stability and Control.* Butterworth-Heinemann, 2011.

[15] Drag estimation. University Handout, 2015.

[16] Williams J.E. *The USAF Stability and Control Digital DATCOM. Volume II.* PN, 1979.

[17] Vargas J. Development of a wave drag prediction tool for the conceptual design phase. Technical report, Delft University of Technology, 2015.

[18] Basavaraj A. Estimation of wave drag of non-transonic airfoils using korn equation. *International Journal of Innovative Research in Science, Engineering and Technology*, 4, 2015.

[19] Lock C.N.H. The ideal drag due to a shock wave. Technical report, Aeronautical Research Council, 1945.

[20] Volume wave drag. University Handout, 2005.

[21] Steenhuizen Ir. D. Wing design part 3. University Lecture Slides, Delft University of Technology, 2013.

[22] van der Vaart J.C. de Weerdt E. de Visser C.C. in 't Veld A.C. Mooij E. Mulder J.A., van Staveren W.H.J.J. Flight dynamics. Technical report, Delft University of Technology, 2013.

[23] Vorley G. Rose R., Nicholas O.P. Flight measurements of the elevator and aileron hinge-moment derivatives of the fairey delta 2 aircraft up to a mach number of 1.6 and comparisons with wind-tunnel results. *Reports and Memoranda No. 3485*, 1967.

[24] Brownson J.J. Jorgensen L.H. Effects of reynolds number and body corner radius on aerodynamic characteristics of a space shuttle-type vehicle at subsonic mach numbers. Technical report, NASA Ames Research Center, 1972.

[25] LaRocca G. Requirement analysis and design principles for a/c stability & control (part 1). University Lecture Slides, Delft University of Technology, Feb. 2016.

[26] Zandbergen B.T.C. Vos R., Melkert J.A. A/c preliminary sizing (class i weight estimation method). University Lecture Slides, Delft University of Technology, Sep. 2014.

[27] Steenhuizen Ir. D. Wing design part 2. University Lecture Slides, Delft University of Technology, 2013.

[28] Seywald K. Wingbox mass prediction considering quasi-static nonlinear aeroelasticity. Master's thesis, technische universität münchen, 2011.

[29] Donachie M.J. *Titanium: A Technical Guide*. ASM International, second edition, 2000.

[30] Anderson J.D. *Fundamentals of Aerodynamics*. McGraw-Hill Book Company, 2011.

[31] Novak K.S. Birur G. Lankford K. Sunada E., Pauken M. Paraffin actuated heat switch for mars surface applications. In *Lunar and Planetary Science and Exploration*. NASA, Feb. 2002.

[32] Hoekstra J. Intro to aerospace engineering. University Lecture Slides, Delft University of Technology, Sep. 2013.

[33] Hibbeler R.C. *Engineering Mechanics: Dynamics*. Pearson, thirteenth edition, 2013.

[34] Küchemann D. *The Aerodynamic Design of Aircraf*. Pergamon Press, 1978.

[35] Kohlman D.L. Flight test data for a cessna cardinal. Technical report, National Aeronautics and Space Administration, 1974.

[36] Heisler M.P. Temperature charts for induction and constant-temperature heating. *Trans. ASME*, 69(2), 1947.

[37] Perkins C.D. *Stability and Control: Flight Testing*. Pergamon Press, second edition, 1959.

[38] Muthukumaraswamy S.A. Rahman H. Preemptive multitasking on atmel®avr®microcontroller. In *Advances in Information Science and Computer Engineering*, Dubai International Academic City United Arab Emirates, 2014. School of Engineering & Physical Sciences, Heriot Watt University Dubai Campus.

[39] Verhagen W. Curran R. Course organization & systems engineering for aerospace. University Lecture Slides, Delft University of Technology, Feb. 2016.

[40] Swinerd G. Fortescue P., Stark J. *Spacecraft Systems Engineering*. Wiley, third edition, 2003.

[41] Van Tooren M. Hamann R. Systems engineering & technical management techniques. University Lecture Slides, Delft University of Technology, Feb. 2007.

[42] Moore J. 2014–15 estimates. Technical report, The Canadian Space Agency, 2014.

[43] Palanisamy S. Dargusch M.S. Xia K. McDonald D.T., Lui E.W. Achieving superior strength and ductility in ti-6al-4v recycled from machining chips by equal channel angular pressing. *Metallurgical and Materials Transactions A*, 45(9):4089–4102, 2014.

[44] NASA. *Risk Management Handbook*. Office of the National Aeronautics and Space Administration, Nov. 2016.

[45] Van Tooren Prof. Dr. Ir. M.J.L. Hamann Ir. R.J. Systems engineering & technical management techniques part ii. University Document, Delft University of Technology, Jan. 2006.

[46] Guerra L. Technical performance measures module. University Lecture Slides, University of Texas at Austin, Mar. 2008.

Appendix A

Functional Breakdown Structure

In this appendix the functional breakdown structure of the ICARUS+ is shown in Figure A.1.

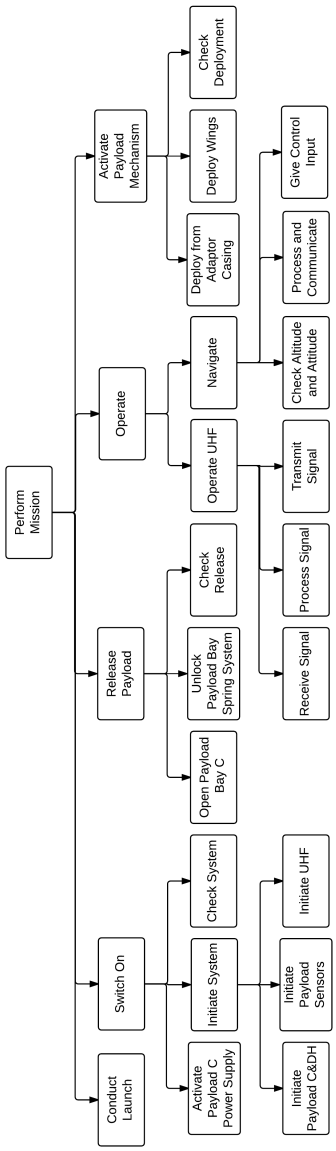

Figure A.1: Functional breakdown structure.

Appendix B

Gantt Chart

In Figure B.1 the Gantt Chart of the entire ICARUS+ project is shown. In Figure B.2 and Figure B.3 the Gantt Chart of the project from group S16 is shown.

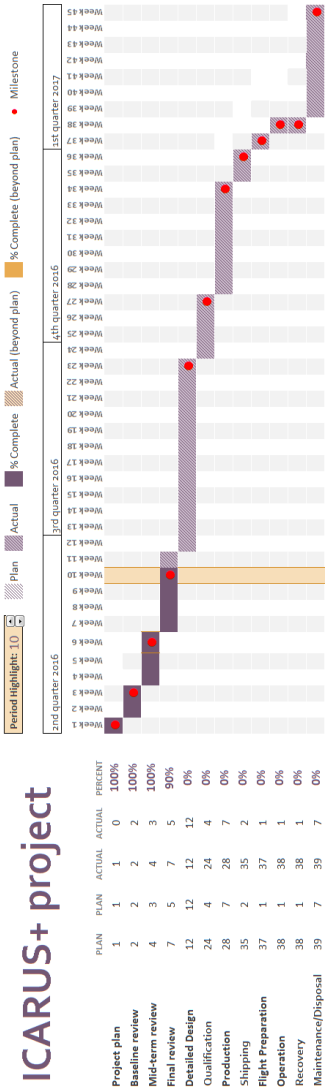

Figure B.1: Gantt chart of the entire ICARUS+ project.

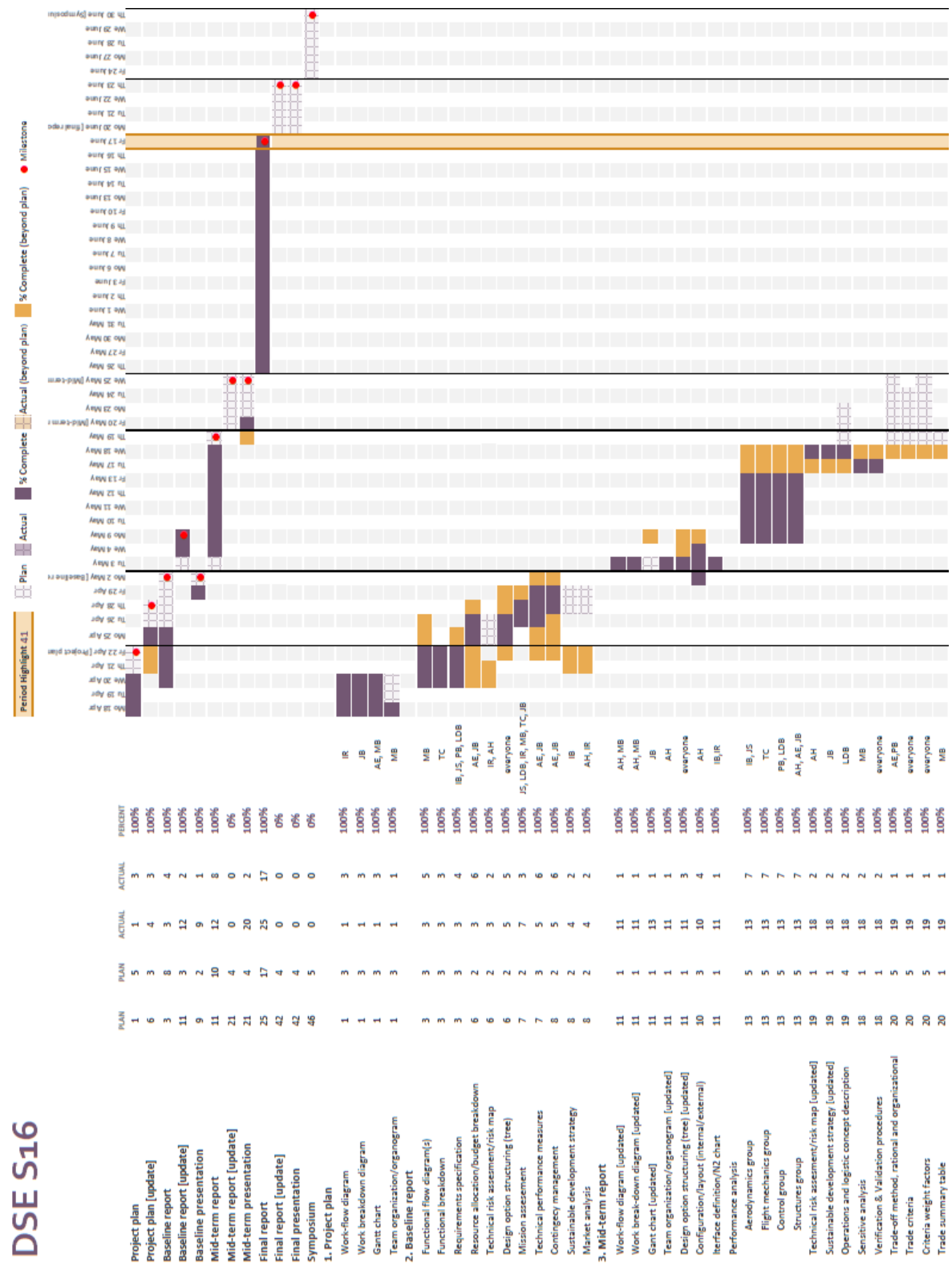

Figure B.2: DSE gantt chart part one (dot is a deadline).

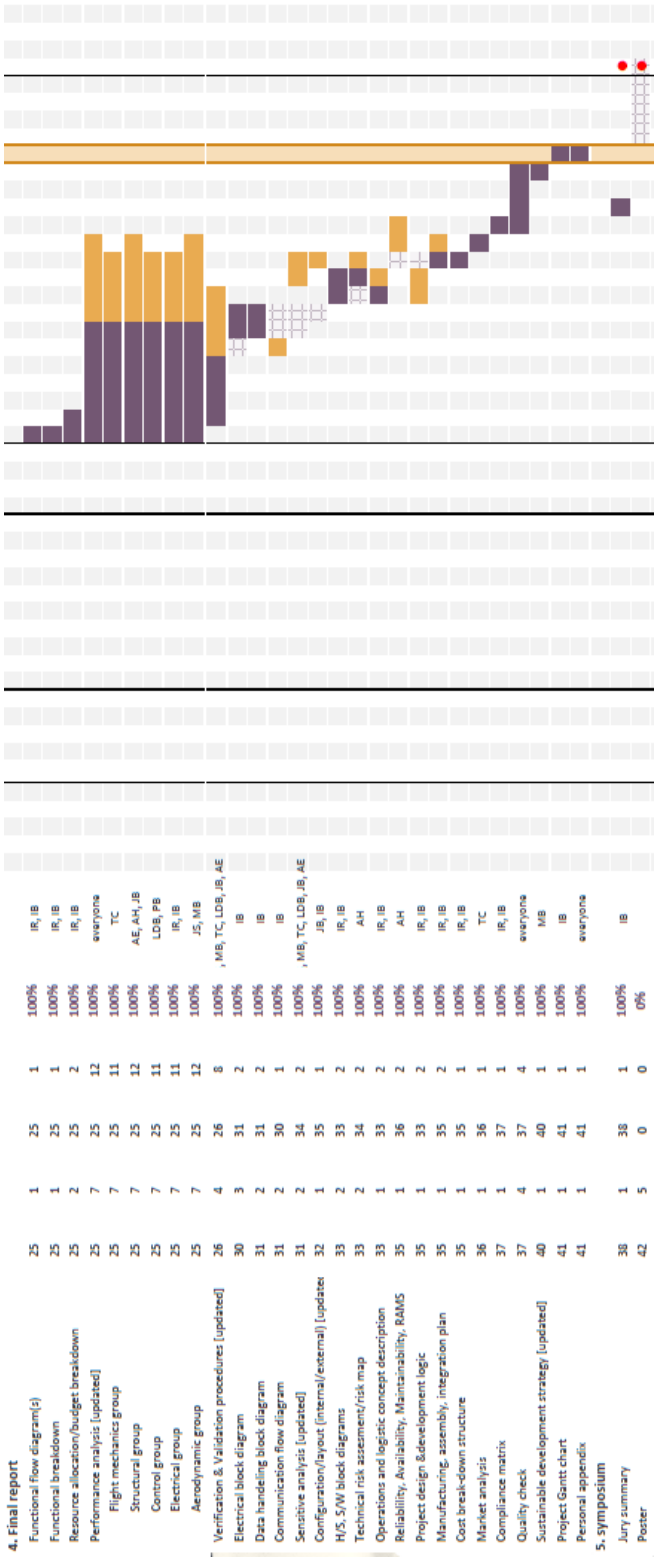

Figure B.3: DSE gantt chart part two (dot is a deadline).

Appendix C

Simulation Models Flow Diagrams

In this appendix the functional flow diagrams for the models used are shown. Figure C.1 shows the functional flow diagram of the stability and control model. Whether or not there is an input of control surfaces and what the input is, is optional and can change every time the program is run.

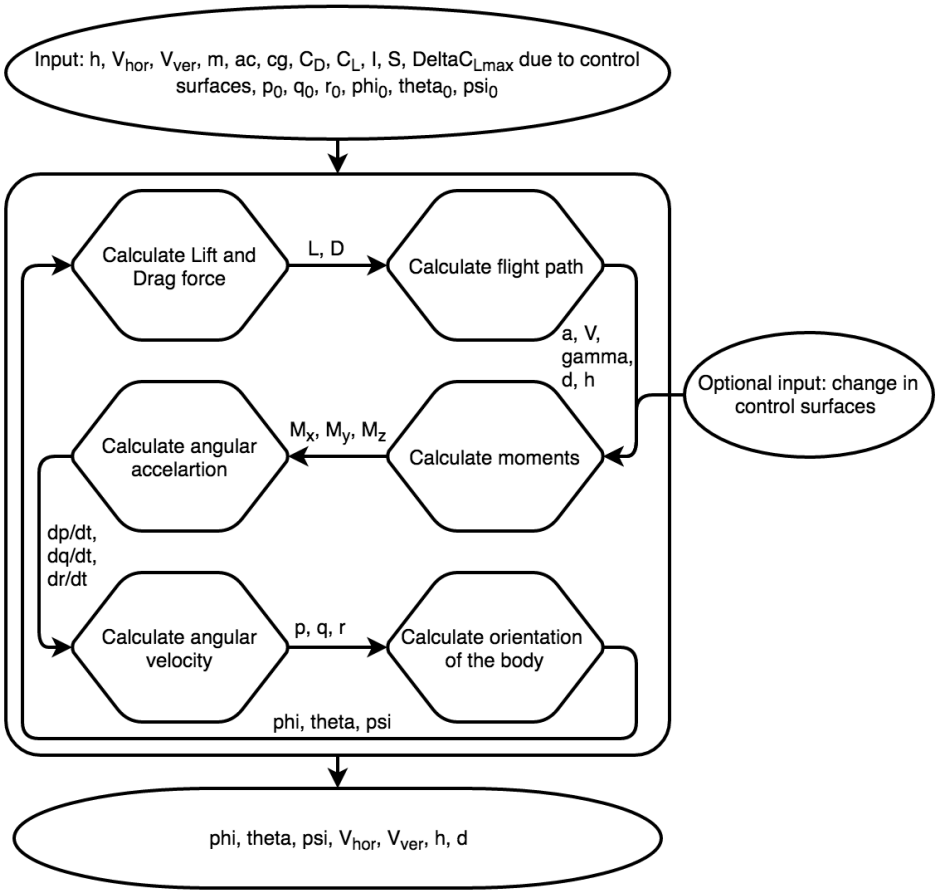

Figure C.1: Functional flow diagram stability and control.

In Figure C.2 the flow of the flight mechanics model is shown. In the first main block the continuous process is shown. These steps are performed every iteration through the program. The second main block shows the main flow of the model with as a final output a range and airborne time.

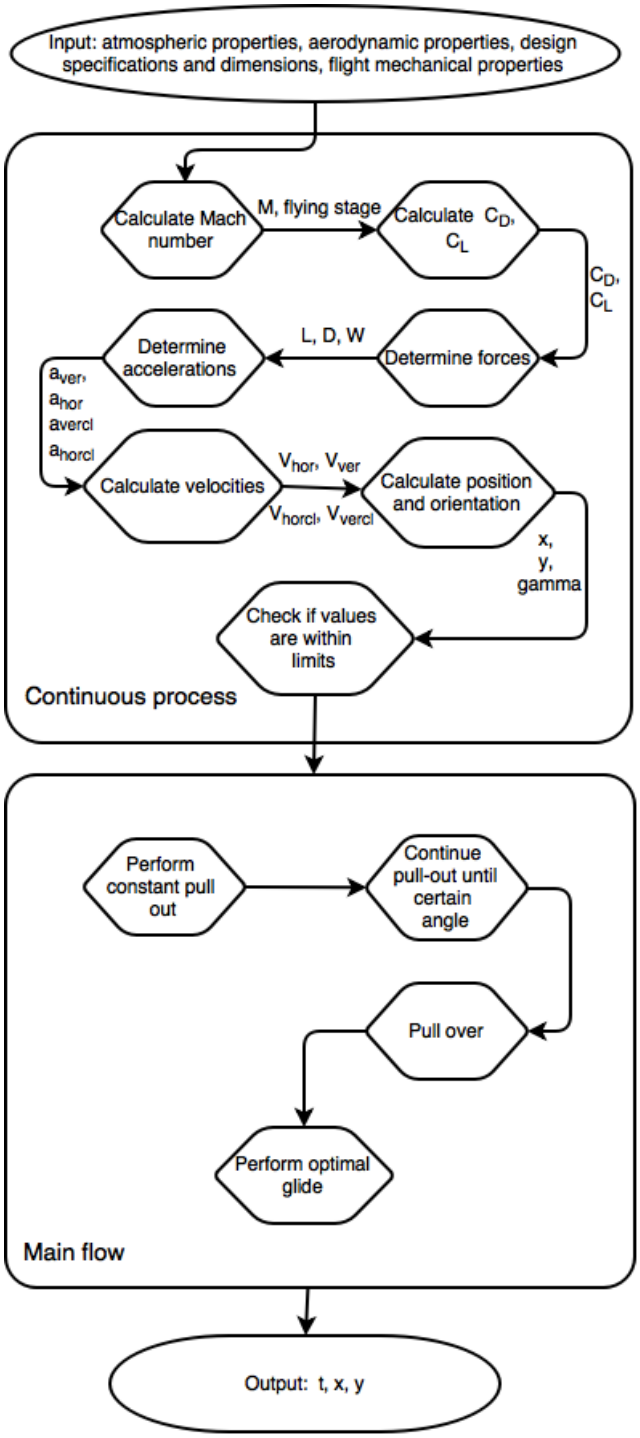

Figure C.2: Functional flow diagram flight mechanics.

Appendix D

ICARUS+ Technical Drawings

In this appendix the technical drawings for the external and internal layout of the ICARUS+are given in Figure D.1 and D.2.

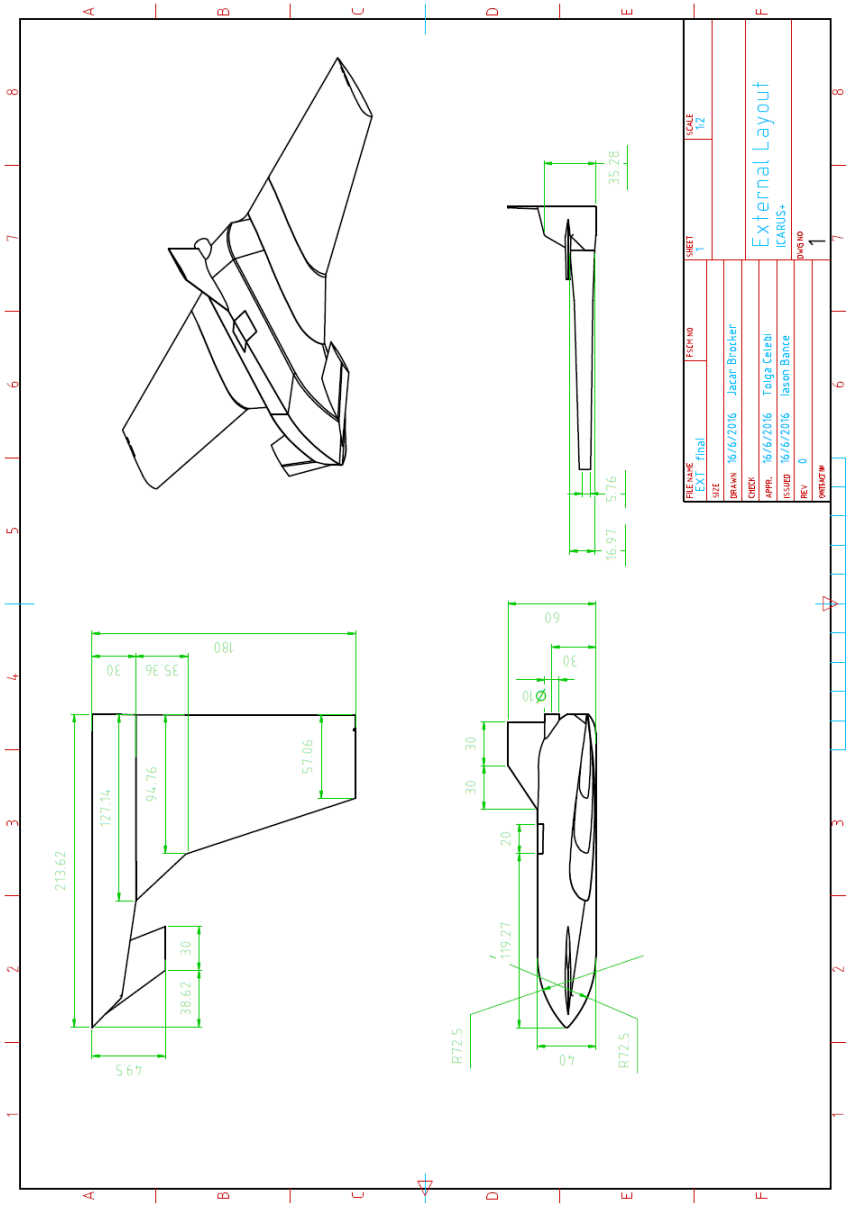

Figure D.1: Technical drawing of the external lay-out of the ICARUS+.

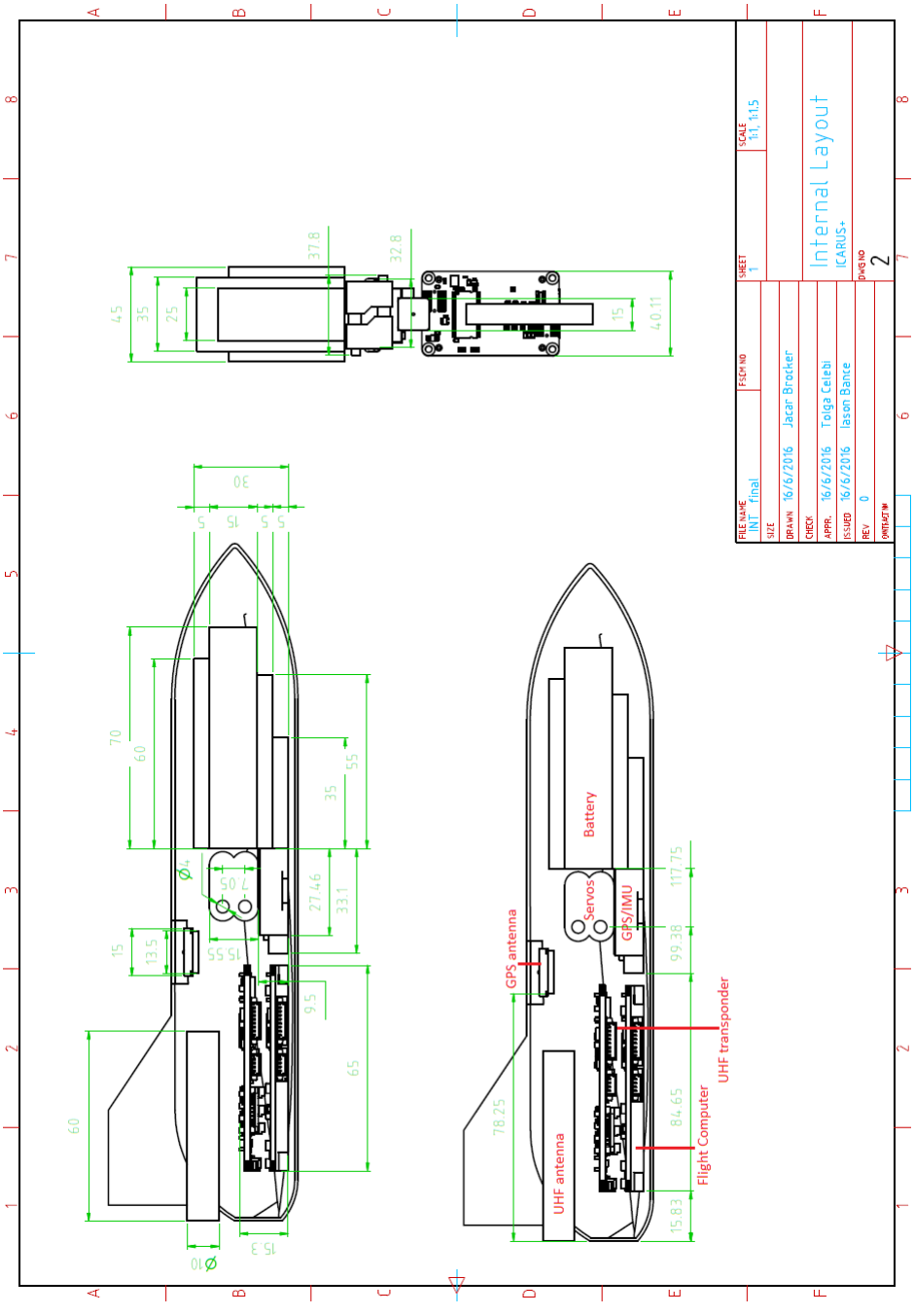

Figure D.2: Technical drawing of the internal lay-out of the ICARUS+.

Appendix E

Work Distribution

In this appendix the work distribution is shown in Table E.1.

Table E.1: Work distribution - Final Report.

Chapter	Worked on
Introduction	Lisa
Summary	Pieter-Bas
Mission Overview	Isa
Functional Breakdown	Isa & Iason
Design Process Overview	Isa & Iason
Meteorological Analysis	Lisa & Annemarie
Flight Mechanics	Tolga
Stability & Control	Lisa & Pieter-Bas
Aerodynamics	Jente & Mitchell
Structures	Adri & Annemarie & Jacar
Electronics	Isa & Iason
Thermal	Jacar
Verification & Validation	Everyone
Sensitivity Analysis	Everyone
Design Iterations	Everyone
Technical Design Overview	Iason
3D Modelling	Adri & Jacar
Recommendations	Everyone
Project Design and Operations	Isa & Iason
Cost Breakdown	Isa
Market Analysis	Tolga
Risk Management	Annemarie
RAMS	Annemarie
Sustainable Development Strategy	Mitchell
Budget Breakdown	Isa & Iason
Compliance Matrix	Isa
Conclusion	Lisa